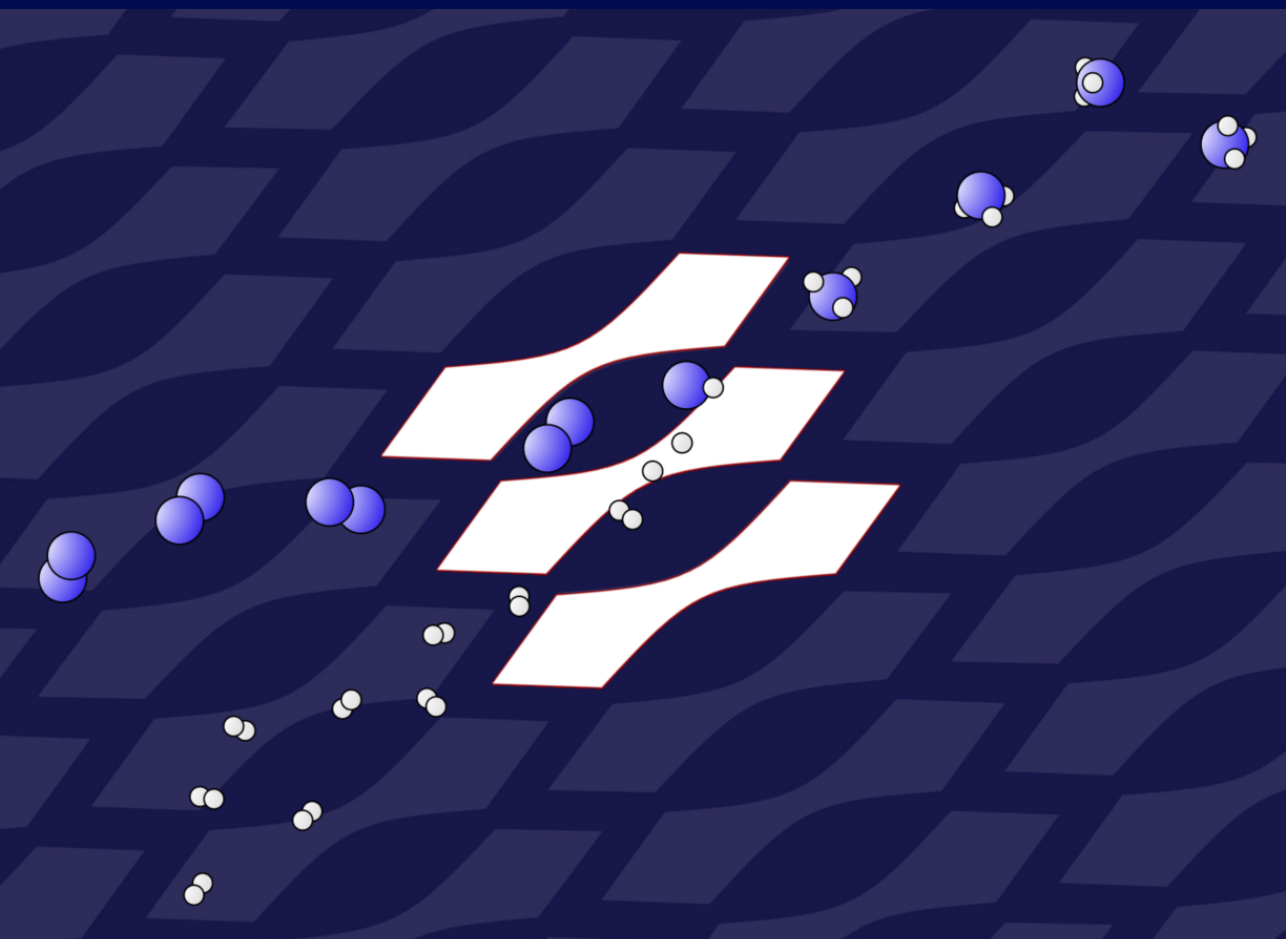


# Upscaling of electrochemical nitrogen reduction to ammonia

*From batch to flow cells*

Jakob Bruun Pedersen

PhD Thesis - April, 2022



**Cover figure**  
**Ammonia formation through the DTU logo**

# Upscaling of electrochemical nitrogen reduction to ammonia

From batch to flow cells

---

Ph.D. thesis

Jakob Bruun Pedersen

Supervisor: Associate Professor Jakob Kibsgaard

Co-supervisor: Professor Ib Chorkendorff

Surface Physics and Catalysis (SurfCat)

Department of Physics

Technical University of Denmark



---

## Abstract

Synthetic production of ammonia was made possible in the beginning of the 20th century, where the Haber-Bosch process was invented. This made it possible to produce large volumes of ammonia, which otherwise was a limited commodity from natural sources. Ammonia is an essential chemical for the world as we know it, since it is mainly used for fertilizers. With synthetic fertilizers, farming can be done much more effectively, increasing the crop-yield. More crops, mean more food to more people. And so, during the last century, the global population has increased four-fold, thanks to the Haber-Bosch process. In this process, nitrogen and methane is converted, forming ammonia and carbon dioxide as a by-product. Splitting inert nitrogen gas is a difficult process, which here requires high temperature and pressure. To do this efficiently, the production-plants are large and centralized. Due to the large scale, and current yearly production volume of >180 million tonnes per year, the process is responsible for more than 1% of the global CO<sub>2</sub>-emissions. With an increase in the global population, the emissions will follow along. So to meet the current climate actions, improvements or alternatives must therefore be found.

In this thesis, an alternative electrochemical method for ammonia synthesis is discussed. It was first proposed in 1930 by Fichter et al., and later again in 1993 by Tsuneto et al. But only within the last few years, the method has gained worldwide attention, after it was proven by Andersen et al. to be able to break the strong nitrogen triple-bond. The synthesis is based on a lithium-mediated reaction, where reactive metallic lithium spontaneously allows the process to proceed. It draws many parallels to battery research, operating in non-aqueous conditions.

Most studies on this electrochemical process, are done in small-scale batches, with minute amounts of ammonia produced. The focus of this thesis, is to develop an upscaled electrochemical cell, not limited by batch-wise production. It should be larger in size, and capable of flowing both liquid electrolyte, and gas reactants. These are key elements for allowing continuous production of ammonia.

The thesis starts with a brief introduction to the importance of ammonia. Subsequently, an introduction to some fundamentals on reactions and catalysis, and the experimental methods used for this work. The following chapter will cover the lithium-mediated reaction, and what we know so far. Then the development process, and challenges faced for realizing a working cell, are described. It will end with measurements on the operation of this cell, where mass spectrometry was used for detection and determination of the origin of reactants.



---

## Resumé

Kunstig produktion af ammoniak blev muliggjort i begyndelsen af det 20. århundrede, hvor Haber-Boschprocessen blev opfundet. Den gjorde det muligt at producere store mængder af ammoniak, hvilket ellers er en begrænset ressource fra naturlige kilder. Ammoniak er et essentielt kemikalie for verden, som vi kender den, eftersom det hovedsagligt bruges til gødning. Med kunstgødning kan landbrug gøres langt mere effektivt og dermed øge mængden af afgrøder. Flere afgrøder betyder mere mad til flere mennesker. Dermed har der været en firefoldig stigning i verdensbefolkningen i løbet af det sidste århundrede takket være Haber-Boschprocessen.

I processen omdannes nitrogen og naturgas til ammoniak med kuldioxid som biprodukt. Det er en svær proces at splitte inert nitrogengas, hvilket her kræver høje temperaturer og tryk. For at gøre dette effektivt er produktionsfabrikkerne store og centraliserede. Grundet den store skala og den nuværende årlige produktionsmængde på mere end 180 millioner ton er denne proces ansvarlig for mere end 1% af den globale udledning af CO<sub>2</sub>. Med en fortsat stigning i verdensbefolkningen vil disse udledninger følge med. Så for at imødekomme de nuværende klimamålsætninger skal forbedringer eller alternativer findes.

I denne afhandling bliver en alternativ elektrokemisk metode til ammoniaksyntese gennemgået. Den blev nævnt første gang i 1930 af Fichter et al., og sidenhen i 1993 af Tsuneto et al. Men først inden for de sidste par år har denne metode vundet genklang verden over, efter det blev påvist af Andersen et al., at den kan bryde den stærke trippelbinding i nitrogen. Syntesen er baseret på en lithiummedieret reaktion, hvor reaktivt metallisk lithium spontant kan starte processen. Den drager mange paralleller til batteriforskning, virkende under ikke-vandige betingelser.

De fleste studier på denne elektrokemiske proces er gjort i lille skala i enkeltvise partier med meget små mængder ammoniak produceret. Fokus for denne afhandling er at udvikle en opskaleret elektrokemisk celle, der ikke er begrænset til produktion i små partier. Den skal være større og være i stand til at have en strøm af både flydende elektrolyt og gasreaktanter. Dette er centrale elementer for at muliggøre kontinuerlig produktion af ammoniak.

Afhandlingen begynder med en kort introduktion til vigtigheden af ammoniak. Derefter gives en introduktion til den fundamentale baggrund for reaktioner og katalyse samt de eksperimentielle metoder brugt i dette arbejde. Det efterfølgende kapitel gennemgår den lithiummedierede proces, og hvad vi kender til om den. Herefter beskrives udviklingsprocessen mod en fungerende celle samt de

---

udfordringer, der blev mødt på vejen. Til slut vil der blive præsenteret egentlige målinger på brug af cellen, hvor massespektrometri blev brugt til at detektere og fastlægge kilden til reaktanter.



---

## Preface

This thesis is submitted in partial fulfilment of the requirements for the Ph.D. degree from the Technical University of Denmark. The work presented in this thesis was conducted under the supervision of Associate Professor Jakob Kibsgaard and Professor Ib Chorkendorff, in connection to the V-Sustain project on electrochemical nitrogen reduction, funded by the Villum Foundation. The work has been carried out at the Department of Physics, Section of Surface Physics and Catalysis (SurfCat), in the period between November 2018 and April 2022.

My experimental work was carried out in close collaboration with other students and colleagues at SurfCat, and with inputs from supervisors and professors involved in the this project. Contributions from my colleagues will be stated in the respective chapters.

Jakob Bruun Pedersen  
April 2022

---

## Acknowledgement

The work for this thesis was funded by the Villum Foundation V-SUSTAIN grant 9455 to the Villum Center for the Science of Sustainable Fuels and Chemicals. The results reported in this thesis were possible due to collaboration and help from many colleagues at SurfCat, who all deserve my gratitude.

I am first and foremost grateful to my supervisors Assoc. Prof. Jakob Kibsgaard and Prof. Ib Chorkendorff for giving me the opportunity to carry out the work in this project. Sharing their insight and giving constructive feedback throughout the entire project, has pushed me and this project forward. And it made this an interesting and exciting journey to be part of. I also would like to thank Prof. Peter C.K. Vesborg and Prof. Jens K. Nørskov, whose input in weekly meetings has expanded my knowledge and way of thinking on this project, and Dr. Debasish Chakraborty for his insights in the ammonia field.

I would like to thank the entire ammonia team for providing help and guidance, both when my chemical understanding reached its limits, and when a helping hand was needed in lab. Dr. Viktor Čolić and Dr. Sungeun Yang helped me get started on the project, and introduced me to the lithium-mediated reaction. I especially would like to thank Dr. Suzanne Z. Andersen, without whom I likely would not have succeeded, showing me that a physicist, also can work with electrochemistry. She gave me a crash-course on the experiments when I started, and has ever since been to great help, always ready to answer questions or help finding the best solution. I owe special thanks to Dr. Mattia Saccoccio, who has been essential in the design and production work, towards realizing an electrochemical cell. His help and broad knowledge, made it possible to succeed. Thanks also go to Dr. Xianbiao Fu, who in short time managed to push the performance of the flow cell forth, and cover many of the ideas, I never got to try out. I owe thanks to all the members of the ammonia group. The Ph.D students Katja Li, Kevin Kreml, and the newest members Bjarke Mygind and Niklas, all help make the days in lab fun. Dr. Rokas Sažinas for learning me a ton of organic chemistry (which still seems like black magic to me) and always ready to answer questions, and Dr. Shaofeng Li for good collaboration in the labs. Some theoreticians have also been part of the weekly discussions, and I thank every one of them for their inputs.

Beyond the ammonia team, I would like to thank all the people at SurfCat. You have all ensured a fun, pleasant, and fruitful work-environment. Special thanks go to Jacqueline McAnulty for assistance in chemistry labs, as well as Birgit Bohn for organization and coordination of the entire section. I owe great thanks to current and former Floormanagers, Brian Knudsen, Jakob Ejler, and

---

Patrick Strøm-Hansen for their technical support in making all the equipment at SurfCat function. I thank the employees at the DTU Physics Workshop for good and precise work, during the manufacturing process of the cell.

I want to thank all the people, whom I have had the joy of sharing office with. Thomas Smitshuysen, Jens-Peter Haraldsted, Suzanne Andersen, Celia Cailloux and Sarah Shapel, together with honorary office member Hjalte Rørbech. Many coffee breaks and good talks have been spent with them. I owe thanks to Alexander Krabbe, who without hesitation came to my help, when I was standing with a new MS-setup that stopped working. Also Asger Moss, has been of great help with discussions on cell assemblies.

I want to thank Jasper Volmer, for proofreading parts of this dissertation, and for being a great friend. I also owe thanks to Suzanne Andersen, Mattia Saccoccio, Rokas Sažinas and Bjarke Mygind for their time on proofreading and valuable feedback on this dissertation.

Finally, I want to thank my family. My parents, Karen and Henrik, my sisters, Hannah and Maria, and my brother-in-laws, Frederik and Kristian. You have always supported me, and given me the encouragement to carry on.

---

## List of publications

### Paper I

#### **Increasing Stability, Efficiency, and Fundamental Understanding of Lithium-Mediated Electrochemical Nitrogen Reduction**

Suzanne Z. Andersen, Michael J. Statt, Vanessa J. Bukas, Sarah G. Shapel, Jakob B. Pedersen, Kevin Kreml, Mattia Saccoccio, Debasish Chakraborty, Jakob Kibsgaard, Peter C.K. Vesborg, Jens Nørskov and Ib Chorkendorff  
*Energy & Environmental Science*, **13**, 4291-4300, (2020)

### Paper II

#### **Towards understanding of electrolyte degradation in lithium-mediated non-aqueous electrochemical ammonia synthesis with gas chromatography-mass spectrometry**

Rokas Sažinas, Suzanne Zamany Andersen, Katja Li, Mattia Saccoccio, Kevin Kreml, Jakob Bruun Pedersen, Jakob Kibsgaard, Peter Christian Kjærgaard Vesborg, Debasish Chakraborty and Ib Chorkendorff  
*RSC Advances*, **11**, 50, 31487-31498, (2021)

### Paper III

#### **Enhancement of lithium-mediated ammonia synthesis by addition of oxygen**

Katja Li, Suzanne Z. Andersen, Michael J. Statt, Mattia Saccoccio, Vanessa J. Bukas, Kevin Kreml, Rokas Sažinas, Jakob B. Pedersen, Vahid Shadravan, Yuanyuan Zhou, Debasish Chakraborty, Jakob Kibsgaard, Peter C.K. Vesborg, Jens K. Nørskov and Ib Chorkendorff  
*Science*, **374**, 6575, 1593-1597, (2021)

---

Paper IV

**Increasing Current Density of Li-Mediated Ammonia Synthesis with High Surface Area Copper Electrodes**

Katja Li, Sarah G. Shapel, Degenhart Hochfilzer, Jakob B. Pedersen, Kevin Kreml, Suzanne Z. Andersen, Rokas Sažinas, Mattia Saccoccio, Shaofeng Li, Debasish Chakraborty, Jakob Kibsgaard, Peter C.K. Vesborg, Jens K. Nørskov, Ib Chorkendorff

*ASC Energy Letters*, **7**, 1, 36-41, (2022)

Paper V

**Electrolyte acidification from anode reactions during lithium mediated ammonia synthesis**

Kevin Kreml\*, Jakob B. Pedersen\*, Jakob Kibsgaard, Peter C.K. Vesborg and Ib Chorkendorff

*Electrochemistry Communications*, **134**, 4, 107186, (2022)

\* these authors contributed equally

---

## List of abbreviations

CA	Chronoamperometry
CE	Counter electrode
CP	Chronopotentiometry
CV	Cyclic voltammetry
PEIS	Potentiostatic Electrochemical Impedance Spectroscopy
HER	Hydrogen Evolution Reaction
LSV	Linear sweep voltammetry
MS	Mass spectrometry
NMR	Nuclear Magnetic Resonance spectroscopy
NRR	Nitrogen reduction reaction
OCP	Open circuit potential
OER	Oxygen evolution reaction
QMS	Quadrupole mass spectrometer
Redox	Coupled reduction-oxidation reaction
RE	Reference electrode
RF	Radio frequency
RHE	Reversible hydrogen electrode
SEI	Solid electrolyte interphase
SEM	Scanning electron microscopy
SHE	Standard hydrogen electrode
SS	Stainless steel
UHV	Ultra high vacuum
UV/Vis	Ultraviolet-visible spectroscopy
WE	Working electrode
XPS	X-ray photoelectron spectroscopy
XRD	X-ray diffraction

## Contents

Abstract . . . . .	i
Resumé . . . . .	ii
Preface . . . . .	iv
Acknowledgement . . . . .	v
List of publications . . . . .	vii
List of abbreviations . . . . .	ix
<b>1 Introduction</b>	<b>1</b>
1.1 Brief history of ammonia . . . . .	1
1.1.1 Natural fixation . . . . .	2
1.1.2 Artificial fixation . . . . .	2
1.2 Thesis outline . . . . .	7
<b>2 Catalysis and reactions</b>	<b>8</b>
2.1 Catalysis . . . . .	8
2.1.1 Basics of catalysis . . . . .	9
2.1.2 Mechanisms of surface reactions . . . . .	10
2.1.3 Choice of catalyst . . . . .	11
2.1.4 Sabatier's principle and scaling relations . . . . .	13
2.1.5 The Haber-Bosch process . . . . .	14
2.1.6 Electrocatalysis and -chemistry . . . . .	16
2.1.7 Lithium-mediated electrochemical process . . . . .	18
2.2 Electrochemical ammonia synthesis in the bigger picture . . . . .	18
2.2.1 Aims of this dissertation . . . . .	19

---

<b>3</b>	<b>Experimental methods</b>	<b>21</b>
3.1	Electrochemical experimentation . . . . .	21
3.1.1	Glovebox . . . . .	21
3.1.2	Electrochemical setup . . . . .	22
3.1.3	Glass cell experiments . . . . .	22
3.1.4	Flow cell experiments . . . . .	23
3.1.5	Electrochemical methods . . . . .	24
3.2	Ammonia quantification . . . . .	28
3.2.1	Colorimetric indophenol method . . . . .	28
3.2.2	Ion Chromatography . . . . .	30
3.2.3	Nuclear Magnetic Resonance Spectroscopy . . . . .	32
3.3	Garm . . . . .	34
3.3.1	Build and components . . . . .	34
3.3.2	Mass spectrometry . . . . .	35
<b>4</b>	<b>Non-aqueous ammonia synthesis</b>	<b>38</b>
4.1	The difficult step - Nitrogen reduction . . . . .	38
4.2	The lithium mediated reaction . . . . .	40
4.3	Stability of organic electrolytes . . . . .	42
4.4	Effect of the SEI layer and potential cycling . . . . .	44
4.4.1	Stability by potential cycling . . . . .	44
4.4.2	Enhancement by oxygen . . . . .	47
4.5	Acidification of electrolyte . . . . .	48
4.6	The other crucial step - Hydrogen oxidation . . . . .	53
<b>5</b>	<b>Flow cell design process</b>	<b>55</b>
5.1	Designing an electrochemical black box . . . . .	55
5.2	Size matters . . . . .	55
5.3	Gas supply . . . . .	56
5.4	Not only a batch . . . . .	58
5.4.1	Design considerations . . . . .	58
5.4.2	Material choice . . . . .	59
5.4.3	O-rings and sealings . . . . .	60
5.5	First iteration . . . . .	60

5.5.1	Evaluation . . . . .	65
5.6	Second iteration . . . . .	67
5.7	Third iteration . . . . .	75
<b>6</b>	<b>The electrochemical flow cell</b>	<b>78</b>
6.1	Objective for the experiments . . . . .	78
6.2	Synthesis with flowing electrolyte . . . . .	80
6.2.1	Electrode areas . . . . .	82
6.3	Mass spectrometry and non-aqueous media . . . . .	83
6.3.1	Preparations . . . . .	84
6.3.2	Measurements on flow cell . . . . .	86
6.3.3	Transport of protons . . . . .	90
6.3.4	Combined NRR and HOR . . . . .	92
6.3.5	Final comments . . . . .	99
<b>7</b>	<b>Conclusion and outlook</b>	<b>100</b>
7.1	Outlook . . . . .	101
<b>Appendices</b>		
<b>A</b>	<b>Useful figures</b>	<b>105</b>
A.1	Urea prices . . . . .	105
A.2	Periodic table . . . . .	106
<b>B</b>	<b>Figures for Chapter 5</b>	<b>107</b>
B.1	Initial tests of membranes . . . . .	107
B.2	Technical drawing . . . . .	109
B.3	Anodization of Al parts . . . . .	110
B.4	Various figures . . . . .	111
B.5	NRR on Cu . . . . .	115
B.6	Electrodeposition of Cu on electrodes . . . . .	116

<b>C</b>	<b>Figures for Chapter 6</b>	<b>117</b>
C.1	Flow cell measurements . . . . .	117
C.2	Mass spec measurements . . . . .	120
C.2.1	Mass spec settings and optimization . . . . .	120
C.2.2	Mass spec calibrations . . . . .	122
C.2.3	Data presentation . . . . .	125
<b>D</b>	<b>Appended Publications</b>	<b>131</b>
	<b>Bibliography</b>	<b>159</b>



# Chapter 1

## Introduction

The PhD project described in this thesis, has in principle focused on two things: ammonia and how to design a device for upscaling electrochemical synthesis of ammonia. This first chapter is meant to be relatively easy to read, giving an overall introduction to the field and motivation for the work. The following chapters will be more technical and probably require an interest in the subject, to enjoy reading.

So before diving into details on the design process we have been through in our group, chemical reactions, measurements and such, I will start with the essentials: What is the deal with ammonia?

### 1.1 Brief history of ammonia

So, what is ammonia? First of all, it is an important molecule that we produce a lot of globally. In 2021 the total global production of ammonia was more than 182 million tonnes [1, 2]. That makes ammonia one of the most produced chemicals in the world together with other important chemicals such as sulfuric acid (231 million tonnes) and ethylene (205 million tonnes) [3–6].

Ammonia in itself is a fairly simple molecule, only consisting of hydrogen (H) and nitrogen (N) and written as  $\text{NH}_3$ . It is mainly ( $\sim 80\%$ ) used as a fertilizer [2, 4], which also explains the importance of producing it. Other applications of ammonia are nitrogen-containing chemicals, polymers and plastics, and explosives such as nitroglycerin and trinitrotoluene also known as TNT [4, 7].

The backbone of ammonia is the nitrogen atom. We have plenty of molecular nitrogen surrounding us, as roughly 80% of the atmosphere is  $\text{N}_2$ . But the nitrogen in our atmosphere is from a thermodynamic perspective very difficult to use. This is due to the nature of the  $\text{N}_2$  molecule. It is symmetric (just two similar N atoms) with a very strong triple bond between the atoms. This makes

$N_2$  very inert and one of the most stable molecules, meaning it prefers to stay as  $N_2$ . It is thus difficult and quite demanding to activate the molecule in order to use it.

### 1.1.1 Natural fixation

Luckily, it is possible. Nature itself is able to do it in a few different ways. One third of the naturally activated nitrogen is from lightning, fires and the like, where nitrogen is oxidized due to the heat. Here the  $N_2$  molecule is split, and reacts with oxygen to form various  $NO_x$  species [7]. A different, and maybe more important route is bacteria using enzymes to form  $NH_3$ . Certain bacteria living in symbiosis with plants and other organisms, such as cyanobacteria or blue-green algae, are able to fix nitrogen on their own. But what is common for them, is an oxygen-free environment, such that anaerobe conditions are met [8, 9]. A nitrogen fixation source many farmers are familiar with is the pea plant family (or leguminous plants). Here bacteria live in symbiosis with the pea plant, and use the nitrogenase enzyme to fix nitrogen. The plant provides energy for the process, and in return the bacteria gives back ammonia, which the plant can use for growth. It is quite fascinating how the enzyme is able to fix nitrogen at room temperature and ambient pressure efficiently [10]. But the process is slow. Hence, artificial fertilizers are needed, in order to meet the growing demand for food, from a globally increasing population [4].

### 1.1.2 Artificial fixation

Rewinding the clock to the early 1900's it had been a long dream for scientists to be able to make synthetic  $NH_3$ . But no one had succeeded, due to the challenging demands and conditions. But then in 1909, something game-changing happened. The German chemist Fritz Haber with coworkers managed to produce ammonia at a considerable rate of 2 kg per day. Today, this does not sound like much, but compared to farming where pea crops are used for natural N-fixation,<sup>1</sup> it corresponds to about 5 hectare of pea plant crops [11]. It did require operation at 175 bar and reactive osmium-based catalysts to achieve this, but synthetic  $NH_3$  production at reasonable rates was now a thing. The chemical company BASF purchased the process, and another German chemist, Carl Bosch, was assigned to scale up the process. He managed to develop the technology from high pressure batch processes into flow reactors operating at high pressures. The following year he succeeded in scaling up Haber's process and produced several tons of ammonia per day at 300 bar [7].

Both of their achievements are absolutely impressive and has since been declared as "the most important discovery of the 20th century" [12, 13]. Accordingly, they were both rewarded with a Nobel price each, Fritz Haber in 1918, and Carl Bosch

---

<sup>1</sup>rotation of pea crops and wheat

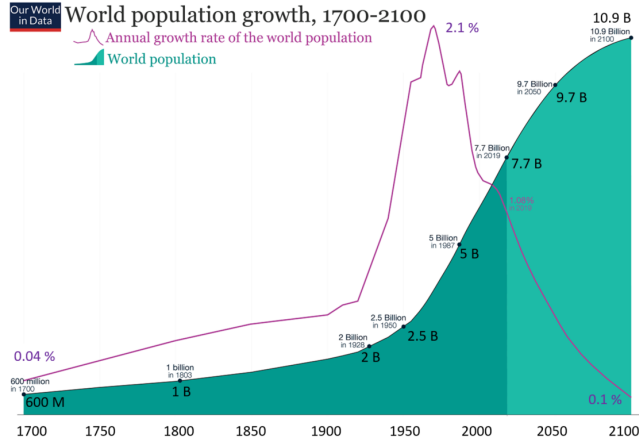


Figure 1.1: Global population growth rate (purple line) and total population (green curve) from 1700 to 2019 and further projected to 2100. A drastic increase in growth rate is seen shortly after the invention of the Haber-Bosch process, reflecting the newfound possibility for producing more crops and food. Projections estimate the global population will stagnate at around 11 billion people a hundred years from now. Figure from Our World in Data [14]

in 1931. This way of producing synthetic ammonia is now referred to as the Haber-Bosch process, reflecting both of their contributions to the development.

The tangible importance of ammonia and the massive impact Haber and Bosch's work has had, is clearly shown in Figures 1.1 and 1.2. Figure 1.1 shows the global population and population increase since 1900. What is very noticeable is how there was an almost explosive increase in the number of people shortly after the development of the Haber-Bosch process. Being able to produce ammonia on demand, allowed for making more fertilizers, producing more crops and thus sustaining a higher food supply. During the 20th century the global population increased more than four-fold! This has only been possible through more efficient farming, by giving more nutrients to the plants. This development has increased ever since, summarized in Figure 1.2. Before the Haber-Bosch process, the only source of fertilizers were natural and organic waste, either from bacteria or using guano from bats, having a relatively high content of fixed nitrogen. We are now at a point, where half the population on earth has a food supply based on synthetic fertilizers [15, 16]. This highlights and underlines why this was the most important discovery, and a crucial product to make. Taking the projected increase of additional approximate 4 billion people in the next hundred years, the importance of synthetic fertilizers is self-evident.

Despite it being developed more than a century ago, the Haber-Bosch process is still the main way of producing ammonia today. Synthetic ammonia is actually almost exclusively produced via the Haber-Bosch process. A lot has happened to the process since Haber and Bosch did the early inventions, namely improved materials and process conditions. But the general synthesis is still the same

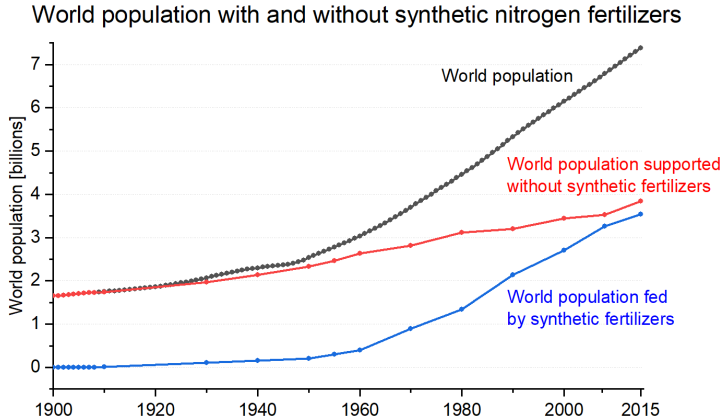


Figure 1.2: The global population from 1900 to 2015 and the estimated proportion that is reliant on nitrogen-containing fertilizers for sustaining their food supply. It is difficult to have exact numbers for this, but best estimates projects that approximately half the world's population is sustained via Haber-Bosch derived fertilizers, who without synthetic fertilizers would not have food to live by. Data from [17] and [18].

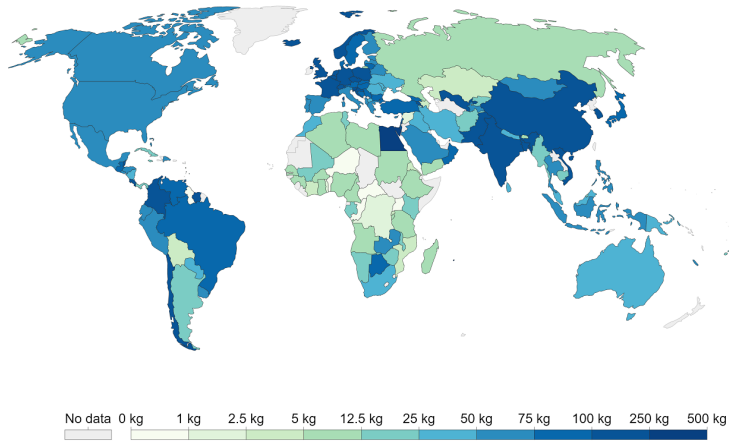
today. I will save the technical details for the next chapter, but the process runs at high pressures and fairly elevated temperatures. This means, that in order to run it efficiently [19], it requires large facilities. Furthermore, due to the high production capacity, a lot of materials need to be provided to the facility - and a lot of products need to be shipped out afterwards. So the facilities not only have to be large, they also have to be centralized, with good infrastructure for shipping materials in and out. When a lot of ammonia is produced, it naturally requires large quantities of both nitrogen and hydrogen. Nitrogen can luckily easily be provided from the surrounding atmosphere, so there is plenty of that. The hydrogen unfortunately cannot be supplied as easily, so the cheapest alternatives are used. Fossil fuels are easy to transport and they do carry quite a lot of hydrogen with them. The hydrogen can be released, but on the cost of emitting a lot of  $\text{CO}_2$  along with it. Summing this up, we now see that the current ammonia production both have a significant energy ( $\sim 2\%$ ) and  $\text{CO}_2$  ( $\sim 1.3\%$ ) footprint [1] from the synthesis - and even higher with the following distribution.

The distribution from the centralized plants has yet another effect. To receive ammonia, it also requires a certain level of infrastructure. This means there is a somewhat skewed distribution of what parts of the world can afford and access ammonia shown in Figure 1.3. This is quite unfortunate, since this also means that there are places lacking access to fertilizers. With a local lack of fertilizers, possible consequences are starvation and inequality [20].

And even in the places where we can access ammonia, it is typically being delivered in bulk. There are different ways to distribute on the fields, which depend

## Nitrogen fertilizer use per hectare of cropland, 2017

Application of nitrogen fertilizer, measured in kilograms of total nutrient per hectare of cropland.



Source: UN Food and Agricultural Organization (FAO)

OurWorldInData.org/fertilizers • CC BY

Figure 1.3: Use of chemical and mineral nitrogen containing fertilizers per area cropland around the world. A noticeable difference is seen in the Sub-Saharan countries, compared to the global use. Data from 2002 to 2017 published by Our World in Data and the Food and Agriculture Organization of the United Nations (FAO) (2020) [17].

on the specific type of fertilizer used. It is possible to use ammonia directly. But ammonia can also be converted to urea, nitrates or other N-containing compounds, which are often preferred by farmers. A common application of nitrogen to the soil, is by knifing it to the ground. It is important for farmers to ensure correct application of fertilizer to their crops, in order for it to grow optimally. This is typically done two to three times per year. Plants can only uptake a certain amount of fertilizers. The excess will simply be washed away with rain or seep through the ground. That does not mean the fertilizers disappear, but they will be part of a different eco-system. It can e.g. run into the ground water and pollute that. Or it can wash out into water streams and lakes - here the N-compounds will improve the growth of whatever plants or algae present, which unfortunately, many times has led to oxygen depletion and lack of sunlight for the ground plants and fish. Reviving such negative impacts on our surroundings are cumbersome, expensive, and difficult, and it should be avoided.

Consequences of  $\text{CO}_2$  emissions to the environment are well known, and has been for a long time [21–25].  $\text{CO}_2$  and other green house gases (GHG) contribute to climate change, by in simple terms, act as a big blanket around the world, keeping in the heat. This is simplified in Figure 1.4. Looking at the atmospheric  $\text{CO}_2$  concentration, it has been fluctuating between about 170 to 300 ppm (parts per million) for the past 800,000 years. But with the industrial revolution, extreme consumption of fossil fuels, and a rapidly increasing population with high living

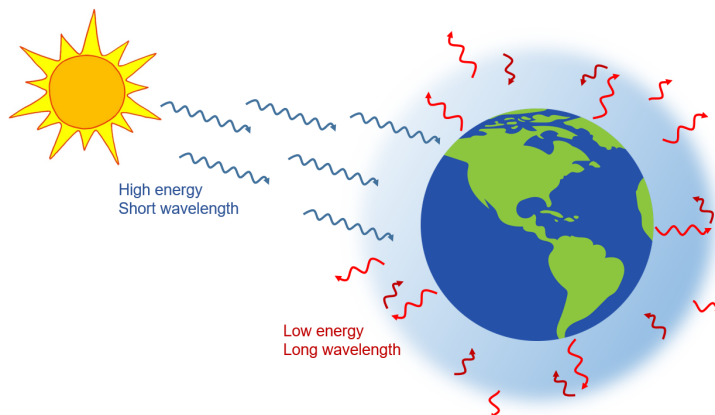


Figure 1.4: Simple schematic showing the effect of green house gases. The presence of GHGs in our atmosphere, such as water,  $\text{CO}_2$  and methane, acts as blanket around the world. High energetic photons from the Sun can pass through, but long wavelength thermal radiation from Earth is absorbed and emitted back to earth. This is why Earth is not too cold for us live here.

standards, the concentration has increased at a rate of more than 1 ppm per year. Today the concentration has passed 415 ppm, and now increasing at a higher rate of more than 2 ppm per year [26]. The blanket around the world, which for thousands of years have provided a nice temperature for humans and animal life to live in, is now starting to become thicker and thicker, and the balance that used to be, is now shifting out of our hands. We can even already now measure and see the effect on global temperature, increased acidity of oceans, the effect on oceanic wild life, and more extreme weather [27]. And what is worse, is the inverted relationship between those who consume and those who pay the price [25], with the biggest climate effects hitting the least wealthy countries, who contributes the least to all of this.

Ammonia production is responsible for approximately 1.3% of the global  $\text{CO}_2$  emissions, and therefore also quite the contributor to all of these problems [28]. I would though take a step back, and remind the reader that ammonia is not all bad, as it does provide food to half the world's population. But nonetheless, it does beg the question: Is there an alternative? A few years ago very interesting and promising work was published, showing how it would be possible to significantly decrease the  $\text{CO}_2$  emissions from the big ammonia production facilities [29], but even this important contribution only solves part of the problem. Because the facilities would still be large, centralized and far from where it is used. So the question remains: are there alternative ways of making ammonia? The thesis title has already given away the answer, as we here at DTU Physics are working on such an alternative, which will be described in greater detailed throughout this thesis.

## 1.2 Thesis outline

Chapter 1 was an introduction to the project, giving a glance on ammonia and the importance of it. In Chapter 2 I will give a description of the chemistry and physics involved in catalysis, which is a crucial part of making reactions occur. Chapter 3 gives a descriptions of the various methods used, while Chapter 4 will focus on the non-aqueous ammonia synthesis reaction that I have relied on for electrochemical ammonia production. Chapters 5 and 6 will focus on a flow cell, which we have built for the ammonia reaction. Chapter five concerns the design process, considerations and iterations that we went through, whereas Chapter six will show how we have managed to make the cell operate. I will finally conclude the work in Chapter 7 together with an outlook for future work.

# Chapter 2

## Catalysis and reactions

This chapter will focus on the physics and chemistry of production of various chemicals is possible. The chapter is divided in three sub-sections, starting with catalysis and surface reactions. It will then move on to a description of the Haber-Bosch process and finally end with putting electrochemical ammonia synthesis into this context. Here I will also define some aims I wish to address throughout this dissertation. Experienced readers can skip to Section 2.2.1 for these aims.

### 2.1 Catalysis

What allows us to produce ammonia, and all other useful chemicals for that matter, is something called catalysis. In layman's terms, a catalyst is a substance that facilitates an easier path from reactants to products, such that the end goal can be reached faster and energetically cheaper. If we take a closer look at it, whatever reactants and products we are working with, it is some kind of molecules. Molecules consists of atoms bonded together. These chemical bonds is associated to some energy, and to break it requires that amount of energy. There can be strong bonds or weak bonds, reflecting how stable a molecule is. The stronger the bond, the more energy is required to break it.

When we want to convert some reactants into some products, we can compare the energy associated to each. More specifically, we describe it by the Gibb's free Energy,  $\Delta G$ . This, in itself, is a combination of other physical measures,<sup>1</sup> but describes the highest reversible work that can be performed by a closed system [30]. There are more layers to the picture here. There are typically some intermediate reaction steps between the starting point (reactants) and the final

---

<sup>1</sup> $\Delta G = \Delta H - T\Delta S$ , where  $H = U + pV$  is the enthalpy, which is the sum of internal energy  $U$  and pressure  $p$  and volume  $V$ .  $T$  and  $S$  denotes temperature and entropy.

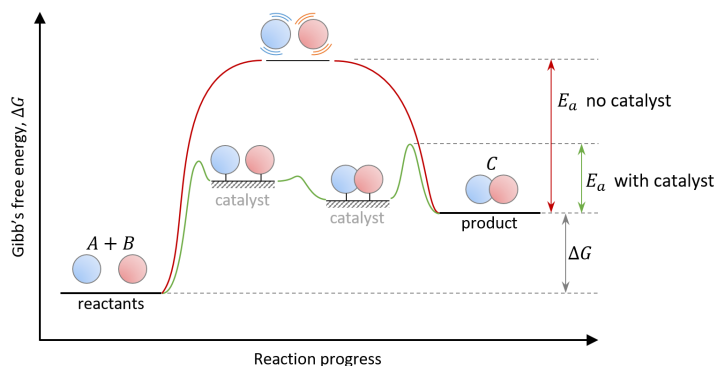


Figure 2.1: Energy diagram of an uphill reaction, where  $A$  and  $B$  reacts to form  $C$ . The red line represents the *non*-catalyzed reaction. The catalyzed reaction (green line), has significant lower energy barrier  $E_a$ , where reactants adsorb and react on the surface of the catalyst.

point (products). These intermediate steps are not as energetically favorable, and therefore require energy to pass. So, apart from the energy in each molecule, it also takes some energy to even begin a reaction. This we call activation energy,  $E_a$ .

With all of this laid out, a reaction path can be presented in a graph. Each reaction step is along the horizontal axis, and the corresponding energy along the vertical axis. In the following, I will describe an arbitrary reaction of two reactants,  $A$  and  $B$ , to one product,  $C$ . In this scenario there is a higher chemical bond in the product than there is in the reactants, so we need to add energy, if we ought to have any chance to make the product. But due to the activation energy of this reaction pathway, the required energy is higher than the difference in free energy of the products and reactants,  $\Delta G = \Delta G_C - \Delta G_{A+B}$ .

### 2.1.1 Basics of catalysis

This is where catalysis comes into play. The catalyst facilitates a different route between  $A$  and  $B$  to  $C$ , which costs less energy than the non-catalyzed pathway. By using the catalyst, we can therefore spend less to produce the same, which means energetically cheaper and faster production.<sup>2</sup>

The difference is depicted in Figure 2.1. Comparing the catalyzed (green line) to the non-catalyzed (red line) pathways, the former is taking a shortcut. I like to compare this with hiking in the mountains. If you need to go from one valley to the neighbouring valley, you can either take the long route over the top of the mountain. Or you might be so lucky there is a tunnel between the two

<sup>2</sup>Cheaper production, w.r.t. economy though, also highly depends on the cost of the catalyst.

valleys. Going through the tunnel, might not give you the same view, but you have saved a lot of energy due to less altitude difference. By introducing the catalyst, the reaction pathway from reactants to products went through different intermediate states. The reactants are allowed to adsorb to the catalyst surface, and go through more favorable steps, which require less energy. The figure is quite simplified, as there often would be multiple intermediate steps, but the story is the same. With a good catalyst less energy is needed to go from reactants to products.

Reactions and the journey from starting point to final point, depends on the specific reactants and the wanted product. Hence, there is not just one catalyst that works for everything, but we need to modify and optimize for the specific needs. Three key parameters are used to describe when a catalyst is good for a reaction. Namely activity, selectivity and stability. The activity is how often it is able to let a reaction occur, whereas the selectivity is a measure of how efficient it only lets one specific, and typically desired, reaction happen. Optimally, your catalyst would be good at both at the same time. If not, you have a trade-off. If you have a very active catalyst, but it makes a bunch of products you are not interested in, you have paid a lot for producing unwanted things and you will have to filter out your product afterwards. On the other hand, you could have a very selective catalyst, that only produces what you want, but the rate is so slow, you never get appreciable amounts of it. Therefore, we need catalysts with just the right properties, such that we can make our desired product at decent rates. Lastly, the equally important factor of stability. Because, in the end, your catalyst is not worth much, if it degrades quickly over time and stops working. Catalysts should, by definition, remain unchanged after reaction, so we continuously can keep on producing for a long time.

### 2.1.2 Mechanisms of surface reactions

So that is the principle of what catalysis does. It can make reactions happen more easily. But what is a catalyst?

The physical way catalysis plays out, can occur via different ways. One way is in biocatalysis, wherein we see enzymes, such as nitrogenase as mentioned in the first chapter. Enzymes are like large proteins with some very shape-specific structures. These structures are created in such a way that they act as active sites and help guide reactants through the reaction. Due to the intricate structure, enzymes are highly efficient catalysts where only specific reactions are allowed. Two other variations are homogeneous and heterogeneous catalysis, referring to whether the catalyst is in the same phase as the reaction medium. This is the case in fully liquid or gaseous systems, where e.g. protons can catalyze the hydrolysis of esters in an aqueous solution. Protons are readily available in acidic media. It speeds up the hydrolysis process but is not consumed during the reaction. Here protons are the catalyst, and exist as a liquid similar to both reactants and products.

This is fundamentally contrasting heterogeneous catalysis, where the catalyst is in a different phase than the reactants and products. This is also what is relevant for this project, and will be described for the remainder of this chapter. There are numerous examples of this from industry, where solid metallic catalysts are used to convert liquids and gases to useful products. The mechanism of the reactions varies, but will involve an initial adsorption process, where interaction of the catalyst to the reactants takes place and lower the reaction energetics. A rare mechanism is when one reactant adsorbs and dissociates on the surface, followed by direct reactions with the remaining reactants and finally desorbs as product (Eley-Rideal mechanism). In heterogeneous catalysis, nearly all reactions happens via the Langmuir-Hinselwood mechanism, where all reactants adsorb to the surface, such that adsorbate electrons interact with the catalyst. In this chemisorbed state, the reaction occur and products are formed. A third possibility is the Mars-van Krevelen reaction, where surface atoms are used for the reaction, and afterwards are replenished by external sources. This is more step-wise than the others, but overall, the catalyst ends in the same state as it was prior to reaction. Exactly which mechanism governs a specific reaction, depends on reaction kinetics. Once knowing this, it is possible to optimize and improve the conditions, and thereby increase the efficiency [7].

Industrial catalysts are often metals. The atoms in a metal sits nicely packed in well defined lattices, which gives them some very specific characteristics. This includes their electronic structure. There are multiple factors that affect the structure, but namely the type of crystal lattice, the number of electrons in the outer-most shell and which electronic orbital this is. Very briefly, the further you move to the right in the periodic system (higher group number), the more electrons (and nuclei) are in the atom. And the further you move down (higher period number), the more orbitals are filled. The periodic table can be found in the Appendix Figure A.2 for reference.

### 2.1.3 Choice of catalyst

There is a group of metals that are widely used in catalysis, which is the d-band metals. The group of metals in the middle of the periodic system has the interesting property, that the outer most electrons are filled into the d-orbital - hence the name of the group. These are widely used and studied for catalysis, due to the way it can interact with molecules, and thereby make these energetically more favorable intermediate states. In order to explain how that is the case, we should take a step back, and start with the principles of solid state physics.

If we consider an electron, it can either be spin up or spin down. Atoms are positive nuclei with electrons orbiting around, so when two atoms are brought together (as in a molecule), the electron wave functions will start overlapping, and new energy levels are created. There will be formed an energy level - or energy state - for each electron, describing the chemical bonding of the molecule. As nature always wants, the electrons will go to the lowest energetic state, which

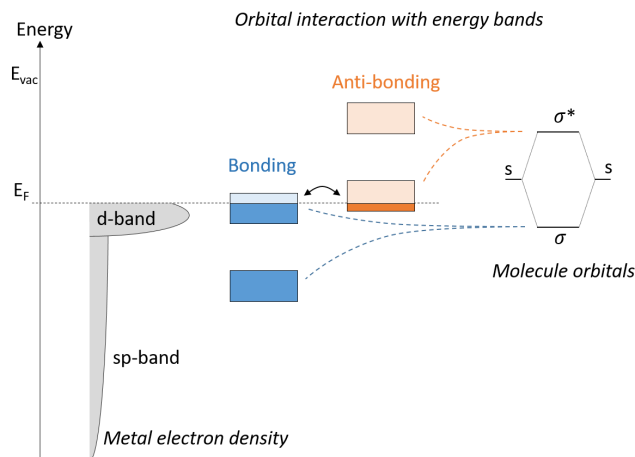


Figure 2.2: Schematic of the interaction between a molecule with a d-band metal. Both bonding and anti-bonding orbitals are split in the interaction with the d-band and shifted down by the sp-band. Here electrons from the bonding orbital starts filling the antibonding orbital, weakening the internal molecule bonding. Inspired from [7].

leads to the two formed states being a bonding and anti-bonding state. When we bring more and more atoms together, each atom will contribute with at state, but can never exist at the exact same energy due to quantum mechanics [31]. In a metal there is a very high number of atoms, described by Avogadro's number in the order of  $10^{23}$ . Even though we know that there is a set of well defined energy states, the energy difference between each of these are now in practice as close to zero as we get, and we now have a continuous band of energy. For the d-band metals, the d-orbital is narrow (as in spatially confined), which from quantum mechanics forces a high electron density. Vice versa, is the s-orbital, which is wide and therefore quite flat and low in density, see left part of Figure 2.2.

As we move from the left to the right in the periodic table, we fill in more and more electrons. Since each electron takes a spot in the vacant band, we start filling up more and more of the bonding states. Eventually, all the bonding states are filled, and the additional electrons will start taking up the anti-bonding states.

If we have a d-band metal, and we move this closer and closer to a molecule, the electrons in the molecule and in the metal will start to interact. The molecules' bonding state ( $\sigma$ ) and anti-bonding state ( $\sigma^*$ ) will split, in a somewhat similar way as was the case for the electron states when creating the molecule, see Figure 2.2. At the same time, interaction with the broad sp-band will lower and broaden each orbital. From the filling degree of the d-band and thus the energy

position compared to the Fermi level,<sup>3</sup> part of the bonding orbital may be shifted above the Fermi-level, while part of the anti-bonding orbital is below. In this scenario, electrons will start filling the anti-bonding orbital, and thus lower the internal binding strength of the molecule. Depending on whether the metal has few electrons, and therefore free bonding-states available (to the left) or many electrons and thus only anti-bonding states available (to the right), the molecule will bind strongly with the bonding states or weakly with the anti-bonding states. Hence, by controlling how filled the d-band is, the molecule will bind strongly or weakly to the metal. This is why atoms to the left are called reactive, while atoms to the right are less reactive.<sup>4</sup> The bonds in the molecule are affected by the interaction between the molecule and the metal. Hence, if the molecule itself is very stable, interaction with a reactive metal will weaken the intramolecular bond, by forcing electrons into the anti-bonding state. Hence, an otherwise very stable molecule can now more easily be split - by the help of a catalyst.

### 2.1.4 Sabatier's principle and scaling relations

The filling of the outer electron band is therefore extremely important for catalysis. But there is a catch to this, and a balance that needs to be considered. The stronger the molecule binds to the metal, the harder it will be to get it off afterwards. Conversely, if it only binds weakly, it will easily be taken off. So we need to make a compromise of how much the molecule should bind to the surface and how weak we want the molecule to become. From the previous discussion on how catalysts provide an alternative and easier reaction pathway from reactants to products, we can now make a similar presentation of how effective a catalyst is (how much energy is saved), by how well we picked the right catalyst to do the job. If the catalyst is too reactive, we can easily split the reactants and form the product, but the product sticks too well to surface, and we cannot get it off. If the reactants bind too weakly, we would easily get the product off, but we cannot start the reaction. Paul Sabatier realized that there had to be an optimum between the rate of catalytic reaction and binding strength. This is thus called Sabatier's principle, and gives rise to the so-called volcano plot, as depicted in Figure 2.3.

Volcano plots are an illustrative way of presenting the required applied energy as a function of the catalyst material. In Figure 2.3, two graphs are shown. The left and right is for (111) and (211) facets respectively (basically the surface geometry of metal atoms), but both graphs gives the same conclusion. The vertical axis is the limiting potential for reaction,  $U_L$ , where more negative numbers mean more energy required. The horizontal axis is the binding energy of nitrogen atoms to the surface,  $\Delta G_N$ . Here more positive numbers mean weaker binding.<sup>5</sup> The

<sup>3</sup>The Fermi level is the energy level of the weakest bound electrons in a solid [7]

<sup>4</sup>And also why noble metals e.g. gold (Au) is to the right - the d-band is filled and reactions with e.g. oxygen in the air is unlikely, and the gold keeps being shiny and non-oxidized.

<sup>5</sup>The less reactive a metal is, the weaker the binding of nitrogen is, hence the order from left to right of the metals in the plot, where Re is in group 7 continuing to Ag in group 11

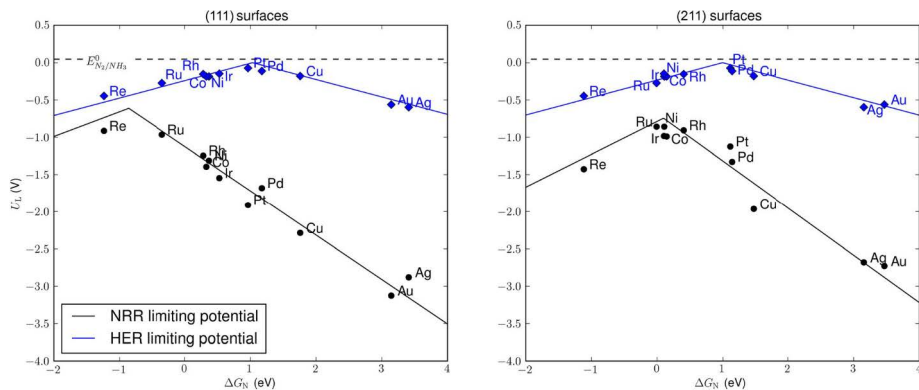


Figure 2.3: Volcano plot of nitrogen reduction (NRR, black line) and hydrogen evolution (HER, blue line) plotted against the  $^*N$ -binding descriptor on two different surfaces. Regardless of the surface HER is more facile than NRR. Figure reprinted with permission from Reference [32]. Copyright 2015 John Wiley & Sons, Inc.

black and blue line show the calculated limiting potentials for hydrogen evolution (HER) and ammonia synthesis (NRR) respectively. Consistently, regardless of the choice of catalyst, the blue hydrogen line is above the black ammonia line, showing how HER has a winning advantage with regards to selectivity over NRR.

It may seem spurious at first, that HER and NRR both can be plotted against nitrogen binding energy, since HER only involves hydrogen and no nitrogen. But it has been shown, that a wide variety of catalytic intermediates across many catalyst surfaces show a very similar behaviour, and they therefore scale to each other. By knowing one, the others can be related to that. This is called scaling relations, and is a very powerful method for summarizing and comparing different catalysts to each other. As seen in Figure 2.3, the different metals fall nicely in two straight lines, suggesting a peak, or optimal binding energy, of nitrogen. Despite ammonia formation being a multi-step process, they can all be described by that single binding energy,  $\Delta G_N$ . Similarly, since nitrogen and hydrogen adsorption also scales, the HER can be plotted simultaneously. With  $\Delta G_N$  being used to describe the entire process, it is fittingly called a descriptor.

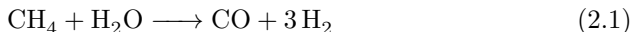
### 2.1.5 The Haber-Bosch process

The Haber-Bosch process is a heterogeneous thermochemical reaction, where air, water, and typically methane<sup>6</sup> is used as feeding stock to produce ammonia. Methane provides plenty of energy while also providing hydrogen. Hydrogen is extracted by steam-reforming, where methane reacts with water to produce

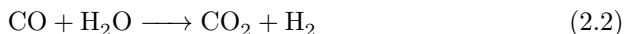
(compare to the periodic system shown in Appendix Figure A.2)

<sup>6</sup>Other fossil fuels, like coal, can also be used, depending on price and accessibility [33]. In 2020 the distribution was 72% methane, 26% coal, 1% oil and a fraction from electrolysis [1].

carbon-monoxide and hydrogen



Some  $\text{CO}_2$  may also be produced in the process, and the mixture of  $\text{CH}_4$ ,  $\text{CO}$ ,  $\text{CO}_2$  and  $\text{H}_2$  is mixed with air. Air is composed of about 78% nitrogen and 21% oxygen, which is used for the subsequent reactions. First oxygen can react with hydrogen and methane in a very exothermic process. This heats up the gas even further to around  $1000^\circ\text{C}$ , which in turn promotes even more conversion of the remaining methane. More hydrogen can be extracted, by water-gas-shift reaction, where  $\text{CO}$  and water reacts to form  $\text{CO}_2$  and hydrogen



This reaction happens at much lower temperatures, so before entering this gas-shift, the gas is cooled down with heat-exchangers. Thereby all the energy from the previous high temperature reaction does not go to waste, but fed back to the initial steam-reforming. It is of upper-most importance that no oxygen is passed along to the following ammonia synthesis, since even trace amounts can completely kill the reaction. This is mainly due to oxygen blocking the active sites of the iron-based ammonia catalysts by forming iron oxides. Water,  $\text{CO}$ , and  $\text{CO}_2$  is also removed, such that a gas composition of 3:1 of nitrogen to hydrogen is compressed to roughly 200 bar and fed to the final ammonia synthesis reactor. The ammonia synthesis reaction is also an exothermic process happening at  $450\text{-}500^\circ\text{C}$ . But only about 15-19% of the nitrogen is converted at a single pass, so ammonia is extracted before being recycled over the catalyst. Since the synthesis reaction is exothermic, the gas mixture heats up as it passes over the catalyst and reacts, but this in turn shifts the equilibrium of reaction unfavorably. Again, a compromise has to be made, where high temperature gives higher rates, and low temperature gives higher conversions. Hence the operating temperature of  $450\text{-}500^\circ\text{C}$  and pressure at around 200 bar. The high pressure in the process, is a benefit for the reaction equilibrium, as four molecules ( $\text{N}_2 + 3\text{H}_2$ ) enter the reaction, but only two molecules ( $2\text{NH}_3$ ) leave as products. By increasing the pressure, the reaction will try to counteract this by making fewer molecules, i.e. converting nitrogen and hydrogen to ammonia. Therefore, as high pressure as possible is desirable, although the cost of building a plant with pipes and reactors capable of producing and maintaining high pressures are expensive. And so, 200 bar is the commonly used pressure.

In the discussion on Sabatier's principle, the choice of catalyst depends on the binding energy of reactant species to the catalyst. For the ammonia reaction, we are of course interested in the binding of nitrogen. But the presence of ammonia will actually affect this binding, as more ammonia corresponds to nitrogen binding less strongly. Consequently, as the nitrogen-hydrogen containing gas passes through the ammonia synthesis reactor, the optimal catalyst for the conversion will slightly change, as the ammonia concentration increases. The optimal setup would therefore be some gradient of catalysts of various alloys, starting with

strong nitrogen binders and subsequently downstream binding more weakly. In practice, a solution is using multiple catalyst beds (or containers of catalyst that the gas passes through) starting with iron-based catalysts leading over to ruthenium-based catalysts.

Summing up the Haber-Bosch process in short: The reaction gases has to be cleaned, heated and pressurized in order to operate the ammonia synthesis efficiently and at high rates. The energy input mainly comes from the methane, which is also the main source of hydrogen to the reaction, where nitrogen is extracted from the surrounding air. And, as a cost of using fossil fuels, 450 million tonnes CO<sub>2</sub> is emitted from the process [1].

### 2.1.6 Electrocatalysis and -chemistry

One more important subject to touch upon is electrochemistry. This is the study of reactions where a chemical change is related to charge transfer. As the name suggests, it is the combination of electricity and movement of charges, and chemistry describing the reaction. There are two sides to an electrochemical reaction. Reactions generally occur at electronic conductors, such as electrodes. There is a positive and a negative electrode, where electrons are released and consumed, respectively. These electrodes are called anode (positive) and cathode (negative).<sup>7</sup> Charge is transferred between these electrodes through an ionic medium, called the electrolyte. Due to conservation of charge, there will be consumed as many electrons at the negative cathode, as there are produced at the positive anode.

With two electrodes present, there will be two reactions happening simultaneously, one at each electrode. These are referred to as half-cell reactions. At the anode, an oxidation reaction occurs where electrons are released. In the context of ammonia synthesis, this could be oxidation of hydrogen:



At this oxidation reaction, hydrogen gas is split into protons, H<sup>+</sup>, that are transferred via the electrolyte, and electrons, e<sup>-</sup>, transferred through electronic conductors and wires. At the negative cathode, electrons are consumed in a reduction reaction. With regards to ammonia, this is the difficult step, where nitrogen gas has to be split.



Combining the two half-cell reactions, we thus get an overall reaction combining nitrogen and hydrogen to ammonia<sup>8</sup>



---

<sup>7</sup>Except when it comes to batteries. Here the nomenclature is opposite, as the flow of charge can be reversed depending on whether it is charging or discharging.

<sup>8</sup>Enthalpy of reaction is  $\Delta H^\circ = -91.8\text{ kJ/mol}$ .

During the previous discussion on Sabatier's Principle, it was mentioned that HER is energetically favorable to NRR. HER is simply just the reverse reaction of the hydrogen oxidation reaction (2.3). This is one of the major reasons why electrochemical ammonia synthesis has been notoriously difficult [34, 35]. As seen in the nitrogen reduction step, (2.4), there has to be protons present to make ammonia. But since hydrogen evolution is an easier reaction, we need to play some tricks in order to prevent the protons from simply forming  $H_2$  at the negative cathode. This will be described in Chapter 4.

To have an actual current between the electrodes, there has to be a closed loop. As described above, that is possible, if the electrodes are electronically connected (e.g. with a wire) and ionically connected via an electrolyte. There is at least one electrolytic phase between the electrodes, but more is also possible. For instance, if it is advantageous to have the anode and cathode in different environments, this can be achieved by separating these with a suitable membrane. This puts a lot of demands on the membrane, namely having a good (selective) conductivity of the ionic species transferred while being stable in the electrolytes. Put in the context of the ammonia reaction, that would for instance mean that such a membrane should be able to conduct protons from the anode to the cathode, and only cause minimal resistive losses. But simultaneously be bad at conducting ammonia from the cathode to the anode, as this could lead to oxidation of ammonia, and reverse the process to form nitrogen or poison the anode.

For any reaction to occur on an electrode, adequate energy must be applied to initiate and run the reaction. Energy is supplied to electrodes by a set potential, which relates to the Gibb's free energy  $\Delta G$  as [36]:

$$\Delta G = -zFU_{cell} \quad (2.6)$$

where  $z$  is the number of electrons transferred in the reaction,  $F$  is Faraday's constant, and  $U_{cell}$  is the cell potential. The negative sign stems from the opposite charge of species in the electrolyte to the charge of electrons. The applied potential on an electrode, will set the energy of the electrons accordingly. If electrons have higher energy than an unoccupied molecular orbital in a reactant molecule, the electrons can flow in the direction towards reactants, in a reduction process like equation (2.4). Similarly, for electrons with lower energy, an oxidation process like equation (2.3) can take place, where electrons flow from the molecule to the electrode. Despite thermodynamics may allow a reaction to take place according to applied energy, the kinetics of the reaction can be slow. To compensate it can be necessary to apply an overpotential to the electrode. This is a more anodic (or cathodic) electrode potential, in order to create a larger driving force for the oxidation (or reduction) reaction.

Since applied potential to the electrode is what drives electrochemical reactions, it is of interest to know what this potential is. Pt is an extraordinary perfect catalyst for hydrogen reactions [37], with negligible overpotential for neither the oxidation nor reduction reaction. With it, the Standard Hydrogen Electrode (SHE) scale is defined, which all other reactions can be correlated to. At 1 atm

$\text{H}_2$  and a hydrogen activity  $a_{\text{H}^+}$  of 1, the hydrogen *reduction-oxidation* (redox) reaction  $2\text{H}^+ + 2\text{e}^- \rightleftharpoons \text{H}_2$  is defined as the zero point for SHE. This only holds true for pH 0 conditions. The  $a_{\text{H}^+}$  changes with pH, but a correction to the scale can be made, such that the potential is constant. This is the Reversible Hydrogen Electrode (RHE):

$$E_{\text{RHE}} = E_{\text{SHE}} - 0.059 \cdot \text{pH} \quad (2.7)$$

These scales are very useful in aqueous systems, but the situation is more difficult for non-aqueous liquids. I have used two guidelines for a relative correlation of potentials to a general scale, namely the efficient hydrogen reactions on Pt, and the redox potential of metallic lithium deposition  $\text{Li}^+ + \text{e}^- \rightleftharpoons \text{Li}_s^0$ , which happens at -3.04 V *vs* SHE under 1 atm, 25 °C,  $a_{\text{Li}^+}$  of 1 [38].

### 2.1.7 Lithium-mediated electrochemical process

After years of work, current and former colleagues of mine managed to unquestionably prove an electrochemical reaction route to synthesize ammonia. A detailed description of this process will be given in Chapter 4, but in short, it is based on plating highly reactive metallic lithium, which can spontaneously break the  $\text{N}_2$  triple bond in organic solvents. Their work was inspired by a nearly 30 year old Japanese paper [39], and draws many parallels to the battery functionality, including formation of an indispensable surface passivation layer.

I will not go into detail here, but only mention it for the continuity of this chapter. Luckily there do exist an electrochemical method for reduction of  $\text{N}_2$  to  $\text{NH}_3$ , albeit it has proven to be challenging.

## 2.2 Electrochemical ammonia synthesis in the bigger picture

With all the ground work laid out, we can resume to set the ammonia synthesis in perspective.

Today synthetic ammonia is produced in very large quantities via the Haber-Bosch process. The thermochemical process has been of immense importance for the living standard and access to food, but comes at a cost. The global  $\text{CO}_2$  footprint is significant, both due to production and following distribution. Activated nitrogen is necessary, but it can come in various forms, such as ammonia,  $\text{NH}_3$ , urea,  $\text{CO}(\text{NH}_2)_2$  and nitric acid,  $\text{HNO}_3$ , and whether you need one or the other depends on industry, application, and price. In farming it can e.g. differ dependent on the type of crop and soil, or the use in greenhouse versus open-air fields.

So as it goes with most things, there are multiple sides to ammonia. On one hand, it is a ground pillar for food supply and growing population. On the other

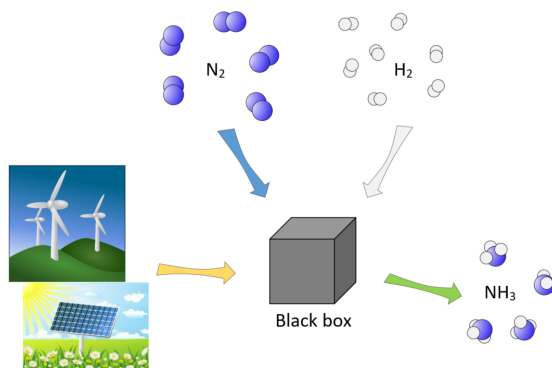


Figure 2.4: A green scenario for ammonia production: Using renewable energy to produce ammonia from nitrogen and a hydrogen source. This requires some *black box*, that allows the synthesis to happen. The black box is essentially what this project is about.

hand, due to current production and distribution, it is a cause of inequality between rich and poor, fortunates and unfortunates.<sup>9</sup> Even the side-effects of high CO<sub>2</sub> emissions and its effect as a GHG, has a skewed effect on developing countries compared to industrial countries, where we have the means to dim the effects on the population.

As thermochemical ammonia production was a game-changer in 1909, electrochemical ammonia synthesis may be a game-changer in the 21st century. At least it opens up the possibility for ammonia production at small scale, under normal pressure and temperature conditions and powered by electricity. All these are key features, possibly enabling *local*, *cheap* and *clean* production. This is at least the dream.

## 2.2.1 Aims of this dissertation

This PhD project was started in the wake of proving the lithium-mediated electrochemical ammonia synthesis as a true positive. The aim was to take what worked in laboratory experiments, and scale it up for performance in a bigger cell. This was a large task, but the hope was that with larger size and different gas supply, improved performance would follow.

In the following chapters I will dive into the efforts we have worked on in our group, and how this has been tried to be implemented into an electrochemical flow cell. Specifically, I list the aims in the following:

1. Can we gain more understanding of how the lithium-mediated process works, and what is necessary for proper performance? This is covered in

<sup>9</sup>See e.g. a price comparison of some Sub-Saharan countries compared to the world average in the Appendix Figure A.1

Chapter 4.

2. How can an electrochemical cell be designed, taking the fundamental knowledge and understanding of the process into account? What challenges and pitfalls follows from working in organic media together with lithium and gasses over large areas and currents? This is scope of Chapter 5.
3. Can we achieve improved results with such a cell? And will it give any new and additional insights to the reaction? The cell should be capable of implementing gasses of both electrodes, but this could also change the conditions compared to the initial fundamental research. This is will be addressed in Chapter 6.
4. With all of this, is it then useful? Or has it just been interesting for the sake of science? The concluding remarks and outlook is given in Chapter 7.

# Chapter 3

## Experimental methods

Throughout this project, my work has relied on a number of different methods depending on the conditions and measurements needed. Most of the work has been *in-situ* monitoring how the experiment developed, but supplemented by *ex-situ* quantification or characterization of electrolyte compounds or electrode deposit. For this, I took part in building and preparing a well-known technique, and adjust it for product detection during ammonia synthesis. This chapter covers a description of the methods and a theoretical background for the techniques used. It is divided into three sections: electrochemical experimentation, ammonia quantification and the Garm setup.

### 3.1 Electrochemical experimentation

The goal for this project is upscaling electrochemical ammonia synthesis. The reaction process was in broad terms already defined, and common pitfalls determined. This especially concerned the ubiquitous nature of ammonia, being present in small concentrations all over the environment. Great care was therefore taken, to keep setups clean and control for contamination. Some electrochemical experiments were carried out in standardized glass cells as reference measurements, but the main focus has been to get the synthesis reaction operating in a dedicated flow cell. A description of the setups utilized will follow here.

#### 3.1.1 Glovebox

In order to maintain non-aqueous conditions and a minimal interference from water, oxygen, and surroundings, organic solvents and various salts were stored in an Ar filled glovebox from Inert. The box pressure was constantly kept 2-8 mbar over ambient pressure, and filled with 5.0 purity Ar. The oxygen and

water content was  $<0.1$  ppm and  $<0.5$  ppm respectively, with the gas constantly circulating through a solvent trap (carbon filter) and gas purifier column, both provided from Inert.

### 3.1.2 Electrochemical setup

Electrochemical experiments were carried out with either 2 or 3 electrodes. There will always be a working electrode (WE) and a counter electrode (CE), but a third reference electrode (RE) can be included. As described in Chapter 2.1.6, electrochemical reactions are divided in two half-cell reactions. By convention, the reaction of interest takes places on the WE, while a necessary opposing reaction takes place on the CE. In the case of nitrogen reduction, the WE would be the cathode, while the oxidation process generating protons and electrons happens on the CE.

While doing electrochemical procedures, it is the WE that is controlled. One can either define the applied potential or a set current. The current will always be between the WE and CE. If only a 2-electrode setup with WE and CE is used, the applied potential will also be the potential difference between the WE and CE. But in this case, there will be no information regarding the potential of either electrode versus a known reference frame. The third RE can be electrically connected via the electrolyte, and should have a known and well-described potential. In this 3-electrode setup, the WE and CE potentials are measured with respect to the RE, providing information of the applied potentials versus a general potential scale, such as V *vs* SHE or RHE, as described in Chapter 2.1.6.

Gasses used for electrochemical tests were: 5.0 purity N<sub>2</sub> passed through a NuPure Eliminator for parts-per-billion (ppb) cleanliness, 5.0 purity Ar, and 5.0 purity H<sub>2</sub> from AirLiquide. Additionally 99.8 atom% D<sub>2</sub> and 98 atom% <sup>15</sup>N<sub>2</sub> from Sigma-Aldrich were used for isotope measurements.

### 3.1.3 Glass cell experiments

Previous work in our laboratories on the lithium-mediated non-aqueous ammonia synthesis, was all done in glass cells with about 10 ml electrolyte volume. My initial work was therefore also in such cells, in order for me to familiarize to the process. Subsequent, I periodically did control experiments in these cells, since environment and conditions can be controlled to a high degree. I have mainly used single compartment glass cells, but a study was also carried out in a larger Rotating Disk Electrode (RDE) compatible cell. The glass cells were all made in borosilicate, and P3 glass frits were used for gas purging and increased solubility. Prior to experiments, all glassware were boiled in ultrapure water (18.2M resistivity, Millipore, Synergy UV System), and dried in air at 100 °C.

Non-aqueous electrolyte was prepared shortly prior to experiments in the Ar glovebox. Mostly, tetrahydrofuran (THF, anhydrous,  $\geq 99.9\%$ , inhibitor-free,

Sigma-Aldrich) was used as solvent, and 1 vol.% ethanol (EtOH, 99.5%, extra dry, AcroSeal or anhydrous, Honeywell) was added as proton donor. Salt-concentrations of 0.2 M to 0.5 M of  $\text{LiClO}_4$  (battery grade, dry, 99.99%, Sigma-Aldrich) was added for ionic conductivity and Li source. Also  $\text{LiBF}_4$  (98%, Sigma-Aldrich) was used as Li containing salt in THF. Other solvents were tested too: 1,2-Dimethoxyethane (DME, 99.5%, inhibitor-free, Sigma-Aldrich), 1,3-Dioxolane (anhydrous, 99.8%, 75 ppm BHT for stabilization, Sigma-aldrich) and 1,4-Dioxane (anhydrous, 99.8%, Sigma-Aldrich). Ferrocene (Fc, 98%, Sigma-Aldrich) was for some measurements added for potential reference.

Various metals were used as WE: Mo foil (+99.9%, Goodfellow), Cu foil (99.8%, Alfa Aesar) and stainless steel mesh (SS, 316 quality, McMaster-Carr). Prior to experiments, Mo and Cu foils were dipped in 2 vol.% HCl (VWR Chemicals) to remove traces of reactive metals, polished with Si-C abrasive paper (Buehler, CarbiMet P1200) and rinsed thoroughly with EtOH and ultrapure water. SS mesh was dipped in 2 vol.%  $\text{H}_2\text{SO}_4$  (VWR Chemicals) and rinsed thoroughly in ultrapure water and EtOH prior to experiment. A Pt mesh (+99.9%, Goodfellow) was almost exclusively used as CE, and a Pt wire (+99.99%, Goodfellow) as a pseudo-reference electrode.

### 3.1.4 Flow cell experiments

Different versions of an electrochemical flow cell for the lithium-mediated ammonia synthesis was used, throughout this project. The versions had parts manufactured in different materials. A chamber for electrolyte was manufactured in aluminium. Compression fittings in Al (Swagelok) were attached, and the Al part was electrochemically oxidized. Initially the part was rinsed in ultrapure water, dipped in 0.1 M NaOH (anhydrous,  $\geq 98\%$ , Sigma-Aldrich), and oxidized in 20 vol.%  $\text{H}_2\text{SO}_4$  (Suprapur, Merck). Gaskets for leak sealing was cut from a sheet of FFKM perfluoroelastomer (Kalrez©6375, DuPont). Other chambers were also manufactured in polyether ether ketone (PEEK). Various electrode parts used in the cell was manufactured in stainless steel 316 (SS), the same quality of SS as used in tubes for gas and electrolyte flow. Gas tubes in polytetrafluoroethylene (PTFE, produced by VICI) was eventually implemented. Electrolyte flow was provided with a 100 ml glass syringe with PTFE seal (100MR-LL-GT, S.G.E.), controlled by a syringe pump (World Precision Instruments).

Carbon cloth (ELAT Hydrophilic plain cloth, Feul Cell Store) was initially used as anode. Stainless steel-based meshes (316 quality, ASTM and FDA compliant, McMaster-Carr) with various mesh sizes ( $400 \times 400$  to  $325 \times 2300$  wires per inch) were used. Also SS-based porous discs (REACH compliant, McMaster-Carr) removing particles from 2 to 40  $\mu\text{m}$  in size were tested.

Prior to experiment, all cell parts (except for PEEK-based chambers) were thoroughly rinsed and boiled in ultrapure water, and dried at 100 °C overnight. When received and prior to subsequent procedures, SS-electrodes were first thoroughly rinsed in EtOH and ultrapure water. Then dipped in 2 vol.%  $\text{H}_2\text{SO}_4$ , followed

by a rinse in ultrapure water. After experiments PEEK electrolyte chambers were thoroughly rinsed in EtOH and acetone, to remove electrolyte and salt leftovers. The syringe was first rinsed in ultrapure water, followed by a dip in boiling water. Some metal electrodes were sputter deposited with platinum (Pt). The base pressure in the sputter deposition chamber, was typically in the order of  $1.2 \times 10^{-7}$  mbar prior to deposition from a 99.99% Pt target. Cu electro-deposition on metal electrodes were done in a solution of 1.5 M  $\text{H}_2\text{SO}_4$  and 0.4 M  $\text{CuSO}_4$  (Merck)

Apart from previously mentioned electrolytes in glass cell experiments, also phenol (PhOH, 99.0%, Sigma-Aldrich), Ethanol-OD (deuterated, 99.5%, Sigma-Aldrich), and tert-butanol (anhydrous, 99.5%, Sigma-Aldrich) was used as replacement of EtOH.

### 3.1.5 Electrochemical methods

A description of the electrochemical techniques used will be given here in broad terms. Measurements were recorded with a potentiostat (Bio-Logic VMP2 and SP-150), capable of control and measurement of potentials and currents to a very high degree. It is though beyond the scope of this thesis to go into details on this.

#### Open circuit voltage (OCV)

During OCV no current can flow between the electrodes, i.e. reactions run forward and backward at the exact same rate. This means the electrodes are disconnected from the power amplifier, but potential measurements are still carried out. The recordings therefore show the rest-potential, and give information about the redox state of species [40].

#### Potentiostatic Electrochemical Impedance Spectroscopy (PEIS)

PEIS studies an electrochemical system's response to an applied low-amplitude sinusoidal electrical perturbation [41]. The frequency of the applied field is varied, and the response in current is measured. Dependent on the system, there may be a delay between the applied potential and response in current, which leads to a phase shift with a certain amplitude.

Since the field is varied, conduction processes occurring over different time-scales can be probed. E.g. ohmic resistance is a fast process, and is therefore seen at high frequencies. Charge transfer processes are oppositely slow, and can be studied at low frequencies.

Due to the similarity between ionic and electric charge transfers, one can infer an equivalent electrical circuit diagram, from the electrochemical PEIS measurement. This includes resistors, capacitors, inductors, etc. A full analysis requires

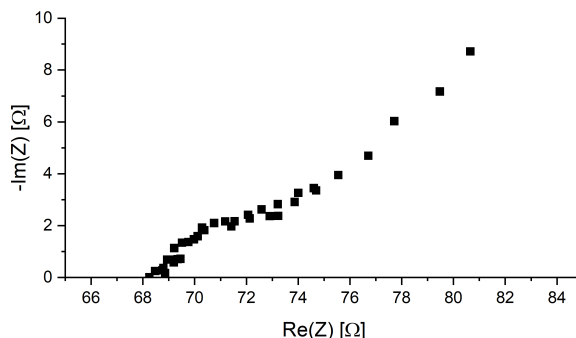


Figure 3.1: Example of a PEIS recording, presented in a Nyquist plot [42], with the real and imaginary part of the impedance plotted along the first and second axis respectively. The high-frequency part is to the left, where the cell-resistance can be determined from the intersection with the  $x$ -axis.

a high degree of knowledge on the system, and is beyond the scope of this thesis. I have therefore only used the high frequency response, to determine the ohmic resistance in the setup.

From Ohm’s law, we know that it requires some potential, to draw a current,  $I$ , through a resistor,  $R$ . When measuring on an electrochemical cell, some of the applied potential will similarly be due to the cell resistance. The measured potential can be compensated for the loss by [36]:

$$U_{measured} = U_{actual} - IR \quad (3.1)$$

giving the actual potential at the electrode for reactions. This IR-compensation is useful to determine the reaction potentials at the working electrode. Though when it comes to energy considerations, the full measured un-compensated cell-potential, is the energy applied to the cell.

### Linear sweep voltammetry (LSV) and cyclic voltammetry (CV)

For Li-mediated ammonia synthesis, the WE must be adequately cathodic for Li-plating. Rather than defining a cathodic potential or current for this reduction, some measurements were initiated with a linear scan of the WE potential. This allows us to monitor, at what potentials cathodic electrochemical reactions occur at the electrode surface. Since, when reactions occur, charges are transferred, resulting in a current. With LSV we could therefore see the onset-potential for Li-deposition, but also if trace amounts of e.g.  $H_2O$  or  $O_2$  are in the electrolyte, or substances are on the electrode surface, as these would reduce at less cathodic potentials.

After a cathodic LSV, the WE potential can also be scanned anodic again. This scanning back and forth of the potential is called cyclic voltammetry (CV) [40]

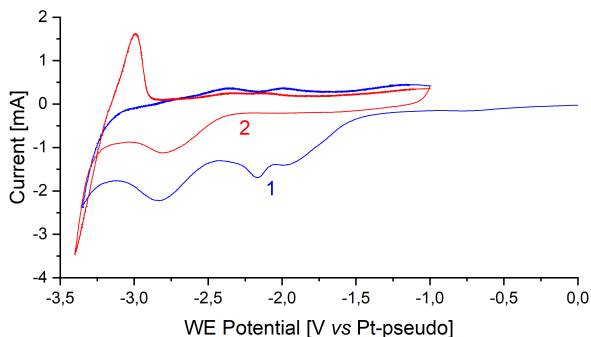


Figure 3.2: Cyclic voltammometry measurements on a Cu foil. Multiple reactions are seen on the first (blue) scan, followed by a cleaner second (red) scan. Li-deposition is seen at -3.25 V *vs* Pt-pseudo reference, which on the second anodic sweep is stripped off. This can be used to define the potential scale.

and an example is given in Figure 3.2. It shows the two first cyclic scans on a Cu electrode in non-aqueous Li-containing electrolyte, measured *vs* a Pt-pseudo reference. In the first (blue) scan, a large cathodic current is drawn at -1.5 V overlaid by a small feature at -2.1 V. Around -2.5 V a new peak arises, followed by an onset at -3.25 V. In the following anodic scan, two small anodic features correlate to the peaks around -2.5 V and -2.1 V. The second (red) scan only shows a reduction feature at -2.5 V, and a sharp onset at -3.25 V, followed by a large anodic peak at -3.2 V, and a small feature at -2.5 V. Combining these observations, we might ascribe the initial cathodic current at -1.5 V and -2.1 V to reduction of  $\text{H}_2\text{O}$  and  $\text{O}_2$  in the electrolyte in the vicinity of the electrode. This being reduced during the first scan, and not present in the second scan [43]. A reoccurring, but limited, surface reaction at -2.5 V may be Cu reacting with the electrolyte. But at -3.25 V the sharp onset shows Li deposition, supported by the following stripping feature in the anodic scan.

### Chronoamperometry (CA) and chronopotentiometry (CP)

An electrochemical system can be controlled, either by defining the WE potential or setting the current between the electrodes.

Chronoamperometry (CA) records the current over time, at a set potential. In a 3-electrode setup, it is the WE potential that is defined. Dependent on the conditions, a certain current can be drawn, and the CE potential may adjust accordingly. E.g. if an applied cathodic WE potential allows much reaction to take place, a high current is drawn. Dependent on the availability of oxidation reactants, the anode may need a more anodic potential, to increase the reaction rate according to the current. Oppositely for chronopotentiometry (CP) it is the current between the WE and CE that is defined, while recording the electrode

potentials over time. Likewise for CA, the electrode potentials must adjust, to have reaction rates set by the current [36].

I have used both techniques for NRR experiments. Whether CA or CP is used, depends on what parameters need to be controlled. E.g. limiting the anodic reactions, by defining the anode potential, can be done with CA. Whereas, reproducible and comparable applied currents can be achieved with CP. From both cases, the accumulated charge passed during an experiment,  $Q$ , can be calculated by integrating the current over time,  $Q = \int I(t)dt$ .

Knowing the applied potentials, current, and charge passed, is important measures for determining how well a system works. For ammonia synthesis, we need to know the efficiency of an experiment. This can be given by two different figures of merit. A commonly used number is the *Faradaic efficiency* (FE). This refers to how efficient the number of charges passed in a system, goes towards product formation. W.r.t. ammonia synthesis, each  $\text{NH}_3$ -molecule has 3 charges, and the FE can thus be calculated as:

$$FE = \frac{3 n_{\text{NH}_3} F}{Q} = \frac{3 m_{\text{NH}_3} F}{M_{\text{NH}_3} Q} \quad (3.2)$$

where  $n_{\text{NH}_3}$  is the moles of product,  $m_{\text{NH}_3}$  is the mass of produced ammonia,  $F$  is the Faraday constant of  $96485 \text{ C/mol}$ ,  $M$  the molar mass of  $\text{NH}_3$  ( $17 \text{ gmol}^{-1}$ ) and  $Q$  the charge passed during reaction. The amount of ammonia produced, can be inferred from subsequent concentration measurements.

Another efficiency statement is *energy efficiency* (EE), which within the last few years is seen more frequently in the NRR literature [44–46]. This does not only take charges into account, but refers to the electrical energy input compared to the chemical energy output from products. It is less agreed upon, what energy inputs should be included (e.g. electrolyte chemicals, gas pressure etc). In our group, we are mainly using the convention:

$$EE = \frac{E_{out}}{E_{in}} = \frac{m_{\text{NH}_3} \delta_{gR}}{\int I(t) V(t) dt} \quad (3.3)$$

where the numerator is the free energy of reaction  $\Delta G_R = m_{\text{NH}_3} \delta_{gR} \delta_{G_r} = 20.055 \text{ mJ}/\mu\text{g}$ . We use the specific free energy ( $\delta_{gR}$ ) of ammonia oxidation to  $\text{N}_2$  and  $\text{H}_2\text{O}$ , in line with the [47], who initially proposed this figure of merit for  $\text{NH}_3$ -synthesis. The integral

$$\int I(t)V(t)dt = \int I(t) \cdot [U_{CE}(t) - U_{WE}(t)] dt \quad (3.4)$$

of the time dependent current  $I(t)$ , and total cell potential  $V(t)$  respectively, gives the electrical energy input. This is where it is important to use the non-compensated electrode potentials,  $U_{CE}$  and  $U_{WE}$ . Otherwise the energy input from the potentiostat is underestimated.

## 3.2 Ammonia quantification

The goal of this thesis is to synthesize ammonia, and preferably in decent amounts. This has to be quantified in reliable ways. Multiple supplementary methods exist for this, and I will here discuss three methods, we use in our labs.

### 3.2.1 Colorimetric indophenol method

An effective and widely used method is the colorimetric Berthelot reaction, producing indophenol in the presence of ammonia [48]. Indophenol is an organic compound with an intense blue color. It is a spectroscopic method, where the test solution turns more and more blue, dependent on the concentration of ammonia. Thereby one can quantify with high certainty how much ammonia is present, as more ammonia leads to formation of more indophenol. Indophenol has a strong absorption of red light, peaking at around 630 nm. And so, one can correlate the strength of absorption,  $A_\lambda$ , to the concentration of ammonia. This is given by the Beer-Lambert law [49]:

$$A_\lambda = \log_{10} \frac{I_0}{I_1} = \epsilon L C \quad (3.5)$$

where  $I_0$  and  $I_1$  are the incident and transmitted intensities. The extinction coefficient is given by  $\epsilon$ , while  $L$  is the photon path length through the medium. Under similar conditions, both  $\epsilon$  and  $L$  are constant. The concentration of absorbing species is  $C$ . Hereby  $A \propto C$ . An example of this is shown in Figure 3.3. The left graph shows six different absorption spectra of solutions with increasing ammonia concentrations. In the clean ammonia-free solution, a flat line is recorded, showing no absorption features in the visible to near-infrared range from 450 to 1000 nm. But as more and more ammonia is added, an increased absorption as seen around 630 nm. The absorption scales linearly with the concentration, so a calibration curve can be made and used for quantification of ammonia in a solution.

The specific slope and interception of the calibration is dependent on the composition of the solution in question. Factors such as solvent and dissolved salts can influence the absorption profiles, and there can even be cross-correlation with other metallic species or the acidity of the solution [48]. One way of avoiding many of these issues, is if the concentration of ammonia in solution is so high, that a significant dilution is necessary. If so, the solution may e.g. be diluted by a factor of 100 in pure water, and obscuring effects may become negligible. The amount of dilution should though always be matched in such a way, that the measured absorption is within the range of the used calibration.

The Berthelot reaction works in alkaline solutions with phenol and hypochlorite, where the reaction can be catalyzed by the presence of nitroprusside as well. [48]. In our lab we use a mixture of alkaline hypochlorite and phenol nitroprusside, to meet the necessary process conditions. Aggressive organic solvents, e.g.

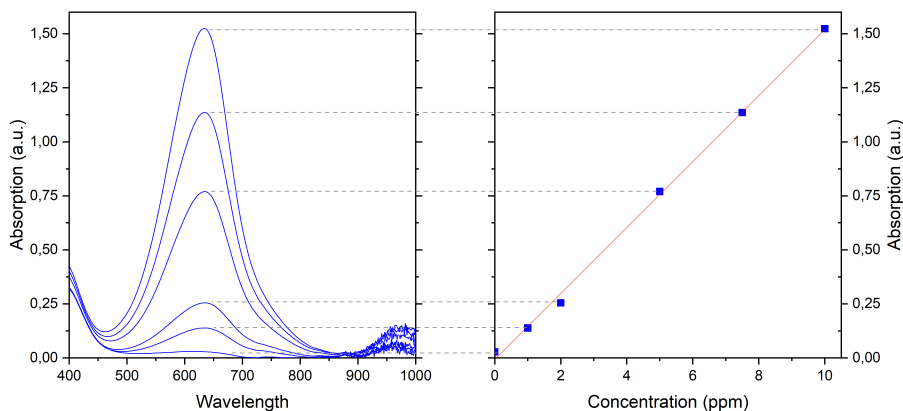


Figure 3.3: Calibration curve with indophenol. A high linearity between absorption and ammonia concentration can be achieved ( $R^2 = 0.998$ ).

THF, require additional steps, to be analyzed. A modified Berthelot reaction was therefore developed by my colleagues [34]. If the concentration of ammonia is relatively low in the tested solution, such that significant dilution is not a possibility, it is possible to evaporate the organic solvent while keeping the ammonia. By first adding acid to the solution, ammonia can uptake a proton and become ammonium,  $\text{NH}_4^+$ . Ammonium has a much lower vapor pressure than ammonia, and will therefore tend to stay in a liquid phase while solution evaporates [50]. We add hydrochloric acid, HCl, before evaporating the solvent. When all liquid has evaporated, the ammonia stays trapped as ammonium chloride,  $\text{NH}_4\text{Cl}$ , which can then be dissolved in pure water. The Berthelot reagents can then be added, and taking other factors, such as salt concentration into account, the amount of trapped ammonia can be quantified.

In case of high ammonia concentrations, the procedure can be much simpler. The final measurements should be in accordance with the suitable calibration. With much dilution and thus a nearly pure water solution, only containing a small amount of dissolved organic solution, the side effects from solvent and salt can be negligible. This is the preferred situation, as it would also mean, that the amount of ammonia produced is significant, and uncertainties of the validity of claiming nitrogen reduction decreases.

Though the indophenol method is a powerful way of measuring ammonia, there are details to be aware of. As shown in Figure 3.4, the effect of what we can call *background* solution measurements, can be important for precise measurements. After trying to see an effect of some additive to the electrochemical procedure, an unknown amount of ammonia was obtained. To quantify this, the solution was measured under various dilution conditions. A 0.5 ml sample from the solution was acidified with HCl, then dried via evaporation of the organic electrolyte,

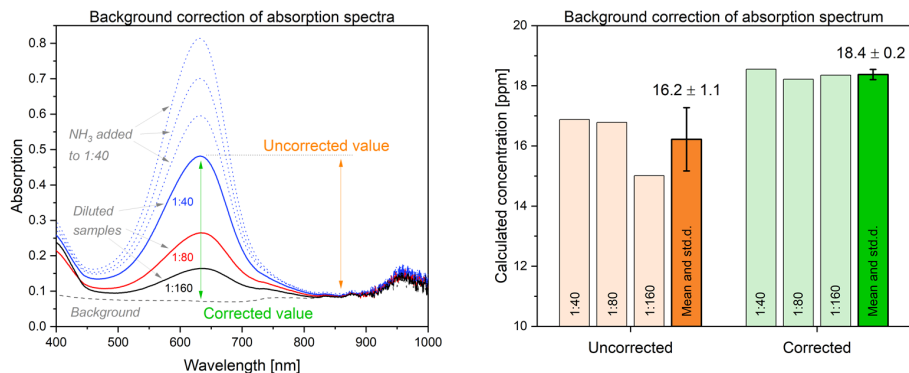


Figure 3.4: Absorption spectra for a sample with different dilution, including a background measurement. Taking the background spectrum into account, gives more correct values with a much smaller spread of values.

followed by dilution in water. By adding different amounts of water, dilution factors of 1:40, 1:80 and 1:160 were made. In each of the cases, a series of samples were prepared. (1) A background solution, consisting of diluted sample, further diluted in pure water. (2) a colorimetric indophenol reaction of the diluted sample itself and (3) colorimetric reaction on the sample with various known amounts of added ammonia [51]. In all cases, the prepared samples were diluted in the same amount of total aqueous liquid, either with or without the indophenol reagents, and with a range of purposely added amounts of ammonia. The shape of the absorption curve, for the purely water diluted sample, was important. It was not flat over the range of wavelengths, but had a lower absorption at the indophenol peak at 630 nm. Compared to the absorption around 860 nm, where all the spectra were nearly overlapping. If this absorption difference was not taken into account, the different dilution factors gave fluctuating indications of the initial concentration of the test liquid. But if the absorption dip was taken into account, all three measurement sets agreed within 1.1 rel.% from each other (compared to 6.8 rel.%). This just exemplifies the importance of being careful with measurements and how to interpret them.

### 3.2.2 Ion Chromatography

Ion chromatography is yet another possibility for measuring ammonia among other compounds. Ion chromatography (IC), measures the presence of ions by detecting the conductivity of a liquid. Ions have a charge and can thus be used for carrying a current between two electrodes. By a clever design, it is possible to separate different ions, and measure the presence of each individual ion [52].

The basics for an IC can be summarized in seven major compounds. First of all, a sample is being carried along and measured in an eluent. The eluent is a liquid, which acts as a carrier and a baseline for the measurement. As the

eluent ensures everything is flowing correctly, this is referred to as the mobile phase. When measuring ammonia in a solution, we measure it as the positively charged cation ammonium,  $\text{NH}_4^+$ , where in an acidic environment it can uptake an additional proton. Though it is possible to set up an IC to measure negatively charged anions, our system is set to measure positive cations. In this case, the eluent will be a dilute acidic medium. We use 6.5 mM nitric acid with 10 vol.% acetone added, where the addition of acetone helps when measuring organic samples, by making the eluent more versatile. Our system is from Metrohm with a high-capacity Metrosep C 6 separation column, coated with a silica gel with carboxyl groups.

As the IC is based on measuring the conductivity of a liquid, it is important that the liquid does not change significantly during the course of a measurement. As the first thing, the eluent therefore passes through a degassing device, which makes sure that no bubbles are carried along and trapped in the liquid. Next is an injector, that controls when sample liquid is mixed with the eluent, and passed along to be analysed, where after the dilute sample in eluent liquid is passing through a guard column, where unwanted parts, such as heavy metals or big solid particles, are removed. The mentioned parts so far, have all been preparation steps, for what allows the IC to do a measurement spectrum of the sample. After the guard column, the sample liquid is passing through a long thin analysis column. The column is coated with a cation exchange resin, where cations will adsorb to. This resin has a certain set of properties, to which cations will have a specific affinity. The higher the affinity, the better an ion will stick to the resin on the surface of the analytical column. The affinity is given by the ion size, charge, electronegativity and other such parameters. As the sample liquid passes through the column, ions will first stick to the surface. But as eluent continuously flows through the column, the ions will slowly be washed or pushed off the resin, and carried along. Since each cation have different affinity, they will stick for a different amount of time on the walls, and so the ions are physically separated in the flow, and therefore also separated in time. An example is shown in Figure 3.5. The ion-separated liquid then passes through a suppressor. The suppressor decreases the background signal of the eluent, which otherwise would have a huge conductivity by itself, due to its acidity. The suppressor can be made by electrolytic reactions and membranes, such that only pure water (rather than acid), the separated ions and the now much diluted organic solvent are passing over to the conductivity detector. Anion exchange membranes can in this way let negatively charged anions away from the stream of liquid, and protons from the acidic eluent can react with hydroxide ( $\text{OH}^-$ -ions) to form pure water.

The conductivity of the sample liquid, is measured with a detector. As charged ions pass through, the conductivity increases and a signal is recorded. The signal scales with the number of ions, and we can therefore quantify these. Due to the analysis column, the different ions will pass the detector at various delayed times, and in that way it is possible to measure and quantify them independently. If anions are still present in the tested liquid, these will pass through the analysis column immediately, as the cation exchange resin will have little to no effect

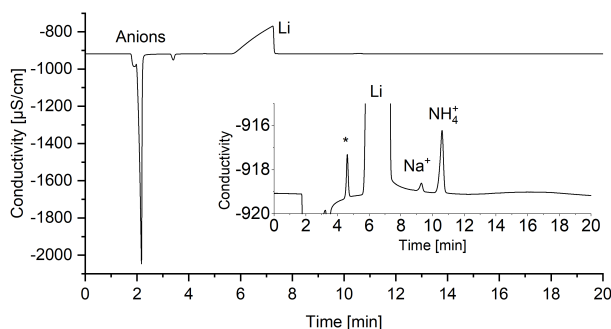


Figure 3.5: Example of IC measurement on a diluted Li-containing electrolyte. Conductivity changes, as ions elute from the analysis column. The initial negative peaks are from anions, followed by a small peak (\*) from unretained cations. The spectrum is dominated by a large  $\text{Li}^+$ -peak, but ammonium is detected after 10.5 min.

on them. Furthermore, they will appear as having a negative conductivity, due to their opposite charge. For consistent and reliable measurements, the flow is precisely controlled with a pump, that has a slow and very well-controlled flow. For our measurements we use a peristaltic pump, where the chemical compatibility to the samples should be considered. Though to have less issues with aggressive solvents to the pump tubing, we have installed the pump as the last part. Hereby, the organic solvent will be much diluted in eluent liquid, before entering the pump.

### 3.2.3 Nuclear Magnetic Resonance Spectroscopy

Reliable reports of  $\text{NH}_3$ -synthesis is important for the development in the electrochemical ammonia field. Results should be reproducible, and supported by control experiments. Protocols have been published on how to do proper demonstration of  $\text{N}_2$  reduction, including Ar blank tests, and quantifiable isotope-labelled control experiments [34, 53, 54]. This is especially important, when small amounts and concentrations are produced. A common way for isotope-labelled ammonia measurements, is quantification with NMR.

Nuclear magnetic resonance (NMR) is a method that can characterize the molecular structure of a material, by recording the interaction of nuclear electronic spin to a powerful magnetic field. Like a spinning top will undergo a precessional motion when slightly misaligned with the gravitational force [55], a nucleus with a magnetic moment will similarly precess in a magnetic field. The precession of the charged nuclei will in turn induce an electric current in the radio frequency coils surrounding the sample. These coils are also used to excite the sample in the first place, by disrupting their alignment with the magnetic field, such that their resonance frequency can be measured. The frequency of the precession

depends on shielding due to local electron density in the molecule, but also the magnetic field strength. More powerful magnets will therefore give more signal. For a  $^1\text{H}$ -NMR, we can observe the types and numbers of protons in the sample. From differences in the chemical structure of the molecule, it is therefore possible to see different groups of protons, as protons that sit in a similar electron density environment, will precess at one frequency. Other protons, in e.g. a higher electron density, will be more shielded thus experience less magnetic field strength, which ultimately leads to a lower frequency of precession. This opens up the possibility to distinguish different molecular structures from each other, as they will have different properties and spin, and thereby have different characteristics when measured with NMR. The spectrum can give insights to chemical shift, i.e. composition of atomic groups in the molecule. The shift turns out from the different precession frequency, that is caused from the local electrical environment as discussed before. Also possible spin-spin coupling constants from adjacent atoms can be seen. Furthermore, it is quantifiable the same way the above-mentioned colorimetric method scaled with concentration, the intensity of the peaks seen in NMR scales with the presence of the specific compounds.

Importantly, it has the ability to distinguish different isotopes. There exist two stable isotopes of nitrogen: 99.6% abundant  $^{14}_7\text{N}$ , and 0.4% of the heavier  $^{15}_7\text{N}$ -isotope [38, 56]. This can be exploited for ammonia measurements, since we thus can produce ammonia from different nitrogen isotopes, resulting in either  $^{14}\text{NH}_3$  or the heavier  $^{15}\text{NH}_3$ . Due to the different nitrogen isotope, the ammonia molecules will not have the same spin coupling, and they are therefore distinguishable with NMR. For detection of ammonia with NMR spectroscopy, one would use  $^1\text{H}$ -NMR. In ammonia, all the hydrogen atoms are similar, and we would therefore expect a singlet from these. It will though be split differently, depending on the N-isotope.  $^{14}\text{N}$  has spin 1, and can therefore be in three different states, +1, 0 or -1. This affects the proton-singlet, which accordingly is split into a triplet for  $^{14}\text{NH}_3$ .  $^{15}\text{N}$  has spin 1/2, with two possible states, +1/2 and -1/2. Accordingly, a doublet appears for  $^{15}\text{NH}_3$ . This follows the rule for peak splitting in NMR, where the number of splits is  $N = 2nl + 1$ , where  $n$  is the number of neighbouring atoms, and  $l$  is the spin. This ultimately means that it is possible to see a difference in ammonia with the normally occurring  $^{14}\text{N}$ , and the heavier, less abundant,  $^{15}\text{N}$ .

Apart from measuring ammonia, NMR spectroscopy can also be used to identify various chemical substances in a sample, to e.g. see if an organic compound has changed form or polymerized. Whether the interest is the carbon atoms (C), hydrogen bonds (H) or maybe fluorine (F), or phosphorous compounds (P), the NMR can be set up accordingly, using relevant isotopes of each. NMR is thereby a very powerful tool for especially organic chemistry analysis.

The NMR spectra were acquired using a Bruker AVANCHE III HD 800 MHz spectrometer, equipped with a 5 mm TCI CryoProbe. It has a high magnetic field of 18.8 T, which with a cryo-cooled NMR probe, easily can distinguish isotopic species to p.p.b. level [34]. Some of the NMR spectra were acquired

using an AVANCE III HD 400 MHz spectrometer equipped with a 5 mm Prodigy probe with either deuterium oxide ( $D_2O$ ) or deuterated chloroform ( $CDCl_3$ ). All the chemical shifts of the samples were normalized to tetramethylsilane (TMS). The very little variation of chemical shift of the NMR signals could appear due to slight differences in the pH, volume, and/or temperature of the samples. The data was analyzed with Topspin 4.1.4 software.

## 3.3 Garm

To measure ammonia and other products, we built a transportable mass spectrometer ("*mass spec*" or just "*MS*"). Placed on a rack on wheels, we even had the possibility to move it around between different setups, and not be limited to only measure at one location. The heart of the equipment is a QMS from an old experimental setup.<sup>1</sup> The new mass spec was called *Garm*, keeping its Norse heritage.<sup>2</sup> For this thesis, Garm has been used for product detection in the flow cell. An image of the setup is shown in Figure 3.6.

### 3.3.1 Build and components

This setup consist of a QMS equipped with a cross-beam emitter, capable of mass-spec measurements with adjustable ionization potentials and high sensitivity. The high vacuum is achieved with a Hipace 300 H Turbo pump from Pfeiffer Vacuum, with the back pressure regulated to rough vacuum with a nXDS10i scroll pump from Edwards Vacuum. The rough and high vacuum pressures are monitored with a Pirani and Ion pressure gauge respectively. The mass spectroscopy is measured with a QMG 420 from Pfeiffer, with a high sensitivity and capability of precise tuning equipment parameters. Importantly, the acceleration voltage is adjustable, which is necessary for being able to distinguish ammonia from water signals [58]. A 1  $\mu m$  orifice (flow calibrated, Lenox Laser), was used to bridge the vacuum chamber to the gas flow for analysis. The chamber was constantly heated to 120  $^{\circ}C$ , to ensure low water signal. Inlet gas tubes were similarly heated to 100  $^{\circ}C$ , both to decrease water signal and to have a lower sticking coefficient of  $NH_3$  to the inner tube walls [59].

---

<sup>1</sup>The old and large setup was fittingly named Yggdrasil, matching its size and height ( $\sim 4$  m in an experimental hall). In Norse mythology, Yggdrasil is the Tree of Life [57], which is almost metaphorical when it has brought life to our new mass spec.

<sup>2</sup>Garm - named by the dog from Norse mythology, who stands guard at the entrance to Hel and howling when someone arrives [57]. This may seem like a fierce name for an equipment, but we found it suitable for its application. The mass spec should detect and measure all sorts of products with a high sensitivity. And like a guardian dog let us know when something - like  $NH_3$  molecules - arrives.

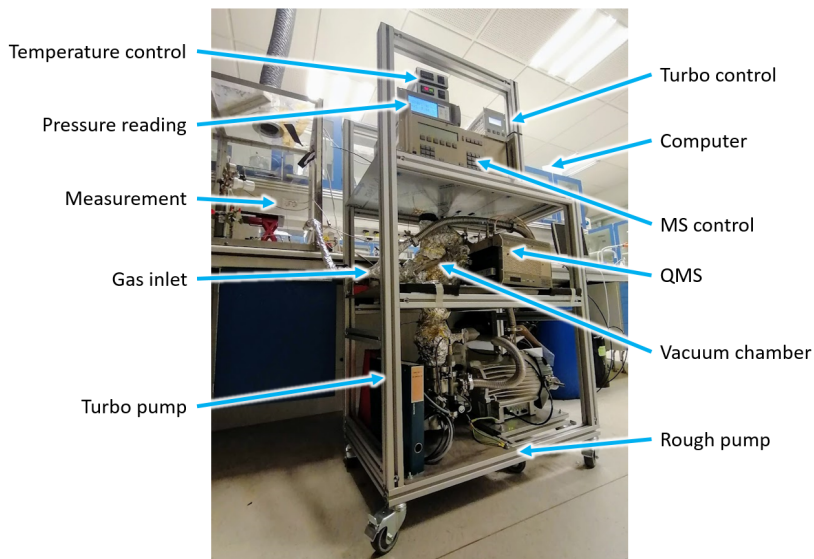


Figure 3.6: Image of the transportable Garm mass spectrometer setup.

### 3.3.2 Mass spectrometry

MS measurements give a spectrum of the atomic masses present for analysis, i.e. the weight of individual atoms and molecules that is analysed. Specifically the mass-to-charge ratio,  $m/z$ , where an atom (or collection of atoms) will have a certain atomic mass. I will refer to these as molecules. The molecules are initially ionized by an electron beam. The vast majority of molecules will only be single-ionized, missing one electron. But dependent on the ionization process, the charge could also be 2 (or seldomly higher). Thus,  $^1\text{H}_2$  is seen at  $m/z$  2, abundant  $^{14}\text{N}_2$  at  $m/z$  28, and double-ionized  $^{14}\text{N}_2$  at  $m/z$  14. With careful and sensitive measurements, the natural abundance of both  $^{14}\text{N}$  and  $^{15}\text{N}$  can be measured, where the 0.4% abundance of the heavier isotope, will show as an accordingly smaller peak in the spectrum. This would mainly be seen at  $m/z$  29 from a  $^{14}\text{N}\equiv^{15}\text{N}$

Mass spectrometry can be achieved in various ways, each with their advantages and disadvantages. Two important ways are based on Time-of-Flight (TOF-MS) and Quadropole separation (QMS). Commonly for both of methods, is they measure on gas-phase products. In TOF-MS, all molecules are accelerated by an electric field. Since heavy molecules travel slower than light molecules, these can be separated by their mass. It is extremely sensitive, but require relatively large equipment [60].

The mass separation technique I have used, is the QMS. The *quadropole* term refers to the heart of the mass filter used. The basic principal is depicted in Figure 3.7. Initially, the gas is ionized with an electron beam. This beam can

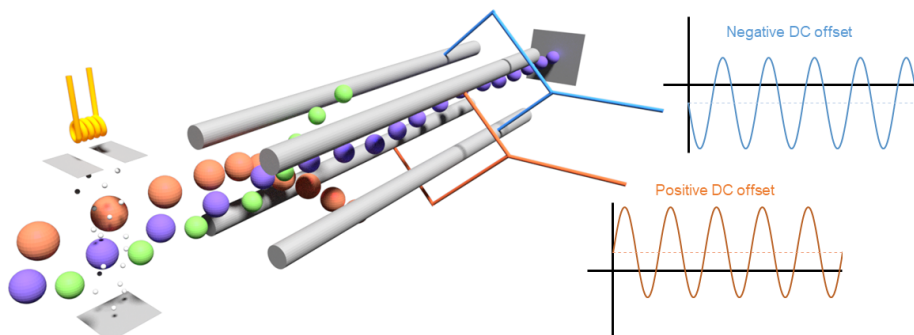


Figure 3.7: Working principle of QMS. Molecules are initially ionized and mass separated by four parallel rods. The rods have an oscillating potential applied ( $\pm U \pm V_0 \cos \omega t$ ), only allowing molecules with a specific  $m/z$  value to travel through and be detected.

kick electrons off the constituent atoms in the molecule, giving the molecule a charge.<sup>3</sup> Four parallel rods, with a certain electrical potential applied to them, create a narrow window for the charged species to travel through. Between the rods, an oscillating electric field is created, such that charged species will have a special trajectory through it. If the charged species are either too light, or too heavy, they will spiral out and be separated away. Only a specific  $m/z$  ratio will have a stable trajectory all the way through, and be measured at the detector. The electric field can thus be changed, allowing for scanning over a wide range of masses, by changing the properties of the stable trajectory between the rods. Two opposing electrodes have the same applied potential, a positive and a negative electrode. The applied potential is an oscillating radio frequency AC field ( $V_0 \cos(\omega t)$ ) on top of a constant DC field ( $U$ ) [61]. Mass sensitivity below 1 amu is easily achievable with a quadrupole mass filter, but not as fine as the TOF. Physically it is much more compact, and can be used for continuous measurements at the same mass. Tracking multiple masses over time can also be done. But each mass would be sampled with some time delay, due to adjustment of applied rod-potentials. After detection of the mass separated ions, adequate processing of the signal is needed. This can e.g. be with a Secondary Electron Multiplier (SEM), where the small current of signals, is increased to measurable and useful numbers [60].

The MS must be under vacuum, both to prevent background signals from other species, but mainly to reduce the risk of ions colliding with other molecules. This could lead to neutralization, scattering or fragmentation of the ions. During measurements, the QMS is typically operating at low vacuum around  $10^{-6}$  mbar,

<sup>3</sup>It can also break bonds in the molecule, causing fractions to appear. E.g. water,  $\text{H}_2\text{O}$ , can give signals at mass 18 ( $\text{H}_2\text{O}$ ), 17 ( $\text{OH}$ ) and 16 ( $\text{O}$ ), but the amount of fractions depends on the energy of the electron beam. At lower beam energy, fewer fractions will be seen with less signal [58].

which is achieved with two pumping stages. A rough pump (approximately  $10^{-3}$  mbar), which provides a vacuum on the outlet of a turbo pump ( $<10^{-6}$  mbar).

## Chapter 4

# Non-aqueous ammonia synthesis

In this chapter, we will focus on the non-aqueous approach for ammonia synthesis. This is the method we have worked on in our group since 2017, where my colleagues described the reliability and possible prospects of it [34]. The notable aspect of this approach, is that it is based on being performed in liquids that are not water. Why that is and what it means follows here.

### 4.1 The difficult step - Nitrogen reduction

As described in Chapter 2 nitrogen reduction and hydrogen evolution is in sharp competition with each other. Under normal conditions, HER would always win over NRR, due to the much simpler reaction. In HER only two protons are needed to be combined, compared to NRR where Nitrogen first has to be adsorbed and split, followed by reaction with six protons to make ammonia molecules. This leads to a lot of reaction steps, where individual tuning of each step unfortunately is not possible - again due to the scaling of each step as described in Chapter 2. The pathway for NRR could be multiple ways. Noticeable ways are dissociative and associative pathways, where the latter can go through both an alternating and a distal reaction mechanism [62]. For the dissociative pathway, the  $\text{N}\equiv\text{N}$  triple bond is split during the adsorption step, and is followed by three protonation steps forming ammonia. For the associative mechanisms,  $\text{N}_2$  adsorbs to the surface, and the last  $\text{N}-\text{N}$  bonding is cleaved together with release of the first ammonia molecule. Whether it is one or the other, depends on the reaction kinetics and thermodynamics. So whichever is the most favorable way will be the reaction mechanism. According to the theoretical studies of [63] the preferred mechanism for catalytic  $\text{NH}_3$  formation depends on the choice of catalyst, due to their different binding strength. Nonetheless, since

HER and NRR is in competition, we need to modify the conditions to improve the reactions towards NRR while making HER less likely to happen.

Sing et al. [64] suggested four possible ways of achieving this, where one way is for instance to decrease the rate of electrons coming to the surface. The idea behind decreasing the rate of electrons is that HER is an electrochemical process, requiring electrons to initially adsorb protons at the surface. The first step in NRR where  $N_2$  adsorbs is purely a chemical step, which is therefore unaffected by the presence of electrons. Decreasing the electron rate should therefore slow down HER while not affecting NRR kinetics. Though this may be possible, there are also some challenges to this. Mainly on controlling the conditions governing the electrodes and modifying the rate of electrons, as they state it requires a *substantially* lower accessibility of electrons. Another interesting way is instead to focus on the protons. Protons are taking part both in NRR and HER, why these are interesting to focus on. The idea behind this approach is to decrease the concentration of protons. In a similar fashion as decreasing the rate of electrons, then by having fewer protons available, we thereby have less favorable conditions for HER, we thus also have much smaller rate of HER. The impact on the NRR rate should be less pronounced compared to HER, why an overall improved ammonia formation is expected. If nitrogen and hydrogen are the only main components present at the vicinity of the electrode, by then decreasing the amount of protons, we will increase the likelihood for nitrogen to adsorb on the surface. If the nitrogen first is adsorbed, the following splitting can then take place, which is obviously a necessity for having any successful ammonia synthesis. With nitrogen being split, it is just a question of when protons arrive at the nitrogen atom and complete the ammonia synthesis.

Most research in electrochemical reactions are made in aqueous solutions, this could be alkaline or acidic.<sup>1</sup> The issue regarding NRR with aqueous systems is water itself. Water has a natural equilibrium between hydroxide ions ( $OH^-$ ), water ( $H_2O$ ) and hydronium ions ( $H_3O^+$ ) [38, 65]. This equilibrium is also what makes water have a pH value of 7 and the ability for either being alkaline or acidic, by shifting the equilibrium to either side. This has multiple implications. One implication is the high availability of protons in aqueous media. Protons can be extracted from  $H_2O$  leaving  $OH^-$ . Also from  $H_3O^+$  protons can obviously also be extracted. Based on the approach of improving NRR by decreasing the availability of protons, water seems to be problematic. There are though another effect of the multiple species of water. The presence of various ions of water, makes water able to conduct protons. Meaning that if we need to transport protons from one place to another, there are species available to do this. E.g. in water, protons can form hydronium, such that the hydronium can be transported where the proton is needed, leaving a water molecule behind again. This ability is very useful and could become an issue to move away from. More on this follow in this thesis.

---

<sup>1</sup>A quick search on [www.scopus.com](http://www.scopus.com) gives >45000 results for keywords "electrochemical aqueous" whereas less than 3000 search results are found with "electrochemical nonaqueous".

Decreasing the proton availability could in principle be achieved by working in purely alkaline environment. This would leave the possibility of using  $\text{H}_2\text{O}$  for proton transport. Before I started on this project, my very talented colleague Dr. Suzanne Zamany together with our two former colleagues Dr. Viktor Colic and Dr. Sungeun Yang tested out a long list of reported possible candidates for NRR. This included a rigorous test of various metals as catalysts in both alkaline and acidic conditions. Unfortunately neither of the aqueous based reactions showed indications of activation and protonation of  $\text{N}_2$ . Not even under alkaline conditions [34]. The issue for the alkaline solutions regarding ammonia synthesis, may be that even under these conditions the proton availability is still too high. This now leads to the other obvious choice for avoiding high presence of protons. That is going completely away from water and work in non-aqueous media [66]. This could be organic liquids. An example of an organic and well know liquid is ethanol ( $\text{EtOH}$ ),  $\text{CH}_3\text{CH}_2\text{OH}$ . Here, all the hydrogen atoms are bound to carbon atoms, except for the  $-\text{OH}$  alcohol group. The  $\text{OH}$ -group makes ethanol protic, meaning it can donate a proton. Other organic solvents does not have this ability. This is the case for tetrahydrofuran (THF). It is a ring of four methyl-groups connected by an oxygen atom. The  $\text{O}$ -atom forces the ring not to be completely planar, and the methyl-groups are not prone to release the  $\text{H}$ -atoms. This makes THF a polar aprotic solvent [67]. There is a long list of organic liquids with differing properties. My colleagues chose to start working with THF, based on a paper from 1993, with a follow up study in 1994, from the three Japanese scientists Tsuneto, Kudo and Sakata [39, 68]. They presented an interesting NRR approach using the organic solvent THF, some  $\text{EtOH}$  and a lithium containing salt, with very promising results. This approach luckily turned out to work and successfully produce ammonia from  $\text{N}_2$ , which was proved by following a rigorous protocol including tests with isotope labelled  $^{15}\text{N}_2$  [34].

## 4.2 The lithium mediated reaction

We have since the rediscovery of the method referred to the non-aqueous electrolyte as "Tsuneto electrolyte" from the first author of the 1993 paper. Though a similar chemistry was also mentioned by a German group all the way back in 1930 [69], they progressed through the reaction under high temperature and extreme pressures. As the reaction is all based on an initial reduction of  $\text{Li}$  ions, which then allows  $\text{N}_2$  to be reduced, it is thus in broad terms called a lithium mediated process. Despite focused research in this particular reaction, both in our group and other prominent research groups around the world [44, 47, 51, 70–75], we still do not know the exact mechanism. But we are starting to understand it more. The first thing to notice, is that it is based on  $\text{Li}$  and non-aqueous media, which immediately will ring a bell for  $\text{Li}$ -ion batteries. As we all know, batteries are essential in nearly every technology we can think of, and has been allowed to grow such from immense research over more than 40 years. Everything from the composition of the electrolyte, to  $\text{Li}$  sources and electrode

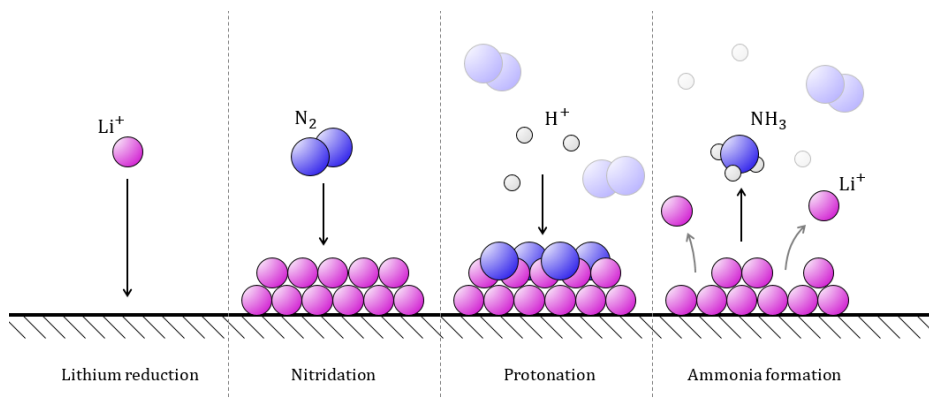


Figure 4.1: Schematic representation of the Li-mediated process, as initially proposed by [68]. Figure reprinted from [79] with permission.

materials have been carefully modified and improved, and it has shed light on what has turned out to be a crucial element in the performance of batteries - the solid-electrolyte-interphase (SEI). And even after all these years, there are still unsolved mysteries regarding this SEI layer [76–78]. In the NRR field we can learn a lot from the battery literature, but it does also give a good reason for why we after some 5 years of work still have not understood it completely [75]. The initial understanding of the process presented by Tsuneto et al. was [68]:



The reaction in equation (4.1) is not balanced but shows the expected necessary steps. These are also presented in Figure 4.1. It also only focuses on the cathodic half-cell reaction, with no concerns to the anode. At first, an adequately negative potential is applied to the cathode in order to plate Li-ions from the dissolved salt as metallic Li. This means applying at least  $-3.04$  V vs SHE. The metallic Li is very reactive and able to activate the otherwise inert  $\text{N}_2$  and form lithium nitride ( $\text{Li}_3\text{N}$ ). Li has thereby done the hard work of breaking the strong triple bond in  $\text{N}_2$ . The role of ethanol (EtOH) is here purely sacrificial as a proton donor, and protonate the nitride forming ammonia and lithium ethoxide (EtOLi).

After a lot of work, both experimentally but certainly also theoretically from our brilliant colleagues at CatTheory, we now know that the reaction process is not quite so simple. This will follow throughout this chapter.

Following their successful work, the ammonia group at SurfCat started to become confident in this approach, and I was then hired to continue along the route with the goal of making it work on a bigger experimental scale. Together with collaborators at Stanford University, we have tested out other possible candidates for the organic solvent and salts. For instance dimethoxyethane (DME), diglyme (DG) and lithium triflate [58, 80]. For the most of my own and my colleague’s

work, we have continued with THF, due to our way of measuring ammonia with the indophenol reaction, as described in Chapter 3.

### 4.3 Stability of organic electrolytes

This approach in nonaqueous media, which differs from most other electrochemical setups, opens up vast possibilities for modifications, such as what solvent to use, additives and its concentration, what salt could be used and so forth. One thing to consider is on the idea of metallic Li being necessary due to its high reactivity stemming from being in the first group in the periodic table, giving it a very reactive lone electron in the outer S-shell [81]. It would be very convenient to move away from Li and use other reactive alkali metals from the same group, such as sodium (Na) or potassium (K). The reason for this being the less reductive potentials needed to plate these metals out, compared to Li.<sup>2</sup> Hereby effectively decreasing the necessary electrical energy input, for allowing the process to occur. Unfortunately, this did not show promising results. We for instance tried replacing the lithium containing salt  $\text{LiClO}_4$  with the corresponding sodium and potassium equivalents ( $\text{NaClO}_4$  and  $\text{KClO}_4$ ), but did not see any ammonia produced. These two perchlorates have a low solubility in THF. Sodium tetraphenylborate is more soluble, but neither here ammonia was produced. This is in correlation to the reportings from Tsuneto et al., who also tried  $\text{NaClO}_4$ . They did not see the same performance with sodium compared to lithium and came to the same conclusion, why we continued basing the synthesis on the lithium-mediated process.

With the electrolyte based on THF, the availability of protons is very limited. As indicated in the beginning of this chapter, we would of course still need some protons available, for being able to synthesize ammonia. To achieve this proton sources can be added. We have used ethanol, as reported initially by Tsuneto et al. [39]. Other additives could be tested out based on their ability to release their protons, i.e. referring to their pKa value [30]. Also the concentration of this additive is a possible modification, which must be optimized regarding the reaction kinetics and conditions. Things as gas flow rate, electrolyte turbidity, electrode substrate and plating rate, and specific experimental setup, may have an influence on how quickly Li is deposited and ready to react with  $\text{N}_2$  and consequently how fast of a protonation is needed to perform more optimal.

Intrinsically by working with organic electrolytes, we have to consider the many reaction routes that can occur. I am not a chemist, but even I can see, how working with an organic solvent (generally some combination of  $\text{C}_x\text{H}_y\text{O}_z$ ) opens up the possibility for numerous different chemical reactions, compared to the simplicity of water ( $\text{H}_2\text{O}$ ). Luckily I have had the pleasure of working with talented colleagues, who are chemists.

---

<sup>2</sup>On the SHE scale the metals plate out at -2.93 V, -2.71 V and -3.04 V vs SHE, respectively for K, Na and Li [38]

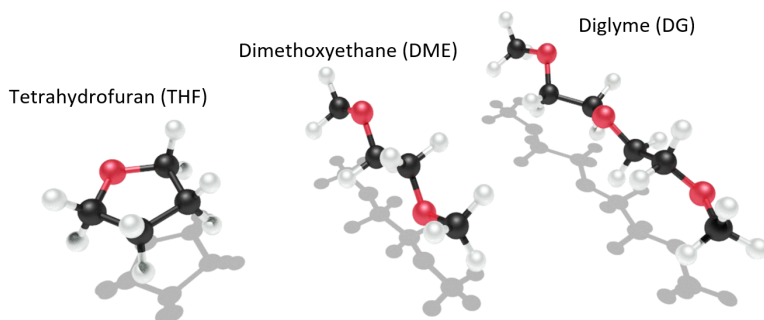


Figure 4.2: Three promising ethers tested for decomposition products during lithium mediated ammonia synthesis. Of these compounds THF showed signs of being most stable.

On this very topic, the brilliant Rokas Sažinas led a study on analysis and identification of soluble side products from the lithium mediated ammonia synthesis reaction (Appended Paper II, [80]). Quantification and identification was done with a gas chromatograph coupled to a mass spectrometer (GCMS), such that species could be separated in time by the GC and detected with the MS at corresponding retention times. Three promising ether based solvents for the lithium-mediated ammonia synthesis was tested for decomposition products. To promote much decomposition, a high charge to electrolyte volume was applied for each solvent, where 90 C of charge was passed through 7 ml electrolyte. The electrolyte mixtures were THF, diglyme (DG) and dimethoxyethane (DME), respectively, all with 1 vol.% EtOH and 0.5 M  $\text{LiClO}_4$  added. The electrochemistry was all done in an Ar filled glovebox with Mo and Pt as the cathode and anode, respectively. The measured GCMS spectra were as expected dominated by the main solvent and EtOH, but many side products were also detected at lower concentrations.

The chemical structure of the three solvents are shown in Figure 4.2. DG is a long linear chain consisting of  $\text{C}_6\text{H}_{14}\text{O}_3$ , and is the heaviest and longest molecule of the tested solvents. It also turned out to be the most unstable electrolyte of the three in this study. This was concluded by detecting the most different compounds after electrochemistry, and also the highest concentration of these. DME also showed more decomposition products at slightly higher concentrations than was the case for THF. Like DG, DME is a linear chain but shorter, consisting of  $\text{C}_4\text{H}_{10}\text{O}_2$ . THF is different from the two other ethers, being a cyclic and smaller molecule with  $\text{C}_4\text{H}_8\text{O}$ . From the decomposition study, there therefore seemed to be a trend of lower stability for longer polyether-based solvents for the lithium-mediated reaction. Nonetheless, in all three electrolytes ammonia could be synthesized by  $\text{N}_2$  reduction at 2-5% FE.

All the electrolytes decomposed during reaction, but the decomposition products depended on the specific solvent. The multitude of products stem from both

electrochemical reactions while somewhat high cell potential is applied, but also chemical reactions with highly reactive metallic lithium, which is plated on the Mo electrode. Though THF seemed to be the most suitable solvent for ammonia synthesis of the three tested here, it still gave at least ten different detectable side products. Some are probably the key to why the  $N_2$  reduction can take place, by manipulation of the formed SEI layer. But it also shows there are limitations to the stability of the synthesis with this electrolyte. At least under the tested conditions.

## 4.4 Effect of the SEI layer and potential cycling

The complexity of reactions may also be the reason why this Li-mediated electrochemical approach has been successful, compared to the multitude of attempts in aqueous conditions [34, 35, 82–84]. Namely the interaction of reactive Li, together with organic solvents and nitrogen, seems to create what can almost best be described as a magical layer, that somehow modifies the diffusion rates of nitrogen and hydrogen just right, allowing ammonia to be formed. This magical layer, is the poorly understood SEI layer. But we have learned a lot.

### 4.4.1 Stability by potential cycling

A microkinetic model was presented by Lazouski et al. from Manthiram’s group [47], showing how the deposited metallic Li could either catalyze an HER reaction or the NRR reaction via a process as described in (4.1). If the concentration of ethanol was too high, the efficiency towards ammonia would decrease and be further out-competed by HER, but with the optimal ethanol concentration, the ammonia formation followed to a certain degree the applied electrical current. According to this study, the catalytic reaction, whether it is HER or NRR, is dependent on the Li being dissolved as a required step. This mechanism may be dependent on the specific experimental conditions, but there may be more to the mechanism. The electrons that in the end drive the reaction, should be available at the surface of the deposited Li, and not necessarily require Li to be dissolved to access them.

With this interesting feature in mind, an experimental and theoretical collaboration from our group was led by Suzanne Andersen together with Michael Statt and Vanessa Bukas (Appended paper I [45]). Here we presented a general molecular-level microkinetic model, to describe the nitrogen reduction mechanism on lithium, and how the plated Li could modify the diffusion rates of protons and nitrogen. Furthermore, we could with the model describe a significant increase in the faradaic efficiency seen experimentally, when allowing the lithium to dissolve without electrical current applied to the electrodes. The continuous alteration of applied potential and no current, we refer to as the *cycling*

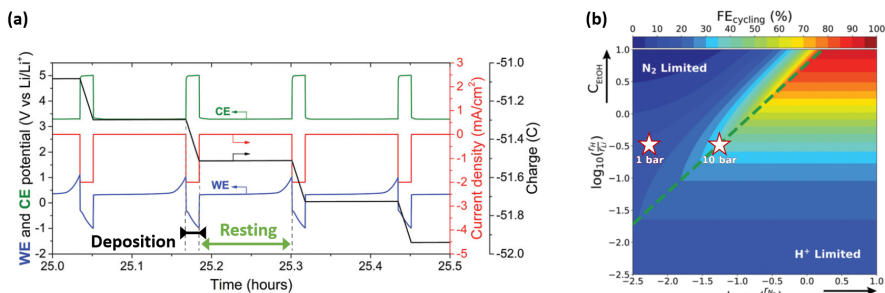


Figure 4.3: (a) Cycling procedure with resting and deposition highlighted, and set from the cathodic potential. (b) Molecular-level model describing the efficiency of NH<sub>3</sub> synthesis dependent on lithium, proton and nitrogen diffusion rates. Stars present experimental measurements. Adapted with permission from [45].

procedure, which we since then have used a lot for achieving improved efficiency results.

The model was based on ten elementary steps, divided into: lithium deposition, hydrogen evolution, and ammonia formation, respectively. In contrast to the microkinetic model by Lazuski et al., there is no step involving lithium dissolution in our molecular-level model. This would mean, that under reductive potentials, a continuous built up of Li-species would be expected. This behaviour was empirically supported from our own experiments where we always would see a visual surface deposition, but also from [70], where a relatively thick lithium containing deposit was observed on the electrode after ammonia synthesis.

If Li continuously is deposited on the electrode there would be at least two effects. For one, the amount of lithium in the system is limited, since it is defined by the amount of Li salt in the electrolyte. Taking it to the extreme, if we would continue to deposit Li, we would expect to eventually deplete the electrolyte for Li ions, and not be able to continue anymore. Apart from the effect of probably stopping the synthesis, it would also have the consequence of increasing the resistance in the electrochemical cell. As mentioned in Chapter 2, the electrolyte is the medium through which the electrodes have ionic contact. Current is running between the electrodes by transferring charges (in the form of charged species). If the supporting electrolyte is depleted of species to carry the charge, charge transfer is hampered and the resistance increases. Meaning that to compensate for this, the energy input must be increased, according to IR-drop.

It is thus not viable, if Li continuously is deposited on the electrode. This is the reasoning behind the cycling procedure as mentioned and shown in Figure 4.3(a). By switching between (1) producing ammonia while depositing Li (referred to as *deposition*), and (2) then being at open circuit potential where no current is passed and thereby allowing the deposited Li to dissolve (referred to as *resting*), we would effectively be in a somewhat similar situation as described by Tsuneto

et al. in equation (4.1), where the Li is being released again from the electrode as ions, and ready to be re-deposited. What we would normally observe when doing experiments in a single compartment glass cell with only  $N_2$  flowing and relying on sacrificial EtOH, is a destabilization of the cathodic electrode potential. The anode potential would often be relatively constant at a high anodic potential, where the electrolyte could be oxidized, in order to provide electrons for the reaction. But the cathode would over time drift more and more cathodic. This was also mentioned in a brief sentence by Tsuneto et al. in their original paper, where they noticed the electrode potential "*shifted gradually in the negative direction during electrolysis*" [39]. But what we observed when applying the cycling procedure was, that during deposition the cathode potential would go to some -3 V or more negative while depositing Li. When switching to OCV, the potential would initially keep being at the  $Li/Li^+$  potential, but suddenly drift less cathodic. We inferred this as a sign of all the deposited Li (or at least most of the accessible Li on the electrode) would at this point have been dissolved. Meaning, that now the cathode potential is no longer defined by the  $Li/Li^+$  redox potential (as it was while  $Li^0$  was present), but the underlying reactions at less cathodic potential would be significant. At this point we would then switch back to deposition conditions again, and repeat the cycle.

The conditions for deposition and rest would not be the same throughout an experiment, but had to be modified throughout the experiment. The modifications was either shortening or prolonging either the deposition or resting time, with which the cathode potential could be shifted more or less cathodic. This allowed us to maintain a stable cathode potential even in experiments lasting multiple days. The downside was though, that the modifications had to be made every few hours. To this I have great respect and admiration for the determination by Suzanne, who sacrificed her sleep in the name of Science, for realizing this and be the main driver for the long experiments. The main reason for the necessity of modifying the deposition and resting times, are very likely the change in electrolyte conditions, since we relied on oxidizing the electrolyte on the anode. This effectively meant that the electrolyte composition would change during the cause of an experiment, which we then had to actively compensate for. The dependence of electrolyte oxidation on the anode thereby also set a limitation for how long experiments were possible - but the limitation was no longer given by the cathodic reduction reactions.<sup>3</sup>

With the cycling procedure, we managed to stabilize the cathode potential, since Li did not built up continuously on the electrode but could be reused, allowing long experiments to run. An equally important observation was a significant increase in the faradaic efficiency towards ammonia. This highlighted that ammonia could be synthesized both during Li deposition but also during Li dissolution while resting. This does agree with both Tsuneto's and Lazouski's work, that ammonia can form during Li dissolution, though it differs with the lack of

---

<sup>3</sup>With the challenges on the cathode starting to be handled, we knew that the anode reaction was an approaching problem to be tackled. Meanwhile I was working on the flow cell with this in mind, which will be described in coming chapters.

applied current. An explanation for the increased FE with the cycling procedure, is that allowing Li to dissolve and take part in the ammonia formation, avoids formation of what could be called *dead lithium*, or inactive lithium for ammonia synthesis. Dead lithium could be seen as Li reacting with the species in the vicinity, such as organic compounds from the electrolyte. Carbonates (especially on reactive metals) are quite stable [78], and if these would first be formed, they are unlikely to dissolve again. Li taking part in formation of e.g.  $\text{LiCO}_3$  or similar, would thus be trapped. The electrons we have paid for when reducing Li ions are therefore lost, resulting in a decrease of FE. On the other hand, the Li that dissolves and participate in ammonia formation, will be recovered and help increasing the FE.

The effect of diffusion of reactant species was seen from pressurization of  $\text{N}_2$ . Experiments were performed in an autoclave, such that the atmosphere could be controlled and pressurized. What we saw was a noticeable increase of the faradaic efficiency, as the pressure was increased from 1 bar to 10 bar of  $\text{N}_2$ . From the model, we could explain this as an increase in the relative diffusion rate of  $\text{N}_2$  compared to Li ions, while the relative proton diffusion was constant, since the electrolyte was unaltered. This shifted the conditions from being in a nitrogen limited regime, closer to an optimal ratio of diffusion rates. Increasing the pressure further to 20 bar  $\text{N}_2$ , did not yield a significant increase in FE, explained by no longer being limited by  $\text{N}_2$  at the electrode surface. This is depicted in Figure 4.3(b) with stars indicating the change of  $\text{N}_2$  diffusion due to increased  $\text{N}_2$  pressure. This co-dependence of diffusion rates points towards that experimental conditions will have a significant impact on the FE and the rate of ammonia formation. Thus changing the electrochemical setup, by e.g. altering whether electrolyte is stagnant or mobile, the composition and concentration of electrolyte, or changing the way nitrogen and protons are supplied to the electrode surface, would all influence the relative reaction pathways towards either HER or NRR and possibly also other side reactions regarding the SEI layer formation.

#### 4.4.2 Enhancement by oxygen

The model was further developed, after the surprising find, that small amounts of oxygen ( $\text{O}_2$ ) added to the system increased the stability and efficiency (Appended paper III [46]). This is a surprising observation, as trace amounts of  $\text{O}_2$  in the Haber-Bosch process, is detrimental for the thermochemical reaction [7].

The study of  $\text{O}_2$ -enhancement to the system, was made in the same autoclave setup, at pressures up to 20 bar. As discussed, the lithium-mediated ammonia synthesis is permitted by the SEI layer on the cathode. What we observed was, that increasing the  $\text{O}_2$  concentration to a few percent, maintained a constant cathode potential for a longer period of time, before eventually destabilize. The stability of the electrode potential was proportional to the  $\text{O}_2$  content. But so was the  $\text{H}_2\text{O}$ -concentration, measured in the electrolyte after experiment. This

suggests, oxygen reduction reaction (ORR) occurs simultaneously with (NRR), as a competing reaction. With no  $O_2$  at 20 bar, the FE was about 20%. This dropped to zero with more than 2%  $O_2$  present. A peak behaviour in FE was seen between these points. At 20 bar  $N_2$ , with 0.8 mol%  $O_2$  (corresponding to 0.16 bar partial pressure), the FE was drastically increased to 78% efficiency. This four-fold increase is very positive news for the lithium-mediated ammonia synthesis. Increased FE means less charges spent on competing side reactions, such as HER and ORR. And with some  $O_2$  in the system, the cathode potential was also stable for longer time. Including the cycling procedure, did not increase the FE further. But it did stabilize the potential, similarly to the initial report, that is already discussed. Furthermore, w.r.t. applicability of the Li-mediated method, less demands on the  $O_2$  cleanliness in  $N_2$  gas, does could lower future installation prices [85].

Taking the microkinetic model, previously developed, into account, the observed ORR was attempted incorporated. This could though not explain the observed increase in FE towards  $NH_3$ . With the initial microkinetic model, a qualitative explanation can be given. If  $O_2$  affects the SEI formation, in such a way that Li diffusion is decreased, while  $N_2$  and  $H^+$  diffusion is unaffected, the FE for NRR should increase. This can be explained from Figure 4.3(b), by moving along the green line towards higher FE. This would be in agreement with [86], who report, that  $O_2$  affects the SEI composition in nonaqueous Li-air batteries, which also diminishes the  $Li^+$  diffusivity.

It is thus clear, that formation of an SEI layer, is crucial for the Li-mediated ammonia synthesis. It also shows, that optimization of the composition and formation of the layer, can lead to improved NRR conditions.

## 4.5 Acidification of electrolyte

One of the side-effects from doing NRR in organic solvents, is an increased acidification of the electrolyte over time. Together with Kevin Krempel, we discussed on this very topic in the Appended Paper V [87]. In this study, we did cyclic voltammetry on a platinum (Pt) disk, to understand the reactions that could happening at the anode during electrochemical NRR. Pt is a commonly used catalyst for hydrogen reactions, as it has near-zero overpotential for both the oxidation and reduction of the hydrogen redox couple,  $H_2 \rightleftharpoons 2H^+ + 2e^-$  [88]. The motivation for the study was to alleviate whether we could see clear indications of hydrogen oxidation in nonaqueuos electrolytes, as the provision of protons not stemming from electrolyte decomposition is an important step for realizing ammonia synthesis from replenisheable hydrogen sources.

The electrolyte was the standard THF based solvent with Li salts. For most of the work we were running with 0.5 M  $LiClO_4$  in THF with or without 1 vol.% EtOH. The slightly higher Li concentration was to compensate for the somewhat high ohmic resistance through the electrolyte, as we separated the

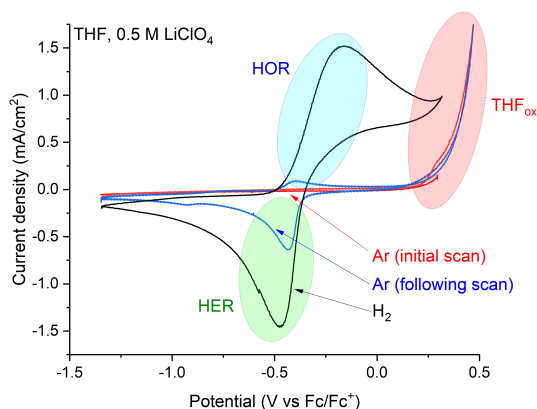


Figure 4.4: CV measurements on Pt in Ar and  $\text{H}_2$  saturated THF with 0.5 M  $\text{LiClO}_4$ . THF oxidation (red shade) is the only feature initially seen in Ar, where after protons are accessible for reduction (green shade). Some  $\text{H}_2$  can be oxidized again (blue shade) afterwards. In  $\text{H}_2$  saturated electrolyte both HOR and HER is clearly seen. Figure adapted from [87] with permission.

Pt disk (working electrode) from the reference and counter electrodes. The separation was to avoid noise in the measurements, from possible side reactions on the counter electrode (here a Li foil), which could both affect the working electrode and the Ag based reference electrode. For the same reason, a Li foil was used to have little effect from possible Li dissolution herefrom. The CV recordings were done with a RDE setup, which gave us some control of the transport kinetics of reactants and species to and from the electrode. In the end, we chose to only exploit this for ensuring proper mixing of gas and electrolyte during experiments, such that we could change the atmosphere and see the effect of hydrogen and inert argon, respectively. By keeping the electrode and electrolyte stagnant we observed an interesting feature.

Representative CV measurements are summarized in Figure 4.4. Irregardless of whether EtOH (normally assigned as being the proton donor, e.g. [34, 47, 68, 70]) was added or not, we would initially not see any HOR or HER activity in an Ar atmosphere, despite being in the potential window where these reactions should take place. Only by going much more anodic, to the point where the supporting electrolyte was oxidized at approximately +0.3 V vs  $\text{Fc}/\text{Fc}^+$  redox couple,<sup>4</sup> we would see a significant oxidation feature occurring. This was followed by a reduction feature close to the expected potential for HER. When scanning the potential anodic again, an oxidation peak was observed, very well correlating to HOR. Compared to the electrolyte oxidation, the new oxidation peak happened at approximately -0.5 V vs  $\text{Fc}/\text{Fc}^+$ , which is much lower. We were now obviously

<sup>4</sup>The ferrocene redox couple  $\text{Fc}/\text{Fc}^+$  was used as a fixed reference frame, such that the Ag wire reference electrode could be calibrated to this redox couple after experiments.

not oxidizing the electrolyte anymore, but given by the potential coupling to the HER peak and the CV *duck-shape* [40], everything pointed towards actual HOR and HER. So with no external hydrogen source, protons can be produced from electrolyte oxidation. These protons are not very mobile and stay at the vicinity of the electrode, and can thus be reduced to hydrogen gas (HER) which in turn can be oxidized back to protons again (HOR).

The same HOR-HER duck-shape was obtained when changing the atmosphere from inert Ar to H<sub>2</sub>. With H<sub>2</sub> present, we did not need to go to the very anodic potential in order to have an oxidation reaction happening, but the same anodic current density could be achieved at the established HOR potential. From here the situation was similar to before, where an HER peak was observed when sweeping the potential cathodic. The HER current density was nearly as high as the anodic peak, but the discrepancy can be explained by some protons reacting with either the solvent or electrolyte salt. So stability may still be an issue. This tells us, that H<sub>2</sub> oxidation is possible in the nonaqueous electrolyte albeit difficult and requires adequate transport of H<sub>2</sub> to a catalytic active anode. It also shows what was already known, namely that protons easily can be provided from "burning" or oxidizing the supporting electrolyte, as long as the anodic potential is high enough [89].

We then combined these measurements with previous observations in the lab, namely that we would normally see nearly all the produced ammonia in the liquid electrolyte phase. This is in contrary to what otherwise is expected, since ammonia is a volatile compound and therefore should be found in gas phase. A possible explanation to this, is that the electrolyte would become acidic during NRR experiments. Additional or available protons could then make ammonia into ammonium, and trap it in the liquid in a similar way as we have exploited for the colorimetric indophenol method described in Chapter 3. We therefore did a series of experiments with *used* electrolyte and compared this to *fresh* unused electrolyte. The used electrolyte was prepared by doing standard Li plating in the nonaqueous electrolyte under Ar atmosphere. Ar atmosphere was chosen in order not to deal with ammonia formation, but otherwise simulate the same conditions as under NRR without N<sub>2</sub> and H<sub>2</sub> gas present, such that protons would be created from electrolyte oxidation. Electrodes were molybdenum (Mo) foil as the cathode, Pt mesh as the anode and a Pt wire as pseudo reference. The applied potentials during 4 mA/cm<sup>2</sup> current density were very representable to normal experiment conditions, with cathodic Li plating on the Mo foil and electrolyte oxidation on the anode. After 15 C had been passed over the 8 ml electrolyte, the used electrolyte was taken out.

From here, two similar experiments were done with this used electrolyte and compared to freshly prepared electrolyte. In both cases, THF saturated Ar was rigorously bubbled through the electrolyte and then passed through a water trap. The electrolyte was initially spiked with a known amount of NH<sub>3</sub> and measured both in the electrolyte and in the water trap. After 45 minutes of rigorous bubbling, the electrolyte and water trap was then quantified for ammonia again.

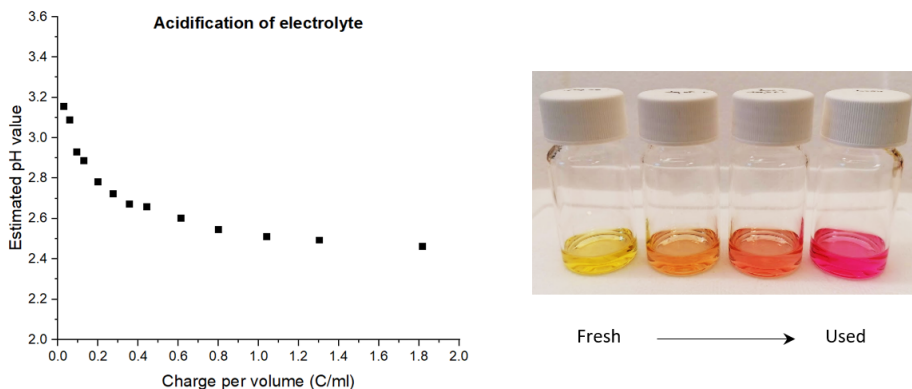


Figure 4.5: Estimated pH value of nonaqueous electrolyte in Ar atmosphere as a function of charge passed. The numbers should not be taken as exact, but an initial quickly acidification is observed.

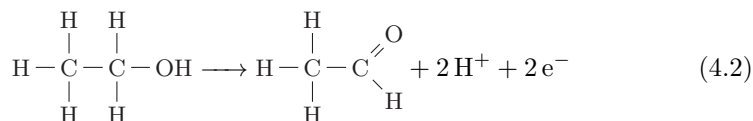
This then clearly showed the suspected behaviour. When measuring on the used electrolyte, all the ammonia was still measured in the electrolyte after Ar bubbling and no increase was measured in the water trap. This was in vast difference to the case of fresh electrolyte, where less than 30% of the ammonia remained in the electrolyte, but instead could be measured in the water trap. This would point towards that in fresh electrolyte, the ammonia stay volatile, due to non-acidic conditions, compared to used electrolyte. To further support this claim, inspired by [90] and discussions with Kevin and Degenhart Hochfilzer I prepared a methyl orange solution containing 3 mM methyl orange in 20 vol.% EtOH in water. Methyl orange has a pH range of 3.1-4.4 [38], and should therefore change colour, if the liquid becomes more acidic than approximately pH 4. This was exactly what we observed, with the fresh electrolyte getting a yellow colour (more alkaline than the turning point) while the used electrolyte turned to a clear purple colour (more acidic than the turning point).

After we successfully could see the effect of acidification I wanted to push this slightly further, and measure how fast the acidification would occur. The setup was simply a one compartment glass cell with the same electrodes as just described from [87], starting out with 15 ml electrolyte and Ar flow, applying 4 mA/cm<sup>2</sup> current, and periodically take samples from the electrolyte. Each of the samples were then added the methyl orange, and titrated with 0.02 M NaOH, to see when the resulting colour would switch back to the non-acidic conditions. The resulting measurements are shown in Figure 4.5. The exact numbers do have quite some uncertainty to them, mainly from whether the turning point was achieved correctly during the titration. But it does nonetheless show, that the electrolyte acidifies very quickly, when only inert gases are passed over the electrodes. This is somewhat in agreement with an old French paper [91], who hypothesis that the anions in salts, can act as a buffer system with the acid-

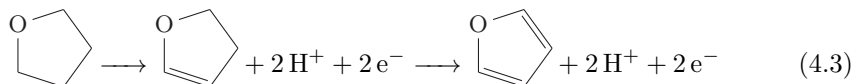
base couple in THF. According to them, proton exchange takes place between  $\text{Li}^+\text{ClO}_4^-$  and  $\text{H}^+\text{ClO}_4^-$ , with a fixed zone of pH at 2-4. Interestingly, the methyl orange experiment, does shown similar tendency.

In order for the electrolyte to acidify, there must be an accumulation of accessible protons in the electrolyte. Ideally, what is produced at one electrode, should be used at the other electrode. Here, I namely refer to protons generated at the anode should be consumed at the cathode. But as the electrolyte acidifies, there must be a misbalance between the rate of proton production and consumption. This could be explained by a combination of multiple factors. One reason is that electrons are consumed at the cathode to plate out metallic Li and not necessarily consume the produced protons. Another factor is the possibility of producing protons both from oxidation reactions at the anode but also reduction processes at the cathode, leading to more protons being produced. This is a possible way of explaining how a total accumulation of protons is possible. This is in good correlation to the many decomposition products seen in the THF based electrolyte, as previously discussed [80]. To just mention some possibilities, four such reactions are listed below.<sup>5</sup>

Oxidation of ethanol



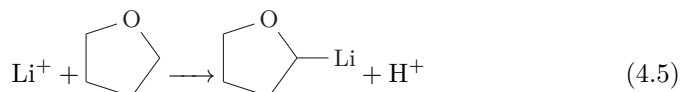
Oxidation of THF



Reduction of THF



Reduction of THF in the presence of Li



This highlights the importance of considering both sides of the electrochemical cell for ammonia synthesis. The cathodic reduction of  $\text{N}_2$  to  $\text{NH}_3$  can be achieved in non-aqueous electrolytes, due to the low and controllable concentration of protons preventing high activity of HER. But as long as we do not have

<sup>5</sup>I owe thanks to Rokas Sažinas and Bjarke Mygind for fruitful discussions and explanations on this topic.

a replenishable source of protons and an adequate transportation mechanism of these, things will, quite literally, go sour. We have to consider the anode as well, and be able to provide protons from a sustainable source. In the publication we suggest the need to find a suitable proton acceptor to add in the electrolyte. It should be electrochemically stable under the applied potentials and not negatively affect the ammonia synthesis reaction. If so, it is plausible it could function as a buffered system, and effectively shuttle protons between the electrodes, without acidification and degradation as a result. To avoid protonation of neither ammonia nor electrolyte, would most likely require a high basicity. Though we have not found the perfect candidate, this challenge still stands. Ethanol has been suggested to be able to function as a proton shuttle [44], but based on our observations of acidification, this may not be an efficient compound.

## 4.6 The other crucial step - Hydrogen oxidation

The section heading will for many people be striking. As mentioned several times, reactions with  $H_2$  is well tested, well described, and well established by now. Built of the smallest and lightest atom, it is the simplest molecule there is. But despite its' small size, that does not mean it is unimportant. Quite on the contrary [92, 93]. There is still some talk about the hydrogen economy [94, 95], and renewable and sustainable production of  $H_2$  is one of the backbones of the transition from fossil fuels to renewable energy and all Power-to-X (PtX) [96, 97] - including electrochemical ammonia synthesis [98].

But electrochemical hydrogen production has mainly and almost exclusively been studied under aqueous conditions. And why not? For the above-mentioned reasons of hydrogen economy and sustainable energy carriers, water is the perfect media. First of all because it is water. Water is everywhere, there is plenty of it and in itself, it is non-toxic. If we split water completely, we are left with hydrogen and oxygen. Again, win-win. And water is also really good at transporting protons, due to the natural equilibrium of  $OH^-$ ,  $H_2O$  and  $H_3O^+$ .

When it comes to working with hydrogen in organic solvents though, the story is very different. Because of the multitude of various routes for organic solvents, it is not straightforward to either take or add protons to the mix, Ideally, we would be in a case, where our solvent stays the same over time, and only two reactions happen.  $H_2$  being oxidized to  $H^+$  on the anode, and  $N_2$  being reduced by  $H^+$  to  $NH_3$ . We could even be realistic and allow for a small part of the  $H^+$  to reduce to  $H_2$  again, meaning a decrease in faradaic efficiency for NRR. But we should by all means not depend on continuously have to burn the electrolyte in order to provide protons for the reaction.

This brings the question back to the stability of the organic electrolytes. So when protons are produced at the anode - preferably from  $H_2$  oxidation,<sup>6</sup> what

<sup>6</sup>One could argue that it would be even more preferred to oxidize water rather than  $H_2$  -

do we then have to transport these protons? From the measurements I did with Kevin [87] mentioned earlier, we saw a tendency for the protons to stay at the vicinity of the electrode, and not easily be transported away. Protons can in general not live on their own in liquids, but have to form some bond to another molecule [30]. I have discussed with many of my brilliant chemist colleagues on this matter, and there is a general consensus, that these organics likely will have to break from their original form, in order to facilitate transport of  $H^+$ . The mechanism of the  $H^+$  transfer is then another question. Whether it is one molecule carrying the proton from the anode to the cathode. Or it happens via a hopping mechanism, where the proton jumps from one molecule to the other, resembling the Grotthuss mechanism in oxides [99].

The mechanism must also depend on which solvent is used. Ethanol is proposed to facilitate transport via ethoxide, and switch between  $EtOH$  and  $EtO^-$  [44]. THF, as an ester, has a dipole moment, and a negative partial charge on the oxygen atom [67]. This negative charge, could therefore move towards the positive anode, and get a proton on the oxygen atom. From here, the proton could be transported in a Grotthuss-type manner. The proton could though also do acidic hydrolysis reaction with THF, and open the C-O bond, leading to polymerization and unwanted breakdown-products [80] A similar transport may be provided by an ester, like dimethyl carbonate (DMC),  $OC(OCH_3)_2$ . As for THF, there is a negative partial charge on the O-atom, due to its higher electronegativity than C. A similar transport could thus be described. The plausible proton bond for DMC is shown below:



Due to the  $C=O$  double bond, DMC should be better and more stable for this specific  $H^+$ -transport mechanism. But hydrolysis, via the methyl-groups, are also likely, why DMC is prone to breaking down too.

At least, we had seen very clear results that it is possible to produce protons from hydrogen gas in the organic electrolyte. But we still needed to see if such protons could then also be used at the cathode for ammonia formation. I will return to this very interesting subject in Chapter 6.

---

but from the initial discussion on water and  $NH_3$  synthesis, I have my doubts to whether that will be possible.

# Chapter 5

## Flow cell design process

### 5.1 Designing an electrochemical black box

I will in this chapter describe the considerations and steps we went through in the design of the electrochemical flow cell we developed for ammonia synthesis. It will be a storytelling of the development process, as it has taken the main focus of my PhD project. The process has been a series of multiple small iterations, but can be divided into three major steps. All of these design steps were done in close collaboration with Dr. Mattia Saccoccio, who also took part in the initial testings, and was a crucial help to me.

### 5.2 Size matters

The initial work on the Li-mediated process, was done in small laboratory scale glass cells, containing some tens of milliliters of electrolyte. Furthermore, the synthesis for these experiments were all batchwise, so limited by a set amount of electrolyte. Most of the following work and experiments done in parallel, has all been in this same order of magnitude, with some modifications in the glass cell designs. But what has been common to them all is the size of the electrodes, all being around  $1 \text{ cm}^2$  in size.

An imperative part of upscaling the Li-mediated ammonia synthesis process, is to make the cell bigger. If this ammonia synthesis method should have any chance of being useful in the real world, we cannot rely on only making a few micrograms ( $\mu\text{g}$ ) of ammonia at a time. Remember the current production is hundreds of millions of tonnes per year - or roughly 500,000 tonnes per day, so 17 orders of magnitude higher! I will say right away, that electrochemical ammonia synthesis will never be able to replace the Haber-Bosch process, but hopefully be a substitute in remote rural areas, where the conventional  $\text{NH}_3$  is not easily

accessible, such as Sub-Saharan Africa (Appendix Figure A.1). The limitation to electrochemical ammonia synthesis lies in the lower energy efficiency (currently limited to  $\sim 30\%$  [46, 85]), compared to that of Haber-Bosch ( $\sim 60\%$  [19]). To realize this, the electrochemical production has to be increased. The line of thoughts is bigger size, gives more current, gives more product.

The fundamentals of how to reduce  $N_2$  to  $NH_3$  has by now been reasonably established. We know what electrode materials to use, the electrolyte and gases needed and the electrochemical conditions required. Electrochemical cells have been designed and tested by many other groups, including some of our colleagues working on electrochemical  $CO_2$  reduction to useful products. As there is no reason to reinvent the wheel, our approach was simple. Take the design they have worked on, and modify it to suit our needs. When I started on the PhD project and we planned our procedure, this sounded easy to me. Little did I know the challenges that followed.

### 5.3 Gas supply

Starting from a known design, the first few obstacles were already included, namely, electrical contact to the electrodes and supply of gas. Gas supply was the first issue we realized that had to be solved for this specific purpose. The cell we started working on, was designed with gas supply from the backside, fed into a small gas channel contacting the electrode. But there was no feature allowing liquid flow of electrolyte through the cell. The membrane-electrode assembly (MEA) type cell is shown in Figure 5.1(a), where an anion-exchange membrane was used for ionic contact between the two electrodes. In our case, we would need to find an electrode that could act as a gas diffusion electrode (GDE) [100, 101], keeping gas on one side and electrolyte on the other side. The principle is sketched in Figure 5.1(b), with liquid on the left side of the electrode and gas on the right. The electrode has a structure, e.g. microporous surface, allowing gas to diffuse to the liquid side, while liquid cannot penetrate. Our challenge was to find a GDE that could work with non-aqueous solvents like THF, having a low surface tension compared to water. Once this was found, the ammonia formation should also be vastly improved, due to much higher availability of  $N_2$ , directly from the gas stream. This compared to being limited by the solubility of  $N_2$  in the electrolyte ( $\sim 5 \times 10^{-5}$  mol/mol) [102, 103], which is the case for the glass cell setups. Thus, a fully saturated THF-solution can contain about 170  $mg_{N_2}/L$ , where complete conversion to  $NH_3$  would give 210 ppm. In practice, it is not possible for us to have a fully saturated liquid without continuous gas flow, due to equilibration to surroundings. Especially, when liquid transfer and flow is taken into account.

A lot of research has been put into developing highly efficient electrodes for e.g. electrolysis cells doing water splitting. The keyword here being electrodes developed to work in aqueous liquids. Water has a high surface tension of  $72 \text{ mJ/m}^2$

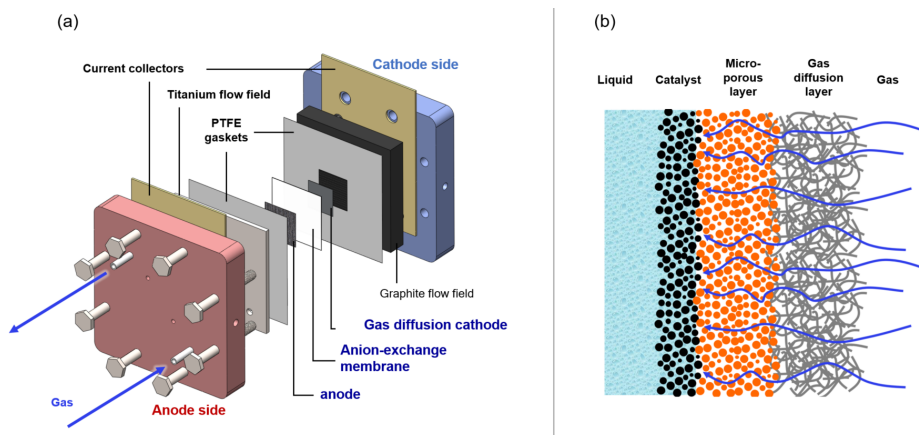


Figure 5.1: (a) Membrane-electrode assembly (MEA) type electrolyzer for  $\text{CO}_2$  reduction used by our colleagues. This cell assembly was the inspiration for the  $\text{NH}_3$  synthesis cell. Reprinted and modified with permission from [104]. Copyright 2019 American Chemical Society. (b) Schematics of a possible gas diffusion electrode (GDE) in aqueous media, with a microporous layer for liquid separation [105, 106].

[38], allowing porous electrodes to function as good gas diffusion electrodes, where water is kept on one side not being able to penetrate through the pores, by carefully modifying the contact angle between liquid and surface [107]. Thereby the GDE is efficient at separating the liquid water on one side from a gas stream on the other side of the electrode.<sup>1</sup>

These are perfect conditions for achieving high currents and conversion efficiencies. Because, there is one more detail to the electrolysis cells. That is the catalysts. As already discussed, reactions on catalysts happen on their surface, so embedding designated catalysts in the GDE, triple phase boundary conditions can be achieved. The reaction will either require gas as reactant (inlet of gas) or have gas as product (gas carried away). As mentioned, electrolyte provides ionic contact and can also be either source of reactants or sink for products. At the same time, the catalyst improves the reaction, so ultimately we need all three phases - gas, liquid, and catalyst - to be present simultaneously. That is the background for triple-phase-boundary and why we need it for optimal performance.

Initially we tested some standard carbon-based GDE materials, but quickly realized that these were not compatible with the organic electrolyte, due to the low surface tension. The membranes were tested inside an Ar-filled glovebox, by adding a known amount of THF to a vial, and close the vial using the membrane as lid. The vial was initially weighed, to know the exact amount of THF. Then four stages were tested and the vial weighed after each: (1) vial standing for one

<sup>1</sup>This is not as easily achieved for non-aqueous liquids with low surface tension, such as ethanol ( $22 \text{ mJ/m}^2$ ) or THF ( $26 \text{ mJ/m}^2$ ) [38].

hour, (2) flipping the vial upside-down for 5 minutes, (3) keeping the vial upside-down an additional hour, (4) letting the vial stand overnight. The vials were weighed after each step, to determine the amount of lost THF. In Appendix Figures B.1 and B.2 an overview of the tests can be seen. For all of the the C-based membranes >99% of the THF was lost after the final stage. Generally, most of the loss occurred when the vial was flipped, while THF was lying directly on the membrane. In this case, THF easily diffused through and evaporated. Apart from C-membranes, two polytetrafluoroethylene (PTFE) membranes of 50  $\mu\text{m}$  and 100  $\mu\text{m}$  thickness respectively, were tested in the same way. In both of these cases, a negligible of THF was lost.

With C-based membranes not compatible with the electrolyte, a silver-based (Ag) porous membrane was tested for applicability with the Li-mediated process. It was a Sterlitech porous silver membrane with nominal pore size of 1.2  $\mu\text{m}$ , that had been used by the  $\text{CO}_2$  group [104]. This was not found suitable with the electrochemical process, as it deformed and became brittle after Li deposition. This is shown in Figure B.3, where Li deposited inside the membrane pores, compromising the structure. We needed to find a different solution, and discussed on various possibilities - including applying pressure to some kind of porous electrodes. Though, we did not pursue this at first, since other cell modifications also were necessary, and chose to postpone the gas delivery issue to later. We knew NRR testing was possible through gas saturated electrolyte, so that would be the first step.

## 5.4 Not only a batch

But we needed to make a chamber for the electrolyte to be in. As a first step, we chose to keep the design as close to the known glass cell experiments as possible, so only having a single compartment. From the very first iteration of the electrolyte chamber, we decided it should have both an inlet and an outlet for liquid. This serves multiple reasons. (1) If electrolyte is lost over time, e.g. due to evaporation from gas flow, this can be refilled, (2) if the electrolyte deteriorates or breaks down, we can replace it with fresh electrolyte, and (3) if we for some reason want to change the composition of the electrolyte, whether it is solvent, additives or salt, this can be done during an experiment. Furthermore it also comes with the advantage, that (4) if synthesized ammonia is stuck in the electrolyte, as observed in acidic cases, this could possibly be taken out and be distilled or separated somehow.

### 5.4.1 Design considerations

The cross section of the chamber was set by the electrode size in the preexisting cell design to be 50x50 mm<sup>2</sup>. From experience we knew the electrolyte has a very limited ionic and electrical conductivity, so to keep resistance losses low,

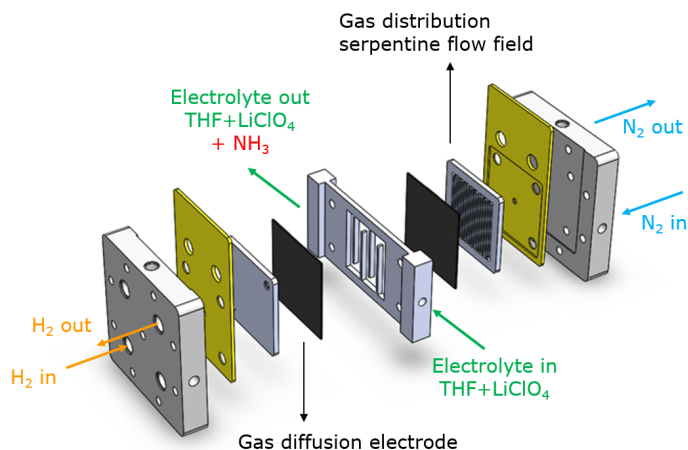


Figure 5.2: Initial envisioning of the electrochemical ammonia flow cell based on a modification to a preexisting cell concept.  $\text{H}_2$  and  $\text{N}_2$  would flow over the anode and cathode respectively with an electrolyte chamber in the center for electrochemical reactions and liquid flow.

the thickness of the chamber had to be kept as small as possible. Accounting for the manufacturing constraints as well as the electrolyte in- and outlet tube sizes, this resulted in a lower limit of the chamber thickness of 4 mm. The electrolyte in- and outlet were positioned in the center axis of the chamber, due to the pre-existing placement of fastening screws. To prevent the flowing electrolyte to 'by-pass' the full electrode area and simply just take the shortest and direct route from in- to outlet, we added fins, to help guide the electrolyte around and flow over all of the electrode. Since these fins would decrease the effective electrode area, as they are covering some of the electrodes, we opted for keeping them as small as possible while still be mechanically rigid. They were therefore 2 mm thick. The cell as envisioned including electrodes and electrolyte chamber is shown in Figure 5.2, and a 3D model with dimensions of the electrolyte chamber is shown in Appendix Figure B.4 together with the predesigned cell in Figure B.5. As shown, small holes were placed along the periphery of the assembly, where screws were placed to compress and tighten the cell.

## 5.4.2 Material choice

Though the idea and principle was simple, we could not be sure if the science would work out the same as we thought. The chamber had to be non-conductive, such that the two electrodes are isolated, and not short-circuited. At the same time, it had to be chemically stable under operating conditions. We therefore chose to manufacture the first chamber in aluminium (Al). This is a fairly cheap alternative and easy for workshops to handle. But more importantly, it can

easily be surface treated and form an aluminium oxide ( $\text{Al}_2\text{O}_3$ ) protective layer. The oxide is also called alumina. This made Al the perfect material candidate. Alumina is a very chemically stable oxide with a high mechanical strength too. Hence it is e.g. being used for prosthetic and orthopedic implants [108]. As an oxide, it is also electrically insulating. Despite only having a thin surface layer of alumina, it should be adequate for meeting the operating requirements for the flow cell.

Producing the chamber in alumina, which would contain and be in direct contact with the electrolyte, made us worried if we could risk having a battery-like behaviour between the chamber and other metals contacting the electrolyte. With electrolyte flowing around, it would come in contact with a lot of surface. Because of this, we therefore ensured, that as much as possible of the chamber and connected fitting-parts, all would be in aluminium, so it all could be oxidized to alumina. This included the chamber it self, electrolyte tubing in and out, and the compression fittings and unions, used for subsequent tube connections. See Appendix Section B.3 for more details on the anodization procedure adopted.

### 5.4.3 O-rings and sealings

Another thing to consider was gaskets and o-rings. These are crucial for being able to make tight connections, especially when pressing different metal parts against each other with a low viscous organic liquid flowing between. Furthermore, we knew we would work with THF as an aggressive solvent, so chemical compatibility would also be of major concern, and did not leave many options open. Hence we have relied nearly exclusively to FFKM perfluoroelastomers, namely Kalrez®6375 elastomers from DuPont. These perfluoroelastomers are known to have long lifespan and being inert to an extensive list of chemicals [109].

## 5.5 First iteration

We now had all the necessary parts for initial tests. A side view of this assembly is sketched in Figure 5.3.

For the first iteration, we did not have any electrodes compatible with gas flow. The focus was instead on electrolyte flow during electrolysis of  $\text{N}_2$ . We therefore built a setup, flowing electrolyte that was pre-saturated with  $\text{N}_2$ . As previously mentioned,  $\text{N}_2$  is only sparsely solvable in the organic solvent, but we knew from glass cell experience, that it should be enough in order to synthesize and measure  $\text{NH}_3$ . For this setup, the electrodes should therefore be closed off, and not allow electrolyte to flow through and out from here.

As schematically shown in Figure 5.3, the first iteration was relatively simple. The outer three parts were the pre-designed parts for  $\text{CO}_2$ -reduction. From

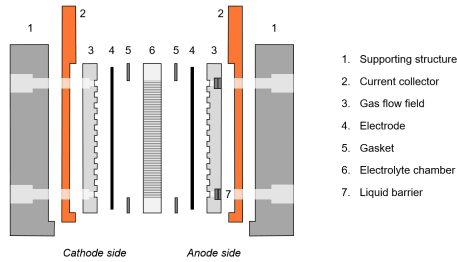


Figure 5.3: Simple cell assembly without gas for the first iteration of the flow cell. Parts (1-3) were from the predesigned cell, with indented slots for alignment. No GDEs were available for electrodes (4), so no gas flow was supplied through the back (1-3). Gaskets (4) ensured a tight seal between (3) and electrolyte chamber (5).

the left, (1) the first block is the *supporting structure*, manufactured in Al and oxidized for stability and electrical isolation. Then there is (2) a copper (Cu) based *current collector*, providing easy electrical access to the electrode. The third part (3) is the *gas flow field* with a meander structure made in titanium (Ti). These three parts have thin carvings or slots, in which each fit and provides guidance for correct placement and alignment. Gas is designed to be provided from the back side, so through the supporting structure all the way to the gas flow field, where a 1/4" tube hole just fit - if everything is perfectly aligned. This then requires a precise length adjustment of gas tube, such that with an o-ring, the tube would seal to the backside of the flow field. But as we would start testing the cell without gas, the holes in the gas flow field should be closed. On the cathode side, this was done by using large molybdenum (Mo) sheets as electrodes (4). These sheets would fill out the meander structure and cover over all the holes. On the anode side, the holes were instead filled with cut pieces of a 1 mm thick FFKM sheet (7), providing some leak tightness. Whether on the cathode or the anode, the *electrode* material was cut out to be slightly smaller than the gas flow field block. Hereby (5) a *gasket* could be fitted around the edge, and provide sealing to the surroundings. The gaskets were also cut out from a Kalrez sheet. These have worked brilliantly once the correct size and combination to the additional parts was found. In the middle (6) the *electrolyte chamber* was placed. Not only did the gaskets ensure a seal between the electrode side to the electrolyte chamber, but it also ensured that there would be no direct electrical contact between the two. Though it should have a surface coating of alumina, there could be scratches or small openings through this layer causing issues. After the electrolyte chamber, the cell assembly is mirrored, just for the opposite electrode instead. The entire assembly was then pressed together with eight screws, placed around the periphery of the supporting structure (and fitted holes in the current collector and electrolyte chamber respectively). Yet again, to ensure no unfortunate short circuits between the two electrode sides, the screws were isolated with PTFE tubes, covering both the screw, bolt and washer.

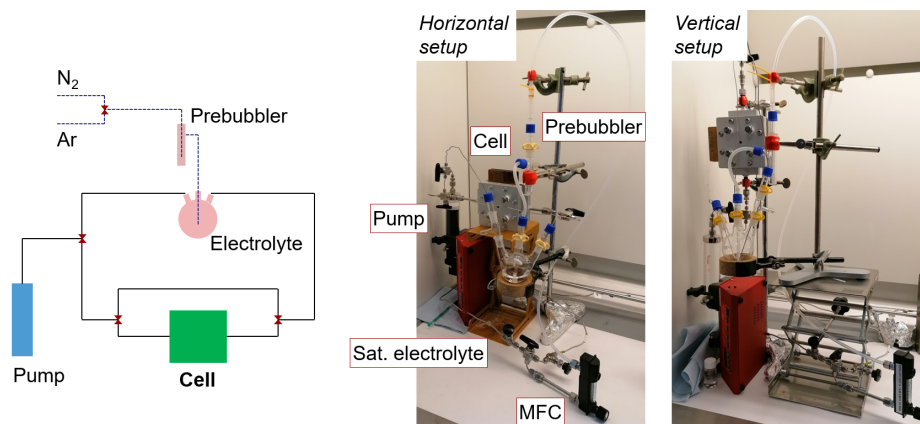


Figure 5.4: First flow cell setup built for nitrogen reduction experiment. Simple setup with no gas flow, but dependent on nitrogen saturated electrolyte. Schematics to the left showing the various components, and photograph of a horizontal and vertical positioned cell to the right.

The very first flow cell experiment we built is shown in Figure 5.4, with images on the right and a schematic on the left. Gas lines are sketched in dotted lines and electrolyte flow with solid line. The setup was built as simple as possible. The only gas flow was  $N_2$ , which could be replaced with Ar for blank tests. Gas lines were PTFE for flexibility, whereas electrolyte tubing was stainless steel. The gas was passed through a pre-bubbler, before entering an electrolyte sample unit. The pre-bubbler is a simple column containing THF, in order to wet the incoming dry gas. This can drastically decrease the evaporation rate of electrolyte, which otherwise can be substantial. The electrolyte sample unit was a glass based 3-neck-flask, with a volume of 100 ml. The three openings were for gas, and electrolyte in- and outlets. The wet gas then bubbled into the electrolyte, in order to pre-saturate this for electrolysis. The electrolyte was pumped around in 1/16" tubing, controlled by a 100 ml syringe pump. We included the possibility for by-passing the flow cell, in order to e.g. pump electrolyte out of tubing, without emptying the cell itself. The 3-way-valves are also marked in the schematics.

Before actually applying current through the cell, the setup was tested for being gas tight, and allowing electrolyte to flow. With this checked out, we were ready to hook up a power supply.

The first tests were done with a Mo foil as a cathode and a carbon (C) paper as the anode. C-paper was an easy way of getting a high area on the anode, and the two electrodes were tested beforehand in a standard glass cell. This test showed a stable current at set electrode potential for an hour, and yielded some 2-3% FE, which we found adequate for proceeding. The measurement is shown in Appendix Figure B.7. In the first iteration, we did not have a reference electrode in the electrolyte, as the original cell design had this included through

the back of the electrodes, in a somewhat similar fashion as gas delivery. This design choice, however, complicated the cell assembly procedure and was often the cause of electrolyte leaks. We therefore did the tests by applying -9 V of potential between the cathode and anode [34]. One could say this is a high potential, but with electrolyte resistance and high overpotential on the anode, this was to ensure an adequate negative potential on the cathode. The electrolyte was the exact same as Tsuneto et al initially reported, consisting of 0.2 M LiClO<sub>4</sub> in THF with 1 vol.% EtOH [39]. The very first test was done with an external power supply, which unfortunately could not register the low current, and we therefore did not know the amount of charge that was passed during the 20 min electrolysis.

We were skeptical about our test, but tried nonetheless to quantify the ammonia. And boy were we excited! We saw blue colour, and had successfully made ammonia. Comparing to a initial blank sample from before applying potential, we measured a concentration increase from 0.14 ppm to 1.74 ppm, corresponding to some 60 µg NH<sub>3</sub>. It is not a lot, but we had finally seen the first indication of success with synthesizing ammonia from N<sub>2</sub> with a flowing electrolyte. Many things were still missing, as we still relied on burning electrolyte for providing protons to the reactions and only having dissolved N<sub>2</sub> in the electrolyte. From the test, we also realized a simple improvement to the setup, in rotating the cell 90 degrees. This was due to the placement of the electrolyte in- and outlets in the chamber. By rotating the cell, the opening would be in the top and bottom of the chamber. Electrolyte would then initially fill the cell from the bottom. Before adding electrolyte, the cell would be flushed with N<sub>2</sub> or Ar. Filling the cell with electrolyte, would then push this gas out through the top. If gas is evolved during electrochemistry, e.g. HER, this gas would then also be pushed out with the continued electrolyte flow. After reaction when the cell should be emptied, electrolyte could be pulled out through the bottom again. The flipped version is also shown in Figure 5.4, with the only downside of the setup being overall much taller now. As it would turn out, the basics and principles behind this setup - using a syringe pump, the 3-neck-flask and tubes for interconnections - got to be overall defining characters for all following setups. Eventually I would make small adjustments to tube dimension and lengths for improved flow, but the ideas were already here seeded.

Following the successful first try we modified the cell direction and changed the power supply to a potentiostat, allowing recording of the potential and current applied. With similar electrolyte and electrodes the cell was run again, but this time in a quantifiable way. At 9 V total cell potential, the current density was only in the range of 1-1.5 mA/cm<sup>2</sup>, but about 10 ppm ammonia was measured afterwards, corresponding to about 5% FE.<sup>2</sup> We were quite happy with those results, resembling the performance of the standard glass cell experiments running parallel to these experiments at the time. Switching the gas stream to an Ar flow, showed no increase in NH<sub>3</sub> concentration during a similar experiment.

---

<sup>2</sup>See Appendix Figure B.8 for recordings

This was all going well, but then issues started to built up. After some successful experiments showing similar performance as glass cells, we started having reproducibility issues. Despite doing our best for setting the experiments up in the same way, the ammonia formation in the flow cell was not consistent, where some experiments had efficiencies around 4% and others below 1% FE.

As a first step for getting more control, we added a reference electrode to the electrolyte chamber. We could do this on the anode side, where we had a C-paper electrode. As mentioned, the reference electrode was inserted from the backside of the cell through the electrode and a small hole in the gas flow field. This solution was not optimal for our case, but we could make it work by isolating the Pt pseudo reference wire (similar electrode as used in glass cell experiments) with Teflon wrap, thereby avoiding short circuits. With the reference electrode, we could start making 3-electrode measurements, and have more knowledge on the actual potentials on both the cathode and the anode.

We also worried whether the reproducibility issues were caused by interference of oxygen and water. This was before realizing the benefits of small controlled amounts of oxygen to the lithium mediated NRR synthesis [46]. We were though aware that these could influence the process. So far we had counteracted this by presaturating the electrolyte with  $N_2$ , both for providing  $N_2$  to the reaction but also to flush out possible trace amounts of  $O_2$ . Prior to electrolysis, we also flushed the cell with either Ar or  $N_2$ , similarly to avoid presence of  $O_2$  in the cell. And we always made sure that cell parts were clean and dry to avoid water. Nonetheless, we could not exclude that trace amounts of water or oxygen could sneak in during experiments, e.g. when flowing around the electrolyte. To accomodate these concerns, we started setting experiments up inside an Ar filled glovebox. As described in Chapter 3, the presence of both water and oxygen can be kept below ppm range, multiple orders of magnitude lower than atmospheric surroundings. On the flip-side, working in a glovebox is also much more cumbersome. Unfortunately, running the cell inside the glovebox did not seem to solve the issues with reproducibility either. Only the initial LSV where scanning the potential cathodic, gave somewhat cleaner data, now that a reference electrode was included. But despite setting the cathodic potential according to the initial LSV procedure, it did not seem to run at an adequate current. This also followed with the total cell potential being around -6 V, taking the anode into account, which was lower than the 2-electrode tests at -9 V.

We then moved on to looking at the electrode. Namely the anode material. We knew C was not optimal for the reaction, as it is not an efficient catalyst for any anodic reaction in our system. Pt on the other hand, should be a prime candidate. An issue would though be to have a large area electrode of Pt, simply due to cost of such an electrode. Instead, we tried to sputter-deposit Pt directly on the block with gas flow field, providing a similar geometric area as the Mo cathode foil. Approximately 4-5 times increase in current density compared to other 3-electrode tests was now achieved, and the LSV showed some distinct and comparable features, as seen in some RDE measurements done parallel to this

work. But yet, still no consistent positive ammonia results.

### 5.5.1 Evaluation

By now we had a lot of experience with assembling the cell, and a reoccurring issue was the reference electrode, inserted from the backside. This led to a modification to the chamber, such that the reference could be inserted from the side instead, directly into the electrolyte compartment. This would alleviate leaks through the multiple layers in the cell with the original design, and instead only lead to a single opening in the chamber. Another issue we could handle here, was the guidance carvings for electrode and current collector placement. These were slightly increased, for easier placement and fitting. As we were now doing modifications, we chose to start focusing on the gas compatible electrodes too. We knew it was a necessary step, and dealing with experimental challenges was starting to be a daily activity. So now was as good a time as any.

The design we started discussing consisted of a number of layers and small parts. Since we had observed the organic electrolyte would leak through the electrode materials we used, we wanted to add a stopping layer of thin PTFE. If porous and enough pressure is applied, gas should be able to diffuse through, while electrolyte does not penetrate. On top a thin porous metallic electrode could then be placed, allowing both gas, electrolyte and electricity. An additional *mask* around the periphery could then be placed on top, to keep everything in place, while gaskets should ensure it to be leak tight. The envisioned layered structure is shown in Figure 5.5. We foresaw some possible issues with this design. Namely the electrode would easily be effectively flooded, meaning electrolyte would fill up the porous structure, also opening up the possibility for depositing Li deep inside those pores. Neither were we sure if the gas supply through a PTFE sheet would be a viable solution, and how the mechanical stability of it would be in the cell. We therefore came up with two versions of this second iteration. A mask solution for thin porous metal sheets ( $\sim 100\ \mu\text{m}$  thickness) and one for thicker metallic porous disks (2 mm thickness, 1.5 inch diameter). This would allow us to try different designs and porosity, and see if either would be beneficial.

In the workshop order, we also included a replacement of the gas flow field for the anode side, making space for a dedicated chamber for the anode reaction. This was to investigate if it was necessary to have separate electrolyte chambers for each half cell reaction, i.e. including a membrane between the two electrodes. The motivation for this was two-fold. Partly (hoping) if  $\text{NH}_3$  concentrations got so high, that anodic oxidation could start to play a role. Though, we knew this was still far from being the case. Secondly, we knew electrolyte decomposition was happening during the current production, but whether the decomposition products had a negative effect on the  $\text{NH}_3$  synthesis was unclear.

While waiting for the new parts to be manufactured, tests continued with the current cell parts. One alteration to previous experiments, was replacing Mo with Cu foils on the cathode, although still dependent on using presaturated

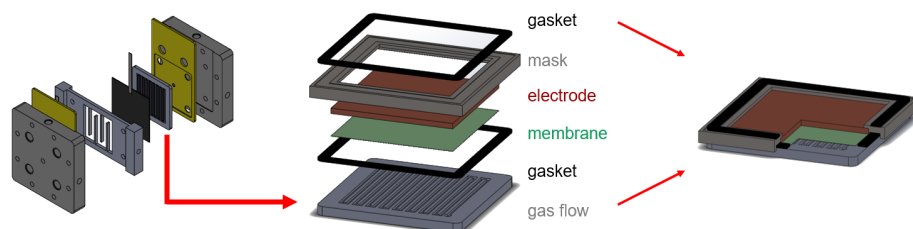


Figure 5.5: Envisioned layered structure for gas diffusion electrodes in the second iteration of the flow cell. A mask would be used to keep electrode structure in place, and gaskets inserted for making the structure leak tight. With an additional membrane only allowing gas penetration.

electrolyte. The now clean LSV profiles we could record, showed clearly different behaviour on Cu compared to Mo (see e.g. Appendix Figure B.9 for recorded LSV), but no major differences in efficiency when experiments worked out. These still yielded results in the order of 3-5% FE, in line with the Mo results. The waiting time was also spent on trying different flow variations out. To see if there would be any noticeable effect of only flowing the electrolyte one way through the cell, or flowing it backwards as well. Also various flow speeds were tested. No obvious improvements were seen from either of these. With regards to the flow rates, this might have been due to too small variations in flow speed. From the flow direction, the trend seemed to point towards a negative effect of time the electrolyte spent "open" to surrounding gas. The experiments were carried out in an Ar glovebox, but as the electrolyte was flowing back and forth, whenever it got collected, it was collected in a vial open to the Ar atmosphere. This was different compared to the closed loop presented in Figure 5.4 with the first iteration, which was done in a fumehood. In the glovebox, space restrictions limited the options for doing the same setup. All this meant, that for each pass, the electrolyte was slowly deaerated of  $N_2$ , and thus  $N_2$  availability decreased over time. Yet another point for pushing on improved gas delivery directly to the electrodes during electrolysis.

Finding suitable membranes for possible future 2-compartment measurements also needed to be done. We did a series of test on two different membranes, before this was commenced. For starters, we tried some *Celgard 3401* membranes [110], which we had prior experience with in our group [34]. Meanwhile, Lazouski et al. [47] had published work on the lithium mediated process, using a *Daramic 175* polyporous polyethylene separator from the lead-battery separator company Daramic [111]. These were tested both in a glass H-cells, i.e. a two-compartment glass cell setup with the membrane separating each compartment. But also in the flow cell. The flow cell tests were done by adding a 5 mm alumina spacer, which we by chance had lying around, into the cell assembly. The spacer had a circumference of similar size as the electrolyte chamber, so by adding a gasket on both sides of the spacer, the membrane could be placed between the

electrolyte chamber and the spacer. The spacer formed in this way a secondary chamber for the anode. By carefully puncturing tiny holes in the corners of the membrane, the secondary anode chamber could be filled together with the cathode electrolyte chamber (see Appendix Figure B.10 for an image of this). The conclusion of the work, was that the membrane added too much resistance between the electrodes. Hereby requiring much higher potentials applied, to compensate for the IR-drop.

After some waiting the new parts finally arrived. The calendar said March 2020. "Covid" and "corona" quickly became a part of everyone's vocabulary.

## 5.6 Second iteration

With access to laboratories again, the first thing needed to be done was cleaning and anodizing aluminium parts again, after they had been modified from the workshop. The next task at hand was to prepare and fit the reference electrode in through the side. We came up with a custom made solution, drilling a thin hole through M2 sized PEEK screws,<sup>3</sup> through which a Pt wire could be placed and then had to be tightened for leaks. See Appendix Figure B.11 for an image. Having the reference inserted from the side, was a huge improvement for the setup, but did require periodic adjustments and remakes of the M2-screw/Pt-wire solution after a number of experiments.

It is always exciting having new equipment to work with. And the first thing to do, was to ensure that the new setup was tight. With the new mask in play additional gaskets had to be added. Meanwhile, Lazowski et al. had managed to publish another great work on the lithium mediated synthesis [44]. This time, incorporating gas diffusion electrodes to work with the non-aqueous electrolyte - so exactly the same challenge we were dealing with. Their cell design was vastly different than our approach, but their electrode solution was very similar to the one we had envisioned to start working with. Apart from showing us we were on the right track, they also inspired me for an experimental test setup to look at the electrode under operation. At least to have a visual inspection of how the electrode would work when flowing gas over it. Seeing the electrodes during operation was otherwise not possible with our flow cell, since the electrodes are buried deep in the assembly. But inspired by the recent publication from Lazowski et al, I only assembled half the cell including electrode and electrolyte chamber, and closed the other end of with a glass plate. This allowed me to watch the electrode (from the electrolyte side) while filling the electrolyte chamber with a liquid (for safety concerns I used EtOH) and flowing gas from the opposite gas side.

A schematics and image of this is shown in Figure 5.6. The half-cell stack was pressed together with clamps as shown in the image. The assembly had to be

---

<sup>3</sup>M2 screws are 2 mm wide in diameter. We drilled out holes <1 mm in diameter through.

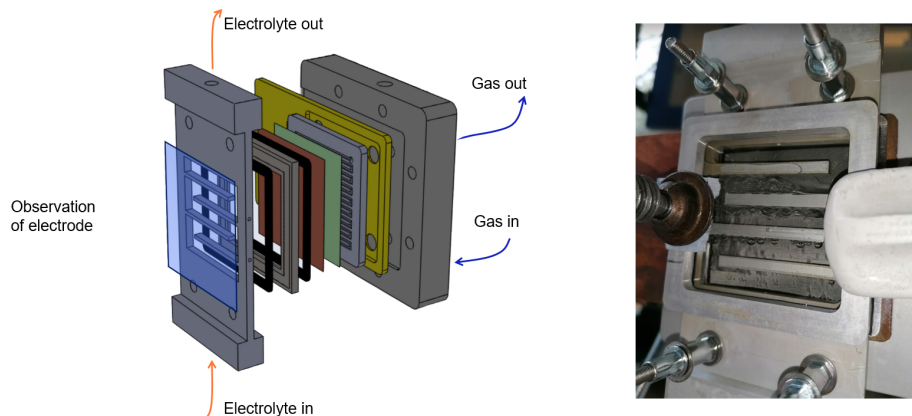


Figure 5.6: Schematics and image of a half cell setup, making it possible to look inside the chamber while flowing gas and electrolyte through the chamber.

pressed very hard together, and in order not to shatter the glass plate, a square frame was used to distribute the pressure around the edge. With this homebuilt setup, we could learn a couple of important things. On the image shown in Figure 5.6 we tried using the same electrode material, as was proposed by [44], and confirmed that this could work - also in our setup. The electrode here is a stainless steel mesh, with  $325 \times 2300$  grid wires per inch and  $5 \mu\text{m}$  pores. We also tried the porous disks mentioned earlier, bought from McMaster-Carr [112]. The meshes and disks are originally intended for particle filter applications. We also had some other meshes, that were thinner and with larger pores. But based on the initial test on C-membranes, and how easily THF could penetrate them, these thinner and semitransparent meshes were not used. When no pressure was applied to the gas stream, the liquid would flow through the mesh and fill up the gas channels. But by increasing the backpressure on the outlet gas, we would eventually see liquid be pressed out of the gas channels, to the point where gas bubbles were forced through the mesh. This is the case shown in Figure 5.6, where a lot of bubbles are observed. This then also gave us another piece of information. Namely, that despite the electrode only being  $50 \times 50 \text{ mm}^2$ , the hydrostatic pressure difference in the top of the cell compared to the bottom of the cell, was large enough to impact how easily the gas could pass through the mesh. As observed, only few and very small bubbles are seen in the bottom, whereas the bubbles are large towards the top. But when pressure was applied, we were able to have gas flowing out of the gas outlet, without liquid following along.

Realizing these electrodes together with an adequate backpressure could be used for separating liquid and gas, was a big step. This suggested we finally had a possible solution to apply gas directly to the electrode in the flow cell. The challenge still remained of keeping control of this balance, as depicted in Appendix

Figure B.12. The necessary backpressure to force gas through the electrode was approximately 50 mbar, measured using a pressure gauge in the half-cell tests. Knowing this, I could now try to implement this in the full assembly of the flow cell. Knowing that including gas pressure would add to the complexity of mechanisms happening simultaneously, the first focus was only adding one single gas stream. And for the first time, I managed to add liquid from the bottom of the cell, while having a gas flow from the side over an electrode, and see the liquid pushed out in the top of the cell, without any dripping or spill from the gas outlet. From here, I started in steps adding more and more gas and electrolyte tubes to the setup, to improve on flow and sampling possibilities. Also the gas outlet tubes were modified, and the necessary pressure drop could be realized by long 1/16" tubes and a small glass vial filled with water.

The next thing was to start applying current to the cell with gas flow. I continued only having  $N_2$  gas flowing, where I managed to increase the current density from 1 to 4 mA/cm<sup>2</sup>, and pass a significant amount of charge. Unfortunately, high efficiencies did not follow along. Only 2-3 ppm ammonia was made corresponding to <1% FE. But a lot of electrolyte decomposition was seen. Repeating this continued presenting some issues. Now the electrodes and electrolyte chamber were visibly affected by the electrolysis happening. Lithium deposition on the cathode suggested that the porous structure, maybe could be filled and block the access of  $N_2$  to the reaction (see Appendix Figure B.13). Since  $H_2$  was not used in these experiments, a stainless steel block replaced the gas flow field on the anode side, such that no holes could give leaks. The block was then sputter deposited with Pt, in order to work well for oxidation reactions. This electrode was visibly damaged after the electrolysis reactions, with a substantially darkened surface. Furthermore, the electrolyte chamber itself was affected on a macroscopic scale, where the surface contacting electrolyte, was roughened as if it had corroded. The side of the chamber (including the reference wire) facing towards the anode was coated with a thin brown layer. This suggested that a lot of side-reactions had happened on the anode, possibly both electrolyte decomposition but also some oxidation reaction with the anode electrode. Since the electrolyte chamber was electrically isolated from the rest of the setup, some chemical reaction had happened there. These observations are summarized in Appendix Figure B.13.

With regards to the electrolyte chamber, the observed surface texturing hinted towards the alumina oxide layer begin incomplete, possibly as a result from multiple times forming the alumina. To have a perfect and fully covering layer, it is important the surface is clean. This requires polishing and pretreatment in alkaline conditions, prior to the oxide formation in acid. It is very possible that, when the chamber was reanodized, an even and well distributed alumina layer was not accomplished. This makes the chamber prone to deterioration in the electrolyte, due to missing a protective layer. Once again, the electrolyte chamber had to be cleaned down and reanodized, hoping for a better result.

The reaction on the anode pushed us to find new ways for introducing Pt electrodes, and we opted for sputter deposit Pt on the stainless steel mesh, as was

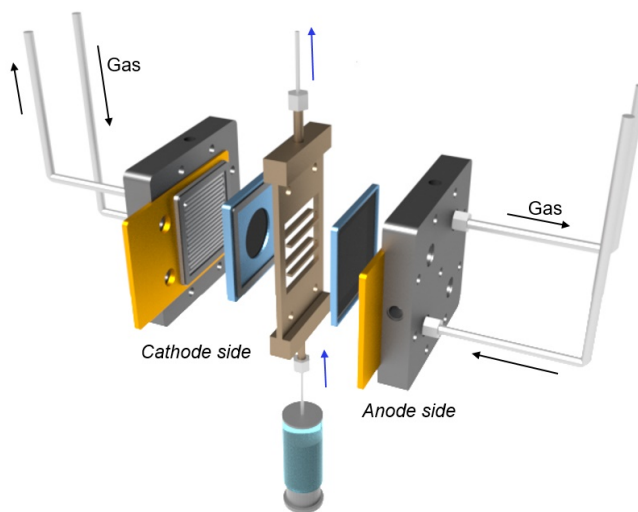


Figure 5.7: Model of the one-compartment second iteration flow cell, flowing gas over both electrodes while flowing electrolyte with a syringe pump.

seen to work with gas flow. The hope being that combined with a  $\text{H}_2$  flow, HOR could be achieved instead of electrolyte oxidation.<sup>4</sup>

We had gotten two different electrode setups prepared and manufactured from the workshop. One based on a thin film or mesh electrode - now dedicated for the anode. And one based on thicker porous disks. The porosity of the disk was chosen to be comparable to the implemented mesh. W.r.t. particle size filtering both the mesh and disk was specified for filtering down to  $5\ \mu\text{m}$  particles. Moving forward was therefore to combine flow of two gases in the electrode. Both on the cathode and also on the anode. We already had gotten some experience with applying backpressure to the gas line, in order to separate gas and liquid. With two gases flowing, it was not possible to look inside the cell, but by doing tests with EtOH and compressed air, a leak tight setup was achieved, Figure 5.7. The porous disk setup was slightly different compared to the thin mesh, and additional gaskets had to be added, to make sure gas and liquid stayed the correct places. By increasing the  $\text{N}_2$  backpressure, some ammonia started to form. But only at around 1-2% FE, so  $\text{N}_2$  availability still seemed to be limited. But it encouraged us to attempt longer experiments and pass more charge. This certainly pushed the setup to its limits, and a number of issues started to arise. First, clear indications of leaching was observed from the stainless steel masks, leaving a thick and dense black deposit on top (Appendix Figure B.14). The electrolyte after electrolysis also got a dark-yellow tint, very similar looking to

<sup>4</sup>I here refer to the previous Chapter 4, for a discussion on HOR and HER in non-aqueous electrolytes.

THF solutions containing ferrocene.<sup>5</sup> If cyclic voltammograms were recorded on the cathode, no clear features were observed, but the resulting current-voltage curve would give a nearly completely straight line, as one normally would see if recording a CV on a resistor, since from Ohm's law we know  $U = R I$ . This made us fear there was some major short circuits in the setup, with a number of possibilities. My main concern regarded the connection of gas lines, as these were stainless steel tubes, potentially making a short from the electrode to the supporting structure. From the previous issue with the electrolyte chamber, it was also plausible that there could be a short between either of the electrodes to the chamber. And on top of all these issues, we could not see any difference whether there was Ar or H<sub>2</sub> flowing over the Pt sputtered anode. In both cases, the anode potential would be at around +4 V, which is a very anodic potential, where the electrolyte is being oxidized. A number of steps were therefore tried out. Gas lines and some of the electrolyte tubes were replaced with PTFE tubes of same dimension. Unfortunately with no improvement, suggesting that the metal lines did not cause any short. After discussions with my colleague Jens-Peter Haraldsted, he suggested that use of ClO<sub>4</sub><sup>-</sup> ions from the lithium salt and the battery-like conditions, could cause problems in the setup [113–115].

After the many problems we started experiencing with the Al based electrolyte chamber, we wanted to change the material to PEEK (polyetheretherketone). This is a semi-crystalline thermoplast, with excellent chemical stability, but less rigid than Al. With the chamber in PEEK, there would be no risk of short circuits and there should be no chemical reactions happening. Having a new chamber produced, we therefore started redesigning the chamber from scratch, fixing as many issues as possible. The new design we came up with is shown in Figure 5.8. The main difference with this improved design compared to the original version, is the position of the electrolyte in- and outlets. On the new design, these are placed in the same side, with access to a corner. Connecting the in- and outlets to the corner positions, was chosen in order to have easier extraction of gas and liquid from the cell. If gas bubbles were formed inside the chamber, for instance from pushing gas through the electrode or having much gas evolution (e.g. HER on the cathode), this gas would seek upwards. Having the electrolyte outlet in the corner, would ease pushing this gas out of the chamber again. From the lower corner connection, it would be much easier to pull out all electrolyte from the cell, compared to accumulating left-over electrolyte drops in the center of the cell. Insertion of the reference electrode was also vastly improved with this design. Where the previous solution was based on custom made holes in tiny M2 screws, this was accomplished with flangeless nuts. The reference wire could be made leak tight, by fitting a 0.5 mm Pt wire through a 1/16" PTFE tube with 0.5 mm inner diameter. Together with ferrules fitting the nut, this could then be inserted between the electrolyte in- and outlet. To avoid reactions with the stainless steel masks, these were spray coated by a Teflon Amorphous Fluoropolymer solution. Together with the new PEEK based chamber, the only electrical surface now was the electrode mesh on the anode and

<sup>5</sup>A comparison is shown in Appendix Figure B.15

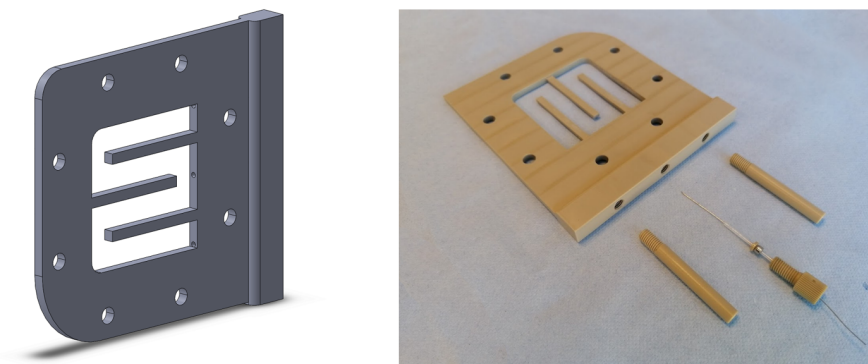


Figure 5.8: Second iteration of the electrolyte chamber made in PEEK. New position of in- and outlet and dedicated space for reference electrode.

the porous disk on the cathode. This was seen from only having Li deposition on the porous disk (and nothing on the mask) after an electrochemical reduction in the electrolyte, and that the measured impedance had increased. The increase in resistance comes from less electrode area, which scales inversely with the cell resistance. The electrode area of the disk electrode is smaller than square mesh electrodes.

$$R_{drop} = \frac{1}{A_e} \frac{d}{\kappa} \quad (5.1)$$

where  $R_{drop}$  is the ohmic drop,  $A_e$  is the electrode area,  $d$  is the distance between electrodes and  $\kappa$  is the conductivity of the solution [116].

With the coated masks and PEEK based chamber very small features started to arise from the CV. But still not nearly as clearly as had been recorded in earlier stages of the process. And despite seeing deposited Li on the porous disk,  $\text{NH}_3$  was still not synthesized in appreciable amounts. Previously we had seen the metallic mesh to work, and fresh batches of Pt sputtered meshes had been prepared. So the only thing left that could cause the issues, was the thick porous disk. To determine if this was the cause of the issue, the disk was covered by a thin sheet of Cu. This blocked the access to  $\text{N}_2$  from the back, so an experiment with  $\text{H}_2$  on the Pt anode and  $\text{N}_2$  saturated electrolyte was performed. Finally a clear blue colour was seen from a flow cell experiment again, where 3 ppm and nearly 200  $\mu\text{g}$   $\text{NH}_3$  was synthesized, corresponding to 3.8% FE ( $\pm 0.1\%$ ). This was perfectly in line with a control glass cell experiment with the same Cu foil, yielding 4.1% FE. Main difference between the two experiments being the much smaller anodic potential in the flow cell experiment, where  $\text{H}_2$  had been present. The two experiments are summarized in Appendix Figures B.16 and B.17 This strongly indicated the porous disk was the cause of the issue.

After the synthesis work with a Cu foil, I tried electrodepositing Cu on the porous disk, following a similar procedure as my helpful colleague Katja Li had

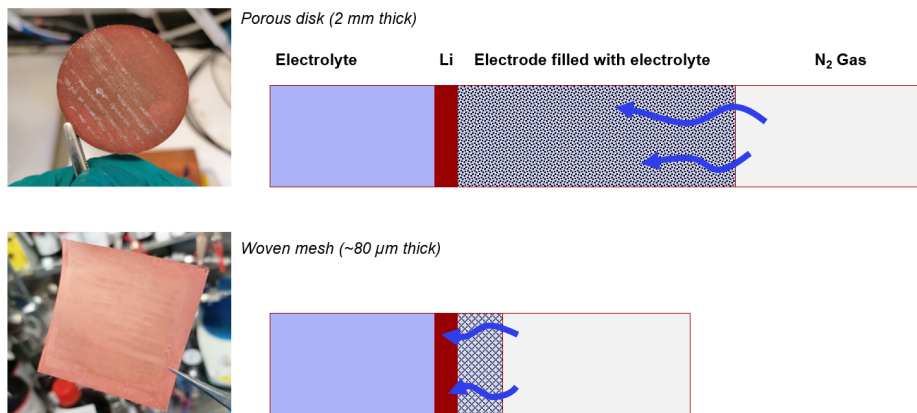


Figure 5.9: Effect of electrode thickness. The thick porous disk turned out to be flooded with electrolyte in the chamber, leaving trace of dry salt on the gas side of the electrode. The flooded disk blocks access of  $N_2$  to electrodeposited Li on the opposite side. Switching to thinner electrodes would allow  $N_2$  to reach the active side of the electrode.

used for high surface area electrodes [117], see Appendix Figure B.18. With the somewhat increased electrochemical surface area on these Cu-deposited electrodes, a higher Li-salt concentration of 1 M compared to previously 0.2 M was also used. These attempts unfortunately did not bring along  $NH_3$  synthesis. But I learned something very important from it.

Figure 5.9 shows an image of a Cu deposited porous disk, after an attempt of electrochemical nitrogen reduction in the flow cell. The photographed side was facing towards the gas meander structure, i.e. away from the electrolyte but on the gas phase side of the electrode. The visible lines are dried electrolyte and thus the leftover Li-salt. This had dried where the grooves in the gas flow field were, showing me that electrolyte had flooded through the porous disk. And due to the flow of gas in the meander structure, dry salt was present there afterwards. This meaning, that though the reduction reaction happens at the electrode-electrolyte interphase, this should mainly be at the side of the electrode facing towards the chamber. But due to the electrode being flooded, the  $N_2$  is not present where the Li is being deposited, and therefore no  $N_2$  reduction reaction.

The solution to this seemed straight forward. Stop using the thick porous disks, and use a thinner electrode instead. We already had a thin electrode material lying around - namely the meshes used at the anode. At this time in our  $NH_3$ -group, Cu deposition for getting higher electrochemical surface area was a popular thing, and following the fairly good results seen on the Cu foil, I continued along this road. Now with Cu deposition on the thinner mesh. Now using two of the meshes as electrode, we did not have enough of the dedicated masks, that we had gotten manufactured to keep the mesh in place. Luckily, we realised that it was possible to fix them directly to the electrolyte chamber, with a gasket

along the edge. An added benefit to this, was a shorter distance between the electrodes. The total cell resistance was now substantially smaller than initially, as a result of (1) large electrode areas, since I used the full chamber cross section with the mesh electrode, (2) higher Li ion concentration and thus higher electrolyte conductivity, and (3) shorter electrode distance. As discussed with equation (5.1), all these factors help to decrease the cell resistance, and thus potential drop. The cell resistance in the first measurements with two gasses flowing, were in the order of  $300\ \Omega$ . The cathode was a porous disk with an area of about  $8\ \text{cm}^2$ , the Li concentration was  $0.2\ \text{M}$ , and the electrode distance was  $\sim 8\ \text{mm}$  including masks and gaskets. With Cu deposition on the disk and increased Li concentration at  $1\ \text{M}$ , the cell resistance decreased to about  $50\ \Omega$ . Changing the cathode to a mesh with a higher area of  $25\ \text{cm}^2$  and a shorter electrode distance of  $\sim 6\ \text{mm}$ , the resistance decreased further to about  $6\ \Omega$ .

The big moment was to see if the thinner electrode would help as hoped. With the increased area from Cu deposition and much thinner electrode, I managed to run the flow cell at the highest permitted current the potentiostat could provide, giving  $9.6\ \text{mA}/\text{cm}^2$  with a low anodic potential well below  $+1\ \text{V}$ , suggesting that the Pt anode was reacting with  $\text{H}_2$  doing HOR, though we at this moment could not confirm this. But more importantly, I measured 5% FE with a clear blue colour from the indophenol reaction. And even better, I could repeat the experiment, and multiple times see FE above 5%. This was like a *eureka moment* for me, as I now finally understood why I for so long had not seen the expected positive results. The electrode choice had been wrong, not giving the high  $\text{N}_2$  availability as planned for.

Since the gas flow was continuously bubbling through a small water column for the backpressure, I could easily take samples during experiment, and monitor how much ammonia got trapped from the gas phase. Sampling for the electrolyte was not as easy - though somewhat possible. But  $\text{NH}_3$  measurements throughout a reduction was a possibility. This turned out to work very well, even when just using ultrapure water as the trap, since water is fairly good at uptaking  $\text{NH}_3$ . It even works so well I completely underestimated the amount of  $\text{NH}_3$  I would find in the gas phase during a NRR experiment in the first attempt. The concentration was much higher in the gas trap than I prepared the indophenol reagents to measure on. The best way to put this electrode setup and  $\text{NH}_3$  synthesis to the test, was to start doing long experiments and passing a lot of charge. The first such experiments are shown in Figure 5.10.

As shown, electrolysis for some 50 minutes at current densities up to  $10\ \text{mA}/\text{cm}^2$  was done passing approximately  $700\ \text{C}$  in total. At the end of the experiment about  $400\text{-}450\ \mu\text{g}\ \text{NH}_3$  was measured from the water-based gas trap downstream on the  $\text{N}_2$  gas outlet, while about  $750\ \mu\text{g}\ \text{NH}_3$  was measured in the electrolyte. The amount of  $\text{NH}_3$  from the gas may have been underestimated, due to using water and not acid in the gas trap. These two measurements were fairly consistent, and show a significant amount of  $\text{NH}_3$  present in the liquid phase, but also in the gas phase. In both cases, the anodic potential was in the range

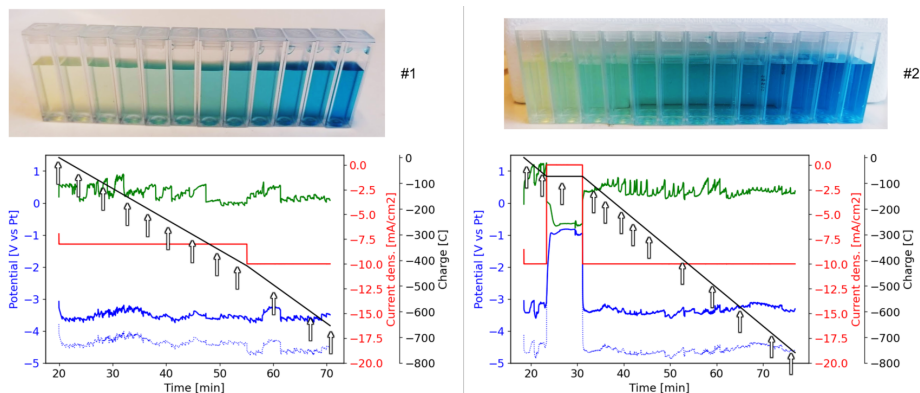


Figure 5.10: Long nitrogen reduction experiments in flow cell, with  $N_2$  and  $H_2$  flowing over the cathode and anode respectively. Taking samples from a gas trap on the  $N_2$  outlet, shows a continuous increase of ammonia from colour development as charge is passed. Notice the duration ( $\sim 50$  min) and amount of charge ( $\sim 700$  C) passed. Experiments labelled *FC314* and *FC315* respectively. Cathode (blue, solid line is IR-compensated for about 5 s), Anode (green), Current density (red), and Charge (black). Potentials measured vs Pt pseudo reference.

between 0 and +1 V vs the Pt pseudo reference. Anodic reaction products were not quantified, but the potential was markedly lower than normal experiments - compare e.g. to the Cu foil experiment in Figure B.17 with anode potential  $>2$  V vs Pt. Both measured and compensated cathode potentials are plotted, with an IR-drop correction to the cathode of about 1-1.5 V, determined from initial PEIS measurements of 4-5  $\Omega$ . From here followed a long line of tests with different Cu deposition conditions. And realization that the Pt sputtered anode electrodes periodically had to be replaced with freshly sputtered electrodes.

## 5.7 Third iteration

Parallel to my work on the flow cell, we had in our ammonia group made a lot of progress on the fundamental understanding of the lithium mediated process and how to improve it. This came in the wake of the work, initially led by Suzanne, testing out the effect of  $N_2$  pressure, where much higher efficiencies towards  $NH_3$  were measured [45]. At increased pressures, we noticed more pronounced effects to the  $NH_3$  synthesis efficiency, from variations to the synthesis and conditions hereof. This led to testing the effect of variations in the reaction atmosphere, which ultimately led to the discovery of oxygen enhancement to the process [46]. With a setup for the flow cell that started to show promising results and continuous ammonia synthesis, we wanted to implement these "tools" for efficiency improvements we had found out so far. I.e. increasing the pressure, including oxygen to the gas flow [46] and do potential cycling on the electrodes [45]. Other variations and modifications to e.g. the electrolyte were possible

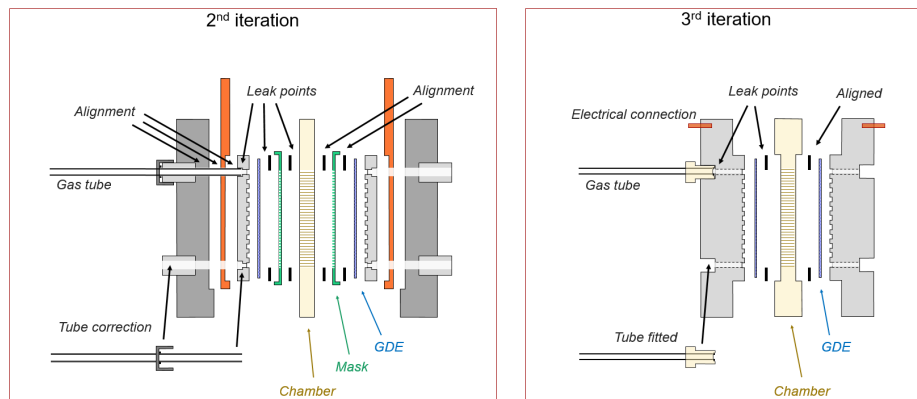


Figure 5.11: Schematics diagram of the second and third iteration of the flow cell, with highlights on the potential leak points and alignment issues. In the third iteration multiple elements are combined in single parts, simplifying the assembly and reducing risk of leaks.

pathways as well.

Increasing the pressure would require modifications to the cell, due to potential leaks. Already at the current stage of the second iteration of the flow cell, it was cumbersome and tedious work to ensure a leak tight cell just at 1 bar. Both with regards to gas and electrolyte. This was due to the multiple layer assembly, both from the preexisting cell, but also on the layered structure at the electrode. In short, every part in an assembly can present a possible leak. If we should increase the pressure to 2, 5, 10 or maybe even 20 bar pressure, this would not be possible. In Figure 5.11, potential leak points are highlighted for the second iteration flow cell.

As highlighted in Figure 5.11, there were many places that presented challenges for the second iteration assembly. For one, the three parts from the predesigned cell, i.e. supporting structure, current collector and gas flow channel, all had to be perfectly positioned and well aligned. If not, feedthrough of gas tubes (with a very specific length) from the backside, would not fit to the gas flow channel connection. This would lead to gas leaks and consequently an uncontrolled pressure loss, which in turn would be detrimental for the gas-liquid separation control. With the multiple layers of electrodes, we used gaskets at every interface of two hard surfaces (metal or PEEK). This was important in order to ensure the cell being tight with regards to both gas and liquid, e.g. when flushing the cell for atmosphere control or when filling the cell with electrolyte. A problem with needing multiple gaskets, was to ensure good alignment of each, and that these during assembly would not slide to one-another.

At this point, my colleague Sarah Shapel joined the discussions with fresh eyes on the design. From these discussions, we came up with a rather new design concept, vastly simplifying and hopefully improving the cell. The solution is

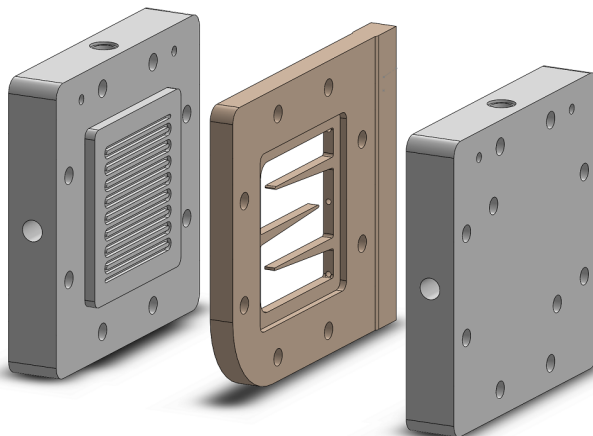


Figure 5.12: 3D model of three main components of the third iteration of the flow cell. The supporting block has embedded gas flow channels and acts as the electrical connection point as well. The electrolyte chamber has built-in masks for easy alignment and positioning of electrodes.

presented schematically in Figure 5.11 and as a 3D model in 5.12. The solution was to combine parts and thus have fewer components and connections. From the preexisting cell, the supporting structure, current collector and gas flow field, were all combined in one single piece, with gas channels embedded within. With the new design, gas connection is tightened at the outside, using a similar flangeless screw connection, as we had had success with, for the new reference connection in the second electrolyte chamber design. This is in contrast to the original design, where gas tubes had to be aligned through the backside of the cell, all the way to a connection (with gasket) at the gas flow field. The difference regarding gas tubes and delivery is also schematically shown in Figure 5.11. Electrical connection is done directly to the outer supporting blocks, which requires that the cell is not placed on a conductive medium or plate during operation causing a short circuit. The electrode positioning with masks are now embedded into the electrolyte chamber. Thereby the previous two masks and one electrolyte chamber is also combined into one piece. Alignment is thus intrinsically ensured as well. With this new improved design, there is only one interface at each electrode side, thereby effectively decreasing the risk of leaks. And as an added benefit, simplified assembly tremendously.

This was the third (and for now final) iteration of the flow cell, which should not only allow gas and liquid flow - but also doing this at elevated pressure.

## Chapter 6

# The electrochemical flow cell

This chapter concerns the operation and measurements of the flow cell we have built. With the flow cell operating with both liquid and gas flow on  $25\text{ cm}^2$  electrodes, we initially only did measurements with a potentiostat combined with ammonia quantification as described in chapter 3. To gain more insight to *in-situ* operation, the transportable mass spec *Garm* was built. Unfortunately, *Garm* was not operating until six months before my PhD project terminated. This set limitations to the extent of quantification and measurements possible, at the time this thesis was handed in. Despite not fully quantified, more knowledge and interesting trends were observed, and will be discussed in the following.

### 6.1 Objective for the experiments

While the third iteration flow cell was being produced (see previous chapter 5.7), we had two subprojects going on.

First of all, we continued doing measurements with the second iteration cell, as gas and liquid flow now was possible. The first measurements were presented in the previous chapter in Figure B.8. With this flow cell, we now had a lot of possibilities to explore. But first of all we needed to get reproducible measurements at higher ammonia yields. As shown in Figure 6.1 and Appendix Figure C.1, as more experiments were done, the efficiency was not impressive. The electrodes used as GDEs, were fine stainless steel (SS) meshes, with a mesh size of  $325 \times 2300$ . The anodes were sputter deposited with Pt, while the cathodes were electrodeposited with Cu.

The synthesized ammonia was both measured from the gas phase and the electrolyte phase. The sum of these, were only around 2-3%. What was interesting

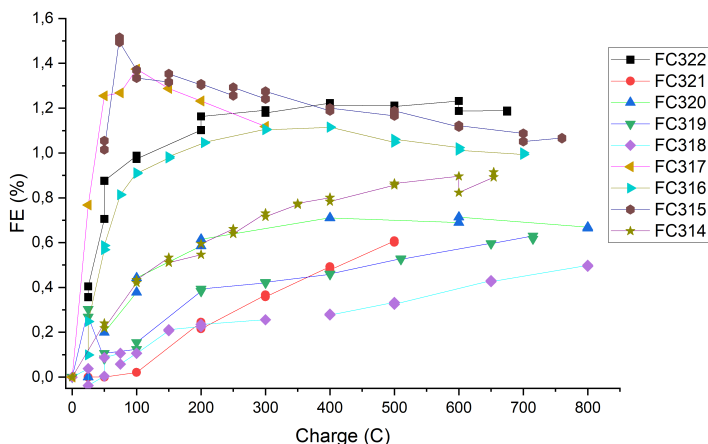


Figure 6.1: Faradaic efficiency calculate for multiple experiments with gas and electrolyte flow in the flow cell. Numbers represent the FE towards  $\text{NH}_3$ , based on measured concentration in gas trap from  $\text{N}_2$  flow. Measurements from the electrolyte, showed similarly scattered performance (Figure C.1).

though, was the relatively low anodic potentials we - for the most part at least - measured during electrolysis. An example is given in Appendix Figure C.2. We expected this to be due to the presence of  $\text{H}_2$  gas on the positive anode, making much more facile HOR possible. Pt can oxidize  $\text{H}_2$  at negligible overpotentials (at least in aqueous conditions [37]), rather than having to go to electrolyte oxidation potentials at approximate  $+0.8$  V compared to HOR [87]. The hope was, that protons could be provided from a hydrogen source, which in this case is  $\text{H}_2$  gas.<sup>1</sup>

With the current setup, we did not have the possibility to measure if HOR provided  $\text{H}^+$  to the reaction, as we during electrolysis only controlled and measured the electrode potentials, and applied current. It would require additional equipment to follow the source of atoms in the reactions. Knowing where the atoms arose from, might give us some insights to why the anode potential sometimes was low, and other times were high.

We did have some techniques available, which for instance was used in some of the other studies, mentioned in Chapter 4. The reason, these techniques had not been used together with the flow cell measurements, were twofold. The electrolyte has to be compatible with the technique. E.g. with fluorine (F) containing electrolytes, such as  $\text{LiBF}_4$ , the F can easily react with H and form the

<sup>1</sup>Other hydrogen sources could also be thought of, which from an economical view might be more interesting. E.g. water is a cheap commodity. But then an additional 1.23 V (plus overpotentials) has to be paid, to split water via electrolysis [93]. In the end, knowing the optimal source is a complex picture [85], but as a first point, we want to not sacrifice the electrolyte.

strong acid HF. This is for instance the issue for GCMS measurements, where the liquid initially is heated up. This speeds up thermal decomposition and formation of HF, which is non-compatible with the internal tubing system. So far, we had not used  $\text{LiBF}_4$  with the flow cell. But this turned out to be a limitation in later flow cell experiments, once we started changing the salt and electrolyte composition. Another reason, for not implementing the techniques, were the inconsistency of measurements. Though we tried preparing and setting up the experiments in the same way, we would not always get the same results. Without control of the process, we would not be able to correlate one measurement to the other. Furthermore, with high anodic potentials, the decomposition of electrolyte would yield a viscous fluid. This could even turn nearly completely solid, within a few days. Unless very good timing between one measurement to the other, the following characterization could measure on a different compound, than was initially formed during the electrochemical reaction. And with regards to NMR measurements, as part of liquid preparation prior to characterization, a reference compound is added. This is required to correlate the chemical shift to a known substance. And in order to trap formed ammonia in solution, an acid is added (to trap it as  $\text{NH}_4^+$ ). If we want to follow the source of protons, these protons can exchange with the added acid, thus blurring the measurement.

We had to be able to monitor the evolution of products *in-situ* during reaction. A candidate for this, which we at SurfCat have a lot of experience with, is mass spectrometry (MS). In the ammonia group, we already had a project going with MS measurements in non-aqueous electrolytes for  $\text{NH}_3$  synthesis, in collaboration with SpectroInlets [58]. The setup is completely different from the flow cell. In these studies, the MS sniffer is directly linked to a thin layer of electrolyte, close to the position of the working electrode. This is made possible, using an engineered membrane to maintain a vacuum for the MS. Such an arrangement would not be possible with the flow cell, but MS measurements could be very useful. It would for instance make it possible to follow where protons are arriving from, by carefully exchanging some sources of hydrogen (H), with the heavier isotope deuterium (D). The nucleus in hydrogen,  $^1\text{H}$ , only consists of a proton. Deuterium,  $^2\text{H}$  also has a neutron in the nucleus, thereby doubling its mass. With mass spectrometry, it should therefore be possible to either use deuterated electrolytes or deuterated gas on the anode, and then measure the mass of the resulting products. Deuterium containing products would thus weigh more, than similar hydrogen containing molecules.

## 6.2 Synthesis with flowing electrolyte

While building the mass spec-setup, experiments were carried out with the flow cell. As shown above, long experiments passing  $>700$  C of charge, gave relatively low FE ( $\sim 3\%$ ), while showing signs of much decomposition of the electrolyte. The low FE measured could be due to a number of factors. E.g. too low backpressure of  $\text{N}_2$ , thus not effectively pushing nitrogen through the GDE to

the reaction surface. A related possibility, is too small pores in the electrode mesh, which would require higher  $N_2$  backpressure. The mesh size ( $325 \times 2300$ ) was chosen to be a finer version, than the reported size by Lazouski et al. [44]. Partly, to not only repeat their experiments, but to make my own. And also for consistency, as the series of tests, had been started using this mesh type. I wanted to get reproducible results, before doing modifications, such that an improved result could be correlated to a change. With Cu electrodeposited, the small pores were also further covered. The low FE could also be a result of side-reactions in the electrolyte, which was based on  $LiClO_4$ . But, at that time, all other experiments in our lab were with this electrolyte. I therefore deemed it unlikely.

With Cu on SS we could go to higher geometric current densities compared to the plain SS mesh. Two things made this possible. First of all, I increased the electrolyte concentration. This was to accommodate Li deposition, and reduced the double layer thickness in the porous electrode surface, such that more area could be accessed [118]. As an added benefit, it decreases the resistance and thus electrode overpotential, as discussed with equation (5.1). Decreasing the overpotential was necessary for applying higher currents.

Having both  $N_2$  and  $H_2$  gasses flowing, the dream was to be able to run at high current and high efficiency. The potentiostat used for potential and current control, was limited to a total of 400 mA, which in the flow cell corresponds to  $16 \text{ mA/cm}^2$ . Trying to operate under these currents, was therefore an initial goal. In the second cell iteration, where the cathode was a porous disk ( $8 \text{ cm}^2$ ), the anode a Pt sputtered mesh, and the electrolyte concentration was 0.2 M, the resistance was measured to be in the order of  $400 \Omega$ . If the highest permitted current was applied here, it would result in  $0.4 \text{ A} \times 400 \Omega = 160 \text{ V}$ . This is way beyond reason! If limiting the allowed overpotential, to be within  $\sim 5 \text{ V}$ , would on the other hand only permit a total current of 12 mA (corresponding to  $1.5 \text{ mA/cm}^2$ ). Increased conductivity was therefore a crucial part for operation. The electrodeposited Cu increased the electrochemical surface area of the electrode. Though, the roughness on the large SS mesh electrodes, were not as high as reported in the published work on this high surface area deposition method (Appended paper IV, [46]). This was also due to current and size limitations. The electrodes, we reported in [46], had a geometric surface area of  $0.5 \text{ cm}^2$ , and Cu-deposited at  $10 \text{ A/cm}^2$ . A potentiostat with a 10 A current booster was used for this, as the specific deposition parameters needed to be controlled. To deposit Cu at the same conditions, on the large  $25 \text{ cm}^2$  mesh electrodes in the flow cell, would thus require 250 A, which again was not feasible. Lower current densities of  $0.2 \text{ A/cm}^2$  for 1.5 minutes, were instead used. This did leave a visible layer of Cu, with micrometer-sized structures (Appendix Figure B.19). We knew this deposition, was far from optimal, but the effect was obvious. With these Cu deposited electrodes, high geometric current densities were possible, at relatively low overpotentials. The overpotential does not only stem from the IR-drop, but also how easy the reactants can get to react [119]. If the reactants have a high surface-coverage (many reactants on small area), competition for having

a surface site to react on, decreases the rate. When increasing the area, more room is left for the reactants, and easier transport to an available site. In our study on high surface area electrodes [46], we found that the higher geometric current densities achieved with the Cu-electrodes, corresponded to the increased roughness factor. Meaning, on a microlevel perspective, the current density for NRR was therefore comparable to flat foil electrodes. Or in other words, the total current scaled with the electrochemical surface area.

Cathodic reactions were hereby improved with Cu deposition. But the anode was unaltered. To have Pt available on the anode, electrode meshes were sputter-deposited with Pt. In the sputter deposition process, the target atoms deposit relatively uniform on the surface. But to avoid exposing SS directly to the electrolyte,  $\sim 350$  nm was deposited. With SS exposed on the anode, Fe and Ni in the SS could be oxidized if the potential is too high [120]. The thick deposit also increase the lifetime for an electrode, as some Pt may dissolve or delaminate during flow. The relative areas of cathode and anode was highly skewed. This could explain the high anodic potentials, as a high current density was applied.

### 6.2.1 Electrode areas

I wanted to test this effect, and see if changing the relative areas, could improve the decomposition seen. Appendix Figure C.3 shows example of flow cell tests, where the anode potential was high. The electrolyte turned dark brown afterwards, clearly indicating decomposition. The high anode potential (indicating electrolyte oxidation), together with the observed change in viscosity and appearance of electrolyte after experiments (Appendix Figure C.4), are in good agreement with [121, 122], reporting anode polymerization of THF.

In the flow cell, I tried decreasing the cathode electrode area. First by using plain SS without additional Cu deposition, which Lazouski et al. [44], also showed promising results with. I then tried to go even further, and cover parts of the cathode, only exposing  $1\text{ cm}^2$  of electrode to the electrolyte.

As shown in Figure 6.2, the anode potential behaved as expected. Under all the experiments, the anode was kept the same. Only the cathode was changed. At high currents applied, the anode potential was at 1-1.5 V *vs* Pt, and thereby beyond the determined potential for electrolyte oxidation. As the current is lowered, the anode potential decreases. Interestingly, it appears like the anode could apply the requested current, when being around 0.3 V. This is seen both at 250 mA (left) and 100 mA (middle). There are some periodic increases in the potential at high currents, which may be due to flooding or too low  $\text{H}_2$  flow. This points towards that  $\text{H}_2$ , at least partially, could provide protons for the reactions. With most of the cathode area covered (see Appendix Figure C.5), less than 50 mA was applied. Under these conditions, the anode area was  $\sim 25$  times larger than the cathode area, and the anode potential dropped to 50 mV *vs* Pt. With the anode potential decreased, two things occurred. The cell resistance increased, due to the smaller area on the cathode (set as

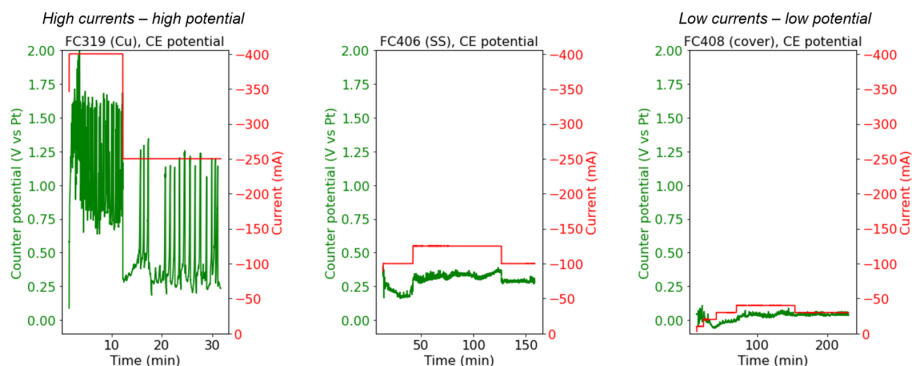


Figure 6.2: Measured anode potentials (labelled as CE) at different applied currents. Cathode area was changed from being Cu deposited SS-mesh, plain SS-mesh, and a covered electrode exposing  $1\text{ cm}^2$  to electrolyte. At currents below 50 mA, the anode potential is at 50 mV, whereas at 400 mA current, it is between 1-1.5 V *vs Pt*.

working electrode). At  $1\text{ cm}^2$  cathode area, the anode potential was negligible during reduction. The applied cathode potential was on the other hand up towards  $-7\text{ V vs Pt}$  (Appendix Figure C.6). Decomposition was still observed in the electrolyte. Since the anode potential was far below electrolyte oxidation potentials, this points towards two possibilities. Either decomposition at the cathode, in agreement with the discussion in Chapter 4.5 on the origin of protons. Or, sidereactions with the electrolyte from e.g.  $\text{H}^+$ , as touched upon in Chapter 4.6.

From these observations, I started to do more experiments on plain SS electrodes. The area of the cathode and anode would also be less skewed. Reports by Suryanto et al. [51], has later shown a similar approach, with a large anode surface area (multiple  $\text{cm}^2$  of Pt mesh), compared to the cathode area ( $0.012\text{ cm}^2$ ).

Following this, our group was expanded with a new team-member: the skilled and productive Dr. Xianbiao Fu. He eventually joined my efforts on the flow cell, and helped test a lot of our ideas.

### 6.3 Mass spectrometry and non-aqueous media

This leads to the second subproject we had going, next to the continued flow cell measurements: getting a mass spec coupled together with the flow cell, for additional insights to operation. For this purpose, *Garm* was built. Multiple people have been a part of getting this mass spec operating and ready for measurements. Initially, Mattia Saccoccio did a lot of work in designing the physical setup and preparing the assembly. And a brilliant student worker, Mathias R. Vinther, prepared the communication software, for controlling the equipment.

This has both the ability to record a mass spectrum, measuring all the signals in a given range, or it can track specific  $m/z$  ratios (simply referred to as masses, and will in plots be written as "m") over time. This technique (called mass-time) is the main use while doing experiments, as it allows recording the development of masses, and thus product formation.

Once we had tested all the individual components, and ensured a low vacuum in the analysis chamber, I could start setting the new equipment up for measurements on the non-aqueous system. By the time Garm was built, the third iteration of the flow cell had arrived, and could be used with the mass spec.

Before Garm was implemented for flow cell measurements, I had personally very limited experience with operation of mass specs. And, as it goes for all new setups, there will be unforeseen hiccups and challenges to solve. Luckily, I have many good and helpful colleagues, who had a lot of experience with similar setups. Especially Alexander Krabbe, Brian Knudsen and Jakob Ejler provided essential guidance in troubleshooting communication errors and access to data.

### 6.3.1 Preparations

With the mass spec, we had two main goals. First of all, to see  $\text{NH}_3$  ammonia formed during reaction, and follow the synthesis. Secondly, we wanted to use isotope labelled gas, to track the origin of products. This led to two obvious candidates regarding  $\text{NH}_3$  synthesis.

$^{15}\text{N}_2$ -gas is an option, but a technique like NMR, would be more suitable for this. The issue with measuring  $^{15}\text{NH}_3$  with a mass spec, is the mass of the molecule. Water signals will always be present, but can be minimized. Nonetheless, both  $^{15}\text{NH}_3$  and  $\text{H}_2\text{O}$  have a mass of 18 amu, and would thus also be hard to distinguish with mass spectrometry. Instead, non-isotope labelled  $^{14}\text{NH}_3$  at mass 17 amu, can be distinguished from water. Though care has to be taken. As mentioned in chapter 3, during the ionization process, necessary for mass separation, molecules can show cracking patterns. Water tends to break into O and OH, thus giving signals at masses 16, 17 and 18 [123]. But by decreasing the ionization energy, cracking becomes less likely, and only the main peak will eventually be seen. This is referred to as *soft ionization*. Measurements showing this behaviour are presented in Appendix Figure C.7. Garm had the capability of doing exactly this, thus making it possible to follow mass 17 from ammonia and 18 from water, which should not interfere.

The other obvious candidate is deuterium ( $^2\text{H}_2$  or simply  $\text{D}_2$ ). In contrary to single compartment glass cells, it would be possible in the flow cell, to flow  $\text{D}_2$  over the anode, and see if D-containing products are formed on the cathode. More on this will follow in chapter 6.3.3. In single compartment glass cells, it is hard to distinguish gas fed in, from gas developed at electrodes. And in two-compartment cells, the resistance and electrode distance is often too high for this to be possible. The flow cell combined with a mass spec, thus opened up a new interesting opportunity.

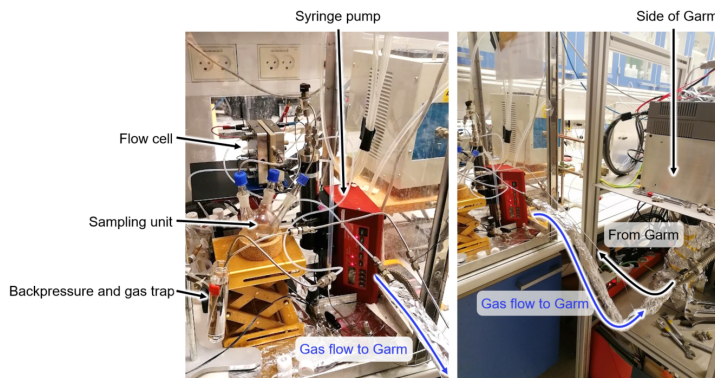


Figure 6.3: Image of the flow cell setup connected to Garm. Noticeable parts are highlighted, including the gas flow from the flow cell to the mass spec. The gas line connected to Garm is heat traced to 100 °C and made as short as feasibly possible, for better detection of  $\text{NH}_3$ .

$^{13}\text{C}$  isotopes could also be used for studying electrolyte decomposition. Though, the extent of gained knowledge would be limited. One could track the development of masses seen, at the main peaks from e.g. THF and the known probable decomposition products [80]. It would though only tell us, that the electrolyte is breaking down, which could be seen from the non-isotope labelled compounds as well. Distinction between solvent (e.g. THF) and additives (e.g. EtOH), may be possible, but other characterization techniques would be more useful. The electrolyte has an impact on the SEI layer formation, why specified techniques for this, should be preferred.<sup>2</sup>

70 eV ionization potential is commonly used in mass spectrometry [123]. With the relatively high potential, a lot of signal can be detected with multiple mass signals from cracking. Cracking signals in mass spectrometry is not necessarily an unwanted thing. Different molecules will have different cracking patterns, so by measuring their spectra, the molecule can be determined. I therefore did some measurements at 70 eV. Mainly to have high signals, but also to compare spectra and patterns to table values. In order to also be able to distinguish molecules by their main peak signal, and avoid cracking patterns, measurements were also done at 26 eV ionization energy. The settings for this soft ionization was optimized for Garm w.r.t. water and ammonia distinction. The standard and optimized settings are listed in Appendix C.2.1.

<sup>2</sup>The possibilities are many. E.g. dissolving the deposit and analysing the liquid with NMR. An exotic technique, like quartz-crystal membranes (QCM), could possibly be used to follow the mass of deposited material - and potentially see differences from isotopes.

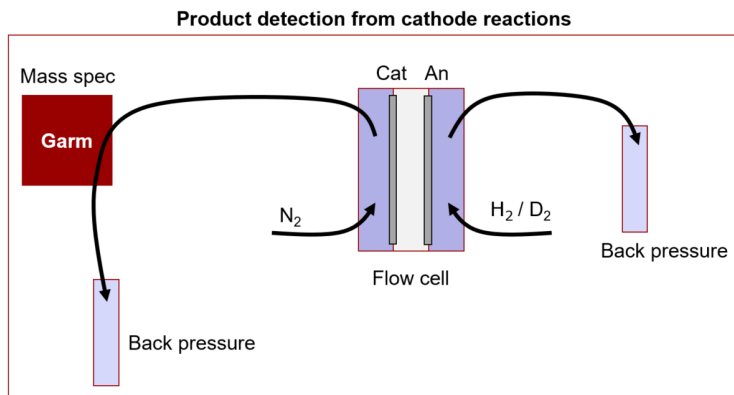


Figure 6.4: Simple schematics of how the mass spec can be combined with the flow cell, only measuring products from one electrode. In this example, Garm is set up to measure on products from the cathode, by being downstream on the  $N_2$  flow. Hereby, it will not measure on a direct flow from the anode gas (e.g.  $H_2$  or  $D_2$ ). Only compounds at the cathode, will be carried to Garm for MS detection.

### 6.3.2 Measurements on flow cell

With Garm prepared and setup for measurements, it was combined with the flow cell. The advantage of using the flow cell with the mass spec, is the opportunity for separating the anode from the cathode. The actual setup is shown in Figure 6.3, and the concept is schematically exemplified in Figure 6.4.

In the simplified schematics, Garm is connected downstream on the  $N_2$  gas line. I.e. products or compounds at the cathode surface (on the gas side of the GDE), can be carried along with the  $N_2$  flow, and measured in the MS. In the example, either  $H_2$  or  $D_2$  is flowing over the anode. Separated by the electrodes and electrolyte layer, this gas stream is not reaching Garm. But if e.g.  $D_2$  is oxidized at the anode, forming  $D^+$ -ions, these could be measured with Garm, if reaching and reacting at the cathode. And since D is heavier than H, gas and electrolyte reactions at the anode can be distinguished from each other. This is the huge advantage and prospects of this setup. Similarly, Garm could be attached on the anode side, and measure anodic products. The only requirement is, that only gas phase products (or volatile species carried with the gas flow) can be detected.

A series of calibration measurements were made. Initially the ability to distinguish  $NH_3$  from  $H_2O$  was confirmed with Garm (see Appendix chapter C.2.2). Later,  $H_2$  and  $NH_3$  calibrations in an  $N_2$  gas flow was made, and shown in Appendix Figures C.12 and C.11.

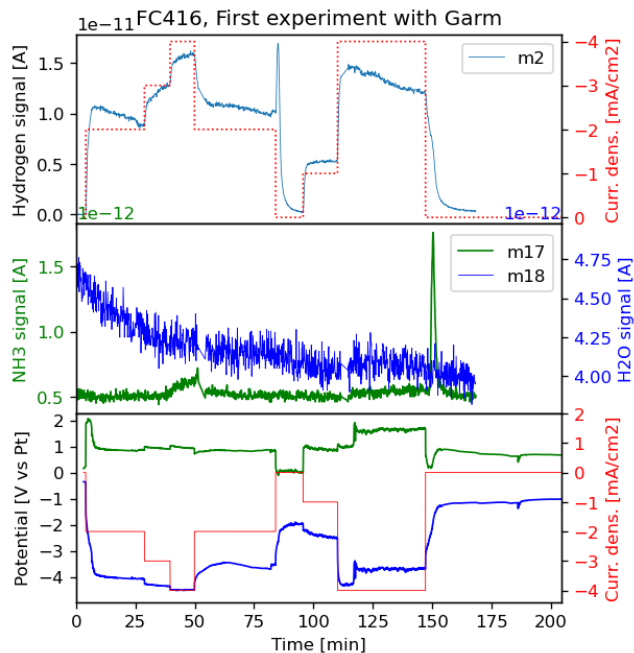


Figure 6.5: H<sub>2</sub>, NH<sub>3</sub>, and H<sub>2</sub>O measurements on the first flow cell experiment (labelled *FC416*), using Garm to measure products from the cathode. (*top*) A reasonable correlation between H<sub>2</sub> signal and applied cell current is seen. (*bottom*) At 4 mA/cm<sup>2</sup>, a small signal increase is seen in the ammonia signal at *m/z* 17, while water at *m/z* 18 decreases. This was the first time ammonia was measured *in-situ* with the flow cell. Measured with soft ionization.

### First look on flow cell reactions

It is well established that HER is a competing reaction with NRR. The first experiments, done with Garm on the operation of the flow cell, was therefore focussed on H<sub>2</sub> evolution. This was to confirm that *in-situ* product measurements on the flow cell was possible. To promote the reaction, a Pt-electrode was used on both the anode and cathode, for HOR and HER respectively. H<sub>2</sub> was flowing on the anode, and N<sub>2</sub> was used as carrier-gas on the cathode. A 1 M LiClO<sub>4</sub> electrolyte-solution with THF and 1% EtOH was used, and in the new flow cell, only 1.8  $\Omega$  was measured with impedance. The mass-time recording of H<sub>2</sub> (m2), NH<sub>3</sub>, and H<sub>2</sub>O, together with the applied cell current is presented in Figure 6.5. All electrochemical data is shown in Appendix Figure C.13.

At this time with the new setup, I did not have the means to precisely control the gas flow rates, and the product formation is therefore not quantified for this experiment. It does, however, provide interesting findings. As seen in the top graph, the hydrogen signal follows, to a reasonable degree, the applied current to the cell. This is very well in line with our expectations. Applying negative

current to a Pt-deposited electrode, would expectedly do HER. As seen, the current was applied in steps, in order to see if the HER rate would follow along. The rate of HER is not steady, during a constant applied current. For instance, during the first step from 0-24 min, A relatively high signal is initially seen, which afterwards decreases. This may be explained by the SEI layer, which we also know deposits under these cathodic conditions. It is plausible, that charges are spent on depositing Li, rather than reacting with protons at the electrode surface. There are some inconsistencies related to this explanation. At higher currents, Li should be plated at an even higher rate, thus preferably out-compete possible HER happening at the same time. Under these conditions, one could expect the behaviour seen at the first step, but the opposite is seen. There are therefore, some missing details to this picture. After all, it was not the objective with this first experiment to explain what happens, but to see the setup work. Which it did.

Two interesting features were observed with the experiment. One regarding hydrogen signal. At 80 min, a high and sharp peak is seen with an exponential decay, when stepping down the current to zero. In light of the cycling paper discussed [45], this could be dissolution of the SEI-layer, and formation of H<sub>2</sub> from H-atoms trapped within the layer. E.g. in the form of LiH. This behaviour was not seen at 150 min, when the current was stepped down again, but the tail of H<sub>2</sub> is observed. This does agree with the proposed SEI-dissolution. The exciting observation was ammonia. With Pt on the cathode, I did not expect to see NH<sub>3</sub>, due to the competition with HER. Luckily I did follow  $m/z$ , as I here saw the first *in-situ* measurement of NH<sub>3</sub> formation. A small increase in the  $m/z$  17 signal is seen when high currents are applied, while the water signal decreased. And interestingly enough, a similar feature, as for H<sub>2</sub>, is seen at the end, where a peak of NH<sub>3</sub> is recorded. This may again be from SEI dissolution, where amine-like (i.e. NH-containing) species are trapped in the layer, forming NH<sub>3</sub> when dissolved. This could be part of the explanation to the increase in FE, observed with the cycling procedure. Whether the intense peak observed here, is from a sudden burst of NH<sub>3</sub>, or an artifact of the short measuring time at each mass, is difficult to say.

From this experiment, I could not determine where the protons were stemming from. Hydrogen could come from both the THF, EtOH and the H<sub>2</sub> gas. From the relatively high anode potentials at +1 V or above (Appendix Figure C.13), it is very likely to come from the electrolyte. But this first experiment was a success, showing both H<sub>2</sub> features - and the first ammonia measurements.

### First deuterated experiment

I followed up on this success, by changing the anode gas to D<sub>2</sub>. As discussed, this would make it possible, to see if the hydrogen signal was a result of protons from

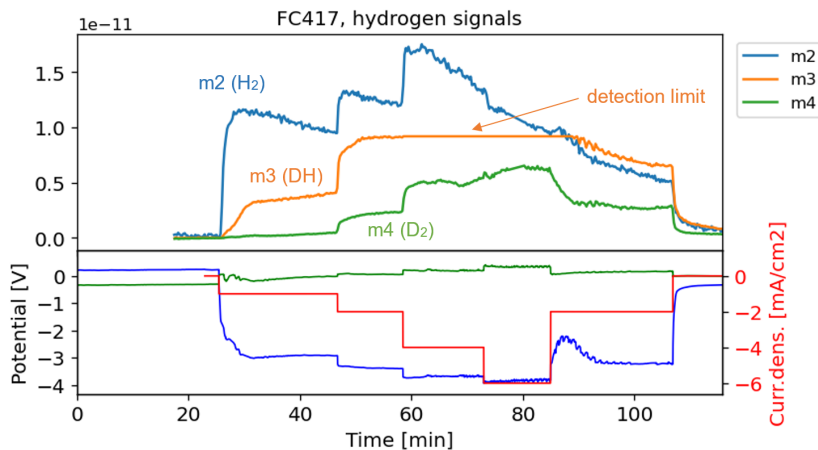


Figure 6.6: Mass spec and electrochemistry measurements on *FC417*. Cathode products are measured, with  $D_2$  flow on anode. Deuterated signals from  $D_2$  oxidation is detected from cathode reactions. Line-colours in lower graph is cathode (blue), anode (green), and current density (red). Measured with soft ionization.

electrolyte oxidation, or from gas oxidation.<sup>3</sup> Since I just saw a small  $NH_3$  signal as well, I wanted to pursue this as well. The cathode was therefore changed to a Cu-deposited electrode. Cu was used, to easily go to high currents on the cathode. The anode was the same type of Pt-electrode, and the electrolyte was again 1 M  $LiClO_4$  in THF and EtOH.

These MS data can not be quantified either, but it still give valuable information. The measured hydrogen and deuterium signals ( $m/z$  2 to 4) are shown in Figure 6.6, together with the electrochemistry data.

The MS data is shifted down, thus showing the measured increase compared to the starting values. When current initially is applied, the  $m/z$  2 signal shoots up. This is in good agreement with our understanding of the Li-mediated system. Here, we have so far talked about the formation of SEI, which is formed as a result of the non-aqueous electrolyte and metallic Li plating. The cathode electrode surface is covered by the organic electrolyte. Hydrogen could be formed directly by reduction of the electrolyte, as discussed in Chapter 4. Or the hydrogen is produced from reaction with Li, while  $Li^0$  reacts with the electrolyte to form the SEI. Both reactions may take place simultaneously.

Most excitingly is the  $m/z$  3 and 4 signals, representing HD and  $D_2$  respectively. After the instant  $H_2$  signal, DH shows a steady increase. This means, that protons from anode oxidation, is at least partially responsible, for the observed hydrogen signal at the cathode. This was the first time, we ever saw direct proof

<sup>3</sup>One could argue, that a deuterium signal in this setup, would be due to  $D_2$ -gas penetrating the GDE, that diffuses to the cathode, and then is measured in the mass spec. I have tested for this, by changing gas and look for traces on the opposite electrode, with no current applied. I concluded that it is not the case.

of HOR products transported to the cathode. Until this point, we could only assume HOR taking place, from the lower oxidation potentials at the anode. The  $D^+$  transport, was even better than I expected, when preparing the experiment. After a few minutes, the rate of  $m/z$  3 increase (i.e. slope of signal) drops. But still with a positive slope under constant current. Meanwhile, the  $m/z$  2 signal decreases. This is very positive, since it suggests that more and more protons over time, stem from HOR, rather than burning the electrolyte. As seen at 50 min, the  $m/z$  3 signal stagnates when increasing the current density, since the signal got higher than the MS-equipment was set up to measure. This is accompanied by an increase in  $m/z$  4, i.e. reduction of two  $D^+$  ions from the anode forming  $D_2$ . Though  $m/z$  3 here is unknown, it is clear that a significant amount of protons eventually stem from HOR. At its peak at 85 min, the 40% of the hydrogen signal is from  $D_2$ , by comparing the  $m/z$  2 and 4 signals.

Ammonia is seen in this experiment too. And much more clearly than the first test, as shown in Appendix Figure C.14. Only masses 17 and 18 were tracked. Most of the signal is seen as  $NH_3$  on  $m/z$  17, but eventually  $m/z$  18 increases too, when the current is increased. This could either be from water production or a sign of  $NHD_2$ . The latter being most interesting. Comparing this increase to measured oxygen signal ( $m/z$  32, not shown), it does correlate to a small decrease. This could point towards  $O_2$ -reduction to water, in line with glass cell measurements [46]. The electrolyte had visibly decomposed during the electrochemical reactions, as shown in Appendix Figure C.15. This is also expected from the MS-measurements, as mainly  $H^+$ -products from electrolyte reactions were observed.

### 6.3.3 Transport of protons

Knowing that the combined mass spec and flow cell setup was able to do product measurements, a series of tests were made. Some for trying to measure  $NH_3$ , and others focussed on detection of proton transport.

I will here discuss one interesting study focussed on proton transport. As was shown for the THF based Tsuneto electrolyte in the previous section 6.3.2, transportation of  $D^+$ -ions from anode oxidation of  $D_2$ , was possible. But electrolyte decomposition was also seen after electrochemistry, showing this electrolyte is not perfect.

As discussed in Chapter 4.3, the ether based electrolytes can break down from acidic hydrolysis. By recommendation of Rokas Sažinas, I tried to study the ester dimethyl carbonate (DMC). As previously mentioned, this ester should be able to transport protons, even better than THF. I therefore set up experiments, using only DMC as solvent and 1 M  $LiClO_4$  as salt, with no extra additives.

I was here mostly interested in DMC's ability to transport protons. With HER being the easiest reaction on the cathode, as also seen from the two previous mentioned experiments, I set up the cell with Pt electrodes on both cathode

and anode - similarly to the very first experiment.<sup>4</sup> To follow the origin of these protons, D<sub>2</sub> was flowing on the anode, while N<sub>2</sub> was used as a carrier gas on the cathode to Garm. The raw data for this experiment is presented in Appendix Figure C.16. Two sets of measurements were included during test. Initially, the anode potential was controlled (CA technique), to ensure it was kept below critically high potentials for solvent oxidation. Based on the observed current during CA, a CP was performed, set to a comparable current.

This was yet another very exciting experiment. Though I have to add, that I was still relatively unexperienced with mass spec measurements. For this specific experiment (which was repeated under same conditions) and some previous variations to it, I took the unfortunate decision, measuring with hard ionization at 70 eV. This means that cracking signals from heavier organic molecules, can interfere with measurements on hydrogen signals. I chose to do this, for getting higher signals. I will return later, to why this has not been redone at soft ionization.

Figure 6.7 shows the relative signal of  $m/z$  2, 3, and 4 compared to each other, during CP at the last part of the test. The first part of the experiment gives the same story. The ratios are calculated as:

$$\eta_i = \frac{m_i}{\sum_{i=2}^4 m_i} \quad (6.1)$$

based on the starting value of each mass, before they increase during applied current. This is an alternative way of presenting the data, where the FE for the hydrogen evolution reaction would be more appropriate. These are calculated and shown in Appendix Figure C.17. The calculated FE are only best estimates. I have, in the limited time available with the two setups operating, realized that calibrations and flow cell measurements do not correlate completely. This is the case, both for NH<sub>3</sub> and for H<sub>2</sub>. For the latter, near unity reactions towards HER on Pt would be expected. Other reactions with SEI formation is also taking place simultaneously. But a significant amount of charges should go towards hydrogen production. This is though not the case, as e.g. seen in this experiment, where <50% is calculated. As for now, these numbers are therefore only best estimates. I therefore use the relative signals, for this discussion.

The mass spec measurements are nonetheless exciting. With DMC as the only molecule present for proton transport, more than 60% of the three hydrogen masses, is eventually the fully deuterated version. And taking into account, that  $m/z$  3 stems from both an H and a D, the relative deuterium to hydrogen products are measured to more than >80% at 270 min (Appendix Figure C.18). This is really impressive, and shows how DMC is able to transport protons from oxidized D<sub>2</sub>, from the anode to the cathode. It also proves yet again, that HOR is possible in the non-aqueous system [87]. And with an adequate shuttle mechanism, these protons can be used for reduction reactions.

<sup>4</sup>One note to this. Pt and Li can alloy, why an old and worn Pt-sputtered mesh was used on the cathode. The electrodes do wear down over time, and this old electrode could therefore be 'sacrificed' for this experiment.

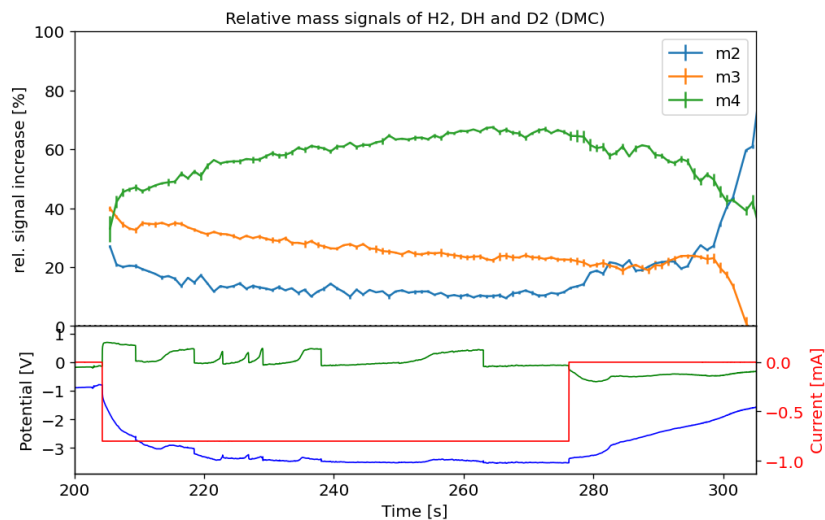


Figure 6.7: Relative measured signals of  $m/z$  2, 3, and 4 during constant current. Increase in  $m/z$  4 signal dominates, indicating much transport of  $D^+$  from the anode to the cathode. Measured with hard ionization.

This would be great to combine with NRR, and see deuterated ammonia species. Unfortunately, I could not see appreciable formation of  $NH_3$ , when I used DMC as solvent. In the presented experiment here, there was a negligible increase in  $m/z$  17, indicating that little ammonia was formed, which was supported by indophenol measurements on the electrolyte. Furthermore, as hard ionization was used, the  $m/z$  17 can not be distinguished from water signal at  $m/z$  18. I also tried to add some tert-butanol to the solvent, proposed to me by colleagues, but with similar lack of ammonia formation.

As discussed in Chapter 4.5, if protons attack the  $OCH_3$ -part of DMC, it can hydrolyse and decompose. Despite very promising measurement on deuterium transport, the electrolyte had visibly decomposed after experiment. These are the reasons why these experiments were not repeated with soft ionization. Though DMC is good at proton-transport, also despite decomposition, what we seek is a way to form ammonia. So the quest continued.

### 6.3.4 Combined NRR and HOR

I have saved the best for last. Which also has been the case for this PhD project. Evidently, it would turn out, that the measurement we had hoped for since the start of my project, could be measured just six weeks before the project was over. This does also mean, that the final measurement, does lack complete quantification. The trends are though clear, and do sum up the project.

While I had worked on the mass spec and flow cell measurements, Xianbiao

continued the tests on the flow cell, which I had started. He managed to get more reproducible results and somewhat higher efficiencies. This was achieved by increasing the flow of  $N_2$  and  $H_2$  over the electrodes. The gas tubes for the new iteration was  $1/8''$ . As the gas tubes have a limited inner diameter of  $\sim 1.6$  mm, an increased flow rate will in turn increase the pressure in the line [107]. Despite the electrode being less than  $<0.1$  mm, flooding will still decrease the efficiency. As discussed in Chapter 5, the break-through for achieving the initial ammonia synthesis in the flow cell, came by changing from thick disk-electrodes, to the much thinner mesh electrodes. Here the flowing gas would have easier access to surface-reactions on the electrodes. If the electrode is flooded, the gas would still have to diffuse through a layer of electrolyte. The continued measurements with the flow cell, and electrodes and electrolyte used so far, resulted in a limitation to the achievable FE for NRR of some 10%. So something had to be changed.

Visible and quantitative signs of electrolyte decomposition was seen by everyone in our ammonia goup. Apart from looking into other solvents, like DMC as just presented, also the Li-containing salt was changed. An issue with  $LiClO_4$ , is its chemical nature as a strong oxidizer [124]. This could also be part of the reason why even at proven cathodic proton consumption stemming from HOR, the electrolyte still showed signs of breakdown. Instead,  $LiBF_4$  [44, 47, 87] was used more frequently.

I had other and thinner electrodes available, that were previously acquired. As mentioned, these had not been tried, from their physical appearance, having large and even transparent pores (see Appendix Figure C.20). In the pursuit of pushing the now reproducible flow cell experiments towards higher efficiencies, two things were implemented. First the cycling procedure was included during NRR. I had tried this a few times at a previous stage, with no markedly improvement. That was while inconsistent measurements were an issue, and thus chosen to be postponed for later. Xianbiao here managed to increase the FE from 10 to 30%.

As decent amounts of ammonia was synthesized in the flow cell, we had to verify the source of nitrogen, and ensure we were not measuring contaminants. Xianbiao and I therefore did a similar cycling-experiment with  $^{15}N_2$ . The gas flow conditions were modified, to accommodate use of the isotope gas, hence a lower FE of 15% was measured. But it confirmed reduction of gaseous  $N_2$  to be the source of  $NH_3$ . The small 5%  $^{14}NH_4^+$ -signal, is from atmospheric  $^{14}N_2$ , introduced as electrolyte is flowing through the cell, and collected in a sampling unit. The Li-mediated process is already proven to work, but the validity of the flow cell operation had to be tested for too [34].

Secondly, the thinner electrodes were tested. I was surprised to hear, that the electrodes were able to separate the gas and liquid, knowing the low viscosity of THF. But with the thinner electrodes higher FE followed. Completely in agreement with how the flow cell first got to work. Even thinner electrodes, lead to even more accessibility of gas. There is one drawback with the thin electrodes. That has to do with the high vapor pressure for THF (143 mm Hg

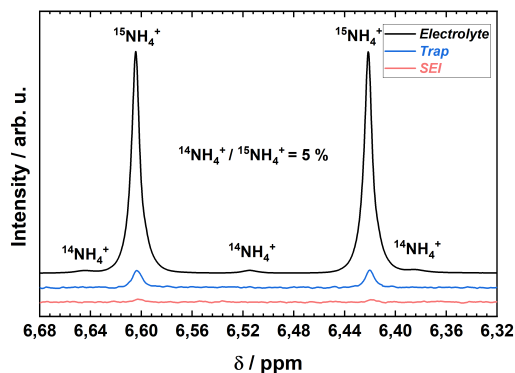


Figure 6.8: Isotope labelled  $^{15}\text{N}$ -test with the flow cell, verifying reduction of gaseous  $\text{N}_2$  as the source of  $\text{NH}_3$ . Courtesy of Rokas Sažinas for acquiring spectra.

at 20 °C) [67]. In the flow cell we have a continuous gas flow over the electrodes. With more contact between gas and liquid, the liquid evaporates even faster. I had very early in the development-process noticed this issue. It was also one of the benefits with the flow cell - that the loss of electrolyte could be compensated for with flow of new electrolyte.

A final thing to notice is the Pt anode. The electrode areas, and thereby current density, has a significant effect on the electrode potentials, as discussed above in Chapter 6.2.1. A higher anode area was needed, similarly to the performance improvement by Cu-electrodeposition. At the same time, the risk of Pt-poisoning [125–127], ought to be considered in these organic electrolytes. To accommodate both of these considerations, Xianbiao made PtAu-electrodeposition on the stainless steel meshes. These electrodes were deposited in a similar way as the Cu electrodes, but in a different electrolyte. The electrolyte used consisted of 10 mM  $\text{H}_2\text{PtCl}_6 \cdot 6\text{H}_2\text{O}$  and 10 mM  $\text{HAuCl}_4 \cdot 4\text{H}_2\text{O}$  in 3 M  $\text{H}_2\text{SO}_4$ , deposited at a negative current of -9.5 A for 2 min, with metallic Pt-mesh as counter electrode. This created a porous deposit of Pt and Au, as shown in Appendix Figure C.19.

All this combined: with the thinner cathode electrode, PtAu-alloy anode, cycling procedure during electrolysis, and an electrolyte with EtOH and  $\text{LiBF}_4$  as Li-source, significantly higher FE towards NRR was achieved by Xianbiao.

## Control experiment

One of the goals with the combined mass spec and flow cell experiments, was to measure ammonia during reaction. With the high efficiencies now realized, it was hopefully time to record promising measurements.<sup>5</sup>

<sup>5</sup>In reality, this experiment took multiple attempts to realize, as the Garm-setup suddenly had communication issues, between different components. I owe Alexander Krabbe, Brian

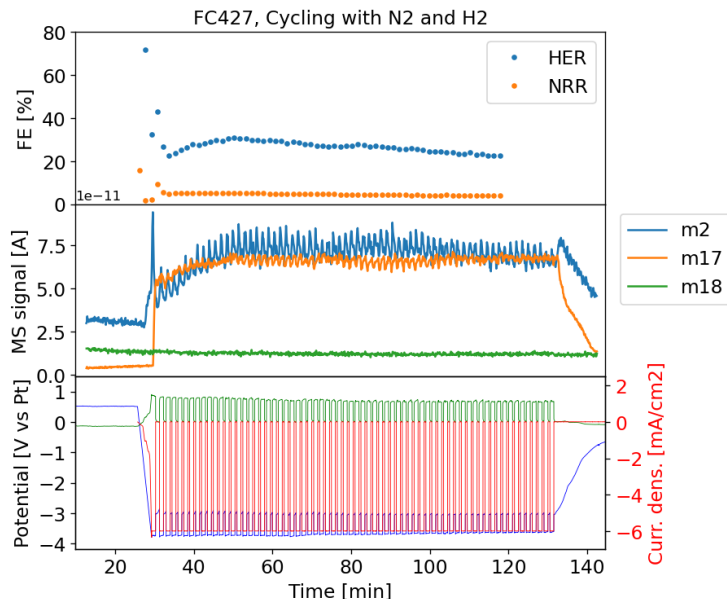


Figure 6.9: Complete overview of an initial cycling experiment with the flow cell. Stainless steel mesh (325x2300) as cathode and PtAu on anode. Electrolyte: 1 M  $\text{LiBF}_4$  in THF with 0.25% EtOH. (*top*) Best estimates of FE for NRR and HER calculated from MS measurements. (*middle*) MS measurements on  $m/z$  2, 17, and 18 from  $\text{H}_2$ ,  $\text{NH}_3$  and  $\text{H}_2\text{O}$  respectively. Notice the constant and low water signal. (*bottom*) Potentials and current during cycling procedure.

These measurements were done with soft ionization, such that there should be no interference from different molecules. Though, before setting up an experiment with  $\text{D}_2$ , to look at protons in the system, a control measurement was done with  $\text{N}_2$  and  $\text{H}_2$  on cathode and anode respectively. This allowed me to distinguish ammonia and water signals from each other, as it was unknown how these would develop over time during cycling. An overview is given in Appendix Figure 6.9. Mass spec measurements are shown for  $m/z$  2, 17, and 18.  $\text{H}_2$  and  $\text{NH}_3$  are nicely following the applied current cycles, while the water signal is completely flat. The ammonia is thus not affected by water. The calculated efficiency for HER is estimated to be 30%, but as previously discussed, this may be an underestimate. When doing a similar estimate for NRR, ammonia synthesis calculated from mass spec data, are in reasonable agreement with indophenol measurements, yielding 5.5% from the gas trap. Including ammonia in the electrolyte, this experiment gave a total of 25% FE, corresponding to 6.7% energy efficiency. And this was with a  $325 \times 2300$  mesh, which ought to be non-ideal. It is possible, that some  $\text{NH}_3$  is lost due to sticking to the inner tube surface, between Garm and the gas trap. This would, however, only mean that 25% FE is underestimated. In short:

---

Knudsen, and Jakob Ejler much gratitude, for help to troubleshoot and (partially) fix the issue.

This started to look quite promising for the flow cell. An interesting feature is seen in the start of the experiment, where the  $m_2$  signal increases before Li deposition. When Li deposits, the  $\text{NH}_3$  quickly increase to a steady state, while  $\text{H}_2$  gives a sudden spike in the signal. With  $\text{H}_2$  flowing on the anode, there is limited knowledge on what causes this. Hence an experiment with  $\text{D}_2$  follows now.

### Deuterium and cycling

For the final experiment, the cathode electrode was changed to the better performing thin mesh (size  $500 \times 500$ ), and a PtAu electrode was used as anode. The electrolyte was Tsuneto based, though with slight modifications, which had been found to perform better: 1 M  $\text{LiBF}_4$  in THF with 0.25 vol.% EtOH. That slightly lower ethanol concentration (0.25 instead of 1%) is better, is suspected to be due to mass transportation. The flow cell setup is different from glass cell setups, which we otherwise have used for investigations. Requiring a setup-specific improvement<sup>6</sup> is therefore also reasonable, as touched upon in Chapter 4.3.

The exciting results, for the cycling experiment with  $\text{D}_2$  on the anode, is shown in Figure 6.10. The upper two graphs show the measured increase in MS signal, for the hydrogen and ammonia related masses. What appears to be noise in the signal, stem from the applied current-cycling procedure, where signals increase as current is applied.

First things first. The reason this experiment is a success, is the development of especially deuterated mass-signals. For the hydrogen-case, initially  $\text{H}_2$  is seen. But over time, partially deuterated HD takes over, followed by fully deuterated  $\text{D}_2$  signal. This general behaviour is in agreement with the earlier observations, discussed regarding Figure 6.6. The exact same thing can be seen for ammonia-related masses. Initially,  $\text{NH}_3$  and partially deuterated  $\text{NDH}_2$  is detected. The  $\text{NH}_3$  signal though decrease over time, as more partially and even fully deuterated  $\text{ND}_3$  is measured. Seeing the  $m/z$  20 signal as the dominating ammonia signal in the end, is quite extraordinary.

Here, we have an *in-situ* measurement, of ammonia synthesized by the two gasses blowing into the flow cell! The two half-cell reactions in equation (2.3) and (2.4), is thus directly measured here.

Electrolyte is still decomposing, but it is a significant improvement. The observant reader, may point out, that  $m/z$  18, 19 and 20, also could be deuteration of water. Two things argue that this is not the case. The water content in the electrolyte was measured before and after the experiment with a Karl Fischer titrator. These measurements showed an increase of 500 ppm, which is similar to what was measured for the control experiment *FC427* with  $\text{H}_2$ . As was shown in Figure 6.9, while the hydrogen and ammonia signal (which behaved

---

<sup>6</sup>Especially considering an upscaling with different gas and liquid flow.

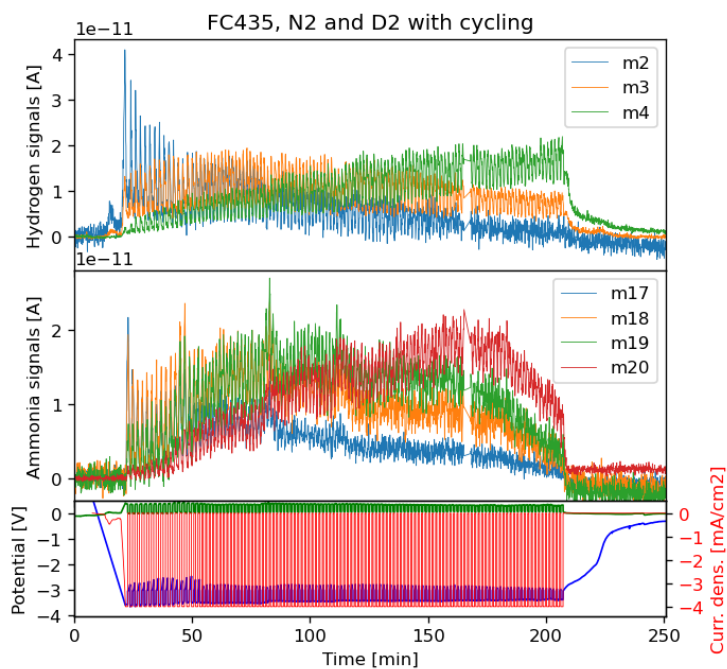


Figure 6.10: (*top*) Mass spec signals for hydrogen signals at  $m/z$  2 ( $H_2$ ), 3 ( $HD$ ), and 4 ( $D_2$ ). (*middle*) Mass spec signals for ammonia signals at  $m/z$  17 ( $NH_3$ ), 18 ( $NDH_2$ ), 19 ( $ND_2H$ ), and 20 ( $ND_3$ ). (*bottom*) Applied potentials and current during cycling procedure.

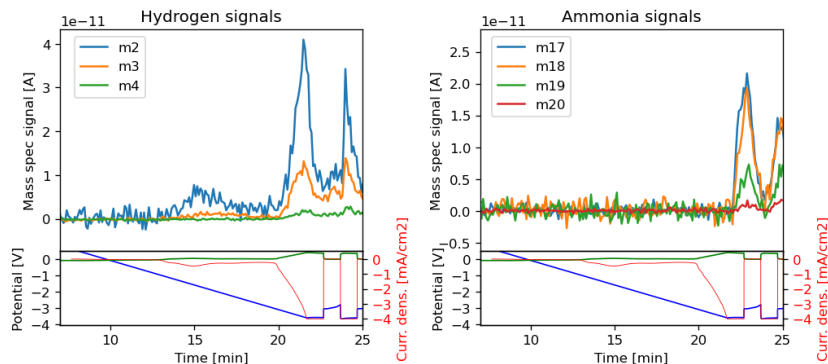


Figure 6.11: Initial sweep of cathode potential, together with hydrogen and ammonia related mass spec signals. An HER occurs a small current around 15 min, is correlated with an  $\text{H}_2$  HD signal. Both hydrogen and ammonia is formed, once the cathode potential is negative enough to plate Li.

exactly as seen in this experiment) increased during applied current, the water signal stayed completely flat. It is therefore safe to assume, that water does not interfere with these measurements.

Looking at the initial sweep of the electrode potential in Figure 6.11, a small current is seen around 15 min, when the cathode potential is between -1 V and -2 V. This is the kind of peak, as was exemplified in Figure 3.2. We see here, that it correlates with hydrogen evolution. But the small increase of HD with  $m/z$  3, shows that it is not only some reduction of electrolyte, but anode products are reduced here as well. As expected, once Li is deposited, both hydrogen and ammonia is produced. Where the hydrogen signals increase immediately with the current, there is a slight delay to the ammonia signal. This is likely due to ammonia sticking to the inner gas-tube surface, thus leading to a delay. With regards to setup improvements, this suggest decreasing the distance between cell and Garm, more heating on gas tubes, and changing tube material to e.g. glass lined steel, which  $\text{NH}_3$  sticks less to [128].

As mentioned multiple times, some work is still missing, on correlating mass spec measurements to other  $\text{NH}_3$ -detecting techniques. Only small adjustments are needed though, as the calculated amount of ammonia does follow the same trend as what is measured with an Ion Chromatograph (IC) C.21. Ammonia synthesis was quantified by periodic samples from the gas trap, and also the final concentration in electrolyte. On top of this, the cathode was submerged in ultra-pure water, to dissolve the deposited and left-over SEI layer. Combining these measurements, the final efficiency was 29.5%, and 12.4 mg of ammonia measured. With the low cell potential, this corresponds to 10.1% energy efficiency.

### 6.3.5 Final comments

We are now not only producing ammonia on microgram-scale but in milligrams. And on top of this, we can show, that the synthesized ammonia, not only stems from  $\text{N}_2$ -reduction, but also (at least partly) from  $\text{H}_2$ -oxidation.

All in all, a successful demonstration of a prototype flow cell is demonstrated. And that is a good way to end the chapter.

# Chapter 7

## Conclusion and outlook

The goal for this project was to create and develop an upscaled electrochemical cell, capable of doing nitrogen reduction to ammonia via the lithium-mediated reaction.

In Chapter 4, four studies on the Li-mediated reaction were presented. What is common for all of these, is the challenging, but necessary, nature of reactions including reactive Li and organic solvents. It was described, how Li reacts with the solvent which forms a protective surface layer (SEI), on top of the negative electrode. This layer modifies the diffusion rate of  $\text{Li}^+$ ,  $\text{N}_2$ , and  $\text{H}^+$ , allowing reduction of nitrogen (NRR) by somewhat impede the competing hydrogen evolution reaction (HER). The surrounding conditions, when forming this layer, has a substantial impact on the performance for ammonia synthesis. Surprisingly, small amounts of  $\text{O}_2$  were found very beneficial for NRR efficiency, which is explained by a slower diffusion of  $\text{Li}^+$ , compared to that of  $\text{N}_2$  and  $\text{H}^+$ . Different organic solvents can support these mechanisms, but their stability has to be considered. During an electrochemical reaction, the bonds in the organic solvents can break, forming a number of by-products. This can also release protons to the solution, which acidifies over time. Rather than depend on oxidation of electrolyte, it would therefore be beneficial to oxidize a hydrogen source instead. It was found to be possible, producing protons from  $\text{H}_2$  in the organic solvent, though transport of these must be improved.

These studies were all done in small-scale glass batch-cells, with a limited amount of electrolyte. Gas supply to the reaction was also restricted, due to the use of submerged and flooded electrodes. An upscaled cell, would therefore require incorporation of gas diffusion electrodes (GDE), facilitating higher accessibility of gas reactants. Furthermore, unlimited access to electrolyte, would be possible with flow of liquid. Chapter 5 described the development process for realizing such an electrochemical cell, through three major iterations. The design process was started with components from a membrane-electrode assembly (MEA) cell. Here supply of gas into the cell was already designed, but without a chamber for

liquid electrolyte. The cell was then modified to accommodate the requirements for Li-mediated ammonia synthesis. First a chamber for electrolyte flow was designed, where ability to produce ammonia with liquid was confirmed. The biggest challenge was to include a GDE, capable of separating liquid and gas. Eventually a thin mesh-type sheet was found able to do so. And with a thin electrode,  $N_2$ -gas could react to form ammonia.

The performance of the cell, was finally tested and measured by means of mass spectrometry. Since the anode and cathode were physically separated, oxidation products could be detected and distinguished at the cathode. With deuterium on the anode, isotope-labelled species could be measured in reduction products, including fully deuterated ammonia,  $ND_3$ . This proved that is possible to combine nitrogen reduction and hydrogen oxidation in the designed flow cell, realizing the goal set for this project.

## 7.1 Outlook

A challenge with the current, and now century old, way of producing ammonia, is the large and centralized production plants. This makes access to ammonia in remote and rural areas, limited and expensive. Electrochemical nitrogen reduction, can change this picture completely. It opens up the possibility for producing ammonia locally, where it is needed, and when it is needed. And since the driving force is electricity, this can be provided from green and renewable sources. Alas, electrochemical ammonia synthesis is currently too small, and limited by design.

The developed cell from this project, aims to change this. Showing that electrochemical ammonia synthesis can be done in larger cells, paves the way forward for meaningful and appreciable production, that could have real impact on people. Though the project was ended with a successful demonstration of a working cell, there are still many challenges to tackle, and paths to explore. The list is long, and the paths are many. I will here just mention a few:

- The organic electrolyte together with lithium, allows the ammonia synthesis to take place. But it also leads to the electrolyte decomposing over time. Can we do something to avoid this? Being inspired from battery research, one might explore the possibility of additives, that initially are sacrificed, but ensures a useful SEI layer. Such candidates would have to be found.
- Can we find stable solvents and electrolytes, that can withstand the tough conditions, with high cell potentials and reactive Li? This should both be stable w.r.t. electrode potentials, but also facilitate transport of protons.
- Are there other alternatives to the organic route? Rigorous testing has so far excluded this. But from a technical viewpoint, it could be very beneficial to not depend on the non-aqueous solvents.

- The developed cell in this project is only a prototype, and should be made even larger. In our group, we believe that a cell with 100 cm<sup>2</sup> area, operating at 100 mA/cm<sup>2</sup> with at least 50% FE, would make commercialization possible and truly impact people.

With many challenges ahead, there is plenty of work to do. I just hope, that the work presented in this thesis, has brought us one step closer.

# Appendices

# Appendix A

## Useful figures

### A.1 Urea prices

Average prices of urea in February 2022 in Sub-Saharan countries. Due to limited accessibility, the prices are significant higher than the world average.

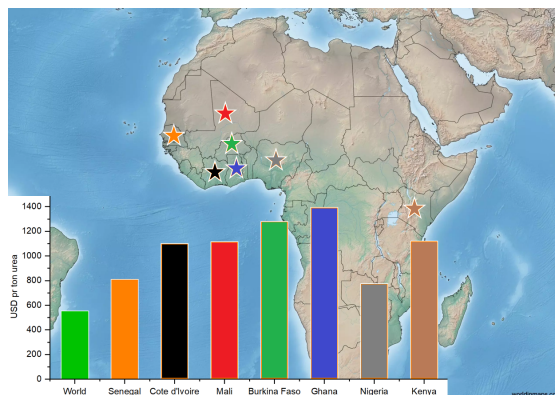


Figure A.1: Average price of urea in February 2022. Map adapted from <https://worldinmaps.com/africa/> and prices sourced from [129].

## A.2 Periodic table

IUPAC Periodic Table of the Elements

1		2		3		4		5		6		7		8		9		10		11		12		13		14		15		16		17		18																																																																																																																																																																																																																																																																																																																																																																																																																																																																																																																																																																																																																																																																																																																																																																																																																																																																																																																																																																																																																																																																																																																																																																																																																																																																																																																									
atomic number	Symbol	atomic number	Symbol	atomic number	Symbol	atomic number	Symbol	atomic number	Symbol	atomic number	Symbol	atomic number	Symbol	atomic number	Symbol	atomic number	Symbol	atomic number	Symbol	atomic number	Symbol	atomic number	Symbol	atomic number	Symbol																																																																																																																																																																																																																																																																																																																																																																																																																																																																																																																																																																																																																																																																																																																																																																																																																																																																																																																																																																																																																																																																																																																																																																																																																																																																																																																																		
name		name		name		name		name		name		name		name		name		name		name		name		name		name		name		name		name		name		name																																																																																																																																																																																																																																																																																																																																																																																																																																																																																																																																																																																																																																																																																																																																																																																																																																																																																																																																																																																																																																																																																																																																																																																																																																																																																																																							
standard atomic weight		standard atomic weight		standard atomic weight		standard atomic weight		standard atomic weight		standard atomic weight		standard atomic weight		standard atomic weight		standard atomic weight		standard atomic weight		standard atomic weight		standard atomic weight		standard atomic weight		standard atomic weight		standard atomic weight		standard atomic weight		standard atomic weight		standard atomic weight		standard atomic weight																																																																																																																																																																																																																																																																																																																																																																																																																																																																																																																																																																																																																																																																																																																																																																																																																																																																																																																																																																																																																																																																																																																																																																																																																																																																																																																							
1	H	hydrogen	2	He	helium	3	Li	lithium	4	Be	beryllium	5	B	boron	6	C	carbon	7	N	nitrogen	8	O	oxygen	9	F	fluorine	10	Ne	neon	11	Na	sodium	12	Mg	magnesium	13	Al	aluminum	14	Si	silicon	15	P	phosphorus	16	S	sulfur	17	Cl	chlorine	18	Ar	argon	19	K	potassium	20	Ca	calcium	21	Sc	scandium	22	Ti	titanium	23	V	vanadium	24	Cr	chromium	25	Mn	manganese	26	Fe	iron	27	Co	cobalt	28	Ni	nickel	29	Cu	copper	30	Zn	zinc	31	Ga	gallium	32	Ge	germanium	33	As	arsenic	34	Se	selenium	35	Br	bromine	36	Kr	krypton	37	Rb	rubidium	38	Sr	strontium	39	Y	yttrium	40	Zr	zirconium	41	Nb	niobium	42	Mo	molybdenum	43	Tc	technetium	44	Ru	rhodium	45	Rh	rhodium	46	Pd	palladium	47	Ag	silver	48	Cd	cadmium	49	In	indium	50	Sn	tin	51	Sb	antimony	52	Te	tellurium	53	I	iodine	54	Xe	xenon	55	Cs	cesium	56	Ba	barium	57-71	lanthanoids	72	Hf	hafnium	73	Ta	tantalum	74	W	tungsten	75	Re	rhodium	76	Os	osmium	77	Ir	iridium	78	Pt	platinum	79	Au	gold	80	Hg	mercury	81	Tl	thallium	82	Pb	lead	83	Bi	bismuth	84	Po	polonium	85	At	astatine	86	Rn	radon	87	Fr	francium	88	Ra	radium	89-103	actinoids	104	Rf	rutherfordium	105	Db	dubnium	106	Sg	seaborgium	107	Bh	bohrium	108	Hs	hassium	109	Mt	meitnerium	110	Ds	darmstadtium	111	Rg	roentgenium	112	Cn	copernicium	113	Nh	nihonium	114	Fl	flerovium	115	Mc	moscovium	116	Lv	livermorium	117	Ts	tennessine	118	Og	oganesson	119	Uu	ununium	120	Uub	ununbium	121	Uut	ununtrium	122	Uuq	ununquadium	123	Uup	ununpentium	124	Uuq	ununhexium	125	Uuh	ununheptium	126	Uuo	ununoctium	127	Uu11	ununundecium	128	Uu12	ununduodecium	129	Uu13	ununtridecium	130	Uu14	ununquadecium	131	Uu15	ununpentadecium	132	Uu16	ununhexadecium	133	Uu17	ununseptadecium	134	Uu18	ununoctadecium	135	Uu19	ununnonadecium	136	Uu20	ununvigintiium	137	Uu21	ununtrigintiium	138	Uu22	ununquadragintiium	139	Uu23	ununquingentiium	140	Uu24	ununsexagintiium	141	Uu25	ununseptuagintiium	142	Uu26	ununoctogintiium	143	Uu27	ununnonagintiium	144	Uu28	ununhundredium	145	Uu29	ununcentium	146	Uu30	ununvigintiium	147	Uu31	ununtrigintiium	148	Uu32	ununquadragintiium	149	Uu33	ununquingentiium	150	Uu34	ununsexagintiium	151	Uu35	ununseptuagintiium	152	Uu36	ununoctogintiium	153	Uu37	ununnonagintiium	154	Uu38	ununhundredium	155	Uu39	ununcentium	156	Uu40	ununvigintiium	157	Uu41	ununtrigintiium	158	Uu42	ununquadragintiium	159	Uu43	ununquingentiium	160	Uu44	ununsexagintiium	161	Uu45	ununseptuagintiium	162	Uu46	ununoctogintiium	163	Uu47	ununnonagintiium	164	Uu48	ununhundredium	165	Uu49	ununcentium	166	Uu50	ununvigintiium	167	Uu51	ununtrigintiium	168	Uu52	ununquadragintiium	169	Uu53	ununquingentiium	170	Uu54	ununsexagintiium	171	Uu55	ununseptuagintiium	172	Uu56	ununoctogintiium	173	Uu57	ununnonagintiium	174	Uu58	ununhundredium	175	Uu59	ununcentium	176	Uu60	ununvigintiium	177	Uu61	ununtrigintiium	178	Uu62	ununquadragintiium	179	Uu63	ununquingentiium	180	Uu64	ununsexagintiium	181	Uu65	ununseptuagintiium	182	Uu66	ununoctogintiium	183	Uu67	ununnonagintiium	184	Uu68	ununhundredium	185	Uu69	ununcentium	186	Uu70	ununvigintiium	187	Uu71	ununtrigintiium	188	Uu72	ununquadragintiium	189	Uu73	ununquingentiium	190	Uu74	ununsexagintiium	191	Uu75	ununseptuagintiium	192	Uu76	ununoctogintiium	193	Uu77	ununnonagintiium	194	Uu78	ununhundredium	195	Uu79	ununcentium	196	Uu80	ununvigintiium	197	Uu81	ununtrigintiium	198	Uu82	ununquadragintiium	199	Uu83	ununquingentiium	200	Uu84	ununsexagintiium	201	Uu85	ununseptuagintiium	202	Uu86	ununoctogintiium	203	Uu87	ununnonagintiium	204	Uu88	ununhundredium	205	Uu89	ununcentium	206	Uu90	ununvigintiium	207	Uu91	ununtrigintiium	208	Uu92	ununquadragintiium	209	Uu93	ununquingentiium	210	Uu94	ununsexagintiium	211	Uu95	ununseptuagintiium	212	Uu96	ununoctogintiium	213	Uu97	ununnonagintiium	214	Uu98	ununhundredium	215	Uu99	ununcentium	216	Uu100	ununvigintiium	217	Uu101	ununtrigintiium	218	Uu102	ununquadragintiium	219	Uu103	ununquingentiium	220	Uu104	ununsexagintiium	221	Uu105	ununseptuagintiium	222	Uu106	ununoctogintiium	223	Uu107	ununnonagintiium	224	Uu108	ununhundredium	225	Uu109	ununcentium	226	Uu110	ununvigintiium	227	Uu111	ununtrigintiium	228	Uu112	ununquadragintiium	229	Uu113	ununquingentiium	230	Uu114	ununsexagintiium	231	Uu115	ununseptuagintiium	232	Uu116	ununoctogintiium	233	Uu117	ununnonagintiium	234	Uu118	ununhundredium	235	Uu119	ununcentium	236	Uu120	ununvigintiium	237	Uu121	ununtrigintiium	238	Uu122	ununquadragintiium	239	Uu123	ununquingentiium	240	Uu124	ununsexagintiium	241	Uu125	ununseptuagintiium	242	Uu126	ununoctogintiium	243	Uu127	ununnonagintiium	244	Uu128	ununhundredium	245	Uu129	ununcentium	246	Uu130	ununvigintiium	247	Uu131	ununtrigintiium	248	Uu132	ununquadragintiium	249	Uu133	ununquingentiium	250	Uu134	ununsexagintiium	251	Uu135	ununseptuagintiium	252	Uu136	ununoctogintiium	253	Uu137	ununnonagintiium	254	Uu138	ununhundredium	255	Uu139	ununcentium	256	Uu140	ununvigintiium	257	Uu141	ununtrigintiium	258	Uu142	ununquadragintiium	259	Uu143	ununquingentiium	260	Uu144	ununsexagintiium	261	Uu145	ununseptuagintiium	262	Uu146	ununoctogintiium	263	Uu147	ununnonagintiium	264	Uu148	ununhundredium	265	Uu149	ununcentium	266	Uu150	ununvigintiium	267	Uu151	ununtrigintiium	268	Uu152	ununquadragintiium	269	Uu153	ununquingentiium	270	Uu154	ununsexagintiium	271	Uu155	ununseptuagintiium	272	Uu156	ununoctogintiium	273	Uu157	ununnonagintiium	274	Uu158	ununhundredium	275	Uu159	ununcentium	276	Uu160	ununvigintiium	277	Uu161	ununtrigintiium	278	Uu162	ununquadragintiium	279	Uu163	ununquingentiium	280	Uu164	ununsexagintiium	281	Uu165	ununseptuagintiium	282	Uu166	ununoctogintiium	283	Uu167	ununnonagintiium	284	Uu168	ununhundredium	285	Uu169	ununcentium	286	Uu170	ununvigintiium	287	Uu171	ununtrigintiium	288	Uu172	ununquadragintiium	289	Uu173	ununquingentiium	290	Uu174	ununsexagintiium	291	Uu175	ununseptuagintiium	292	Uu176	ununoctogintiium	293	Uu177	ununnonagintiium	294	Uu178	ununhundredium	295	Uu179	ununcentium	296	Uu180	ununvigintiium	297	Uu181	ununtrigintiium	298	Uu182	ununquadragintiium	299	Uu183	ununquingentiium	300	Uu184	ununsexagintiium	301	Uu185	ununseptuagintiium	302	Uu186	ununoctogintiium	303	Uu187	ununnonagintiium	304	Uu188	ununhundredium	305	Uu189	ununcentium	306	Uu190	ununvigintiium	307	Uu191	ununtrigintiium	308	Uu192	ununquadragintiium	309	Uu193	ununquingentiium	310	Uu194	ununsexagintiium	311	Uu195	ununseptuagintiium	312	Uu196	ununoctogintiium	313	Uu197	ununnonagintiium	314	Uu198	ununhundredium	315	Uu199	ununcentium	316	Uu200	ununvigintiium	317	Uu201	ununtrigintiium	318	Uu202	ununquadragintiium	319	Uu203	ununquingentiium	320	Uu204	ununsexagintiium	321	Uu205	ununseptuagintiium	322	Uu206	ununoctogintiium	323	Uu207	ununnonagintiium	324	Uu208	ununhundredium	325	Uu209	ununcentium	326	Uu210	ununvigintiium	327	Uu211	ununtrigintiium	328	Uu212	ununquadragintiium	329	Uu213	ununquingentiium	330	Uu214	ununsexagintiium	331	Uu215	ununseptuagintiium	332	Uu216	ununoctogintiium	333	Uu217	ununnonagintiium	334	Uu218	ununhundredium	335	Uu219	ununcentium	336	Uu220	ununvigintiium	337	Uu221	ununtrigintiium	338	Uu222	ununquadragintiium	339	Uu223	ununquingentiium	340	Uu224	ununsexagintiium	341	Uu225	ununseptuagintiium	342	Uu226	ununoctogintiium	343	Uu227	ununnonagintiium	344	Uu228	ununhundredium	345	Uu229	ununcentium	346	Uu230	ununvigintiium	347	Uu231	ununtrigintiium	348	Uu232	ununquadragintiium	349	Uu233	ununquingentiium	350	Uu234	ununsexagintiium	351	Uu235	ununseptuagintiium	352	Uu236	ununoctogintiium	353	Uu237	ununnonagintiium	354	Uu238	ununhundredium	355	Uu239	ununcentium	356	Uu240	ununvigintiium	357	Uu241	ununtrigintiium	358	Uu242	ununquadragintiium	359	Uu243	ununquingentiium	360	Uu244	ununsexagintiium	361	Uu245	ununseptuagintiium	362	Uu246	ununoctogintiium	363	Uu247	ununnonagintiium	364	Uu248	ununhundredium	365	Uu249	ununcentium	366	Uu250	ununvigintiium	367	Uu251	ununtrigintiium	368	Uu252	ununquadragintiium	369	Uu253	ununquingentiium	370	Uu254	ununsexagintiium	371	Uu255	ununseptuagintiium	372	Uu256	ununoctogintiium	373	Uu257	ununnonagintiium	374	Uu258	ununhundredium	375	Uu259	ununcentium	376	Uu260	ununvigintiium	377	Uu261	ununtrigintiium	378	Uu262	ununquadragintiium	379	Uu263	ununquingentiium	380	Uu264	ununsexagintiium	381	Uu265	ununseptuagintiium	382	Uu266	ununoctogintiium	383	Uu267	ununnonagintiium	384	Uu268	ununhundredium	385	Uu269	ununcentium	386	Uu270	ununvigintiium	387	Uu271	ununtrigintiium	388	Uu272	ununquadragintiium	389	Uu273	ununquingentiium	390	Uu274	ununsexagintiium	391	Uu275	ununseptuagintiium	392	Uu276	ununoctogintiium	393	Uu277	ununnonagintiium	394	Uu278	ununhundredium	395	Uu279	ununcentium	396	Uu280	ununvigintiium	397	Uu281	ununtrigintiium	398	Uu282	ununquadragintiium	399	Uu283	ununquingentiium	400	Uu284	ununsexagintiium	401	Uu285	ununseptuagintiium	402	Uu286	ununoctogintiium	403	Uu287	ununnonagintiium	404	Uu288	ununhundredium	405	Uu289	ununcentium	406	Uu290	ununvigintiium	407	Uu291	ununtrigintiium	408	Uu292	ununquadragintiium	409	Uu293	ununquingentiium	410	Uu294	ununsexagintiium	411	Uu295	ununseptuagintiium	412	Uu296	ununoctogintiium	413	Uu297	ununnonagintiium	414	Uu298	ununhundredium	415	Uu299	ununcentium	416	Uu300	ununvigintiium	417	Uu301	ununtrigintiium	418	Uu302	ununquadragintiium	419	Uu303	ununquingentiium	420	Uu304	ununsexagintiium	421	Uu305	ununseptuagintiium	422	Uu306	ununoctogintiium	423	Uu307	ununnonagintiium	424	Uu308	ununhundredium	425	Uu309	ununcentium	426	Uu310	ununvigintiium	427	Uu311	ununtrigintiium	428	Uu312	ununquadragintiium	429	Uu313	ununquingentiium	430	Uu314	ununsexagintiium	431	Uu315	ununseptuagintiium	432	Uu316	ununoctogintiium	433	Uu317	ununnonagintiium	434	Uu318	ununhundredium	435	Uu319	ununcentium	436	Uu320	ununvigintiium	437	Uu321	ununtrigintiium	438	Uu322	ununquadragintiium	439	Uu323	ununquingentiium	440	Uu324	ununsexagintiium	441	Uu325	ununseptuagintiium	442	Uu326	ununoctogintiium	443	Uu327	ununnonagintiium	444	Uu328	ununhundredium	445	Uu329	ununcentium	446	Uu330	ununvigintiium	447	Uu331	ununtrigintiium	448	Uu332	ununquadragintiium	449	Uu333	ununquingentiium	450	Uu334	ununsexagintiium	451	Uu335	ununseptuagintiium	452	Uu336	ununoctogintiium	453	Uu337	ununnonagintiium	454	Uu338	ununhundredium	455	Uu339	ununcentium	456	Uu340	ununvigintiium	457	Uu341	ununtrigintiium	458	Uu342	ununquadragintiium	459	Uu343	ununquingentiium	460	Uu344	ununsexagintiium	461	Uu345	ununseptuagintiium	462	Uu346	ununoctogintiium	463	Uu347	ununnonagintiium	464	Uu348	ununhundredium	465	Uu349

# Appendix B

## Figures for Chapter 5

Section for figures and additional discussion for Chapter 5 on the flow cell design process.

### B.1 Initial tests of membranes

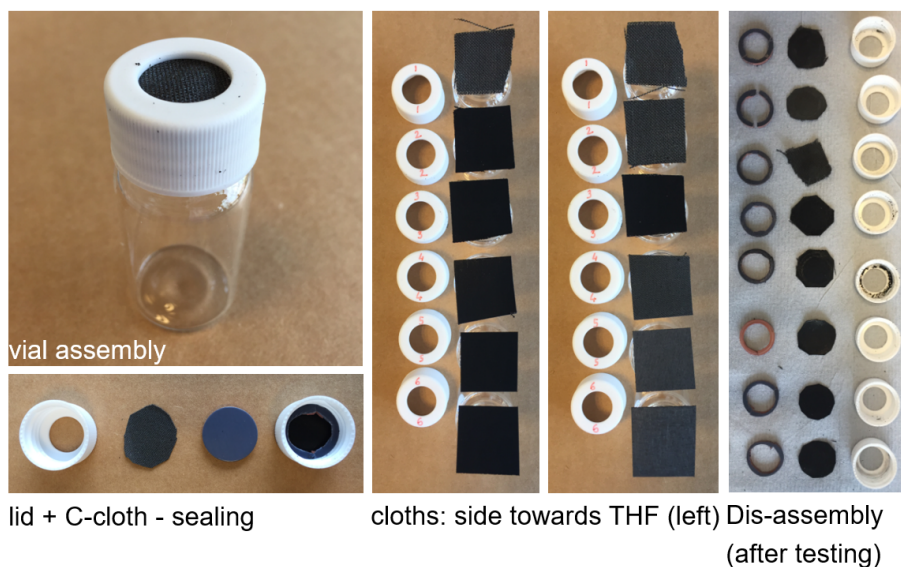


Figure B.1: Image of tests of various carbon based membranes, and their applicability with the organic solvent. Courtesy of Mattia Saccoccio.

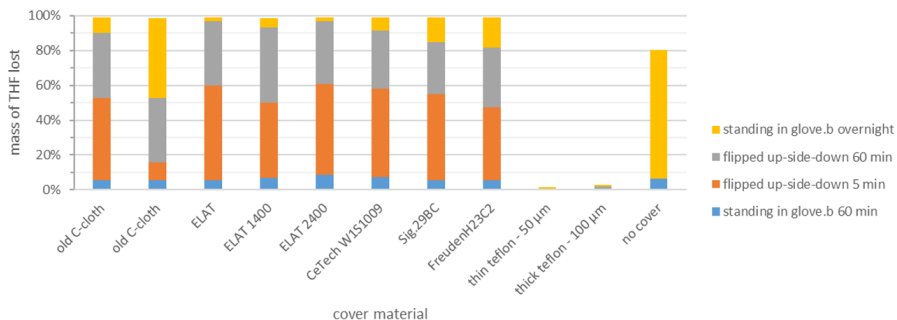


Figure B.2: Summary of membrane tests. The organic solvent evaporated through all the carbon membranes overnight. Only Teflon membranes could contain the solvent. Courtesy of Mattia Saccoccio.

Tests of various membranes' ability to keep electrolyte over time. A known amount of solvent was added to a vial, and the vial was closed with the specific membrane. The organic electrolyte evaporated through the C-membranes - even significant amounts within a short time period. Polytetrafluoroethylene (PTFE) was the only membrane that showed negligible evaporation over the course of a day.

The tested membranes were: ELAT (*hydrophilic plain cloth*), ELAT (*LT1400*) and ELAT (*LT2400*) from NuVant Systems; carbon cloth with microporous layer (*W1S1009*) from CeTech; Sigracet (*29 BC*) from SGL Carbon; and Freudenberg (*H23C2*) from FuelCellStore.

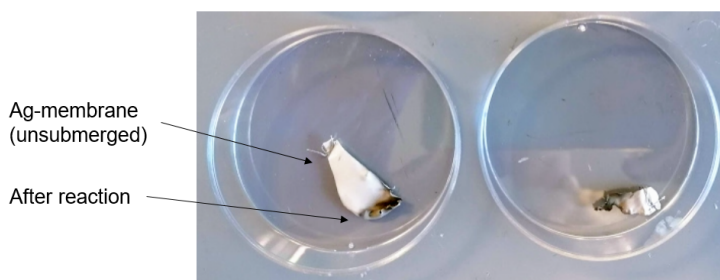


Figure B.3: Silver membrane tested for Li-mediated reaction. The membrane itself is white, but crumpled up and turned black after reaction.

Thin porous Ag membranes (1.2  $\mu\text{m}$  pore size, Sterlitech) neither showed usefulness in the Li-mediated process. Similarly to the C-based membranes, THF evaporated through while standing in a glovebox. The membrane itself was white, but after reaction with Li, it crumpled together and changed its texture. This was due to Li deposition within the pore structure, and since the sheet was so thin, it could not maintain its shape.

## B.2 Technical drawing

3D model of the first iteration of the flow cell electrolyte chamber. Chamber manufactured in Al, and later electrochemically oxidized for chemical and mechanical stability.

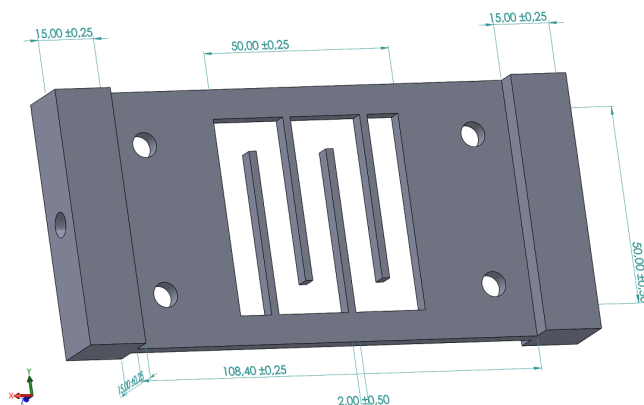


Figure B.4: 3D model of the first iteration of the electrolyte chamber. The chamber itself is 50 mm×50 mm, with four fingers to guide the electrolyte around.

A combined and exploded view of the predesigned cell parts from the CO<sub>2</sub> electrolysis group. The three parts are the supporting Al structure, a Cu current collector and a Ti gas flow field.

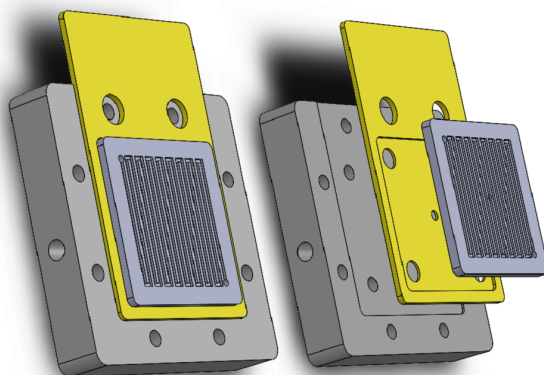


Figure B.5: 3D model of the predesigned cell parts, used in the first iteration of the flow cell.

### B.3 Anodization of Al parts

In the first iteration of the flow cell, the supporting structure and the electrolyte chamber were manufactured in aluminium (Al), as this could be electrochemically oxidized afterwards. Oxidation of the Al parts would form an alumina ( $\text{Al}_2\text{O}_3$ ) surface layer, which is both non-conductive, chemically resistant and mechanically hard. The oxidation procedure followed these steps:

- Polish the Al part with abrasive paper
- Clean part in de-ionized or ultrapure water
- Dip in 0.1 M NaOH solution for about 5 min
- Rinse in de-ionized or ultrapure water
- Connect Al-wires to the Al part
- Immerse it in 20 vol.%  $\text{H}_2\text{SO}_4$  and apply positive current on Al part (about  $10 \text{ mA/cm}^2$ ). The negative counter electrode should be a sacrificial piece of aluminium.
- Boil at  $100^\circ \text{C}$  in water for 1 hour to close pores
- Concentration of NaOH and  $\text{H}_2\text{SO}_4$  can be higher than mentioned.

The parts were always cleaned using ultrapure water (Milli-Q). If needed, an additional cleaning step with ethanol was included. An image of the anodization step in  $\text{H}_2\text{SO}_4$  for both the electrolyte chamber and one of the supporting structures, are shown in Figure B.6.



Figure B.6: Electrochemical anodization of aluminium parts for creating a surface protecting layer.

## B.4 Various figures

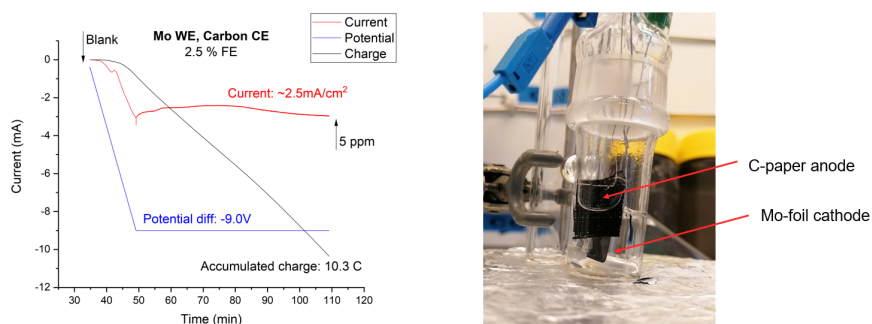


Figure B.7: Initial test of electrode materials for first iteration. C-paper as anode and Mo-foil as anode. Applying -9 V across the electrodes yielded stable currents and 2.5% FE.

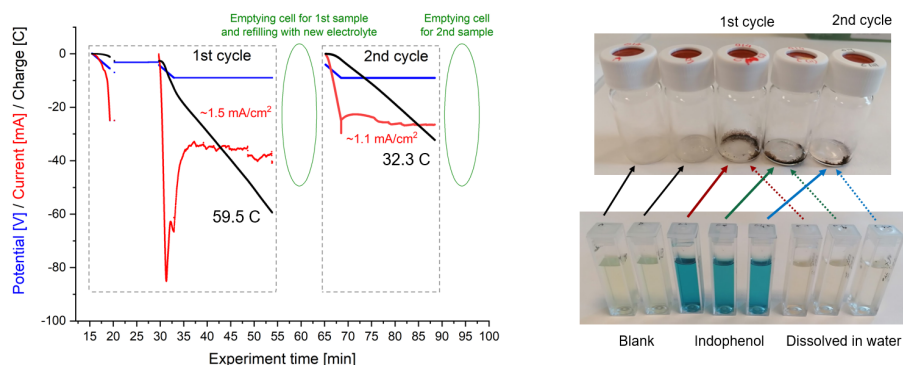


Figure B.8: First recorded successful ammonia synthesis in the first iteration of the flow cell. 2-electrode setup with -9 V applied. Ammonia synthesis measured with indophenol reaction, showing about 10 ppm ammonia in solution corresponding to ~5% FE.

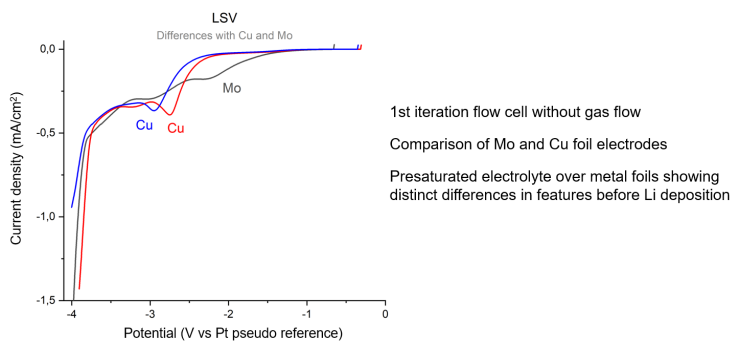


Figure B.9: Linear sweep voltammetry (LSV) on Mo and Cu foils measured in the first iteration of the flow cell. No gas is flowing on the electrodes, but  $N_2$ -saturated electrolyte is flowing through the electrolyte chamber.

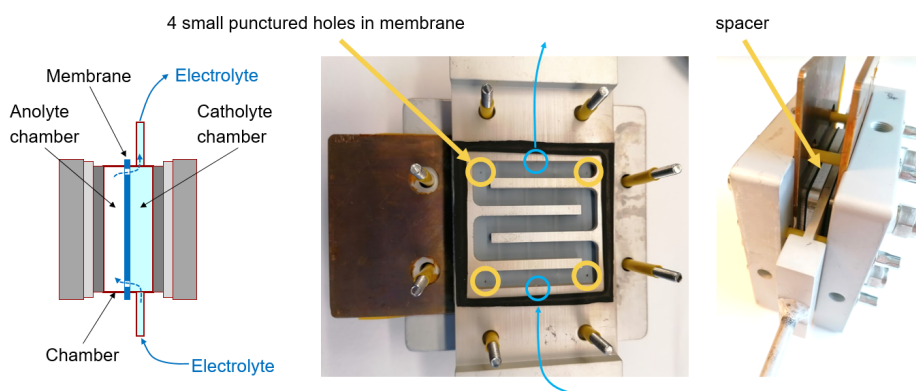


Figure B.10: Explanatory schematics and images on testing membranes for 2-chamber measurements. A spacer was used for creating room for the second anode chamber. Since the second chamber had no electrolyte in- or outlets, the chamber was filled through small punctured holes in the membrane.

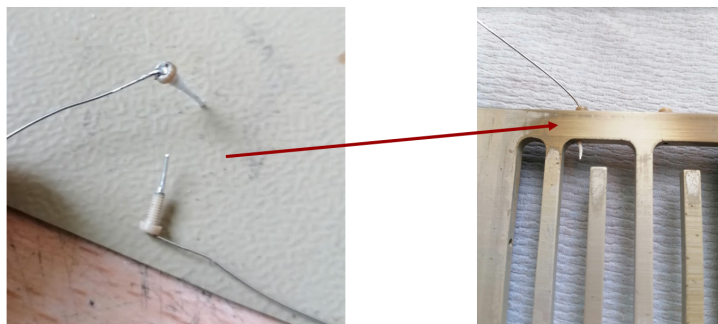


Figure B.11: New solution for introducing reference wire into electrolyte chamber through the side. Custom made fittings with small 2 mm PEEK screws.

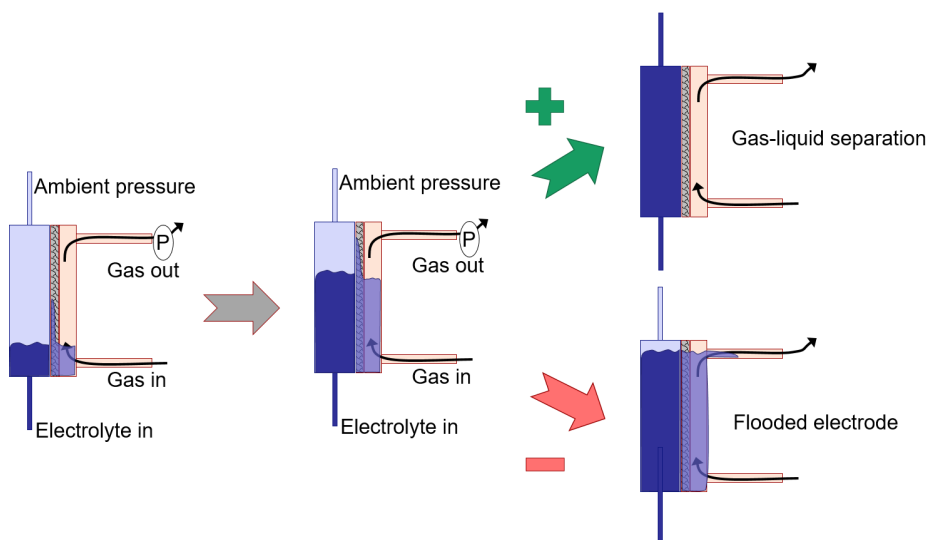


Figure B.12: Drawings of the challenges faced with gas diffusion electrodes (GDEs) in the flow cell. With no control, the electrolyte go through the electrode and can flood out the gas lines. The aim is to achieve a liquid-gas separation, keeping gas on one side and liquid on the other side of the electrode.



Figure B.13: Overview of a number of problems that started occurring after repeated experiments. (1) During Li deposition, the porous structure could be filled and block access to gas from the backside. (2) The Pt sputtered anode block was visibly damaged from surface reactions. (3) The surface of the electrolyte chamber got a grainy surface texture after some chemical reaction. (4) The reference electrode had a thin brown deposit on the side facing the anode, from some leftover electrolyte decomposition products.



Figure B.14: Reactions of stainless steel with either electrolyte or Li. Thick black deposits on the cathode was observed after a reduction experiment, where also the anode had remnants on its surface. This lead to much colouration of electrolyte (see next figure), probably from iron leaching from the stainless steel.

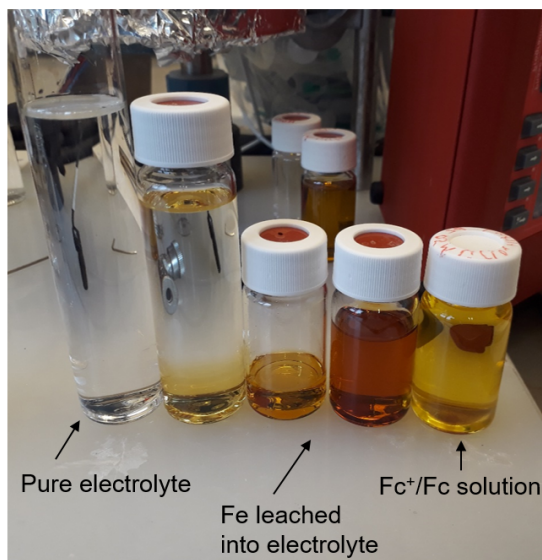


Figure B.15: Visible comparison of electrolyte extracted from the flow cell, after Fe had leached out of the stainless steel mask components. The yellow and red solutions are the part containing Fe compounds. The different shades depend on the concentration of these compounds, as electrolyte was pulled out of the cell. The electrolyte is visibly compared to a ferrocene containing THF solution to the right.

## B.5 NRR on Cu

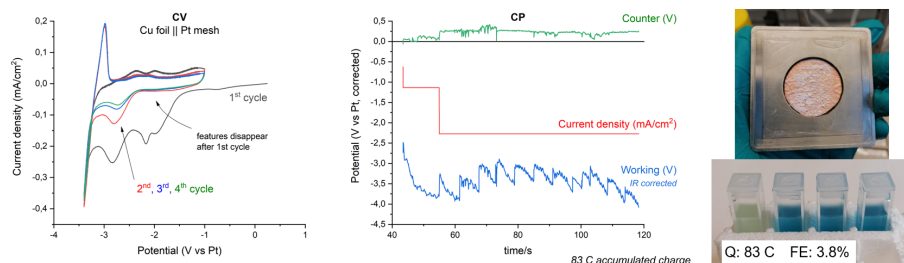


Figure B.16: Nitrogen reduction on a Cu foil in the flow cell.  $N_2$  saturated electrolyte used.

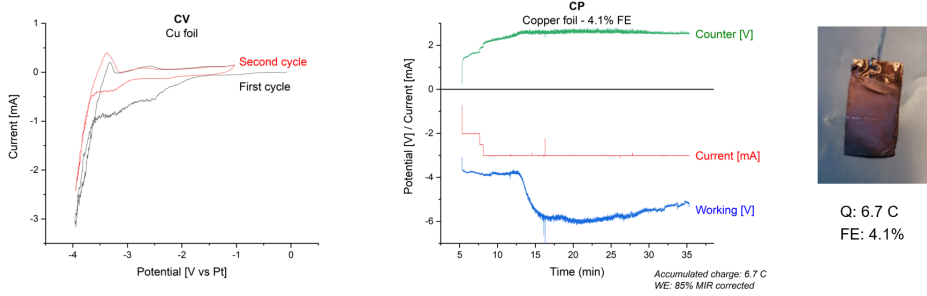


Figure B.17: Nitrogen reduction on a Cu foil in a glass cell as control experiment.  $N_2$  bubbling in electrolyte during electrolysis.

## B.6 Electrodeposition of Cu on electrodes



Figure B.18: Electrochemical Cu deposition on porous disk and SEM image of surface morphology. The Cu deposition gives the electrode a red colour and the SEM image shows deposition of small structures.

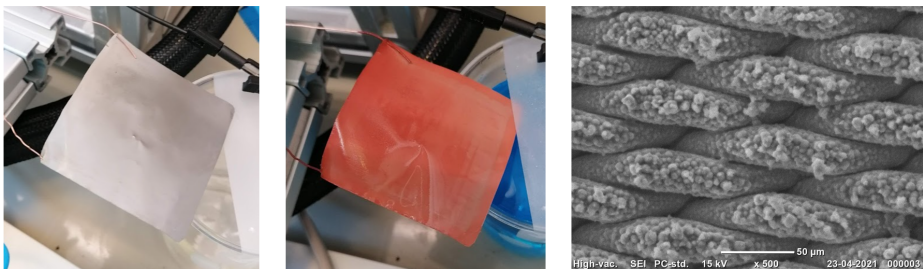


Figure B.19: Electrochemical Cu deposition on woven mesh and SEM image of surface morphology. The Cu deposition gives the mesh a red colour and the SEM image shows deposition of small micrometer-sized structures.

# Appendix C

## Figures for Chapter 6

Section for figures and additional discussion for Chapter 6 on the flow cell measurements.

### C.1 Flow cell measurements

Repeated measurements in the flow cell, showed low FE and non-reproducible operation. Calculations based on electrolyte samples.

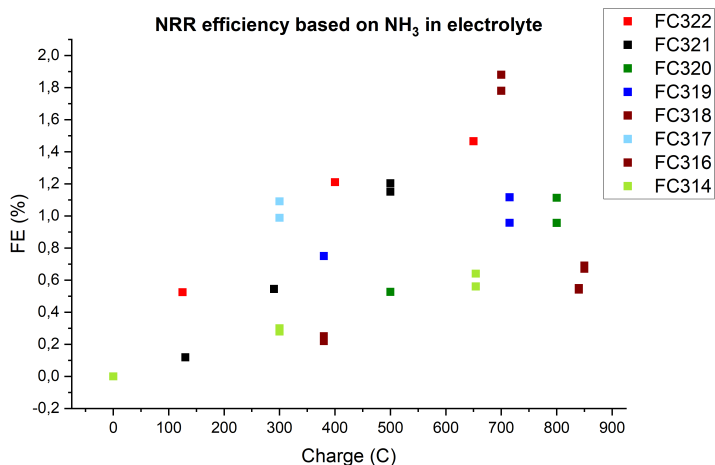


Figure C.1: Faradaic efficiency calculation for multiple experiments with gas and electrolyte flow in the flow cell. Numbers represent the FE towards NH<sub>3</sub>, based on measured concentration in the electrolyte. Measurements from same experiments as shown in Figure 6.1.

Electrochemical data, from a representative experiment (label: *FC317*), with 1 M  $\text{LiClO}_4$  in THF with 1 vol.% EtOH. Cathode was a stainless steel mesh (mesh size  $325 \times 2300$ ) with electrodeposited Cu. Anode was similar mesh, but sputter deposited Pt. Notice the anode potential, that at all times are below +1 V *vs* Pt pseudo reference. Initially fluctuating around +0.5 V, but decreased to about +0.1 V at 32 min. At this point, the flow of  $\text{H}_2$  to the anode was increased.

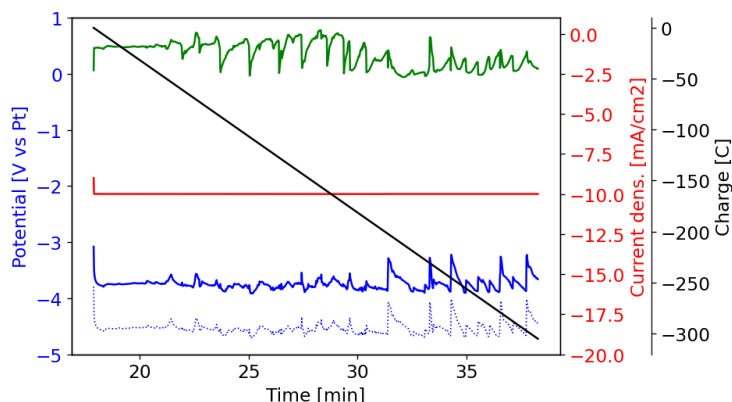


Figure C.2: EC-data from a representative flow cell experiment *FC317*. This experiment was only run for 20 minutes, passing 300 C of charge. Cathode (blue), Anode (green), Current density (red), and Charge (black). Blue stipulated line is uncompensated potential, whereas solid line is IR-corrected (3.6).

Electrochemical data, from a long experiment (label: *FC319*). Similar electrodes and electrolyte as for *FC317*. Experiment was momentarily stopped, due to an overload of the potentiostat (current beyond 400 mA) at 28 min. The reference is initially shifted, where the IR-compensated solid blue line during Li-deposition is at -2.5 V. When experiment is restarted, the cathode potential is at the expected -3 V as  $\text{Li}^+/\text{Li}^0$  potential. During high current density ( $16 \text{ mA/cm}^2$ ), the anode potential is very anodic (1-2 V *vs* Pt at 31-42 mins), but drops to  $\sim +0.5$  V at  $10 \text{ mA/cm}^2$ . The noise on the anode potential, may be due to periodic flooding of the electrode.

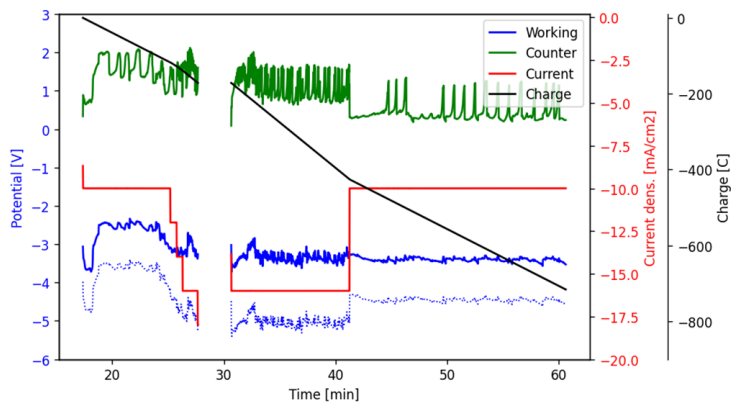


Figure C.3: EC-data from a longer flow cell experiment *FC319*, where 700 C of charge was passed. Cathode (blue, solid line IR corrected for 4.2 ), Anode (green), Current density (red), and Charge (black). Blue stipulated line is uncompensated potential, whereas blue line is IR-corrected (3.6 ).

After the above experiment (*FC319*), Li-deposits could be seen on the cathode. We know Li is necessary for the NRR reaction, which was measured to 1.7%. The electrolyte had visibly decomposed substantially, turning dark brown after electrolysis.

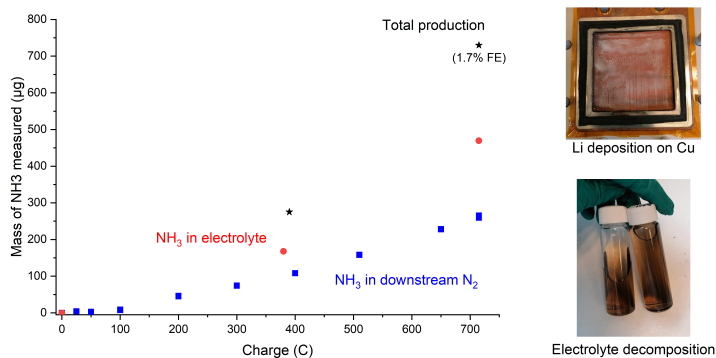


Figure C.4: Ammonia synthesis for *FC319*, measured in both gas and electrolyte phase. The reaction is followed with substantial electrolyte decomposition.

Covered cathode electrode, for lower surface area during NRR.

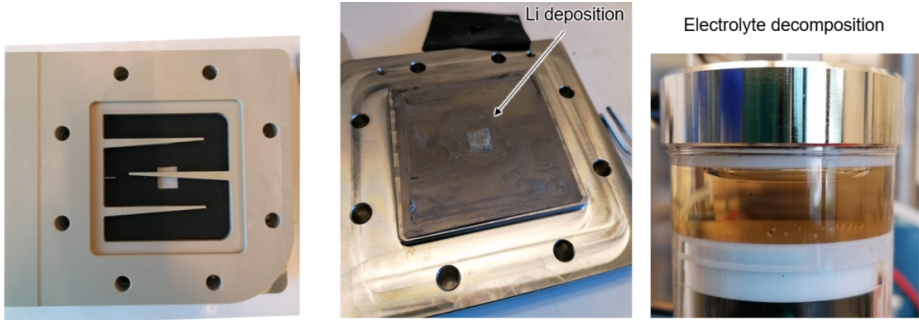


Figure C.5: (left) Covered cathode area with a FFKM perfluoroelastomer sheet. 1 cm<sup>2</sup> was hereby exposed to electrolyte. (middle) After a total of 415 C was passed, a thick layer of Li had been deposited. (right) Despite a low anodic potential of 50 mV was measured, electrolyte still showed decomposition products.

Covered cathode electrode, for lower surface area during NRR.

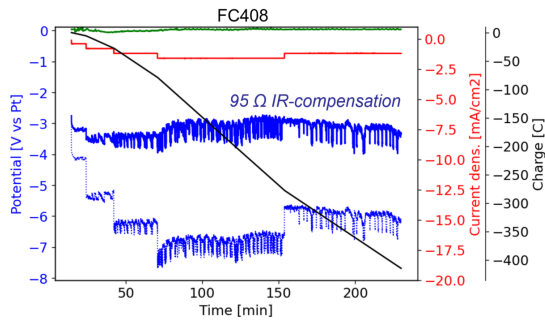


Figure C.6: Measured EC-data for *FC408* experiment, with covered cathode area. Due to the smaller area, the resistance was markedly higher (95  $\Omega$ ) than a non-covered electrode ( $\sim 4$   $\Omega$ ). Calculated IR-compensation, showed the cathode to be at -3 V vs Pt, as expected for Li deposition (and seen in C.5).

## C.2 Mass spec measurements

Various measurements regarding the performance of the mass spec setup Garm.

### C.2.1 Mass spec settings and optimization

The QMG420 mass spec, had the possibility to adjust a number of parameters. The standard settings for potentials are listed below:

V1	Ion reference (anode)	90 V
<b>V2</b>	<b>Cathode</b>	<b>70 V</b>
V3	Focus	20
V4	Field axis	15
V5	Extraction field	250
V6	Inner deflector	300
V7	Outer deflector	0
V8		0
V9	Wehnelt	30

The cathode or ionization potential is V2. As written in bold, the standard parameter is set to 70 eV. At 70 eV ionization, there much signal is detected. A low beam current of 0.1 mA was therefore used.

By successively change and optimize the potentials, settings for soft ionization at 26 eV was determined as follows:

V1	Ion ref	90 V
<b>V2</b>	<b>Cathode</b>	<b>26 V</b>
V3	Focus	16
V4	Field axis	15
V5	Extraction field	250
V6	Inner deflector	300
V7	Outer deflector	0
V8		0
V9	Wehnelt	20

Many of the standard potentials, was found to be fine for lower ionization potentials as well. The V9 was recommended by the supplier to be set at 20 V, when decreasing V2 below 40 V. At decreased ionization potential, the signal was lower, and compensated for by increasing the current to 0.2 mA.

The effect of soft ionization is shown in Figure C.7, measured by bubbling N<sub>2</sub> through a glass cell containing THF. Gas flow out of the cell is directed over Garm for MS detection. At 70 eV ionization, many peaks are seen. The peaks decrease as the potential is lowered. Cracking patterns decrease as well, where e.g.  $m/z$  1 and 14 disappear below 40 eV. At 20 eV, no signal is measured at any mass, and only a small signal is seen at  $m/z$  18 at 25 eV

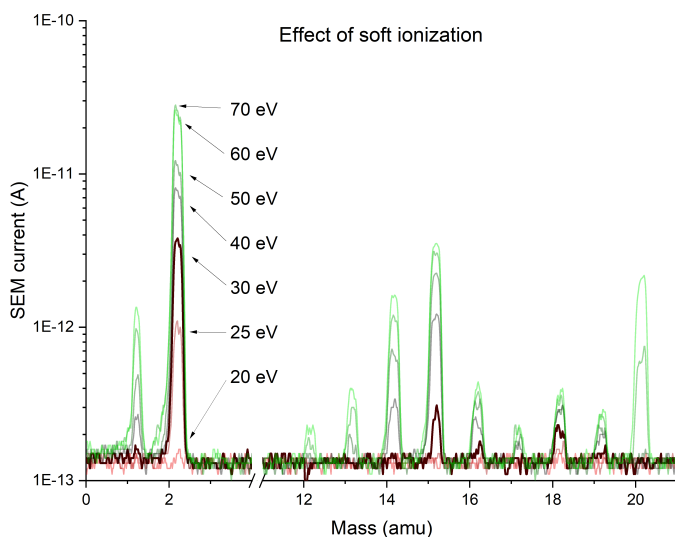


Figure C.7: Mass spectra measured from bubbling  $N_2$  through THF in a glass cell. Spectrum for 30 eV is highlighted for reference.

## C.2.2 Mass spec calibrations

### Soft ionization for water and ammonia detection

The ability to distinguish  $NH_3$  from  $H_2O$  signals with Garm on the flow cell, is shown in Figure C.8. Setup is depicted in Figure C.9. An ethanol solution containing aqueous ammonium hydroxide was added to the electrolyte sampling unit. The solution was pulled into the syringe pump, and pushed through the cell. Initially at a high flow rate (15 ml/min), in order to quickly replace the liquid already in the cell. Eventually, an ethanol solution with water was added the same way. At this point, despite an increase in  $m/z$  18 from water, no increase is seen in  $m/z$  17 from ammonia. Water content was determined with a Karl-Fischer titrator, and  $NH_3$  using the indophenol method. The resulting calibration is presented in Figure C.10, showing very good linearity in measurements. Though, the MS settings for measurements were later adjusted, why the calibration curves are not strictly applicable.

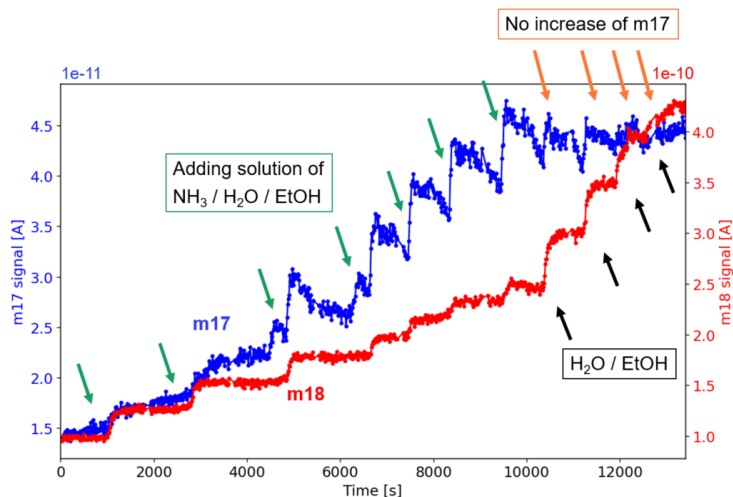


Figure C.8: Mass-time measurements of  $m/z$  17 and 18, in an  $N_2$  flow over one electrode in the flow cell. The cell was successively filled with ethanol solution, containing water and ammonia in increased concentrations. When only ethanol with water is added, there is no signal increase for  $m/z$  17 while 18 increases significantly.

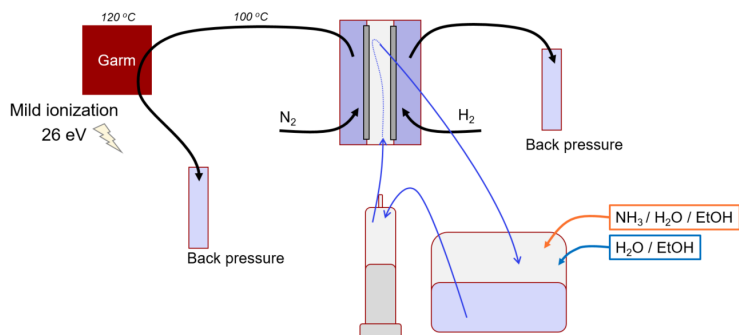


Figure C.9: Schematics of measurement setup, for showing distinction of water and ammonia signals with Garm using soft ionization. Ethanol solution containing either aqueous ammonia, or water, is added to the electrolyte sampling unit. With a syringe pump, the solution is flown through the cell, and measured with Garm.

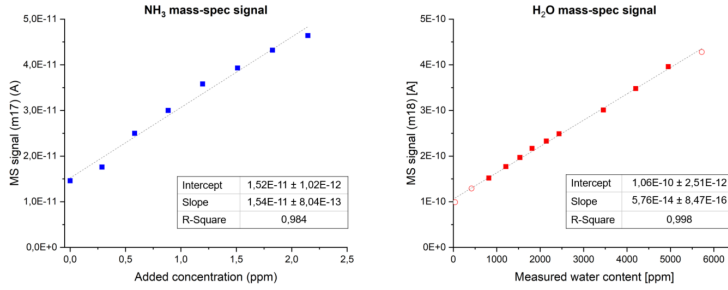


Figure C.10: The resulting measurements show good linearity for both NH<sub>3</sub> and H<sub>2</sub>O measurements. Settings were though later adjusted, and numbers therefore not strictly applicable.

### Gas calibrations

Gas calibrations were made, by controlling the gas flow of N<sub>2</sub>, and H<sub>2</sub> or NH<sub>3</sub> respectively, with a mass flow controller (MFC) from Brooks. The two gasses were mixed through a gas tube, leading to Garm for detection. Gasses used were 5.0 N<sub>2</sub>, 5.0 H<sub>2</sub> and 300 ppm NH<sub>3</sub> in N<sub>2</sub> from Air Liquide.

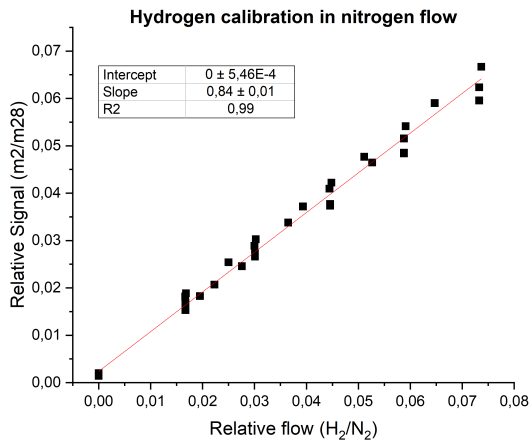
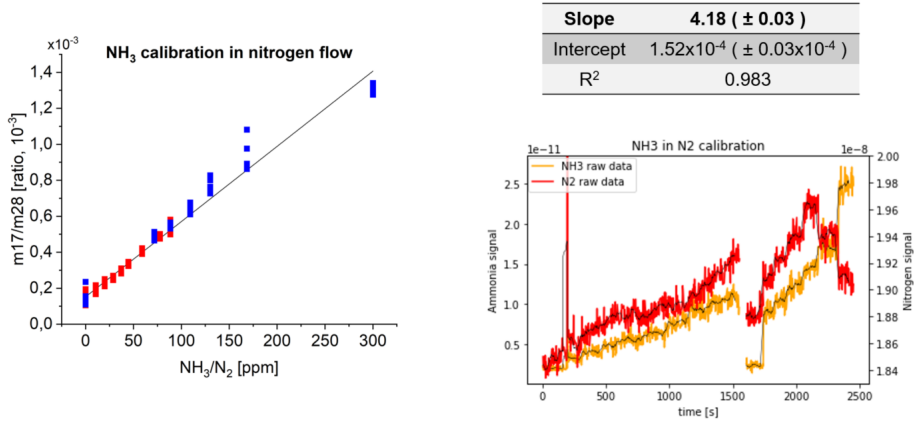


Figure C.11: Gas calibration-curve for H<sub>2</sub> diluted in N<sub>2</sub>.


 Figure C.12: Gas calibration-curve for NH<sub>3</sub> diluted in N<sub>2</sub>.

The FE for NRR and HER can then be calculated as follows

$$FE_{HER} = \frac{m2}{m28} \times \dot{V}_{N_2} \times \frac{1}{22400 \text{ mol/L}} \times \frac{1}{60 \text{ s/min}} \times F \times \frac{7/6}{\beta_{H_2}} \times \frac{1}{I_{cell}} \quad (\text{C.1})$$

$$FE_{NRR} = \frac{m17}{m28} \times \dot{V}_{N_2} \times \frac{1}{22400 \text{ mol/L}} \times \frac{1}{60 \text{ s/min}} \times F \times \frac{7/6}{\beta_{NH_3}} \times \frac{1}{I_{cell}} \quad (\text{C.2})$$

where  $m2$ ,  $m17$ , and  $m28$  are the MS measurements on the respective masses.  $\dot{V}_{N_2}$  is the N<sub>2</sub> flow rate,  $F$  is Faraday's constant, and the factor  $7/6$ , is a correction to the flow provided by the MFC.

### C.2.3 Data presentation

Graphs of various data Figures for discussion on the flow cell operation.

First mass spec-flow cell measurement (*FC416*).

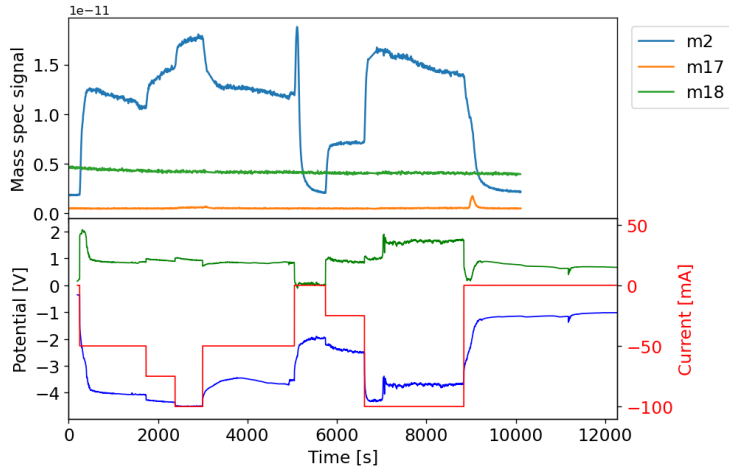


Figure C.13: Electrochemical data combined with mass spec measurements, on the first mass spec/flow cell experiment ( $FC_{416}$ ). Line-colours in lower graph is cathode (blue), anode (green), and current density (red). Measured with soft ionization.

Ammonia signal in  $FC_{417}$ . Tracking  $m/z$  17 and 18.

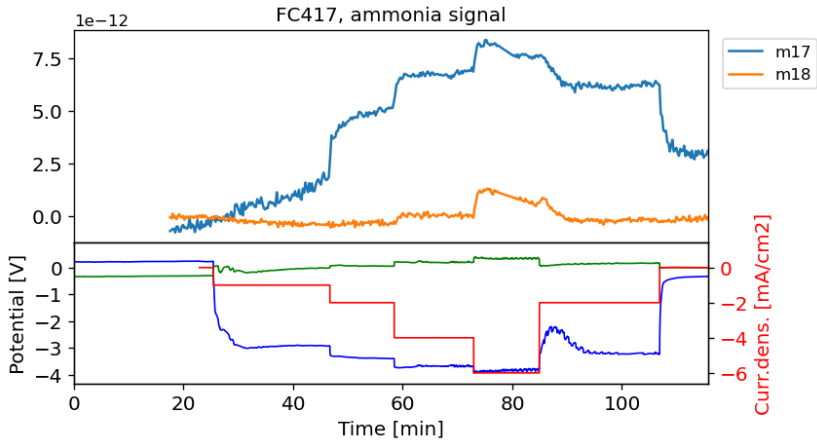


Figure C.14: Mass spec and electrochemistry measurements on  $FC_{417}$ . Increase of ammonia signal at  $m/z$  17. Under high currents,  $m/z$  18 increases too. Either from water ( $H_2O$ ) or partially deuterated ammonia ( $NDH_2$ ). Measured with soft ionization.

Electrolyte decomposition observed after  $FC_{417}$  experiment.

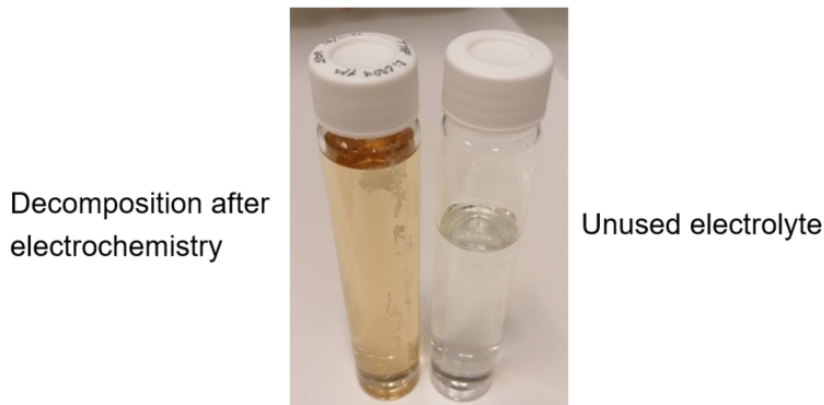


Figure C.15: Visible signs of electrolyte decomposition, after  $FC_{417}$  experiment, where both  $H^+$  and  $D^+$  was observed.

Raw MS-data on  $m/z$  2-4 together with EC-data for  $FC_{425}$ .

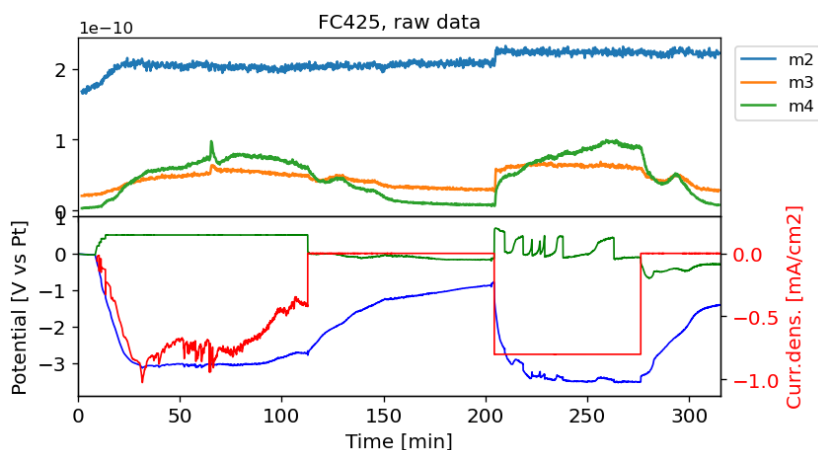


Figure C.16: Mass spec and electrochemistry measurements on  $FC_{425}$  experiment. Initially a CA (controlled anode potential) and later a CP (controlled cell current) was applied.

The behaviour of the anode potential is spurious, but can be explained by a shift in the reference potential. For one thing, the Pt pseudo reference electrode, is known to not be stable, but can drift during experiments [79]. Secondly, the reference potential is dependent on the hydrogen activity,  $a_H$ , which may be affected by the transport of protons through the cell. Lastly, the reference electrode itself, may have been compromised by Li. If Li, from a previous experiment, had started to either alloy or interfere with the Pt wire, this could affect the measured potentials.

Best estimates of hydrogen evolution FE in *FC425*, based on gas flow and calibration.

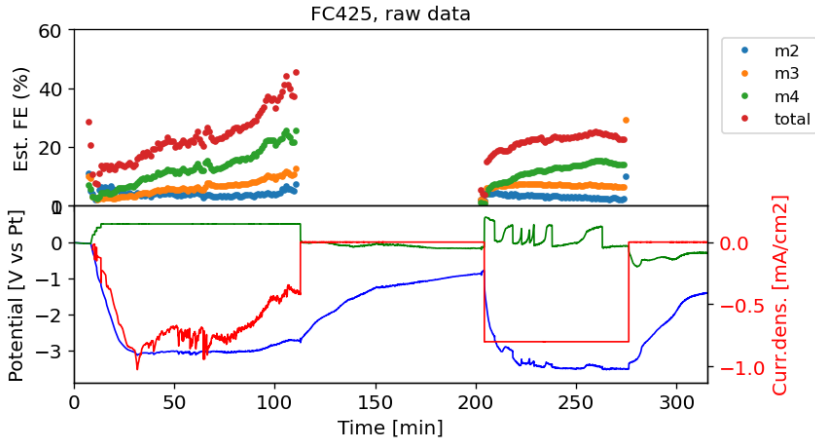


Figure C.17: Mass spec and electrochemistry measurements on *FC425* experiment. Initially a CA (controlled anode potential) and later a CP (controlled cell current) was applied.

Best estimates of hydrogen evolution FE in *FC425*, based on gas flow and calibration.

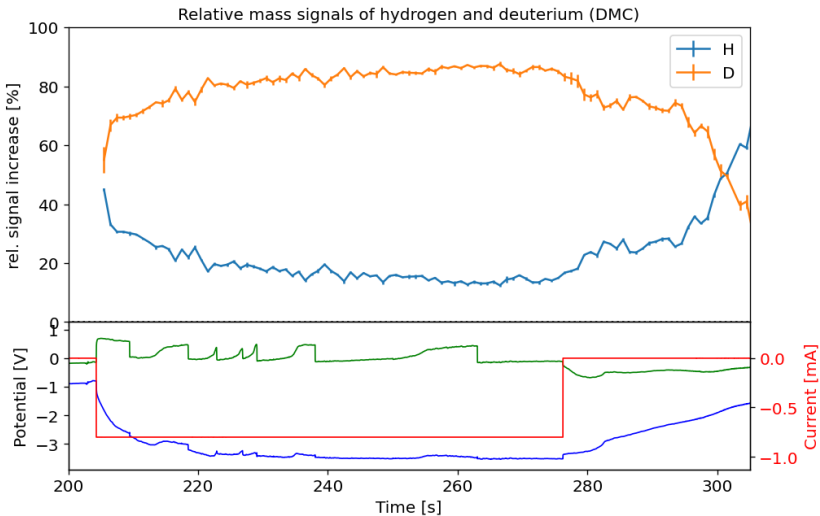


Figure C.18: Relative measured signals of  $m/z$  2 and 4 during constant current, as an indicator for the ratio of H and D in the cathode reactions. Eventually, more than 80% of the hydrogen signals at the cathode are from oxidized deuterium from the anode.

PtAu-alloy electrodeposited electrode mesh, used as a high surface-area anode. Incorporation of Au in the alloy, may help prevent poisoning of Pt, and a resulting lower activity for oxidation reaction.

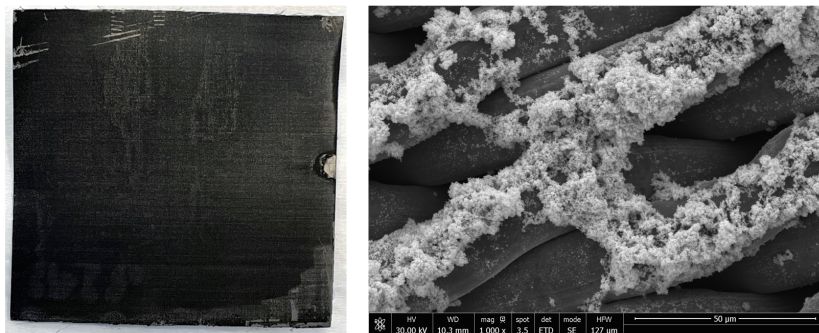


Figure C.19: (left) Photograph of the PtAu electrode. The surface has a black appearance, as a physical consequence of nano-sized particulates. Courtesy of Xianbiao Fu. (right) SEM image of the surface morphology of the PtAu electrodes. The porous structure of the deposit, increases the electrochemical surface area, similarly to the Cu-deposition method [117]. Scale bar is 50  $\mu\text{m}$ . Courtesy of Xianbiao Fu and Katja Li.

Visual comparison of two different mesh-types. Left is a 325x2300 mesh (wires per inch), with a pore size of 5  $\mu\text{m}$  and 80  $\mu\text{m}$  thickness. This electrode was initially used for flow cell experiments. The right electrode is a 500x500 mesh, with 30  $\mu\text{m}$  pores and 30  $\mu\text{m}$  thickness. This thinner electrode gave much higher efficiency towards NRR.

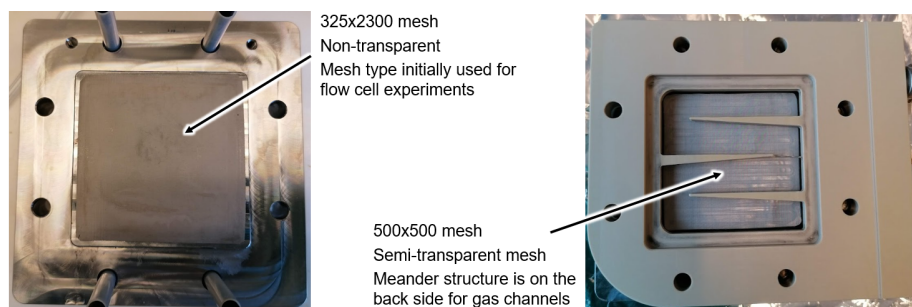


Figure C.20: Visual comparison of stainless steel meshes used as GDE, with 325x2300 and 500x500 wires per inch, respectively.

Calculated ammonia synthesis based on MS data compared to what is measured with an Ion Chromatograph. The MS measurements correlate well, and is only off by a scaling.

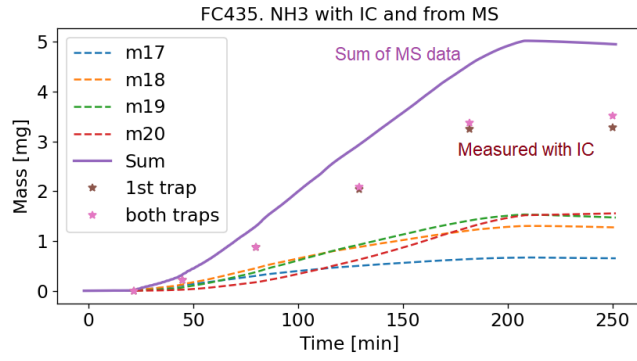


Figure C.21: Stars represent measured amount of  $\text{NH}_3$  with an Ion Chromatograph. Dashed lines are the best estimate of ammonia synthesis from each related mass. Solid line is the sum of all these signals.

## Appendix D

# Appended Publications

Paper I

**Increasing Stability, Efficiency, and Fundamental Understanding of Lithium-Mediated Electrochemical Nitrogen Reduction**

Suzanne Z. Andersen, Michael J. Statt, Vanessa J. Bukas, Sarah G. Shapel, Jakob B. Pedersen, Kevin Kreml, Mattia Saccoccio, Debasish Chakraborty , Jakob Kibsgaard, Peter C.K. Vesborg, Jens Nørskov and Ib Chorkendorff  
*Energy & Environmental Science*, **13**, 4291-4300, (2020)



Cite this: DOI: 10.1039/d0ee02246b

# Increasing stability, efficiency, and fundamental understanding of lithium-mediated electrochemical nitrogen reduction†

Suzanne Z. Andersen,  <sup>‡</sup><sup>a</sup> Michael J. Statt,  <sup>‡</sup><sup>b</sup> Vanessa J. Bukas,  <sup>‡</sup><sup>a</sup> Sarah G. Shapel,<sup>a</sup> Jakob B. Pedersen,  <sup>a</sup> Kevin Krempf,  <sup>a</sup> Mattia Saccoccio,  <sup>a</sup> Debasish Chakraborty,  <sup>a</sup> Jakob Kibsgaard,  <sup>a</sup> Peter C. K. Vesborg,  <sup>a</sup> Jens Nørskov  <sup>\*a</sup> and Ib Chorkendorff  <sup>\*a</sup>Received 15th July 2020.  
Accepted 30th September 2020

DOI: 10.1039/d0ee02246b

rsc.li/ees

Lithium-mediated nitrogen reduction is a proven method to electrochemically synthesize ammonia; yet the process has so far been unstable, and the continuous deposition of lithium limits its practical applicability. One major problem of further developing this process is that very little is understood about the mechanism. We develop a model to start understanding the kinetics and we use our understanding to develop a potential cycling procedure. We show experimentally that it improves stability of the system, and leads to a significant increase in faradaic efficiency.

## Broader context

The production of ammonia, and its subsequent use in fertilizer, is one of the most environmentally impactful industrial processes today. Conventional ammonia synthesis uses 1% of the world's energy while emitting 1% of the world's CO<sub>2</sub>. Additionally, the harsh process conditions require a centralized production of fertilizer, which leads to an expensive distribution system and inefficient utilization at the farm. Electrochemical nitrogen reduction (eNRR) could circumvent these issues by utilizing non-fossil fuel derived protons and renewable electricity whilst operating at near ambient conditions, enabling distributed ammonia production. Recently, lithium-mediated eNRR has gained renewed attention due to its moderate faradaic efficiencies and reproducible results. However, significant stability issues and low energy efficiencies still limit the practical viability of lithium-mediated eNRR. Herein, we develop a kinetic model to improve the understanding of lithium-mediated eNRR. The results of the model are then used to motivate and develop a voltage cycling procedure that significantly increases both the energy and faradaic efficiency. Additionally, the cycling procedure greatly improves the stability of the system. These promising results, coupled with the insights from our model, present a significant step forward towards the practical viability of lithium-mediated eNRR.

## Introduction

Ammonia is currently the second most produced industrial chemical, with annual production exceeding 172 Mt.<sup>1</sup> It is primarily used as a fertilizer and has played a central role in sustaining the growing world population over the last century.<sup>2,3</sup> Ammonia is also an essential base chemical in industry and, importantly, holds promise as a potential energy vector if production is efficiently coupled to a renewable energy source like solar or wind.<sup>4,5</sup> Currently, the production of ammonia relies on the catalytic Haber–Bosch process, which

thermally reduces atmospheric nitrogen with hydrogen, *i.e.*,  $N_2 + 3H_2 \rightarrow 2NH_3$ , at high temperatures (350–500 °C) and pressures (150–200 bar).<sup>6,7</sup> The energy demand of this process presently amounts to ~1% of the global energy consumption<sup>8</sup> and gives rise to significant CO<sub>2</sub> emissions,<sup>9,10</sup> mainly due to the required H<sub>2</sub> production *via* steam-reforming of fossil fuels.<sup>11</sup> Additionally, the needed high-pressure reaction conditions call for large centralized facilities with a large cost of installation and additional cost for transporting ammonia to the point of use.

The carbon footprint of hydrogen production for the Haber–Bosch process can be reduced substantially by electrifying the heating in the steam reforming process<sup>11</sup> or by using water electrolysis. Alternatively, a direct electrochemical synthesis of ammonia, *i.e.*,  $N_2 + 6H^+ + 6e^- \rightarrow 2NH_3$ , presents an extremely attractive substitute to the Haber–Bosch process.<sup>8,12</sup> Such a synthesis route can, in principle, operate under mild conditions of <100 °C and near-atmospheric pressure, while simultaneously

<sup>a</sup> Department of Physics, Technical University of Denmark, Kongens Lyngby, Denmark. E-mail: jkno@dtu.dk, ibchork@fysik.dtu.dk

<sup>b</sup> SUNCAT Center for Interface Science and Catalysis, Department of Chemical Engineering, Stanford University, Stanford, CA, USA

† Electronic supplementary information (ESI) available. See DOI: 10.1039/d0ee02246b

‡ These authors have contributed equally.

## Paper II

### **Towards understanding of electrolyte degradation in lithium-mediated non-aqueous electrochemical ammonia synthesis with gas chromatography-mass spectrometry**

Rokas Sažinas, Suzanne Zamany Andersen, Katja Li, Mattia Saccoccio, Kevin Kreml, Jakob Bruun Pedersen, Jakob Kibsgaard, Peter Christian Kjærgaard Vesborg, Debasish Chakraborty and Ib Chorkendorff

*RSC Advances*, **11**, 50, 31487-31498, (2021)


 Cite this: *RSC Adv.*, 2021, 11, 31487

# Towards understanding of electrolyte degradation in lithium-mediated non-aqueous electrochemical ammonia synthesis with gas chromatography-mass spectrometry†

 Rokas Sažinas,  Suzanne Zamany Andersen,  Katja Li,  Mattia Saccoccio,   
 Kevin Krempel,  Jakob Bruun Pedersen,  Jakob Kibsgaard,   
 Peter Christian Kjærgaard Vesborg,  Debasish Chakraborty and Ib Chorkendorff \*

Lithium-mediated electrochemical ammonia synthesis (LiMEAS) in non-aqueous media is a promising technique for efficient and green ammonia synthesis. Compared to the widely used Haber–Bosch process, the method reduces CO<sub>2</sub> emissions to zero due to the application of green hydrogen. However, the non-aqueous medium encounters the alkali metal lithium and organic components at high negative potentials of electrolysis, which leads to formation of byproducts. To assess the environmental risk of this synthesis method, standardized analytical methods towards understanding of the degradation level and consequences are needed. Here we report on the implementation of an approach to analyze the liquid electrolytes after electrochemical ammonia synthesis via high-resolution gas chromatography-mass spectrometry (GCMS). To characterize the molecular species formed after electrolysis, electron ionization high-resolution mass spectrometry (EI-MS) was applied. The fragmentation patterns enabled the elucidation of the mechanisms of byproduct formation. Several organic electrolytes were analyzed and compared both qualitatively and quantitatively to ascertain molecular composition and degradation products. It was found that the organic solvent in contact with metallic electrodeposited lithium induces solvent degradation, and the extent of this decomposition to different organic molecules depends on the organic solvent used. Our results show GCMS as a suitable technique for monitoring non-aqueous electrochemical ammonia synthesis in different organic electrolytes.

 Received 6th August 2021  
 Accepted 8th September 2021

DOI: 10.1039/d1ra05963g

[rsc.li/rsc-advances](https://rsc.li/rsc-advances)

## Introduction

Lithium-mediated electrochemical ammonia synthesis (LiMEAS) is a promising alternative to the traditional complex thermochemical Haber–Bosch process,<sup>1–5</sup> which predominantly requires high temperatures (400–500 °C) and pressures (150–200 bar) coupled with a steam reforming plant for hydrogen (H<sub>2</sub>) production.<sup>6</sup> On the other hand, the LiMEAS is thermodynamically driven by an electrical potential instead of high temperatures and pressures, and the chemical reactivity of lithium towards nitrogen gas (N<sub>2</sub>).<sup>7</sup> By utilization of green electricity from *e.g.* wind or solar energy sources, the process can be considered a renewable alternative. This enables softer operation conditions in a modular fashion, similar to a flow reactor,<sup>8</sup> and leads to lower capital costs for the process without greenhouse gas emissions compared to the 1.4% of global CO<sub>2</sub>

emissions for ammonia (NH<sub>3</sub>) production by the Haber–Bosch process. The LiMEAS could be operated on a local level *e.g.* individual farms or greenhouses, thereby further eliminating the need for transportation and storage. This alternative decentralized NH<sub>3</sub> production method turns against the centralized nature of Haber–Bosch making ammonia accessible at a local scale and employing renewable energy sources *e.g.* wind or solar. The production of H<sub>2</sub> (for example, water splitting) may overcome some of the issues associated with the traditional Haber–Bosch process, such as the large amount of CO<sub>2</sub> from steam reforming<sup>9</sup> emissions and high cost.<sup>2</sup>

A typical LiMEAS cell consists of a noble metal anode *e.g.* platinum (Pt) and transition metal cathode which does not interact or alloy with lithium (Li) *e.g.* molybdenum (Mo).<sup>10,11</sup> The electrodes are usually submerged in the non-aqueous organic electrolyte with or without a membrane or separator. The electrolyte is composed of a conducting Li salt and a solvent, typically lithium perchlorate (LiClO<sub>4</sub>)<sup>12</sup> and tetrahydrofuran (THF), respectively.<sup>10,13</sup> Other mostly ether-based solvents, such as dimethoxyethane (DME) or diethyleneglycol dimethyl ether or diglyme (DG) can also be used for LiMEAS. Thus, the influence

Department of Physics, Technical University of Denmark, Kongens Lyngby, 2800, Denmark. E-mail: [ibchork@fysik.dtu.dk](mailto:ibchork@fysik.dtu.dk)

† Electronic supplementary information (ESI) available. See DOI: 10.1039/d1ra05963g

### Paper III

#### **Enhancement of lithium-mediated ammonia synthesis by addition of oxygen**

Katja Li, Suzanne Z. Andersen, Michael J. Statt, Mattia Saccoccio, Vanessa J. Bukas, Kevin Kreml, Rokas Sažinas, Jakob B. Pedersen, Vahid Shadravan, Yuanyuan Zhou, Debasish Chakraborty, Jakob Kibsgaard, Peter C.K. Vesborg, Jens K. Nørskov and Ib Chorkendorff  
*Science*, **374**, 6575, 1593-1597, (2021)

## ELECTROCHEMISTRY

# Enhancement of lithium-mediated ammonia synthesis by addition of oxygen

Katja Li<sup>1</sup>†, Suzanne Z. Andersen<sup>1</sup>†, Michael J. Statt<sup>2</sup>†, Mattia Saccoccio<sup>1</sup>, Vanessa J. Bukas<sup>1</sup>†, Kevin Kremp<sup>1</sup>, Rokas Sažinas<sup>1</sup>, Jakob B. Pedersen<sup>1</sup>, Vahid Shadravan<sup>1</sup>, Yuanyuan Zhou<sup>1</sup>, Debashish Chakraborty<sup>1</sup>, Jakob Kibsgaard<sup>1</sup>, Peter C. K. Vesborg<sup>1</sup>, Jens K. Nørskov<sup>1,\*</sup>, Ib Chorkendorff<sup>1,\*</sup>

Owing to the worrying increase in carbon dioxide concentrations in the atmosphere, there is a need to electrify fossil-fuel-powered chemical processes such as the Haber-Bosch ammonia synthesis. Lithium-mediated electrochemical nitrogen reduction has shown preliminary promise but still lacks sufficient faradaic efficiency and ammonia formation rate to be industrially relevant. Here, we show that oxygen, previously believed to hinder the reaction, actually greatly improves the faradaic efficiency and stability of the lithium-mediated nitrogen reduction when added to the reaction atmosphere in small amounts. With this counterintuitive discovery, we reach record high faradaic efficiencies of up to  $78.0 \pm 1.3\%$  at 0.6 to 0.8 mole % oxygen in 20 bar of nitrogen. Experimental x-ray analysis and theoretical microkinetic modeling shed light on the underlying mechanism.

Ammonia ( $\text{NH}_3$ ) is one of the most abundantly manufactured chemicals worldwide, with a yearly production of over 182 million tonnes (1). Its main use is as a synthetic fertilizer (~80%) and as the source of all activated nitrogen in the chemical industry, but it has recently also been considered as a carbon-free energy carrier (2–4). Currently, ammonia is produced from nitrogen and hydrogen through the thermally catalyzed Haber-Bosch process, which operates under harsh conditions ( $350^\circ$  to  $450^\circ\text{C}$ , 100 to 200 bar), requiring large centralized plants and high capital investment (5, 6). To satisfy the commercial demands, about ~1% of global energy consumption is used in the process (7). Additionally, the Haber-Bosch process is responsible for about 1.4% of the annual  $\text{CO}_2$  emissions, as the supplied  $\text{H}_2$  originates from steam reforming of methane (8–10). An alternative, environmentally sustainable way to produce ammonia is through an electrochemical pathway, with the electrical energy provided from renewable sources such as wind or solar power. Recently, efforts toward electrochemical synthesis of ammonia have increased substantially (11–14); however, the field has been hampered by various issues. One major concern in the literature is related to contamination of the input gases, chemicals, and catalysts by ammonia and other labile nitrogen compounds (15, 16), which may result in an erroneously high reported faradaic efficiency (FE). Several protocols (16–18) have been published on proper contaminant iden-

tification and rigorous experimentation, and some of the erroneous reports are being corrected or withdrawn as scientists retest and reevaluate methods and systems (19, 20). In a recent paper, Choi *et al.* investigated over 130 publications on electrochemical ammonia synthesis, concluding it highly likely that none of the aqueous systems produce ammonia and that the most reliable method presently is lithium-mediated nitrogen reduction (LiNR) in nonaqueous electrolytes (16). A similar lithium-mediated method was first published by Fichter *et al.* in 1930 (21) and later investigated with a near-aprotic solvent by Tsuneto *et al.* in the 1990s (22, 23). Currently, the Tsuneto-based system has been revisited by several groups (11, 12, 17, 18, 24–28); however, the exact mechanism is still not fully understood. It is generally accepted that the LiNR takes place in three steps (25), the first one being the electrochemical reduction of  $\text{Li}^+$  ions in the electrolyte to metallic Li, which is a very reactive material. This freshly plated Li is believed to then dissociate  $\text{N}_2$ , and the N at the surface is finally reduced in a series of electron and proton transfers to form  $\text{NH}_3$  by using a suitable proton source, like ethanol (EtOH). An important component of the LiNR system is the solid electrolyte interface (SEI) that forms from decomposition products of an organic electrolyte during Li deposition on the cathode. The SEI provides a porous passivation layer over the electrode surface that is electronically insulating but ionically conducting. Its exact composition and mechanistic role in the LiNR process are still unclear and difficult to determine, because it is strongly dependent on experimental conditions and sensitive to air exposure. Nevertheless, the process reliably forms ammonia from  $\text{N}_2$  and a proton source at ambient conditions, typically achieving a FE of around 5 to 20% (17, 25, 29), with a recent breakthrough in

FE of up to 69% by Suryanto *et al.* (11) under 20-bar  $\text{N}_2$ . Lazouski *et al.* implemented this process using a gas diffusion electrode (GDE) setup with reported efficiencies of 30%, but the system was only stable for a few minutes and exhibited high cell potentials (12). Instability of this process was already described by Tsuneto *et al.* (22), and recently mitigated by Andersen *et al.* with a potential cycling strategy (24), which enabled stability over several days and increased the FE at 10-bar  $\text{N}_2$  from 20% without cycling to 37% with cycling at an energy efficiency (EE) of 7%. However, the REFUEL program of the US Department of Energy set a target of 90% FE at 300 mA/cm<sup>2</sup> and an EE of 60% (30). The current state of the lithium-mediated process is clearly far from this target. Especially the EE is currently a major problem in the LiNR, because Li plating requires largely negative potentials (~3.04 V versus SHE). The overpotential losses of the LiNR are portrayed and discussed in fig. S1. If all overpotentials are minimized and hydrogen oxidation reaction (HOR) is utilized at the counter electrode (CE), the resulting EE would be 26%, assuming 80% FE.

Here we show that adding small amounts of  $\text{O}_2$  to the feed gas has a positive effect on both the FE and the stability of the system. A FE of up to  $78.0 \pm 1.3\%$  at 20-bar  $\text{N}_2$  can be achieved by adding 0.5 to 0.8 mol %  $\text{O}_2$ , resulting in an EE of  $11.7 \pm 0.5\%$  (calculation in supplementary materials). This EE calculation accounts for neither EtOH as sacrificial proton donor nor for the energy of pressurizing the system. We used this framework as a basis for comparison to results from literature (24, 25). Using hydrogen oxidation at the CE in a GDE-type system has previously been shown to prevent solvent oxidation (12), and the use of a phosphonium proton shuttle has been experimentally verified to successfully shuttle the newly created protons to the working electrode while the phosphonium ylide becomes reprotonated at the anode (11), thereby circumventing the sacrificial ethanol issue. Our focus in this study lies on the finding that oxygen increases the FE and not on the sacrificial proton donor issue, but we expect that the previously reported solutions will also apply to our system. The positive effect of small amounts of oxygen is counterintuitive; one would expect oxygen to contaminate the active phase and result in loss of efficiency because of the oxygen reduction reaction (ORR). Indeed, early experiments by Tsuneto *et al.* showed that higher oxygen content in the gas feed (synthetic air with 20%  $\text{O}_2$ ) lowered the FE considerably from ~50 to 0.1% at 50 bar (23). We investigated the origin of the oxygen promotion using a microkinetic model, suggesting that the higher FE is related to slower  $\text{Li}^+$  diffusion through the SEI layer formed in the presence of  $\text{O}_2$  as observed by Wang *et al.* in

<sup>1</sup>Department of Physics, Technical University of Denmark, Kongens Lyngby, Denmark. <sup>2</sup>SUNCAT Center for Interface Science and Catalysis, Department of Chemical Engineering, Stanford University, Stanford, CA, USA.

\*Corresponding author. Email: jkno@dtu.dk (J.K.N.); ibchork@fysik.dtu.dk (I.C.)

†These authors contributed equally to this work.

‡Present address: Fritz-Haber-Institut der Max-Planck-Gesellschaft, 14195 Berlin, Germany.

## Paper IV

### **Increasing Current Density of Li-Mediated Ammonia Synthesis with High Surface Area Copper Electrodes**

Katja Li, Sarah G. Shapel, Degenhart Hochfilzer, Jakob B. Pedersen, Kevin Kreml, Suzanne Z. Andersen, Rokas Sažinas, Mattia Saccoccio, Shaofeng Li, Debasish Chakraborty, Jakob Kibsgaard, Peter C.K. Vesborg, Jens K. Nørskov, Ib Chorkendorff

*ASC Energy Letters*, **7**, 1, 36-41, (2022)

# Increasing Current Density of Li-Mediated Ammonia Synthesis with High Surface Area Copper Electrodes

Katja Li,<sup>†</sup> Sarah G. Shapel, Degenhart Hochfilzer, Jakob B. Pedersen, Kevin Krempel, Suzanne Z. Andersen, Rokas Sažinas, Mattia Saccoccio, Shaofeng Li, Debasish Chakraborty, Jakob Kibsgaard, Peter C. K. Vesborg, Jens K. Nørskov, and Ib Chorkendorff\*



Cite This: *ACS Energy Lett.* 2022, 7, 36–41



Read Online

ACCESS |



Metrics & More

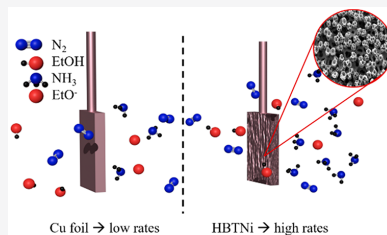


Article Recommendations



Supporting Information

**ABSTRACT:** The lithium-mediated ammonia synthesis is so far the only proven electrochemical way to produce ammonia with promising faradaic efficiencies (FEs). However, to make this process commercially competitive, the ammonia formation rates per geometric surface area need to be increased significantly. In this study, we increased the current density by synthesizing high surface area Cu electrodes through hydrogen bubbling templating (HBT) on Ni foam substrates. With these electrodes, we achieved high ammonia formation rates of  $46.0 \pm 6.8 \text{ nmol s}^{-1} \text{ cm}_{\text{geo}}^{-2}$ , at a current density of  $-100 \text{ mA/cm}_{\text{geo}}^{-2}$  at 20 bar nitrogen atmosphere and comparable cell potentials to flat foil electrodes. The FE and energy efficiency (EE) under these conditions were  $13.3 \pm 2.0\%$  and  $2.3 \pm 0.3\%$ , respectively. Additionally, we found that increasing the electrolyte salt concentration improves the stability of the system, which is attributed to a change of Li deposition and/or solid electrolyte interphase.



Global warming is arguably one of the biggest problems of our current society. It is caused by greenhouse gases such as  $\text{CO}_2$ , whose emissions are increasing constantly. To counteract this, all possible  $\text{CO}_2$  emissions should be reduced. The ammonia production by itself is the cause of  $\sim 1.4\%$  of the global annual  $\text{CO}_2$  emission, since it utilizes steam reforming to obtain  $\text{H}_2$ , which is then reacting with  $\text{N}_2$  to form ammonia in the Haber-Bosch process.<sup>1–5</sup> This is not only harming the environment but is also heavily energy consuming (1% of total yearly energy consumption) because of its harsh conditions (100–200 bar, 350–450 °C).<sup>6–8</sup> Hence, finding a sustainable alternative to the Haber-Bosch process would be a huge step in mitigating climate change. One way to achieve this is by electrifying ammonia synthesis, since electricity can be acquired from renewable energy sources. Although the area of electrochemical ammonia synthesis has gained much scientific interest due to the large positive implications,<sup>9–17</sup> it still has some complications such as impurities in the gas feed or chemicals and selectivity issues, leading to erroneous reports and small faradaic efficiencies.<sup>18–21</sup> Recently, protocols of how to conduct experiments in this field and measure ammonia correctly were published, which will help move the research in the right direction.<sup>18,22–24</sup> So far it is believed that the only reliable way to make ammonia electrochemically is the Li-mediated ammonia synthesis which

was initially developed by Fichter et al. in 1930<sup>25</sup> and later also studied by Tsuneto et al. over 60 years later.<sup>4,5</sup> This method uses a nonaqueous electrolyte to minimize the competing hydrogen evolution reaction (HER). The exact mechanism is yet to be elucidated, but most agree that it involves three main steps.<sup>26</sup> The first step is plating out metallic Li from a Li-salt, which then reacts in the second step with dissolved  $\text{N}_2$  in the electrolyte, therefore splitting the stable triple bond and forming  $\text{Li}_3\text{N}$  or other N-containing compounds. Finally, ammonia is made after protonation by a suitable proton source like EtOH. Tsuneto et al. reported moderate faradaic efficiencies (FEs) of around 6% at ambient conditions and the inherent instability of the system,<sup>4</sup> but since the rediscovery of this process by many groups, the FE and the stability have increased.<sup>11,18,26–30</sup> Up to this point, the highest FE reported is 69% at 20 bar  $\text{N}_2$ ,<sup>27</sup> where the sacrificial proton donor was replaced with an ionic liquid based proton shuttle.

Received: September 27, 2021

Accepted: November 19, 2021

Published: November 24, 2021



Paper V

**Electrolyte acidification from anode reactions during lithium mediated ammonia synthesis**

Kevin Krempf\*, Jakob B. Pedersen\*, Jakob Kibsgaard, Peter C.K. Vesborg and Ib Chorkendorff

*Electrochemistry Communications*, **134**, 4, 107186, (2022)

\* these authors contributed equally

# Electrolyte acidification from anode reactions during lithium mediated ammonia synthesis

Kevin Krempel,<sup>†,‡</sup> Jakob B. Pedersen,<sup>†,‡</sup> Jakob Kibsgaard,<sup>†</sup> Peter C. K. Vesborg,<sup>†</sup>  
and Ib Chorkendorff<sup>\*,†</sup>

<sup>†</sup>*Department of Physics, Technical University of Denmark, DK-2800 Kgs. Lyngby, Denmark*

<sup>‡</sup>*Contributed equally to this work*

E-mail: [ibchork@fysik.dtu.dk](mailto:ibchork@fysik.dtu.dk)

## Abstract

Li-mediated electrochemical ammonia synthesis (LiMEAS), a potential alternative to conventional thermochemical synthesis, is enabled by non-aqueous electrolytes with precisely controlled proton activity. However, the effects of proton generating anode reactions, such as hydrogen or electrolyte oxidation, is unknown but crucially important for enabling a steady-state LiMEAS without the need of sacrificial proton sources. By employing cyclic voltammetry on a platinum electrode, we demonstrate that protons are generated not only by hydrogen oxidation but also electrolyte oxidation, which has the consequence of a continuous acidification of the electrolyte over the course of a LiMEAS experiment. In addition, the cyclic voltammograms reveal that the generated protons show reactivity towards electrolyte components, which would disrupt the replenishment of the added proton source. We therefore suggest to design new electrolytes that also contain proton acceptors, ultimately resulting in a buffered electrolyte with a stable proton activity.

**Keywords:** Ammonia, Electrochemistry, Anode reactions, Acidification

## 1 Introduction

Li-mediated electrochemical ammonia synthesis (LiMEAS) has recently gained much interest, as a process to unambiguously activate unreactive nitrogen and convert it into ammonia.<sup>[1]</sup> The Li-mediated nitrogen reduction process requires a non-aqueous electrolyte, such that the proton availability can be controlled by addition of appropriate amounts of a proton source.<sup>[2]</sup> In that regard, most reports on Li-mediated nitrogen reduction closely resemble the original reports by Tsuneto *et al.*, who used tetrahydrofuran (THF) as a solvent and ethanol as proton source with a Li-containing electrolyte in a single compartment electrochemical cell.<sup>[3]</sup> Most studies have so far focused on the processes occurring at the ammonia producing cathode, such as solid-electrolyte-interface (SEI) formation<sup>[4]</sup> or Li-metal deposition and corrosion,<sup>[5]</sup> as well as the effect of proton donor concentration or nitrogen pressure.<sup>[6,7]</sup> A fully integrated, steady-state LiMEAS as depicted in Figure 1A however requires not only ammonia being produced at the cathode but also a suitable oxidation reaction on the anode, that is able to selectively regenerate the deprotonated proton source. For this purpose, Lazouski *et al.* have demonstrated the use of hydrogen oxidation reaction (HOR) in a separated gas-diffusion electrode set-up, which can selectively provide protons and replace the electrolyte oxidation reactions encountered in single compartment cells when no hydrogen is provided.<sup>[8]</sup> In combination with a suitable proton donor/acceptor system, for example phosphonium ions,<sup>[9]</sup> a steady-state LiMEAS can be imagined. While the HOR can conceptually provide protons necessary for this,<sup>[10,11]</sup> the interaction of the generated protons with the electrolyte is rarely studied in the context of LiMEAS. In this letter, we present cyclic voltammetry studies on platinum disk electrodes of both anode reactions, electrolyte oxidation and HOR, in order to clarify their role in LiMEAS. Based on the results, we discuss the conditions that must be fulfilled to enable steady-state electrochemical LiMEAS in non-aqueous electrolytes and point out potential future research directions.

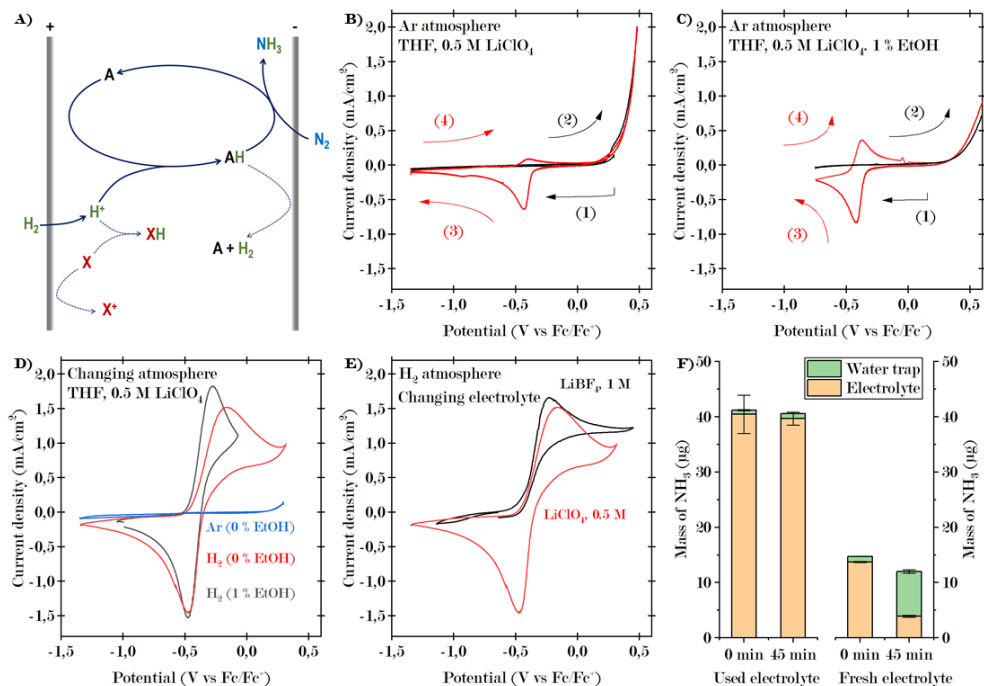


Figure 1: **(A)** Potential reaction pathways for protons generated during hydrogen oxidation illustrating the selectivity challenge encountered in non-aqueous electrolytes. A illustrating a proton shuttle and X electrolyte components. **(B-E)** CVs showing electrolyte oxidation and HOR/HER features in THF based electrolytes saturated with either Ar or H<sub>2</sub>. **(B)** and **(C)**: Appearance of an additional redox feature (red curve) at -0.4 V vs Fc/Fc<sup>+</sup> after electrolyte oxidation in Ar saturated THF/LiClO<sub>4</sub> electrolyte with and without EtOH. **(D)**: CVs in H<sub>2</sub> sat. THF/LiClO<sub>4</sub> electrolyte show the same feature as observed after electrolyte oxidation, while in Ar sat. electrolyte no feature is observed. **(E)**: CV in HER/HOR region in THF based electrolyte with either LiBF<sub>4</sub> or LiClO<sub>4</sub>. A cathodic HER peak is not seen in LiBF<sub>4</sub> containing electrolyte, while anodic peak is seen in both. **(F)** Amounts of NH<sub>3</sub> in electrolyte and in downstream water trap during evaporation experiments in used and fresh electrolyte demonstrating acidification of electrolyte.

## 2 Results and discussion

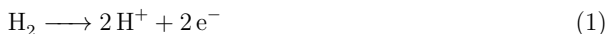
### 2.1 Oxidation and reduction features

As a first step, we measured cyclic voltammograms on a platinum disk electrode in a THF based 0.5 M LiClO<sub>4</sub> electrolyte under static electrolyte conditions (see Supporting Information for details) in order to take a closer look at the anode reaction in conventional single-compartment cells. In order to obtain the potential on an absolute scale and therefore allow comparison between different electrolytes, the Ag-wire pseudo-reference electrode was calibrated against the Fc/Fc<sup>+</sup> redox couple after each measurement. As shown in Figure 1B, the first cathodic sweep does not show any redox features as expected for an aprotic electrolyte. Even with the addition of the proton source, Figure 1C, in this case ethanol, no reductive feature is observed in this potential range indicating that protons provided by ethanol are only reduced at more cathodic potentials. This is in line with the high pK<sub>a</sub> value of ethanol in non-aqueous solvents, which is significantly higher than in an aqueous system.<sup>[12]</sup> On the subsequent anodic sweep, the onset of electrolyte oxidation can be observed at around +0.3 V vs Fc/Fc<sup>+</sup> with a less pronounced increase in oxidative current for the ethanol containing electrolyte. It appears that ethanol partly inhibits the anode reaction, which in this case is probably the anodic polymerization of THF.<sup>[13,14]</sup> At the same time, the oxidation of ethanol itself cannot be excluded. However, an important consequence of electrolyte oxidation becomes apparent on the second cathodic sweep in Figure 1B and 1C, where a pronounced reduction feature appears that goes in hand with another oxidative feature on the subsequent anodic sweep. Hatsukade *et al.* have also shown similar behaviour in an ethylenecarbonate:ethylmethylcarbonate (EC:EMC) based electrolyte, and have ascribed the reductive feature to the reduction of protons formed during electrolyte oxidation.<sup>[15]</sup> In line with this, the oxidative feature on the subsequent anodic sweep would then be the hydrogen oxidation reaction (HOR).

To further substantiate that the redox feature appearing after electrolyte oxidation is as-

sociated with proton reduction and hydrogen oxidation, we also measured CVs in a hydrogen saturated electrolyte. In hydrogen, a clear duck-shaped voltammogram arises at the same potential as the redox couple observed after electrolyte oxidation, while under inert Ar gas the voltammogram remains featureless (see Figure 1D) supporting the presumption of production of protons during electrolyte oxidation. Unlike in the case of electrolyte oxidation, the presence of ethanol appears to improve the kinetics of the HOR since the separation between the anodic and cathodic peak, a measure for the degree of irreversibility of a redox couple, decreases.<sup>[16]</sup> A possible explanation for this could be the higher dielectric constant of ethanol compared to THF. The addition of ethanol increases the dielectric constant of the solvent, which in turn leads to a better stabilization of the charged transition state during HOR. Moreover, measurements in EC:EMC based electrolyte carried out by Hatsukade *et al.*, show an almost reversible redox behaviour for the HOR, which would be consistent with the substantially higher dielectric constant of organic carbonate solvents compared to THF. Another conclusion that can be drawn from these measurements is that the HOR provides protons to the electrolyte, similar to electrolyte oxidation. Moreover, these protons are at a substantially higher chemical potential than the protons provided by ethanol, since no reductive feature is observed without the presence of hydrogen in this potential range, Figure 1D. A higher chemical potential of the generated protons, or in other words, a higher acidity of the generated protons can potentially also lead to higher effective reactivity. This effective reactivity of the generated protons can be assessed by comparing the anodic and cathodic peak current densities of the cyclic voltammogram under hydrogen atmosphere. Since the cathodic peak ( $-1.53 \text{ mA/cm}^2$ ) is at lower current density than the anodic peak ( $1.82 \text{ mA/cm}^2$ ), it indicates that the generated protons are reacting with the electrolyte salt or solvent instead of being reduced. This is also in line with the observation of liquid decomposition products that can be detected in the electrolyte after long-term experiments.<sup>[17]</sup> For example, it is known that THF can undergo cationic polymerization when initiated with strong proton acids.<sup>[18,19]</sup> The instability of the generated protons becomes even more ap-

parent when  $\text{LiClO}_4$  is replaced by  $\text{LiBF}_4$ , where no reductive feature can be observed at all, see Figure 1E. Here, the generated protons most likely immediately react with the  $\text{BF}_4^-$  anion to form HF and  $\text{BF}_3$  according to equation (2), a reaction that is observed for most fluoride based anions.<sup>[20,21]</sup>



## 2.2 Acidification of electrolyte

The formation of readily reducible protons through electrolyte oxidation, but also through hydrogen oxidation, at the anode, has important implications for LiMEAS experiments. First of all, the generation of protons at the anode introduces non-steady-state conditions during ammonia synthesis experiments as the electrolyte becomes more acidic over time. Using methyl orange as a colorimetric pH indicator solution, the used electrolyte was found to be more acidic compared to freshly prepared electrolyte (Figure S6). Electrolyte acidification is also evident by the observation that synthesized ammonia can typically only be detected in the liquid electrolyte after an experiment and no  $\text{NH}_3$  is recovered from the gas phase. Ammonia however is a volatile compound, with a Henry constant in water of  $59 \text{ M bar}^{-1}$ ,<sup>[22]</sup> and would be expected to evaporate, particularly if a high  $\text{N}_2$  gas flow is used to saturate the electrochemical cell. To verify this, we spiked freshly prepared electrolyte with an ammonia containing solution of THF and purged it with an Ar gas flow for 45 minutes. As a result, the  $\text{NH}_3$  was evaporated and could be recovered in a downstream water trap. On the other hand, if the same experiment is carried out with used electrolyte, the ammonia remains entirely in the liquid, see Fig. 1F and S5. The experimental details can be found in the Supporting Information. This indicates that the generated protons increase the acidity of the electrolyte over the course of the experiment such that  $\text{NH}_3$  is protonated to form  $\text{NH}_4^+$  ions, which do not evaporate into the gas phase. The acidification of the electrolyte by the anode reaction is therefore responsible that no  $\text{NH}_3$  is lost through evaporation and accurate

quantification can be performed by sampling the liquid electrolyte. It is to be pointed out, that this however might not be the case for different cell geometries, where counter and working electrode are separated, or when the anode reaction is changed so that no acidic protons are generated. In addition, the effect of this acidification on ammonia synthesis rates can potentially be profound, as the acidity and concentration of the proton source are hypothesized to play a key role in enabling efficient LiMEAS.<sup>[23]</sup>

Besides the protonation of synthesized ammonia, our CV measurements in the previous section also provide evidence for the protonation and subsequent decomposition of electrolyte components. This of course is in contrast to what would be required for a fully integrated steady-state LiMEAS system, where the generated protons should selectively recombine with the deprotonated form of the added proton source instead of with electrolyte components or with synthesized ammonia. In order to alleviate this issues and design a suitable electrolyte for a fully integrated steady-state LiMEAS, we believe it will be necessary to also provide a suitable proton acceptor in the electrolyte. As long as the proton acceptor is sufficiently stable in the electrolyte, this would result in a buffered system where protons can be effectively shuttled between working and counter electrode. Such proton acceptors should however be of high basicity, so that neither ammonia nor other electrolyte components are protonated. Moreover, the proton acceptors must not negatively affect the ammonia synthesis rate at the cathode, e.g. by altering the composition of the SEI. An added advantage of having a high basicity proton acceptor in the electrolyte would also be that the equilibrium potential for HOR is shifted to less oxidizing potentials compared to Li electroplating, which can potentially reduce the overall cell potential.

### 3 Conclusion

In summary, this study highlights the selectivity challenge encountered during proton generation for LiMEAS. We believe that further understanding of proton equilibria in non-aqueous electrolytes will play a crucial role in designing suitable electrolytes that allow for a fully in-

tegrated LiMEAS. In addition, the ability to precisely control proton activity in non-aqueous electrolytes can also open up new avenues for other reactions such as CO<sub>2</sub> reduction or organic electrosynthesis, where the proton chemical potential also plays an important role. The simple methodology based on cyclic voltammetry in hydrogen and Ar saturated electrolyte presented in this study, can give insight into the chemical potential but also into the stability of the protons in non-aqueous electrolytes. Applying this method to electrolytes typically used for LiMEAS, we uncovered the fate of anodically generated protons and showed that the interaction of protons with electrolyte components or ammonia itself must be considered when assessing the viability of the electrolyte for fully integrated LiMEAS. Based on the findings, we propose the addition of proton acceptors into the electrolyte in order to obtain a buffered system, which conceptually should provide a stable proton chemical potential and allow for effective shuttling of protons from the anode to the ammonia producing cathode.

**Author contributions.** KK and JP contributed equally to the work, supervised by JK, PV and IC. All authors contributed to the editing of the manuscript.

**Conflicts of interest.** Authors declare no competing interests.

**Acknowledgements.** We gratefully acknowledge the funding by Villum Fonden, part of the Villum Center for the Science of Sustainable Fuels and Chemicals (V-SUSTAIN grant 9455) and E-Ammonia project funded by Innovation Fund Denmark (IFD) ref. no. 9067-00010B.

**Data availability.** Data is available by reasonable request to IC.

# Supporting Information Available

## A Additional information on experiments

### A.1 Chemicals

Tetrahydrofuran (THF, anhydrous, >99.9 %, inhibitor-free, Sigma Aldrich), ethanol (EtOH, anhydrous, Honeywell), lithium perchlorate ( $\text{LiClO}_4$ , Battery grade, dry, 99.99 %, Sigma Aldrich) and lithium tetrafluoroborate ( $\text{LiBF}_4$ , 98 %, Sigma Aldrich) were used for electrolyte solutions and ferrocene (98 %, Sigma Aldrich) for reference calibration. Methyl orange (a.c.s. grade reagent, Sigma Aldrich) was mixed with ultra-pure water (18.2 M $\Omega$  resistivity, Millipore, Synergy UV system) and ethanol absolute (99.97 % assay (V/V), VWR Chemicals) for pH indicator solution. Methanesulfonic acid ( $\geq 99.0$  %, Sigma Aldrich) diluted in THF and sodium hydroxide (NaOH, anhydrous, 98 %, Sigma Aldrich) diluted in ultra-pure water was used to alter electrolyte pH conditions. Polycrystalline platinum stub (Pt, 5.03 mm  $\times$  3 mm, 99.99 %, MaTeck), Li foil (99.9 %, Sigma Aldrich) and Pt wire (99.99 %, Goodfellow) were used as working, counter and reference electrodes.

### A.2 Setup

All electrochemical cyclic voltammetry results presented in this work were obtained in a custom made rotating disk electrode (RDE) glass cell. The glass cell has five openings. A central 24 mm opening, fitting a standard RDE shaft, with a tight fit ensured with an o-ring. Four additional neck openings are used for inserting reference electrode, counter electrode, gas inlet and electrolyte transfer respectively. The openings for counter electrode, reference electrode and electrolyte transfer were all sealed closed with Thermogreen Septas.

A 5 mm Pt stub (0.196 cm<sup>2</sup> geometric area), mounted to the RDE shaft, was used as a working electrode. The Pt stub was stored in ultra clean water, and flame annealed in air prior to experiments. The RDE shaft is made of PEEK with a PTFE U-cup for mounting the working electrode stub.

A 0.5 mm Ag wire was used as reference electrode, separated to the main compartment by a 0.5 mm diameter capillary. The reference electrode potential was calibrated using 2 mM ferrocene in THF after each experiment. See example in S1.

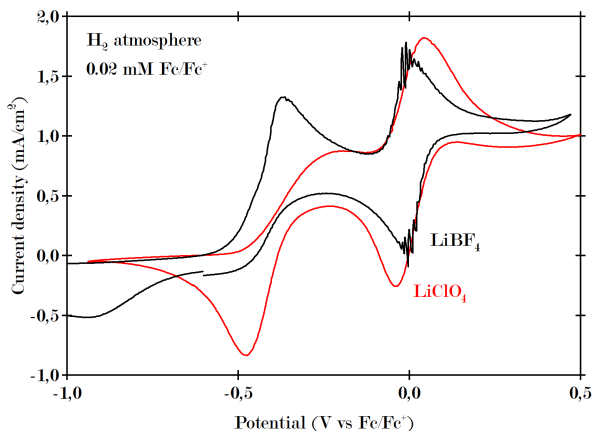


Figure S1: Example of calibrated CV after adding ferrocene to electrolyte solution

The counter electrode was made of a Li foil connected with a Pt wire. The counter electrode was placed in a small approximately 1 ml compartment filled with electrolyte, separated from the main compartment by a glass frit, to limit potential cross-over of anodic breakdown products of electrolyte to the working electrode.

A schematics of the setup is shown in Figure S2

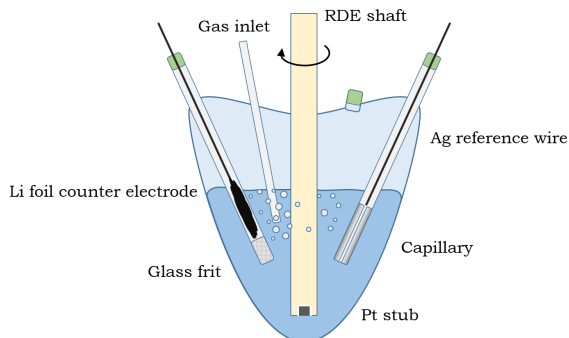


Figure S2: Schematics of the RDE setup used for CV measurements

### A.3 Measurement procedure

All cell parts were rinsed and boiled in ultrapure water ( $18.2 \text{ M}\Omega \cdot \text{cm}$  resistivity), then dried at 100 degree C in air and finally transferred to an Ar-filled glove box for assembly. After cell assembly in the glove box, the cell was transferred to a fume hood and immediately flushed with a continuous flow of Ar gas, to maintain an inert atmosphere and avoid oxygen to leak into the system. Hereafter, electrolyte was added and measurements collected.

After the electrolyte was added to the compartment, and good electrochemical contact between the three electrodes were ensured, the cell impedance was measured before cyclic voltammetry was commenced. When saturating electrolyte with either Ar or  $\text{H}_2$  gas, a high RDE rotation was used, to help mixing and stirring of liquid and gas. When static electrolyte was needed for measurements, the RDE rotation was turned off, such that electrolyte was allowed to be stagnant. The typical cell resistance was measured with impedance spectroscopy to be in the order of  $1 \text{ k}\Omega$ , which was compensated for when post-processing data.

All electrochemical measurements was made on a VMP2 potentiostat with the BioLogic 11.36 software. RDE rotation was controlled with a Rotating Electrode Speed Control from Pine Research Instrumentation. UV-vis absorption measurements were done on a Shimadzu UV-2600 UV-vis spectrophotometer in fast setting mode with  $1 \text{ nm}$  resolution.

### A.4 Ammonia trapping experiment

For clear exemplification of the ammonia trapping effect in used electrolyte, a high Ar gas flow of  $50 \text{ ml/min}$  for 45 minutes was used. As the Ar is a dry gas, a substantial amount of electrolyte would evaporate under these conditions. To prevent this, the Ar was presaturated by THF and ethanol. Before introduction to the primary glass cell containing electrolyte, the Ar gas was flowing through a secondary glass cell containing  $1 \text{ vol}\%$  ethanol in THF. Hereby, the loss of electrolyte was kept below  $1 \text{ ml}$  throughout the duration of the experiment. From the primary glass cell, the outlet gas was bubbling through a downstream  $3 \text{ ml}$  water trap, to catch possible  $\text{NH}_3$  in the gas. See Figure S3

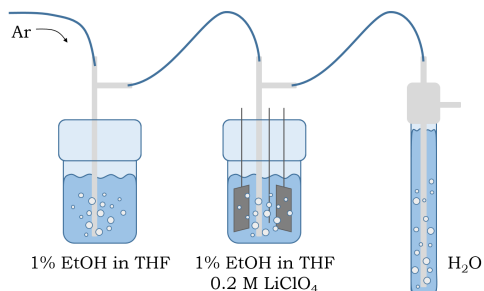


Figure S3: Schematics of  $\text{NH}_3$  trapping experiment setup

0.2 M  $\text{LiClO}_4$  in 1 vol% ethanol in THF was used as electrolyte. 8 ml of freshly prepared electrolyte was added to the glass cell, from which 0.5 ml electrolyte was sampled. Two samples from the downstream water trap was then taken, before the solution was spiked by adding 25  $\mu\text{l}$  of ammonia solution in THF. The solution was quickly well mixed due to the high bubbling rate of Ar, and two samples of the spiked solution was taken. After 45 minutes of rigorous bubbling two more samples were taken of the electrolyte and also of the water trap.

In the same cleaned setup a standard 3 electrode electrochemical Ar blank experiment was prepared, following the same procedure as earlier works.<sup>[1,5]</sup> A 1  $\text{cm}^2$  Mo foil, a 1  $\text{cm}^2$  Pt mesh and a Pt wire was used as the working, counter and reference electrode respectively. An impedance of 520  $\Omega$  was measured between the reference and working electrode. A total charge of 15 C at 4  $\text{mA}/\text{cm}^2$  was passed through the electrolyte, which can be seen together with the electrode potentials and current in Figure S4. The current in the Ar blank experiment mainly goes towards HER and Li plating on the Mo foil cathode, and requires the Pt anode to go to highly anodic potentials (approximately +4 V vs Pt pseudo reference potential).

After the electrochemical experiment, an electrolyte sample was taken and the electrodes were taken out. From here, the process steps were exactly as described above. Two samples were taken of the water trap, the electrolyte was spiked from which two samples were taken.

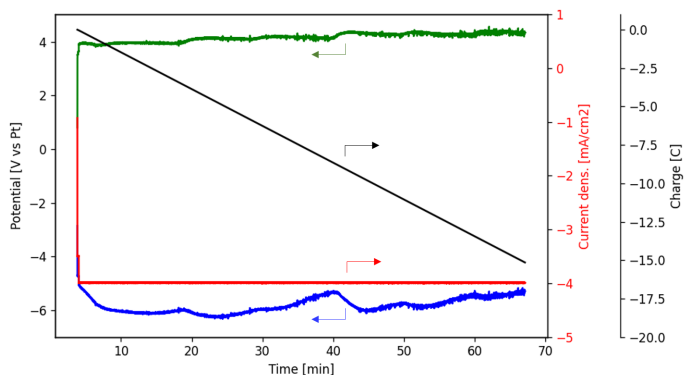


Figure S4: Potential vs Pt pseudo reference, current and charge curves during an Ar-blank experiment prior to the above-mentioned  $\text{NH}_3$  trapping experiment.

After 45 minutes of rigorous bubbling, two new samples were taken from both the water trap and the electrolyte.

$\text{NH}_3$  measurements were quantified as described in previous work.<sup>[1,5]</sup> The  $\text{NH}_3$  measurements are collected and shown in Figure S5 and 1B in terms of concentration and mass respectively. In the case of used electrolyte, the  $\text{NH}_3$  concentration increases with 1 ppm in the electrolyte, while being constant in the water trap. The increase of concentration is due to some evaporation of electrolyte during Ar bubbling. This shows how well the  $\text{NH}_3$  is being trapped in the acidified used electrolyte, and preferably stays in the liquid phase rather than being carried with the evaporated electrolyte. When comparing to freshly prepared electrolyte, the picture is quite different. Starting out with an initially slightly smaller  $\text{NH}_3$  concentration in the electrolyte, a significant decrease of 1.5 ppm  $\text{NH}_3$  concentration during the 45 minutes of bubbling is seen in the electrolyte. Meanwhile the  $\text{NH}_3$  concentration in downstream water trap increases with 2.5 ppm. With regards to the mass of  $\text{NH}_3$  in fresh electrolyte (see Fig. 1B), there is a small discrepancy in the total amount of  $\text{NH}_3$  before and after bubbling. The discrepancy may be due to ammonia sticking to PTFE gas tubing between the spiked electrochemical glass cell and the glass water trap.

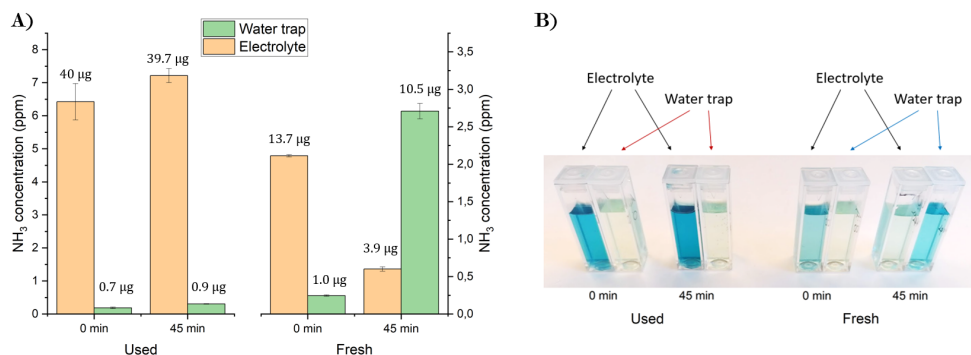


Figure S5: **(A)** Measuring concentration of ammonia in used (left) and freshly prepared (right) electrolyte and gas phase after spiking electrolyte with an ammonia solution and having rigorous Ar bubbling. **(B)** Picture of color reaction, used for quantification in left bar plot (A). Two samples were taken for each measurement, which was used to determine uncertainties for bar plot. As evident from the picture, the NH<sub>3</sub> trapping was visibly significant.

### A.5 pH indication using methyl orange

The methyl orange indicator solution was prepared, by mixing 0.02 gram methyl orange powder in 16 ml ultrapure water and 4 ml ethanol. After stirring the solution, all powder was dissolved and a deep red color obtained.

Multiple 3 ml samples of as-prepared electrolyte and used electrolyte was collected in glass vials. 10  $\mu$ l of the methyl orange indicator solution was added to each, and the solutions shaken.

For the as prepared electrolyte solution, the colour turned bright yellow - the same colour as for an alkaline solution. In the case of used electrolyte, the solution turned bright pink, as is the case for acidic solutions.

As a reference to the samples, acidic and alkaline solutions were prepared from as-prepared electrolyte. The acidic solution was made, by adding 100  $\mu$ l of 0.08 M methanesulphonic acid (diluted in THF) to 3 ml as-prepared electrolyte. The alkaline solution was similarly prepared by adding 100  $\mu$ l of 0.1 M NaOH to 3 ml as-prepared electrolyte. Adding the methyl orange solution to the acidified and alkaline electrolyte solutions, yielded the

same colors as for the fresh and used electrolyte samples, which can be seen in Figure S6.

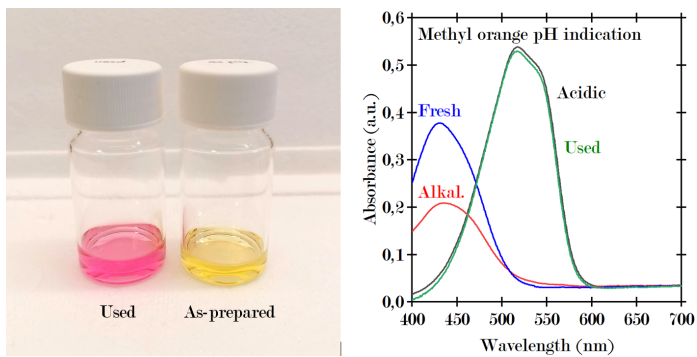


Figure S6: Photograph and UV-vis spectra of electrolyte samples with methyl orange pH indicator solution added. Acidic solutions turn pink while alkaline solutions are yellow. The absorption spectra in the right graph, show a complete overlay how used electrolyte gets the same colour as acidic solutions, while fresh electrolyte is more alkaline.

## References

- (1) Andersen, S. Z. et al. A rigorous electrochemical ammonia synthesis protocol with quantitative isotope measurements. *Nature* **2019**, *570*, 504–508.
- (2) Singh, A. R.; Rohr, B. A.; Schwalbe, J. A.; Cargnello, M.; Chan, K.; Jaramillo, T. F.; Chorkendorff, I.; Nørskov, J. K. Electrochemical Ammonia Synthesis—The Selectivity Challenge. *ACS Catalysis* **2017**, *7*, 706–709.
- (3) Tsuneto, A.; Kudo, A.; Sakata, T. Efficient Electrochemical Reduction of N<sub>2</sub> to NH<sub>3</sub> Catalyzed by Lithium. *Chemistry Letters* **1993**, *22*, 851–854.
- (4) Schwalbe, J. A.; Statt, M. J.; Chosy, C.; Singh, A. R.; Rohr, B. A.; Nielander, A. C.; Andersen, S. Z.; McEnaney, J. M.; Baker, J. G.; Jaramillo, T. F.; Nørskov, J. K.; Cargnello, M. A Combined Theory-Experiment analysis of the Surface Species in Lithium Mediated NH<sub>3</sub> Electrosynthesis. *ChemElectroChem* **2020**, *7*, 1542–1549.
- (5) Andersen, S. Z.; Statt, M. J.; Bukas, V. J.; Shapel, S. G.; Pedersen, J. B.; Kreml, K.; Saccoccio, M.; Chakraborty, D.; Kibsgaard, J.; Vesborg, P. C. K.; Nørskov, J.; Chorkendorff, I. Increasing stability, efficiency, and fundamental understanding of lithium-mediated electrochemical nitrogen reduction. *Energy & Environmental Science* **2020**, *13*, 4291–4300.
- (6) Lazouski, N.; Schiffer, Z. J.; Williams, K.; Manthiram, K. Understanding Continuous Lithium-Mediated Electrochemical Nitrogen Reduction. *Joule* **2019**, *3*, 1127–1139.
- (7) Cherepanov, P. V.; Krebsz, M.; Hodgetts, R. Y.; Simonov, A. N.; MacFarlane, D. R. Understanding the Factors Determining the Faradaic Efficiency and Rate of the Lithium Redox-Mediated N<sub>2</sub> Reduction to Ammonia. *The Journal of Physical Chemistry C* **2021**, *125*, 11402–11410.

- (8) Lazouski, N.; Chung, M.; Williams, K.; Gala, M. L.; Manthiram, K. Non-aqueous gas diffusion electrodes for rapid ammonia synthesis from nitrogen and water-splitting-derived hydrogen. *Nature Catalysis* **2020**, *3*, 463–469.
- (9) Suryanto, B. H. R.; Matuszek, K.; Choi, J.; Hodgetts, R. Y.; Du, H.-L.; Bakker, J. M.; Kang, C. S. M.; Cherepanov, P. V.; Simonov, A. N.; MacFarlane, D. R. Nitrogen reduction to ammonia at high efficiency and rates based on a phosphonium proton shuttle. *Science* **2021**, *372*, 1187–1191.
- (10) Wise, C. F.; Agarwal, R. G.; Mayer, J. M. Determining Proton-Coupled Standard Potentials and X-H Bond Dissociation Free Energies in Nonaqueous Solvents Using Open-Circuit Potential Measurements. *Journal of the American Chemical Society* **2020**, *142*, 10681–10691.
- (11) Ledezma-Yanez, I.; Díaz-Morales, O.; Figueiredo, M. C.; Koper, M. T. Hydrogen oxidation and hydrogen evolution on a platinum electrode in acetonitrile. *ChemElectroChem* **2015**, *2*, 1612–1622.
- (12) Olmstead, W. N.; Margolin, Z.; Bordwell, F. G. Acidities of water and simple alcohols in dimethyl sulfoxide solution. *The Journal of Organic Chemistry* **1980**, *45*, 3295–3299.
- (13) Nakahama, S.; Hashimoto, K.; Yamazaki, N. Anode-Initiated Polymerizations of Olefins and Tetrahydrofuran. *Polymer Journal* **1973**, *4*, 437–445.
- (14) Dey, A. N.; Rudd, E. J. Electroinitiated Polymerization of Tetrahydrofuran. *Electrochem. Soc.* **1974**, *121*, 1294–1298.
- (15) Hatsukade, T.; Zorko, M.; Haering, D.; Markovic, N. M.; Stamenkovic, V. R.; Strmcnik, D. Detection of protons using the rotating ring disk electrode method during electrochemical oxidation of battery electrolytes. *Electrochemistry Communications* **2020**, *120*, 106785.

- (16) Elgrishi, N.; Rountree, K. J.; McCarthy, B. D.; Rountree, E. S.; Eisenhart, T. T.; Dempsey, J. L. A Practical Beginner’s Guide to Cyclic Voltammetry. *Journal of Chemical Education* **2018**, *95*, 197–206.
- (17) Sazinas, R.; Andersen, S. Z.; Li, K.; Saccocio, M.; Kreml, K.; Pedersen, J. B.; Kibsgaard, J.; Vesborg, P. C. K.; Chakraborty, D.; Chorkendorff, I. Towards understanding of electrolyte degradation in lithium-mediated non-aqueous electrochemical ammonia synthesis with gas chromatography-mass spectrometry. *RSC Adv.* **2021**, *11*, 31487–31498.
- (18) Pruckmayr, G.; Wu, T. K. Polymerization of Tetrahydrofuran by Proton Acids. *Macromolecules* **1978**, *11*, 662–668.
- (19) Pruckmayr, G.; Wu, T. K. Macrocyclic Tetrahydrofuran Oligomers. 2. Formation of Macrocycles in the Polymerization of Tetrahydrofuran with Triflic Acid. *Macromolecules* **1978**, *11*, 265–270.
- (20) Freire, M. G.; Neves, C. M. S. S.; Marrucho, I. M.; Coutinho, J. A. P.; Fernandes, A. M. Hydrolysis of Tetrafluoroborate and Hexafluorophosphate Counter Ions in Imidazolium-Based Ionic Liquids. *The Journal of Physical Chemistry A* **2010**, *114*, 3744–3749.
- (21) Solchenbach, S.; Metzger, M.; Egawa, M.; Beyer, H.; Gasteiger, H. A. Quantification of PF 5 and POF 3 from Side Reactions of LiPF 6 in Li-Ion Batteries. *Journal of The Electrochemical Society* **2018**, *165*, A3022–A3028.
- (22) Sander, R. Compilation of Henry’s law constants (version 4.0) for water as solvent. *Atmos. chem. phys.* **2015**, *15*, 4399–4981.
- (23) Singh, A. R.; Rohr, B. A.; Statt, M. J.; Schwalbe, J. A.; Cargnello, M.; Nørskov, J. K. Strategies toward Selective Electrochemical Ammonia Synthesis. *ACS Catalysis* **2019**, *9*, 8316–8324.

# Bibliography

1. Gül, T. *Ammonia Technology Roadmap - Towards more sustainable nitrogen fertiliser production* tech. rep. (International Energy Agency, IEA, 2021), 1–168. <https://www.iea.org/reports/ammonia-technology-roadmap>.
2. Apodaca, L. E. *Mineral Commodity Summaries 2022* tech. rep. (U.S. Geological Survey, Reston, Virginia, Jan. 2022), 118–119.
3. NOAH Chemicals. *5 Most Common Industrial Chemicals* Aug. 2017. <https://noahchemicals.com/blog/5-most-common-industrial-chemicals/> (2022).
4. Lim, J., Fernández, C. A., Lee, S. W. & Hatzell, M. C. Ammonia and Nitric Acid Demands for Fertilizer Use in 2050. *ACS Energy Letters* **6**, 3676–3685. ISSN: 23808195 (Oct. 2021).
5. Lazonby, J. & Waddington, D. *Sulfuric acid* Oct. 2016. <https://www.essentialchemicalindustry.org/chemicals/sulfuric-acid.html> (2022).
6. Tiseo, I. *Global ethylene demand & capacity 2015-2022* Mar. 2022. <https://www.statista.com/statistics/1246694/ethylene-demand-capacity-forecast-worldwide/> (2022).
7. Chorkendorff, I. & Niemantsverdriet, J. W. *Concepts of Modern Catalysis and Kinetics* (WILEY-VCH Verlag GmbH and Co. KGaA, Weinheim, 2003).
8. Parrott-Sheffer, C. *Blue-green algae* Dec. 2017. <https://www.britannica.com/science/blue-green-algae> (2022).
9. Petruzzello, M. *Nitrogen fixation* July 2021. <https://www.britannica.com/science/nitrogen-fixation> (2022).
10. Hoffman, B. M., Lukoyanov, D., Yang, Z. Y., Dean, D. R. & Seefeldt, L. C. Mechanism of nitrogen fixation by nitrogenase: The next stage. *Chemical Reviews* **114**, 4041–4062. ISSN: 15206890. <https://pubs.acs.org/doi/full/10.1021/cr400641x> (Apr. 2014).
11. Knight, J. D. Frequency of field pea in rotations impacts biological nitrogen fixation. *Canadian Journal of Plant Science* **92**, 1005–1011. ISSN: 00084220. <https://cdnsiencepub.com/doi/full/10.4141/cjps2011-274> (Nov. 2012).
12. Smil, V. Detonator of the population explosion. *Nature* 1999 400:6743 **400**, 415–415. ISSN: 1476-4687. <https://www.nature.com/articles/22672> (July 1999).

13. Barona, A., Etxebarria, B., Aleksanyan, A., Gallastegui, G., Rojo, N. & Diaz-Tena, E. A Unique Historical Case to Understand the Present Sustainable Development. *Science and Engineering Ethics* **24**, 261–274. ISSN: 14715546. <https://link.springer.com/article/10.1007/s11948-017-9891-5> (Feb. 2018).
14. Roser, M., Ritchie, H. & Ortiz-Ospina, E. *World Population Growth* May 2019. [https://ourworldindata.org/world-population-growth?utm\\_content=bufferd03f5%5C&utm\\_medium=social%5C&utm\\_source=twitter.com%5C&utm\\_campaign=buffer](https://ourworldindata.org/world-population-growth?utm_content=bufferd03f5%5C&utm_medium=social%5C&utm_source=twitter.com%5C&utm_campaign=buffer) (2022).
15. Stewart, W. M., Dibb, D. W., Johnston, A. E. & Smyth, T. J. The contribution of commercial fertilizer nutrients to food production. *Agronomy Journal* **97**, 1–6. ISSN: 00021962 (2005).
16. Westhead, O., Jervis, R. & Stephens, I. E. Is lithium the key for nitrogen electroreduction? *Science* **372**, 1149–1150. ISSN: 10959203 (June 2021).
17. Ritchie, H. & Roser, M. Fertilizers. *Our World in Data*. <https://ourworldindata.org/fertilizers> (2013).
18. Erisman, J. W., Sutton, M. A., Galloway, J., Klimont, Z. & Winiwarter, W. How a century of ammonia synthesis changed the world. *Nature Geoscience* **1**, 636–639 (10 Oct. 2008).
19. Martín, A. J., Shinagawa, T. & Pérez-Ramírez, J. Electrocatalytic Reduction of Nitrogen: From Haber-Bosch to Ammonia Artificial Leaf. *Chem* **5**, 263–283. ISSN: 24519294 (Feb. 2019).
20. Trepelkov, A. *THE 17 GOALS | Sustainable Development* 2015. <https://sdgs.un.org/goals> (2022).
21. Broecker, W. S. Climate Change: Are We on the Brink of a Pronounced Global Warming? *Science* **189**, 460–463 (1975).
22. Wang, W. C., Yung, Y. L., Lacis, A. A., Mo, T. & Hansen, J. E. Greenhouse Effects due to Man-Made Perturbations of Trace Gases. *New Series* **194**, 685–690 (Nov. 1976).
23. Hansen, J., Johnson, D., Lacis, A., Lebedeff, S., Lee, P., Rind, D. & Russell, G. Climate Impact of Increasing Atmospheric Carbon Dioxide. *New Series* **213**, 957–966 (Aug. 1981).
24. Jain, P. C. Greenhouse Effect and Climate Change: Scientific Basis and Overview. *Renewable Energy* **3**, 403–420. ISSN: 09601481 (1993).
25. Rich, N. & Steinmetz, G. *Losing Earth: The Decade We Almost Stopped Climate Change* Aug. 2018. <https://www.nytimes.com/interactive/2018/08/01/magazine/climate-change-losing-earth.html> (2022).
26. McGee, M. Daily CO<sub>2</sub>. *CO<sub>2</sub>.Earth*. <https://www.co2.earth/daily-co2>, accessed 21/03-2022 (2022).
27. Lindsey, R. Climate Change: Atmospheric Carbon Dioxide. *Climate.gov*. <https://www.climate.gov/news-features/understanding-climate/climate-change-atmospheric-carbon-dioxide>, accessed 21/03-2022 (2021).
28. Kyriakou, V., Garagounis, I., Vourros, A., Vasileiou, E. & Stoukides, M. An Electrochemical Haber-Bosch Process. *Joule* **4**, 142–158. <https://doi.org/10.1016/j.joule.2019.10.006> (Jan. 2020).

29. Wismann, S. T., Engbæk, J. S., Vendelbo, S. B., Bendixen, F. B., Eriksen, W. L., Aasberg-Petersen, K., Frandsen, C., Chorkendorff, I. & Mortensen, P. M. Electrified methane reforming: A compact approach to greener industrial hydrogen production. *Science* **364**, 756–759. ISSN: 10959203. <https://www.science.org/doi/abs/10.1126/science.aaw8775> (May 2019).
30. Zumdahl, S. S. & DeCoste, D. J. *Chemical Principles* 7th ed. (ed Lockwood, L.) 1199. ISBN: 978-1-111-58065-0 (Cengage Learning EMEA, Belmont, CA, 2013).
31. Ballentine, L. E. *Quantum Mechanics - A Modern Development* 2nd ed., 722. ISBN: 9789814578585 (World Scientific Publishing Co Pte, Singapore, 2014).
32. Montoya, J. H., Tsai, C., Vojvodic, A. & Nørskov, J. K. The Challenge of Electrochemical Ammonia Synthesis: A New Perspective on the Role of Nitrogen Scaling Relations. *ChemSusChem* **8**, 2180–2186. ISSN: 18645631. <http://doi.wiley.com/10.1002/cssc.201500322> (July 2015).
33. Parkinson, B., Tabatabaei, M., Upham, D. C., Ballinger, B., Greig, C., Smart, S. & McFarland, E. Hydrogen production using methane: Techno-economics of decarbonizing fuels and chemicals. *International Journal of Hydrogen Energy* **43**, 2540–2555. ISSN: 0360-3199 (Feb. 2018).
34. Andersen, S. Z., Čolić, V., Yang, S., Schwalbe, J. A., Nielander, A. C., McEnaney, J. M., Enemark-Rasmussen, K., Baker, J. G., Singh, A. R., Rohr, B. A., Statt, M. J., Blair, S. J., Mezzavilla, S., Kibsgaard, J., Vesborg, P. C., Cargnello, M., Bent, S. F., Jaramillo, T. F., Stephens, I. E., Nørskov, J. K. & Chorkendorff, I. A rigorous electrochemical ammonia synthesis protocol with quantitative isotope measurements. *Nature* **570**, 504–508. ISSN: 14764687. <http://dx.doi.org/10.1038/s41586-019-1260-x> (2019).
35. Choi, J., Suryanto, B. H., Wang, D., Du, H. L., Hodgetts, R. Y., Ferrero Vallana, F. M., MacFarlane, D. R. & Simonov, A. N. Identification and elimination of false positives in electrochemical nitrogen reduction studies. *Nature Communications* **2020 11:1** **11**, 1–10. ISSN: 2041-1723. <https://www.nature.com/articles/s41467-020-19130-z> (Nov. 2020).
36. Bard, A. J. & Faulkner, L. R. *Electrochemical methods: fundamentals and application* 2nd, 833. ISBN: 0471043729 (cloth alk. paper). Publisher % 20description% 20http://www.loc.gov/catdir/description/wiley031/00038210.html% 20Table% 20of% 20Contents% 20http://www.loc.gov/catdir/toc/onix01/00038210.html (Wiley, New York, 2001).
37. Hansen, J. N., Prats, H., Toudahl, K. K., Mørch Secher, N., Chan, K., Kibsgaard, J. & Chorkendorff, I. Is There Anything Better than Pt for HER? *ACS Energy Letters* **6**, 1175–1180. ISSN: 23808195. <https://pubs.acs.org/doi/full/10.1021/acsenerylett.1c00246> (Apr. 2021).
38. Rumble, J. R., Lide, D. R. & Bruno, T. J. *Handbook of Chemistry and Physics* 98th edition (ed Rumble, J. R.) ISBN: 978-1-4987-8454-2 (CRC Press, Boca Raton, Florida, 2017).
39. Tsuneto, A., Kudo, A. & Sakata, T. Efficient Electrochemical Reduction of N<sub>2</sub> to NH<sub>3</sub> Catalyzed by Lithium. *Chemistry Letters* **22**, 851–854. ISSN: 0366-7022. <http://www.journal.csj.jp/doi/10.1246/cl.1993.851> (May 1993).

40. Elgrishi, N., Rountree, K. J., McCarthy, B. D., Rountree, E. S., Eisenhart, T. T. & Dempsey, J. L. A Practical Beginner's Guide to Cyclic Voltammetry. *Journal of Chemical Education* **95**, 197–206. ISSN: 19381328. <https://pubs.acs.org/doi/full/10.1021/acs.jchemed.7b00361> (Feb. 2018).
41. Barsoukov, E. & Macdonald, J. R. *Impedance Spectroscopy - Theory, Experiment, and Applications*. 2nd ed., 606. ISBN: 0-471-64749-7 (John Wiley & Sons, Inc., Hoboken, New Jersey, 2005).
42. Arbizzani, C., Yu, Y., Li, J., Xiao, J., Yao Xia, Y., Yang, Y., Santato, C., Raccichini, R. & Passerini, S. Good practice guide for papers on supercapacitors and related hybrid capacitors for the Journal of Power Sources. *Journal of Power Sources* **450**, 227636. ISSN: 0378-7753 (Feb. 2020).
43. Aurbach, D., Daroux, M., Faguy, P. & Yeager, E. The electrochemistry of noble metal electrodes in aprotic organic solvents containing lithium salts. *Journal of Electroanalytical Chemistry and Interfacial Electrochemistry* **297**, 225–244. ISSN: 0022-0728 (Jan. 1991).
44. Lazouski, N., Chung, M., Williams, K., Gala, M. L. & Manthiram, K. Non-aqueous gas diffusion electrodes for rapid ammonia synthesis from nitrogen and water-splitting-derived hydrogen. *Nature Catalysis* *2020* **3:5** **3**, 463–469. ISSN: 2520-1158. <https://www.nature.com/articles/s41929-020-0455-8> (May 2020).
45. Andersen, S. Z., Statt, M. J., Bukas, V. J., Shapel, S. G., Pedersen, J. B., Krempl, K., Saccoccio, M., Chakraborty, D., Kibsgaard, J., Vesborg, P. C., Nørskov, J. & Chorkendorff, I. Increasing stability, efficiency, and fundamental understanding of lithium-mediated electrochemical nitrogen reduction. *Energy & Environmental Science* **13**, 4291–4300. ISSN: 1754-5706. <https://pubs.rsc.org/en/content/articlehtml/2020/ee/d0ee02246b> <https://pubs.rsc.org/en/content/articlelanding/2020/ee/d0ee02246b> (Nov. 2020).
46. Li, K., Andersen, S. Z., Statt, M. J., Saccoccio, M., Bukas, V. J., Krempl, K., Sažinas, R., Pedersen, J. B., Shadravan, V., Zhou, Y., Chakraborty, D., Kibsgaard, J., Vesborg, P. C., Nørskov, J. K. & Chorkendorff, I. Enhancement of lithium-mediated ammonia synthesis by addition of oxygen. *Science* **374**, 1593–1597. ISSN: 10959203. <https://www.science.org/doi/abs/10.1126/science.abl4300> (Dec. 2021).
47. Lazouski, N., Schiffer, Z. J., Williams, K. & Manthiram, K. Understanding Continuous Lithium-Mediated Electrochemical Nitrogen Reduction. *Joule* **3**, 1127–1139. ISSN: 2542-4351 (Apr. 2019).
48. Searle, P. L. The berthelot or indophenol reaction and its use in the analytical chemistry of nitrogen. A review. *The Analyst* **109**, 549. ISSN: 0003-2654. <http://xlink.rsc.org/?DOI=an9840900549> (1984).
49. Wypych, G. in *Handbook of material weathering* 6th ed., 1–26 (Elsevier Science, 2018). ISBN: 9781927885321.
50. Scott, W. D. & Cattell, F. C. Vapor pressure of ammonium sulfates. *Atmospheric Environment (1967)* **13**, 307–317. ISSN: 0004-6981 (Jan. 1979).

51. Suryanto, B. H., Matuszek, K., Choi, J., Hodgetts, R. Y., Du, H. L., Bakker, J. M., Kang, C. S., Cherepanov, P. V., Simonov, A. N. & MacFarlane, D. R. Nitrogen reduction to ammonia at high efficiency and rates based on a phosphonium proton shuttle. *Science* **372**, 1187–1191. ISSN: 10959203 (June 2021).
52. SeQuant. *A Practical Guide to Ion Chromatography* 2nd ed., 1–26. ISBN: 9789163180569. [www.sequant.com](http://www.sequant.com) (SeQuant AB, Umeaa, Sweden, Mar. 2007).
53. Suryanto, B. H., Du, H. L., Wang, D., Chen, J., Simonov, A. N. & MacFarlane, D. R. Challenges and prospects in the catalysis of electroreduction of nitrogen to ammonia. *Nature Catalysis* 2019 2:4 **2**, 290–296. ISSN: 2520-1158. <https://www.nature.com/articles/s41929-019-0252-4> (Mar. 2019).
54. Greenlee, L. F., Renner, J. N. & Foster, S. L. The Use of Controls for Consistent and Accurate Measurements of Electrocatalytic Ammonia Synthesis from Dinitrogen. *ACS Catalysis* **8**, 7820–7827. ISSN: 21555435. <https://pubs.acs.org/doi/full/10.1021/acscatal.8b02120> (Sept. 2018).
55. Knudsen, C. & Pedersen, M. B. *Mechanics and Physical Modelling* Second Custom Edition (ed Florence, I.) 334–337. ISBN: 978-1-4080-7432-9 (Cengage Learning EMEA, Hampshire, UK, 2012).
56. De Laeter, J. R., Böhlke, J. K., De Bièvre, P., Hidaka, H., Peiser, H. S., Rosman, K. J. R. & Taylor, P. D. P. *Atomic Weights of the Elements: Review 2000* tech. rep. 6 (International Union of Pure and Applied Chemistry, 2003), 683–800.
57. Crawford, J. *The Poetic Edda : stories of the Norse gods and heroes* ISBN: 9781624663567 (Hackett Publishing Co, Inc, Mar. 2015).
58. Krempl, K., Hochfilzer, D., Cavalca, F., Saccoccio, M., Kibsgaard, J., Vesborg, P. C. K. & Chorkendorff, I. Quantitative Operando Detection of Electro Synthesized Ammonia Using Mass Spectrometry. *ChemElectroChem* **9**, 1–5. <https://doi.org/10.1002/celec.202101713> (Feb. 2022).
59. Minissale, M., Faure, J.-B., Dunand, A., Angot, T., De Temmerman, G. & Bisson, R. Ammonia Molecules on Tungsten and 316L Stainless Steel Surfaces. *Journal of Physical Chemistry C* **124**, 17566–17577. <https://hal-amu.archives-ouvertes.fr/hal-03046773> (2020).
60. Somogyi, Á. in *Medical Applications of Mass Spectrometry* (eds Vékey, K., Telekes, A. & Vertes, A.) 1st ed., 93–140 (Elsevier, 2008). ISBN: 9780444519801.
61. Hoffmann, E. D. & Stroobant, V. *Mass spectrometry: Principles and Applications* 3rd ed., 502. ISBN: 9780470033104 (John Wiley & Sons Inc, 2007).
62. Van der Ham, C. J. M., Koper, M. T. M. & Hetterscheid, D. G. H. Challenges in reduction of dinitrogen by proton and electron transfer. *Chem. Soc. Rev.* **43**, 5183–5191. ISSN: 0306-0012. <http://xlink.rsc.org/?DOI=C4CS00085D> (2014).
63. Skúlason, E., Bligaard, T., Gudmundsdóttir, S., Studt, F., Rossmeisl, J., Abild-Pedersen, F., Vegge, T., Jónsson, H. & Nørskov, J. K. A theoretical evaluation of possible transition metal electro-catalysts for N<sub>2</sub> reduction. *Physical Chemistry Chemical Physics* **14**, 1235–1245. ISSN: 1463-9084. <https://pubs.rsc.org/en/content/articlehtml/2012/cp/c1cp22271f> <https://pubs.rsc.org/en/content/articlelanding/2012/cp/c1cp22271f> (Dec. 2011).

64. Singh, A. R., Rohr, B. A., Schwalbe, J. A., Cargnello, M., Chan, K., Jaramillo, T. F., Chorkendorff, I. & Nørskov, J. K. Electrochemical Ammonia Synthesis - The Selectivity Challenge. *ACS Catalysis* **7**, 706–709. ISSN: 21555435. <https://pubs-acrs-org.proxy.findit.cvt.dk/doi/full/10.1021/acscatal.6b03035> (Jan. 2017).
65. Dooley, R. *Revised Release on the Ionization Constant of Water and Steam (2019)* tech. rep. (The International Association for the Properties of Water and Steam, Banff, Canada, Oct. 2019), 1–7. <http://www.iapws.org>.
66. Zhou, F., Azofra, L. M., Ali, M., Kar, M., Simonov, A. N., McDonnell-Worth, C., Sun, C., Zhang, X. & Macfarlane, D. R. Electro-synthesis of ammonia from nitrogen at ambient temperature and pressure in ionic liquids † Broader context. *Energy & Environmental Science* **10**, 2516 (2017).
67. PubChem. *PubChem Compound Summary for CID 8028, Tetrahydrofuran* 2018. <https://pubchem.ncbi.nlm.nih.gov/compound/Tetrahydrofuran>.
68. Tsuneto, A., Kudo, A. & Sakata, T. Lithium-mediated electrochemical reduction of high pressure N<sub>2</sub> to NH<sub>3</sub>. *Journal of Electroanalytical Chemistry* **367**, 183–188. ISSN: 15726657. <http://linkinghub.elsevier.com/retrieve/pii/S002207289303025K> (Mar. 1994).
69. Fichter, F., Girard, P. & Erlenmeyer, H. Elektrolytische Bindung von komprimiertem Stickstoff bei gewöhnlicher Temperatur. *Helvetica Chimica Acta* **13**, 1228–1236. ISSN: 1522-2675. <https://onlinelibrary.wiley.com/doi/full/10.1002/hlca.19300130604><https://onlinelibrary.wiley.com/doi/abs/10.1002/hlca.19300130604><https://onlinelibrary.wiley.com/doi/10.1002/hlca.19300130604> (Dec. 1930).
70. Schwalbe, J. A., Statt, M. J., Chosy, C., Singh, A. R., Rohr, B. A., Nielander, A. C., Andersen, S. Z., McEnaney, J. M., Baker, J. G., Jaramillo, T. F., Nørskov, J. K. & Cargnello, M. A Combined Theory-Experiment Analysis of the Surface Species in Lithium-Mediated NH<sub>3</sub> Electrosynthesis. *ChemElectroChem* **7**, 1542–1549. ISSN: 2196-0216. <https://onlinelibrary.wiley.com/doi/full/10.1002/celec.201902124><https://onlinelibrary.wiley.com/doi/abs/10.1002/celec.201902124><https://chemistry-europe.onlinelibrary.wiley.com/doi/abs/10.1002/celec.201902124> (Apr. 2020).
71. Cherepanov, P. V., Krebsz, M., Hodgetts, R. Y., Simonov, A. N. & Macfarlane, D. R. Understanding the Factors Determining the Faradaic Efficiency and Rate of the Lithium Redox-Mediated N<sub>2</sub>Reduction to Ammonia. *Journal of Physical Chemistry C* **125**, 11402–11410. ISSN: 19327455. <https://pubs.acs.org/doi/abs/10.1021/acs.jpcc.1c02494> (June 2021).
72. Cai, X., Fu, C., Iriawan, H., Yang, F., Wu, A., Luo, L., Shen, S., Wei, G., Shao-Horn, Y. & Zhang, J. Lithium-mediated electrochemical nitrogen reduction: Mechanistic insights to enhance performance. *iScience* **24**, 103105. ISSN: 2589-0042 (Oct. 2021).
73. Krishnamurthy, D., Lazouski, N., Gala, M. L., Manthiram, K. & Viswanathan, V. Closed-Loop Electrolyte Design for Lithium-Mediated Ammonia Synthesis. *ACS Central Science* **7**, 2073–2082. ISSN: 23747951. <https://doi.org/10.1021/acscentsci.1c01151> (Dec. 2021).

74. Lazouski, N., Steinberg, K. J., Gala, M. L., Krishnamurthy, D., Viswanathan, V. & Manthiram, K. Proton Donors Induce a Differential Transport Effect for Selectivity toward Ammonia in Lithium-Mediated Nitrogen Reduction. *ACS Catalysis*, 5197–5208. ISSN: 2155-5435. <https://pubs.acs.org/doi/abs/10.1021/acscatal.2c00389> (Apr. 2022).
75. Steinberg, K., Yuan, X., Lazouski, N., Klein, C. K., Manthiram, K. & Li, Y. *Imaging nitrogen fixation at lithium solid electrolyte interphases via cryo-electron microscopy* Cambridge, Apr. 2022. <https://chemrxiv.org/engage/chemrxiv/article-details/624f326685d81418ed012332>.
76. Peled, E. The Electrochemical Behavior of Alkali and Alkaline Earth Metals in Nonaqueous Battery Systems—The Solid Electrolyte Interphase Model. *Journal of The Electrochemical Society* **126**, 2047–2051. ISSN: 0013-4651. <https://iopscience.iop.org/article/10.1149/1.2128859><https://iopscience.iop.org/article/10.1149/1.2128859/meta> (Dec. 1979).
77. Peled, E., Golodnitsky, D. & Ardel, G. Advanced Model for Solid Electrolyte Interphase Electrodes in Liquid and Polymer Electrolytes. *Journal of The Electrochemical Society* **144**, L208–L210. ISSN: 0013-4651 (Aug. 1997).
78. Peled, E. & Menkin, S. Review—SEI: Past, Present and Future. *Journal of The Electrochemical Society* **164**, A1703–A1719. ISSN: 0013-4651. <https://iopscience-iop-org.proxy.findit.cvt.dk/article/10.1149/2.1441707jes><https://iopscience-iop-org.proxy.findit.cvt.dk/article/10.1149/2.1441707jes/meta> (June 2017).
79. Andersen, S. Z. *Electrochemical Nitrogen Reduction Under (Near) Ambient Conditions* PhD thesis. PhD thesis (Technical University of Denmark, Kongens Lyngby, Denmark, 2020), 1–157. <https://findit.dtu.dk/en/catalog/6080a074d9001d013e164532>.
80. Sažinas, R., Andersen, S. Z., Li, K., Saccoccio, M., Krempl, K., Pedersen, J. B., Kibsgaard, J., Vesborg, P. C. K., Chakraborty, D. & Chorkendorff, I. Towards understanding of electrolyte degradation in lithium-mediated non-aqueous electrochemical ammonia synthesis with gas chromatography-mass spectrometry. *RSC Advances* **11**, 31487–31498. ISSN: 2046-2069. <https://pubs.rsc.org/en/content/articlehtml/2021/ra/d1ra05963g><https://pubs.rsc.org/en/content/articlelanding/2021/ra/d1ra05963g> (Sept. 2021).
81. Szeloing, K. & Fan, K. *Chemistry of Lithium (Z=3)* Aug. 2020. <https://chem.libretexts.org/@go/page/591> (2022).
82. Kibsgaard, J., Nørskov, J. K. & Chorkendorff, I. The Difficulty of Proving Electrochemical Ammonia Synthesis. *ACS Energy Letters* **4**, 2986–2988. ISSN: 23808195. <https://pubs.acs.org/doi/full/10.1021/acsenerylett.9b02286> (Dec. 2019).
83. Choi, J., Choi, J., Du, H. L., Du, H. L., Nguyen, C. K., Nguyen, C. K., Suryanto, B. H., Simonov, A. N., Simonov, A. N., MacFarlane, D. R. & MacFarlane, D. R. Electroreduction of Nitrates, Nitrites, and Gaseous Nitrogen Oxides: A Potential Source of Ammonia in Dinitrogen Reduction Studies. *ACS Energy Letters* **5**, 2095–2097. ISSN: 23808195. <https://pubs.acs.org/doi/abs/10.1021/acsenerylett.0c00924> (June 2020).

84. Chen, Y., Liu, H., Ha, N., Licht, S., Gu, S. & Li, W. Revealing nitrogen-containing species in commercial catalysts used for ammonia electrosynthesis. *Nature Catalysis* 2020 3:12 **3**, 1055–1061. ISSN: 2520-1158. <https://www.nature.com/articles/s41929-020-00527-4> (Oct. 2020).
85. Lazouski, N., Limaye, A., Bose, A., Gala, M. L., Manthiram, K. & Mallapragada, D. S. Cost and performance targets for fully electrochemical ammonia production under flexible operation. *ChemRxiv. Cambridge: Cambridge Open Engage*. <https://chemrxiv.org/engage/chemrxiv/article-details/6230f749d6d3ed3d2f931fe1> (Mar. 2022).
86. Wang, E., Dey, S., Liu, T., Menkin, S. & Grey, C. P. Effects of Atmospheric Gases on Li Metal Cyclability and Solid-Electrolyte Interphase Formation. *ACS Energy Letters* **5**, 1088–1094. ISSN: 23808195. <https://pubs.acs.org/doi/full/10.1021/acsenergylett.0c00257> (Apr. 2020).
87. Krempel, K., Pedersen, J. B., Kibsgaard, J., Vesborg, P. C. & Chorkendorff, I. Electrolyte acidification from anode reactions during lithium mediated ammonia synthesis. *Electrochemistry Communications* **134**, 107186. ISSN: 1388-2481 (Jan. 2022).
88. Skúlason, E., Tripkovic, V., Björketun, M. E., Gudmundsdóttir, S., Karlberg, G., Rossmeis, J., Bligaard, T., Jónsson, H. & Nørskov, J. K. Modeling the Electrochemical Hydrogen Oxidation and Evolution Reactions on the Basis of Density Functional Theory Calculations. *The Journal of Physical Chemistry C* **114**, 22374–22374. ISSN: 1932-7447. <http://pubs.acs.org/doi/10.1021/jp110913n> (Dec. 2010).
89. Hatsukade, T., Zorko, M., Haering, D., Markovic, N. M., Stamenkovic, V. R. & Strmcnik, D. Detection of protons using the rotating ring disk electrode method during electrochemical oxidation of battery electrolytes. *Electrochemistry Communications* **120**, 106785. ISSN: 1388-2481 (Nov. 2020).
90. Choudhary, A. *Preparation of Indicator Solutions* Sept. 2010. <https://www.pharmaguideline.com/2010/09/preparation-of-indicator-solutions.html> (2021).
91. Perichon, J. & Buvet, R. No. 646 - Électrochimie en solution dans le tétrahydrofurane. I. - Fixation et détermination expérimentale de l'acidité dans le tétrahydrofurane. *Bulletin de la Société Chimique de France* **10**, 3697–3706 (1967).
92. Lewis, N. S. & Nocera, D. G. Powering the planet: Chemical challenges in solar energy utilization. *Proceedings of the National Academy of Sciences of the United States of America* **103**, 15729–15735. ISSN: 00278424. [www.pnas.org/cgi/doi/10.1073/pnas.0603395103](http://www.pnas.org/cgi/doi/10.1073/pnas.0603395103) (Oct. 2006).
93. Schmidt, O., Gambhir, A., Staffell, I., Hawkes, A., Nelson, J. & Few, S. Future cost and performance of water electrolysis: An expert elicitation study. *International Journal of Hydrogen Energy* **42**, 30470–30492. ISSN: 0360-3199 (Dec. 2017).
94. Bockris, J. O. The hydrogen economy: Its history. *International Journal of Hydrogen Energy* **38**, 2579–2588. ISSN: 0360-3199 (Feb. 2013).

95. Dillman, K. & Heinonen, J. A ‘Safe’ Hydrogen Economy: An Absolute Environmental Sustainability Assessment of the Hydrogen Economy. *SSRN Electronic Journal*. ISSN: 1556-5068. <https://papers.ssrn.com/abstract=4081110> (Apr. 2022).
96. Balat, M. Potential importance of hydrogen as a future solution to environmental and transportation problems. *International Journal of Hydrogen Energy* **33**, 4013–4029. ISSN: 0360-3199 (Aug. 2008).
97. Gahleitner, G. Hydrogen from renewable electricity: An international review of power-to-gas pilot plants for stationary applications. *International Journal of Hydrogen Energy* **38**, 2039–2061. ISSN: 0360-3199 (Feb. 2013).
98. Jones, M., Rouwenhorst, K. H. R., Travis, A. S. & Lefferts, L. 1921–2021: A Century of Renewable Ammonia Synthesis. *Sustainable Chemistry 2022, Vol. 3, Pages 149–171* **3**, 149–171. ISSN: 2673-4079. <https://www.mdpi.com/2673-4079/3/2/11/html><https://www.mdpi.com/2673-4079/3/2/11> (Apr. 2022).
99. Roberts, S. T., Ramasesha, K., Petersen, P. B., Mandal, A. & Tokmakoff, A. Proton transfer in concentrated aqueous hydroxide visualized using ultrafast infrared spectroscopy. *Journal of Physical Chemistry A* **115**, 3957–3972. ISSN: 10895639. <https://pubs.acs.org/doi/abs/10.1021/jp108474p> (Apr. 2011).
100. Rabiee, H., Ge, L., Zhang, X., Hu, S., Li, M. & Yuan, Z. Gas diffusion electrodes (GDEs) for electrochemical reduction of carbon dioxide, carbon monoxide, and dinitrogen to value-added products: A review. *Energy and Environmental Science* **14**, 1959–2008. ISSN: 17545706 (Apr. 2021).
101. Wakerley, D., Lamaison, S., Wicks, J., Clemens, A., Feaster, J. & Corral, D. Gas diffusion electrodes, reactor designs and key metrics of low-temperature CO<sub>2</sub> electrolyzers. *Nature Energy* **7**, 130–143. <https://doi.org/10.1038/s41560-021-00973-9> (2022).
102. Battino, R., Rettich, T. R. & Tominaga, T. The Solubility of Nitrogen and Air in Liquids. *Journal of Physical and Chemical Reference Data* **13**, 563–600. ISSN: 15297845 (1984).
103. Gibanel, F., López, M. C., Royo, F. M., Santafé, J. & Urieta, J. S. Solubility of nonpolar gases in tetrahydrofuran at 0 to 30°C and 101.33 kPa partial pressure of gas. *Journal of Solution Chemistry* *1993 22:3* **22**, 211–217. ISSN: 1572-8927. <https://link.springer.com/article/10.1007/BF00649244> (Mar. 1993).
104. Larrazábal, G. O., Strøm-Hansen, P., Heli, J. P., Zeiter, K., Therkildsen, K. T., Chorkendorff, I. & Seger, B. Analysis of Mass Flows and Membrane Cross-over in CO<sub>2</sub> Reduction at High Current Densities in an MEA-Type Electrolyzer. *ACS Applied Materials and Interfaces* **11**, 41281–41288. ISSN: 19448252 (2019).
105. Li, Y. & Dai, H. Recent advances in zinc–air batteries. *Chemical Society Reviews* **43**, 5257–5275. ISSN: 1460-4744. <https://pubs.rsc.org/en/content/articlehtml/2014/cs/c4cs00015c><https://pubs.rsc.org/en/content/articlelanding/2014/cs/c4cs00015c> (July 2014).
106. Weng, L. C., Bell, A. T. & Weber, A. Z. Modeling gas-diffusion electrodes for CO<sub>2</sub> reduction. *Physical Chemistry Chemical Physics* **20**, 16973–16984. ISSN: 1463-9084. <https://pubs.rsc.org/en/content/articlehtml/2018/cp/c8cp01319e><https://pubs.rsc.org/en/content/articlelanding/2018/cp/c8cp01319e> (June 2018).

107. Lautrup, B. in *Physics of Continuous Matter: Exotic and Everyday Phenomena in the Macroscopic World* 2nd ed., 69–96 (CRC Press, Boca Raton, Florida, Mar. 2011). ISBN: 9781439894200.
108. Jin, W. & Chu, P. K. Orthopedic Implants. *Encyclopedia of Biomedical Engineering* **1-3**, 425–439 (Jan. 2019).
109. DuPont. *Stable in Harsh Environments* 2022. <https://www.dupont.com/kalrez.html> (2022).
110. Celgard. *About us* 2022. <https://www.celgard.com/about/> (2022).
111. Daramic. *About Daramic* 2022. <https://daramic.com/about-us> (2022).
112. McMaster-Carr. *Filtering* 2022. <https://www.mcmaster.com/browse-filtering/> (2022).
113. Ujvári, M., Láng, G. & Horányi, G. Stability of perchlorate ions in acid medium: Interaction with zinc and aluminium. *Journal of Applied Electrochemistry* **32**, 581–582. ISSN: 0021891X (2002).
114. Láng, G., Ujvári, M. & Horányi, G. On the reduction of ClO<sub>4</sub><sup>-</sup> ions in the course of metal dissolution in HClO<sub>4</sub> solutions. *Corrosion Science* **45**, 1–5. ISSN: 0010938X (2003).
115. Ma, T., Xu, G. L., Li, Y., Wang, L., He, X., Zheng, J., Liu, J., Engelhard, M. H., Zapol, P., Curtiss, L. A., Jorne, J., Amine, K. & Chen, Z. Revisiting the Corrosion of the Aluminum Current Collector in Lithium-Ion Batteries. *Journal of Physical Chemistry Letters* **8**, 1072–1077. ISSN: 19487185 (2017).
116. Noël, T., Cao, Y. & Laudadio, G. The Fundamentals Behind the Use of Flow Reactors in Electrochemistry. *Accounts of Chemical Research* **52**, 2858–2869. ISSN: 15204898. <https://pubs.acs.org/doi/full/10.1021/acs.accounts.9b00412> (Oct. 2019).
117. Li, K., Shapel, S. G., Hochfilzer, D., Pedersen, J. B., Krempel, K., Andersen, S. Z., Sažinas, R., Saccoccio, M., Li, S., Chakraborty, D., Kibsgaard, J., Vesborg, P. C., Nørskov, J. K. & Chorkendorff, I. Increasing Current Density of Li-Mediated Ammonia Synthesis with High Surface Area Copper Electrodes. *ACS Energy Letters* **7**, 36–41. ISSN: 23808195. <https://pubs.acs.org/doi/abs/10.1021/acsenerylett.1c02104> (Jan. 2022).
118. Boo, H., Park, S., Ku, B., Kim, Y., Park, J. H., Kim, H. C. & Chung, T. D. Ionic Strength-Controlled Virtual Area of Mesoporous Platinum Electrode. *Journal of the American Chemical Society* **126**, 4524–4525. ISSN: 00027863. <https://pubs.acs.org/doi/abs/10.1021/ja0398316> (Apr. 2004).
119. Kadyk, T., Bruce, D. & Eikerling, M. How to Enhance Gas Removal from Porous Electrodes? *Scientific Reports 2016 6:1* **6**, 1–14. ISSN: 2045-2322. <https://www.nature.com/articles/srep38780> (Dec. 2016).
120. Davalos Monteiro, R., van de Wetering, J., Krawczyk, B. & Engelberg, D. L. Corrosion Behaviour of Type 316L Stainless Steel in Hot Caustic Aqueous Environments. *Metals and Materials International* **26**, 630–640. ISSN: 20054149. <https://link.springer.com/article/10.1007/s12540-019-00403-2> (May 2020).
121. Nakahama, S., Hashimoto, K. & Yamazaki, N. Anode-Initiated Polymerizations of Olefins and Tetrahydrofuran. *Polymer Journal* **4**, 437–445 (1973).

122. Dey, A. N. & Rudd, E. J. Electroinitiated Polymerization of Tetrahydrofuran. *Journal of the Electrochemical Society* **14**, 1294–1298 (1974).
123. NIST. *NIST Standard Reference Database Number 69* Jan. 2022. <https://webbook.nist.gov/chemistry/> (2022).
124. PubChem. *PubChem Compound Summary for CID 23665649, Lithium perchlorate* 2022. <https://pubchem.ncbi.nlm.nih.gov/compound/Lithium-perchlorate>.
125. Sung, Y. E., Chrzanowski, W., Zolfaghari, A., Jerkiewicz, G. & Wieckowski, A. Structure of chemisorbed sulfur on a Pt(111) electrode. *Journal of the American Chemical Society* **119**, 194–200. ISSN: 00027863. <https://pubs.acs.org/doi/abs/10.1021/ja962637h> (Jan. 1997).
126. Trens, P., Durand, R., Coq, B., Coutanceau, C., Rousseau, S. & Lamy, C. Poisoning of Pt/C catalysts by CO and its consequences over the kinetics of hydrogen chemisorption. *Applied Catalysis B: Environmental* **92**, 280–284. ISSN: 0926-3373 (Nov. 2009).
127. Jung, N., Cho, Y. H., Ahn, M., Lim, J. W., Kang, Y. S., Chung, D. Y., Kim, J., Cho, Y. H. & Sung, Y. E. Methanol-tolerant cathode electrode structure composed of heterogeneous composites to overcome methanol crossover effects for direct methanol fuel cell. *International Journal of Hydrogen Energy* **36**, 15731–15738. ISSN: 0360-3199 (Dec. 2011).
128. Vaittinen, O., Metsälä, M., Persijn, S., Vainio, M. & Halonen, L. Adsorption of ammonia on treated stainless steel and polymer surfaces. *Applied Physics B: Lasers and Optics* **115**, 185–196. ISSN: 09462171. <https://link.springer.com/article/10.1007/s00340-013-5590-3> (Aug. 2014).
129. AfricaFertilizer.org. National Fertilizer Prices. *AfricaFertilizer.org*. <https://africafertilizer.org/national/>, accessed 01/04-2022 (2022).

**Supervisor: Associate Professor Jakob Kibsgaard**

**Co-supervisor: Professor Ib Chorkendorff**

Technical University of Denmark

Surface Physics and Catalysis

Department of Physics

Fysikvej, Building 307

2800 Kongens Lyngby

[www.fysik.dtu.dk](http://www.fysik.dtu.dk)

©**Jakob Bruun Pedersen**